CRANFIELD UNIVERSITY

LEE AIK SOON

TWO-COMBUSTOR ENGINE FOR MILITARY APPLICATIONS

SCHOOL OF ENGINEERING

DEPARTMENT OF POWER AND PROPULSION

PhD THESIS

Academic Year: 2006 - 09

Supervisor: R. Singh

August 2009

CRANFIELD UNIVERSITY

SCHOOL OF ENGINEERING

DEPARTMENT OF POWER AND PROPULSION

PhD THESIS

Academic Year: 2006 - 2009

LEE AIK SOON

Two-combustor Engine for Military Applications

Supervisor: R. Singh

August 2009

Abstract

The key requirements for military aircraft are high survivability and mission success rate: the former will "exponentially" increase the latter. The survivability of the aircraft depends crucially on its performance and energy signatures, to which its propulsion system contributes significantly. Therefore this imposes demands upon future propulsion systems for a better aerothermodynamics performance with a lower energy-signature. However, the performances achievable with conventional engine-cycles may be reaching their limits. Therefore, the author was motivated to investigate the potential of the two-combustor engine for military-fighter applications; with respect to its aerothermodynamics performance and infrared-signature.

An extensive literature survey was conducted to identify the up-to-date research for the two-combustor engine. Based on the collected information, systematic approaches were formatted with proven analytical methodologies for conducting the present study. A proven conventional engine (i.e. F100-PW229 engine, based on "open-publication"), for powering military fighter aircraft, was selected for benchmarking purposes in order to identify the prospect of the two-combustor engine. With an engine performance-simulation program of high fidelity and a detail engine model, the accuracy of the predictions of the engines' performances are greatly improved. The key contribution is the establishment on the influences of the two-combustor engine on the performances of the selected fighter aircraft, in particular the transient behaviour, steady-state flight characteristics (e.g. flight-envelope) and infrared signatures. This research relates the performance of the two-combustor engine to that of the aircraft, which was not found in any up-to-date publication. The availability of this research will allow engine and aircraft studies to include two-combustor solution in a more secure way than it was possible.

In this investigation, the main analytical tool employed is a Cranfield University in-house developed engine performance-simulation program, TURBOMATCH. The author has implemented various sub-programs to interface with TURBOMATCH in order to conduct specific simulations, e.g. transient-behaviour predictions. All the analyses have been undertaken using data from the published literature.

Acknowledgements

The author is grateful to the DSO National Laboratories, Singapore, for providing the scholarship, which enables him to pursue a postgraduate-degree course.

The author would like to thank his research advisor, Prof R. Singh, for his constant guidance and encouragement in this research work. Of course, the author has also gained valuable knowledge from Prof Singh on subjects beyond the scope of this research.

The author would like to express his appreciation to Prof S. D. Probert for proof-read the author's publications. Prof Probert has provided valuable advice on the subject of technical writing, whereby the author will benefit in the future as well.

The author would also like to give credit to the staff in the Department of Power and Propulsion toward the completion of this research work. Prof P. Pilidis, in particular, for been a member in the research-progress review panels.

Finally, the author would like to dedicate this thesis to his family members, in particular his wife, Miss Ong Ching Ching. Without their constant support and encouragement, this thesis would not have been completed "ON-TIME".

Agenda

List of Figures

List of Tables

Notation and Abbreviation

a_0	$m\ s^{-1}$	Sonic speed
A	m^2	Area
AoA	rad	Angle of attack
$A_{flametube}$	m^2	Flame tube's cross-section flow area
Bi_{metal}	-	Biot number of metal
Bi_{tbc}	-	Biot number of thermal barrier coating
Bi_{total}	-	Total Biot number
C_D	-	Drag coefficient
C_{Do}	-	Parasitic drag coefficient
C_L	-	Lift coefficient
Cp	$kJ\ kg^{-1}\ K^{-1}$	Specific heat capacity at constant pressure
Cp_{air}	$kJ\ kg^{-1}\ K^{-1}$	Specific heat capacity, at constant pressure, for the air
$Cp_{product}$	$kJ\ kg^{-1}\ K^{-1}$	Specific heat capacity, at constant pressure, for the product of fuel-air mixture
D	N	Drag
D_{ann}	m	Depth of annulur
D_{comb}	m	Depth of combustor
$D_{diff\text{-}in}$	m	Depth of diffuser's inlet
$D_{diff\text{-}out}$	m	Depth of diffuser's outlet
$D_{flametube}$	m	Depth of flame tube
D_{itb}	m	Depth of inter-stage turbine burner
E_{flt}	s	Flight endurance
F_{net}	N	Net thrust
FAR	-	Fuel-air-ratio
H	km or kft	Flight altitude
HPTET	K	High-pressure turbine's entry-temperature
$\dot{H}$	$m\ s^{-1}$	Rate of climb
I	$W\ atm^{-1}\ m^{-3}$	Combustion intensity
J	$W\ sr^{-1}$	Radiant intensity
J	$kg\ m^2$	Polar moment of inertia
K_{comb}	-	Combustion pattern factor
k	-	k^{th} time-step
k_1 , k_2	-	Factor for lift induced drag
K_{cool}	-	Cooling-flow factor
L	N	Lift
L_{ab}	m	Length of afterburner

$L_{exh\text{-}sys}$	m	Length of exhaust system (afterburner+exhaust nozzle)
L_H	N	The component of the lift acting in the horizontal direction
L_{inj}	m	Length of fuel injector
L_{itb}	m	Length of inter-stage turbine burner
L_V	N	The component of the lift acting in the vertical direction
L_{zone}	m	Length of respective zone in the combustor
LPTET	K	Low-pressure turbine's entry-temperature
m	-	m^{th} time-step
m	kg	Mass
M	-	Mach number
M	-	M^{th} time-step
MFF	-	Mass-flow function
M_0	-	Free-stream/Flight Mach-number
M_λ	W m^{-3}	Spectral radiant exitance
n	-	Load factor
N	RPM	Spool's rotational-speed
N	W sr^{-1} m^{-2}	Radiance
$\dot{N}$	RPM s^{-1}	Rate of change of spool's rotational-speed
P_0	K	Freestream pressure
P_s	m s^{-1}	Rate of climb
P_t	Pa	Total pressure
q	N m^{-2}	Dynamics pressure
Q	-	Correction factor for drag calculation
$\dot{Q}$	J	Heat input
R	kJ kg^{-1} K^{-1}	Gas constant
R_{ab}	m	Radius of the afterburner
R_{flt}	m	Range
R_i	m	Inner radius
$R_{noz\text{-}exit}$	m	Nozzle exit radius
$R_{noz\text{-}throat}$	m	Nozzle throat radius
R_o	m	Outer radius
RPM	RPM	Revolution per minute
S	J kg^{-1} K^{-1}	Entropy
SFC	kg s^{-1} N^{-1}	Specific fuel-consumption rate
SOT	K	Stator's outlet-temperature
ST	N s kg^{-1}	Specific thrust
S_{Ref}	m^2	Nozzle exit area

t	s	time
T_0	K	Freestream temperature
T_{metal}	K	Temperature of the metal
T_t	K	Total temperature
$T_{t/noz\text{-}exit}$	K	Total temperature at the nozzle's exit
$T_{t/plume}$	K	Total temperature at the exhaust plume
TET	K	Turbine's entry-temperature
W	kg s^{-1}	Mass-flow rate
W_{fuel}	kg s^{-1}	Fuel-flow rate
w_{fuel}	kg	Fuel flow
Wt	kg	Weight
WD	W	Work
V	m s^{-1}	Velocity
Vol	m^{-3}	Volume
Z	%	Compressor's surge line
ΔP_t	Pa	Change in the total pressure
Δt	s	Time step
ΔT	K	Change in the total temperature
ΔWD	W	Work imbalance in the spool

Greek Scripts

α	-	Bypass ratio
δ	-	Temperature correction factor
ε	-	Emissivity
ε_0	-	Cooling effectiveness
ε_e	-	Effective emissivity
ε_{film}	-	Film cooling effectiveness
ϕ_{cl}	-	Cooling air mass-flow rate to relative to mass-flow rate
Φ	-	Work potential of turbine's cooling-flow
γ	-	Cp/Cv
η	-	Efficiency
η_{int}	-	Internal cooling efficiency
η_{isen}	-	Isentropic efficiency
η_{mech}	-	Mechanical efficiency
η_{poly}	-	Polytropic efficiency
η_{prop}	-	Propulsive efficiency
η_{th}	-	Thermal efficiency

φ	rad	Angle between IR sensor line-of-sight and nozzle exhaust axis
λ	μm	Wavelength
Λ_{LE}	rad	Angle of the leading edge of aircraft's wing
$\prod$	-	Pressure ratio
θ	rad	Pressure correction factor
θ_{ab}	$Pa^{1.4}\ m^3\ kg^{-1}\ s$	Afterburner's sizing parameters
θ_{comb}	$Pa^{1.75}\ m^{2.75}\ kg^{-1}\ s$	Combustor's sizing parameters
τ	-	Temperature ratio
ξ	-	Turbine work distribution, ratio of work generate by respective stage of turbine over total work generate by the turbine
$\dot{\psi}$	$deg\ s^{-1}$	Rate of turn

Subscripts

0	Engine's inlet ; Time step zero
ab	Afterburner
ann	Annulur
bp	Bypass
calc	Calculation
cl	Cooling flow
clean-cfg	Clean configuration
cold	Cold (pressure) loss
com	Combustor
diff	Diffuser
dp	Design point
fan	Fan
flametube	Flametube of the combustor
gas	Gas
hg	Hot gas
hot	Hot (pressure) loss
hp	High pressure
hpc	High-pressure compressor
hpt	High-pressure turbine
i	Segment
in	Inlet
intake	engine's intake
itb	Inter-stage turbine burner
J	Engine's exhaust

k	k^{th} time-step
lp	Low pressure spool
lpc	Low-pressure compressor
lpt	Low-pressure turbine
m	m^{th} time-step
max	Maximum
mb	Main burner
mean	Mean
ngv	Nozzle-guiding-vanes
ngv1	Nozzle-guiding-vanes in the 1^{st}-stage of a two-stage turbine
ngv2	Nozzle-guiding-vanes in the 2^{nd}-stage of a two-stage turbine
ngv-eq	Nozzle-guiding-vane in an equivalent single-stage turbine
noz	Nozzle
out	Outlet
pri-zone	Primary zone of the combustor
ram	Ram
ref	Reference
rotor1	Rotor in the 1^{st}-stage of a two-stage turbine
rotor2	Rotor in the 2^{nd}-stage of a two-stage turbine
rotor-eq	Rotor in an equivalent single-stage turbine
R	Reference
sim	Simulation
sot	Stator-outlet temperature
target	Target
tolerance	Tolerance
turb	Turbine
tbc	Thermal barrier coating
T1, T2	Turbine 1 and Turbine 2
TJ	Turbojet
TF	Turbofan
wm	Windmilling

Superscripts

0	zero time-step
max	Maximum
n	n^{th} time-step ; n^{th} iteration

Constant

A1	$0.03 \rightarrow 0.07$	Depending on the turbine's cooling technologies
B1	3.74177×104 W μm^4 cm^{-2}	Coefficients for calculation of spectral radiant exitance
B2	1.43877×104 μm K	
$C_0,\ldots,C_7$	Constant values for calculating the value for Cp_{air}	
$D_0,\ldots,D_7$	Constant values for calculating the value for $Cp_{product}$	
g	9.81 ms-2	Gravity
Q_{fuel}	43124 kJ kg^{-1}	Fuel low heating value
σ	5.67 x 10-8 W m^{-2} K^{-4} K	Stefan-Boltzmann constant

Abbreviations

AB	Afterburner
AR	Aspect ratio
A/C	Aircraft
BLE	Baseline engine
BPR	Bypass ratio
C1, C2, C3, C4	Compressor 1 to compressor 4
Cfg	Configuration
CD	Convergent-divergent
CE	Conventional engine
CFD	Computational fluid dynamics
CFT	Conformal fuel-tank
CO_2	Carbon dioxide
CSH	Constant specific-heat model
CTB	Constant temperature turbine
CTT	Constant-temperature turbine
CU	Cranfield University
DP	Design-point condition
DP-A	Design-point condition A
DP-B	Design-point condition B
Fan	Fan
FLPTNGV	Fixed low-pressure turbine's nozzle-guiding-vane
fn	Function
FPR	Fan's pressure-ratio
GT	GasTurb
hg	Hot gas
H_2O	Water vapour
HP	High-pressure
HPC	High-pressure compressor

HPT	High-pressure turbine
IPC	Intermediate-pressure compressor
ISH	Improved specific heat model
ITB	Inter-stage turbine burner
LE	Leading edge
LP	Low pressure
LPC	Low-pressure compressor
LPT	Low-pressure turbine
MB	Main burner
MSH	Modified specific-heat model
MWIR	Mid-wave infrared
N.A.	Not applicable
NGV	Nozzle-guiding vanes
Noz	Nozzle
OD	Off-design condition
OPR	Overall pressure-ratio
PHI	Equivalent ratio for combustor's fuel-air-ratio
PR	Pressure ratio
Ram	Ram
Ref	Reference
Rotor	Rotor blade
SCC	Sequential combustion cycle
SEAD	Suppression of enemy air defences
SOT	Stator-outlet temperature
STOVL	Short take-off and vertical landing
SWIR	Short-wave infrared
T1, T2	Turbine 1 and Turbine 2
TBC	Thermal barrier coating
TCE	Two-combustor engine
TM	TURBOMATCH
T/0	Take-off
UCC	Ultra-compact combustor
VLPTNGV	Variable low-pressure turbine's nozzle-guiding-vane
VSH	Variable specific-heat model
VEAS	Equivalent air-speed

Glossaries

Afterburner	device (mounted between the final stage of the turbine and the exhaust nozzle) into which fuel is injected in order to achieve additional combustion with the un-burnt air and hence supplementary thrust.
Air-to-Air Configuration	aircraft equipped with avionics and weapon systems to perform air-to-air combat missions.
Air-to-Ground Configuration	aircraft mounted with avionics and weapon-system to conduct air-to-ground mission, e.g. strikes.
Bypass	passage to enable air to flow through the fan, but around the engine core, to the exhaust.
Bypass ratio	ratio of the rates of mass flow through the bypass passage to that through the engine's core.
Cold loss	The cold loss is mainly due to the injection of cooling-air through the liner into the combustion and dilution zone.
Combustor	chamber in which fuel is introduced, mixed with air and ignited to achieve combustion.
Compressor	component of the engine that compresses the air, prior to its entry to the combustion chamber.
Core	gas-generator component of a gas-turbine engine.
Design-point	the specific operating point (e.g. defining the flight condition and the compressor's pressure-ratio) which the engine has been designed to satisfy. Design point is also referred to as the on-design point in this thesis.
Drag polar	the aircraft's drag-coefficient to lift-coefficient.

Dry thrust	the thrust produced by an engine without the use of an afterbruner.
Dump diffuser	A short conventional diffuser used at the upstream of the combustor to reduce flow velocity over a short distance.
Fan	rotating bladed device for moving air: in the present context, the component that compresses the air upstream of the core and bypass splitter.
Flight envelope	flying condition, in terms of altitude and speed, within which the aircraft or engine is capable of operating.
Full-throttle	engine operating at its maximum allowable thrust.
Hot loss	The hot loss occurs, generally, in the main combustion section; whereby the combustion increases the temperature, causes a drop in the gas density and in turn an increase in the gases velocity. Based on momentum change, there would be a pressure loss.
NGVs	ring of radially-positioned aerofoils (at each stage of the turbine) which accelerate the gases emerging from the combustion chamber and direct them on to the first rotating turbine stage.
Nozzle	this exhaust-nozzle is a convergent duct designed to accelerate the flow in order to produce the engine's jet at the exit and so achieve thrust.
Off-design point	any operating point, within the engine's operating-envelope, except the design point.
Partial-throttle	engine operating at below its maximum allowable thrust condition for the flight condition.
Pay-load	personnel, equipment and consumable items (bullets, bombs, etc) carried onboard an aircraft, but which are

	non-essential to the aircraft's flying performance.
Spool	engine's centreline shaft, which transmits the turbine's work to the compressor.
Stator's outlet-temperature	the gas temperature at the outlet of the stator where the stator is the first NGV before entering the rotor blade
Super-cruiser	aircraft with the ability to cruise at supersonic speeds.
True airspeed	the physical speed of the aircraft relative to the speed of the air surrounding the aircraft
Turbine	component of the engine that extracts energy from the flow and which is used to power the compressor or perform auxiliary tasks.
Turbofan	gas-turbine jet engine with a bypass stream, i.e. part of the power developed is harnessed by a fan mounted inside a duct.
Turbine's entry-temperature	the temperature at the turbine inlet prior to mixing with cooling-flow: some text refer it to the temperature after the mixing with the NGV cooling flow
Wet thrust	the thrust achievable by an engine with an afterburner in operation
Windmilling condition	the condition in which an aero-engine if flame-off during flight

Chapter 1. Introduction

1.1 Introduction

Shortly after aircraft were invented, they were engaged in both commercial and military applications. Prior to the invention of the jet engine, aircraft were powered by reciprocating engines. The introduction of the jet engine revolutionalized the way that aircraft were been propelled: the aircraft envelope has been expanded to higher altitudes and flight speeds. With pertinent development in technology and science, aircraft use in both commercial and military applications have greatly increased. The latter is the focus of this thesis.

The propulsion system is an inevitable component of the aircraft. Apart from its influences on the design of the airframe, the propulsion system chosen has significant impacts on the aircraft's aerodynamic-performance. Assuming all other influential factors remain invariant, an aircraft's performance and capabilities will depend on its propulsion system.

Table 1.1 shows the diversity of typical missions [1-6] conducted by military aircraft; where the type of propulsion system is dependent upon the type of mission to be conducted. The increasing demands for aircraft with multi-role, short take-off and vertical landing (STOVL) and super-cruise capabilities have imposed more stringent design requirements on the propulsion system [7, 8].

1.2 Aircraft's Survivability versus Mission Rate of Success

During military operations, the main concerns are the success of the mission and survivability of the aircraft, i.e. the aircraft would have to survive both natural and man-make hostile environments, also to complete their operations successfully. Volpe and Schiavone [9] claim that the success of an operation "increases exponentially" with linear increases in the aircraft's survivability. The aircraft's survivability depends on factors such as its behavioural capabilities, energy signatures, operating environments and the tactics employed during the

operation. The propulsion system contributes significantly to the aircraft's behavioural capabilities and energy signatures, which in turn should dictate the tactics employed.

Table 1.1. Requirements imposed on military aircraft and their propulsion systems [1-6].

Mission Type	**Obligatory Attribute of the Aircraft**	**Stipulation Imposed on the Propulsion System**
Airborne control & command	Acceptable flight-distances and/or on-station loiter-periods	Turboprop or high bypass turbofan with an acceptable SFC
Bombing, SEAD, sweep and escort	Ability to operate well inside enemy-territory	Compromise between low SFC and high specific-thrust
Combat air-patrol	Endurance to achieve prolonged on-station loiter-periods	Compromise between low SFC and high specific-thrust
Interception	Take-off in shortest period and distance when scrambling to intercept incoming hostile-aircraft	High specific-thrust is the key requirement; low fuel-consumption is a secondary consideration
Transportation	Capability for carrying heavy loads over long flight-distances	Compromise between a low SFC and a high specific-thrust

1.3 Propulsion-system Contributions to an Aircraft's Performance and Its Infrared-Signature

The propulsion system influences the aircraft's performance and capabilities mainly with respect to the maximum achievable-thrust, lowest achievable specific fuel-consumption rate (SFC), shortest transient response-time and the minimum energy-signature. Factors such as the size and weight of the aircraft, which are equally important considerations are not included in this thesis.

The stealth attribute is now a critical factor influencing a military aircraft's survivability. The achievement of stealth requires a low radar cross-section, as well as small infrared, visual and acoustic signatures [10-15]: the attention is limited to the infrared signature in this study.

The propulsion system is a significant contributor to an aircraft's infrared-signature – see Table 1.2 [13-20]. Provided other influential contributions remain invariant, a reduction in the propulsion system's infrared-signature would reduce the likelihood of the aircraft being detected. The use of infrared countermeasures [21-23] will only be effective in enhancing the aircraft survivability if the aircraft's infrared-signature is appreciably lower [10, 17] Hence it is desirable to investigate the means for reducing the aircraft's inherent infrared-signature.

Table 1.2. Aircraft's main infrared-radiation signature sources [13-20].

Source	**Source of Contribution**	**Waveband***
Airframe	Aerodynamic friction heating; and heat transfers from heat sources in the aircraft	3→5μm [16] 8→14μm [16]
Propulsion-system's hot-parts	Turbine blade, tail-pipe, nozzle, and flame holder	1→3μm [14] 3→5μm [14, 16]
Engine's exhaust-plume	Carbon dioxide (CO_2) and water vapour (H_2O) in the exhaust-plume	2.7μm [16] 4.3μm [14, 15] 4.7μm [16]
Incident radiation reflected by the aircraft	Reflection of solar radiation	1→3μm [14] 2→3μm [16]

* There is no "official" standard [14]

1.4 Future Requirements for Aircraft and their Propulsion-systems

Air superiority will continue to be a crucial factor to the success of military campaigns for the foreseeable future. The strategic and tactical operations under-taken by military aircraft are constantly being refined, and shape the future

requirements imposed on military aircraft. The main requirements for future aircraft are listed below [7, 8, 24-27]; trade-offs in the requirements are often necessary in the aircraft's development process.

- ✓ Improvement in performance: The increase in an aircraft's thrust-to-weight (F_{net}/Wt) ratio and decrease in SFC remain the primary goals. The former will increase the aircraft's capabilities and/or reduce the size of the aircraft, while the latter will enable a longer operating-range and/or lower operating-cost.
- ✓ Increase in capabilities: The ability to improve/increase the aircraft's capabilities will enhance its flexibility on the conduct of missions. This will reduce the needs for a large fleet of aircraft for single-purpose tactical missions.
- ✓ Low observable characteristics (e.g. improved stealth): The reduction in the aircraft's energy-signatures will enhance its survivability during the conduct of a mission.
- ✓ Survivability: The improvement in the survivability of the aircraft will increase the rate of success of its mission [9]; thus reducing the cost of owning a large fleet of aircraft.
- ✓ Reliability and availability: These two factors measure the readiness of the aircraft. Increases in both reliability and availability will reduce the maintenance cost and probably the size of the fleet.
- ✓ Affordability: Increases in the aircraft's performance and capabilities are achieved by the introduction of leading-edge technologies, which increase the unit cost of the aircraft. Therefore "affordable capability" would be a more appropriate term to describe the requirements for the capabilities of future aircraft.

Being a vital component for propelling the aircraft, the propulsion system plays an important role in achieving the aims for future aircraft. Quantitatively, the set of requirements imposed on future aircraft directly affect its propulsion system [7, 8, 24-29] (see Section 2.4).

1.5 Motivation for the Investigation of the Novel Engine Concept: i.e. the Two-combustor Engine for Military Applications

Although great improvements in the engine performance have been achieved over the last sixty years, it might be reaching its limits (see Sections 2.3 and 2.5). Therefore researchers have been motivated to investigate the performances of novel engine-cycles in order to satisfy future requirements on both the aircraft and its propulsion system.

A two-combustor engine has a second combustor installed between the turbines, usually the high-pressure and low-pressure turbines (the HPT and LPT, respectively). Researches [30-43] have identified the benefits of higher achievable thrusts associated with the two-combustor engine in comparison with that achievable by the conventional engine. However, there remain zones of ignorance concerning the performance and operation of the two-combustor engine. This motivated the present author to investigate the potential of the two-combustor engine concept for military applications, and in particular for fighter aircraft.

1.6 Contributions to Knowledge

Literature survey was conducted to identify the analytical approaches and the findings for the studies on the two-combustor engine. Subsequently, systematic approaches were formatted with proven analytical methodologies for conducting the present study. The engine performance-simulation program employed is of high fidelity with generic components' maps to improve the accuracy and reliability of the simulation results. The engine model created also incorporated the exact requirement on the turbines' cooling-flow rate, which further enhanced the accuracy and reliability of the simulated engines' performances. Apart from revealing the exact performance of a two-combustor engine, the key contribution is the establishment on the influences of the two-combustor engine on the performances of the selected fighter aircraft, in particular

the transient behaviour, steady-state flight characteristics (e.g. flight-envelope) and infrared signatures. In order to ascertain the prospects and shortfalls of a two-combustor engine for military fighter, a proven conventional engine (i.e. F100-PW229 engine), for powering military fighter aircraft, was selected for benchmarking purposes. This research has revealed the potential of a two-combustor engine, relative to a proven conventional engine, on the enhancement of performances for a military fighter aircraft; with respect to both the aerothermodynamics and infrared characteristics. The adopted analytical approaches for this research, also the findings and the conclusions drawn are not found in any up-to-date publication. The availability of this research will allow engine and aircraft studies to include two-combustor solution in a more secure way than it was possible.

1.7 Thesis Structure and Convention

In this research, the key objective is to investigate the potential of the two-combustor engine for military-fighter applications; with respect to its aerothermodynamics performance and infrared-signature. To fulfill this objective, this research has been broken-down into different subjects pertaining to the performance of the two-combustor engine and its influences on the aircraft's behaviour. Each subject can be regarded as an independent study; thus the results, findings and conclusions are presented in as an independent chapter in the thesis. In the final chapter, only the main conclusions are summarized with emphasis on the prospects and drawbacks of the two-combustor engine for the military fighter aircraft. The layout and the conventions in the thesis are stated in the next paragraph.

Extensive literature surveys were conducted in order to understand the present and future requirements on aero-engines for future military aircraft. A literature survey will be presented in Chapter 2, but limited to the subject of gas-turbine. The analytical approaches and tools are described in Chapter 3. Chapter 4 presents the mis-leading findings published by researchers on the topic of two-combustor engines. The present aim can be divided into two categories: (i) the

study of the steady-state performance of the two-combustor engine under design and off-design conditions; and (ii) the investigation of the impacts of the two-combustor engine on the aircraft's performance. To ascertain the potential of the two-combustor engine, a baseline engine was identified for benchmarking purposes. The predictions and observations will be presented in subsequent chapters. The final chapter will present the conclusions drawn based on the present investigation and the recommendations for future work. For the ease of reference, the following conventions are adopted: -

- ✓ Unless otherwise stated, the terms gas turbine and propulsion system are used interchangeably to describe an aero-engine.
- ✓ The term "two-combustor engine" is designated to describe a gas-turbine with a main combustor installed directly downstream of the compressor-system. The second combustor is installed between the turbines, whereby the latter will be termed as the inter-stage turbine burner (abbreviated to ITB). Therefore the phase "ITB engine" is also used to refer to the "two-combustor engine"
- ✓ High-pressure and low-pressure turbines' entry-temperatures (HPTET and LPTET) refer to the gas temperatures prior to entering the high-pressure and low-pressure turbines (HPT and LPT), respectively.
- ✓ For the conventional engine, the terms HPTET and TET is used to refer to the gas temperature before entering the HPT. In the two-combustor engine, TETs is used to refer to both the HPTET and LPTET. The turbine's entry-temperature is also known as the combustor's exit-temperature: the latter parameter is not used in this investigation.

Chapter 2. Literature Survey

2.1 Introduction

An extensive literature survey was conducted to (i) appreciate the current and further operation-requirements of a fighter aircraft as well as (ii) identify the requirements imposed on its propulsion system. This chapter will discuss the evolvement of the propulsion system (see Figure 2.1). The early developments of the gas-turbine and the improvements in gas-turbine's performance over the last sixty years has been briefly summarized. The limitations of present-generation aero-engines have been identified, which are the motivations for researchers to investigate the performances of various novel engine-cycles. The engine with the capability of "heat-addition in the expansion process" was then shortlisted for special investigation here. The concept can be achieved through "constant-temperature" or "constant-pressure" processes: the latter is the focus for this study. The development of the hardware for achieving "heat-addition in the expansion process" has also described.

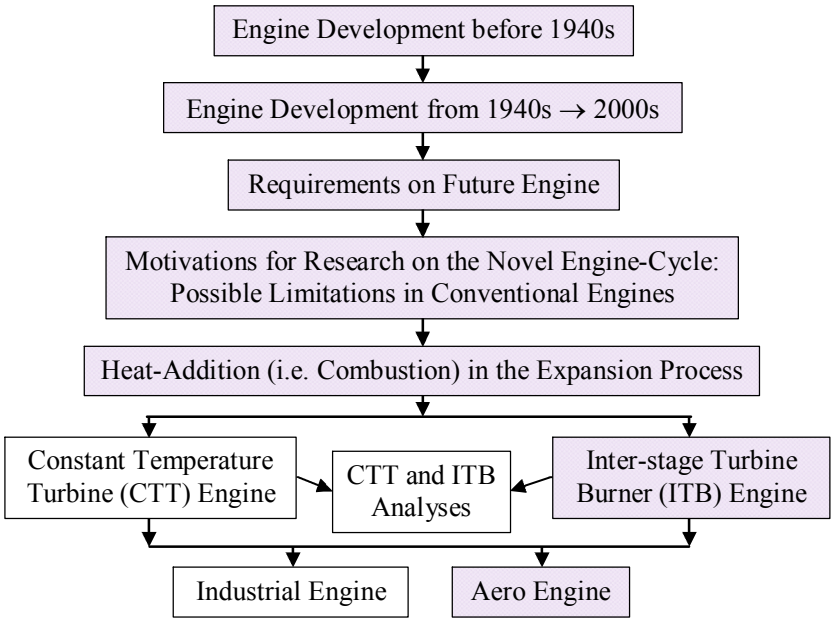

Figure 2.1. The layout on the presentation of the literature survey.

2.2 Developments in Gas Turbines prior to 1940s

John Barber patented the first gas turbine, with thermodynamic of modern cycle, in 1791 [44] (see Figure 2.2). From 1791 to the 1940s, researchers made several advances in the development of the gas turbine [44-47]: those in England, Germany, Italy and America are considered to be the main contributors.

- ✓ England: Frank Whittle patented a jet-engine design in 1930: it was run in a test-bed in 1937 [44, 45] (see Figure 2.3).

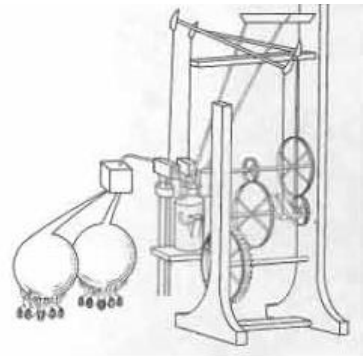

Figure 2.2. Schematic diagram of Barber's gas-turbine engine [44].

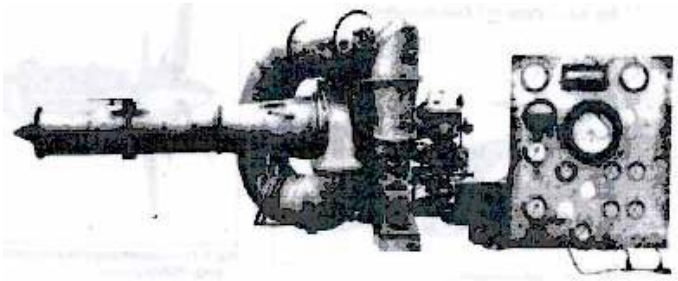

Figure 2.3. Whittle's first gas-turbine engine which was tested in 1937 [44].

- ✓ Germany: Hans von Ohain and Max Hahn patented their gas-turbine design, which had an operating principle similar to that employed in the Whittle's engine [44]: it was successful demonstrated in 1936 [45].
- ✓ Italy: Secundo Campini designed, produced and flight tested a gas turbine in late 1939: its compressor was driven by a reciprocating engine [45].

- ✓ USA: Based on the Whittle W1X engine and the W2B engine design, General Electric developed America's first turbojet prototype (GE-1-A), which was flight-tested in 1942 [44].

2.3 Advances in Gas-Turbine Engines Since 1940s

Figure 2.4(a) shows the ideal Brayton-cycle, which can be used to describe the operation of a simple gas turbine undergoing isentropic compression and expansion processes. The air at an aero-engine's inlet is compressed (also known as ram effect) due to its aircraft forward motion. The air pressure is further raised using a compressor before it enters the combustor. Fuel is added-to and burnt-in the compressed air in order to increase the entropy of the fuel-air mixture. Work is thereby produced, to drive the compressor, when the high-energy fuel-air mixture undergoes the expansion process in the turbine. The turbine's exit-flow, with relatively high energy, will produce shaft power or thrust. In an actual cycle, the efficiencies of the compression and expansion processes fall below 100%; also there exists pressure-drops for the gases passing through various components (e.g. the combustor) – see Figure 2.4(b).

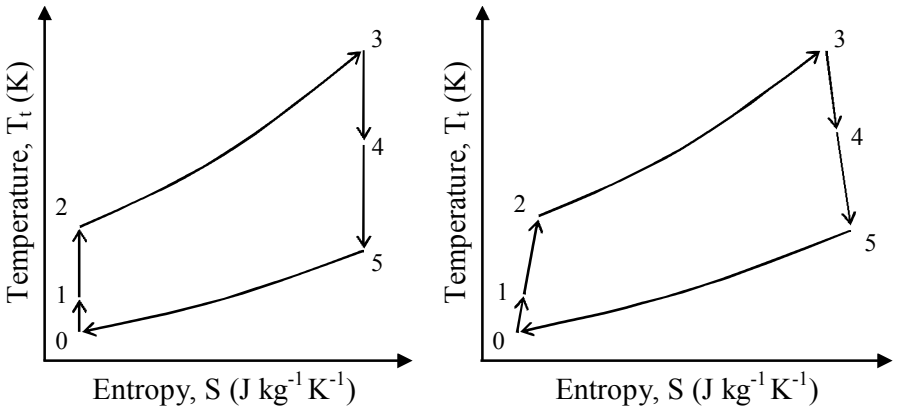

Figure 2.4. Temperature versus entropy diagram for a Brayton cycle
[0→1 Ram Compression 1→2 Compression by Compressor
2→3 Combustion 3→4 Expansion by Turbine
4→5 Expansion by Turbine or Nozzle].

Different types of propulsion system, for aero applications, were developed after the initial employment of the simple turbojet engine (see Figure 2.5). For an open-looped air-breathing engine, except for a ramjet, the core engine resembles that of a simple turbojet-engine cycle. Nevertheless, the operating principle of a ramjet can also be described by the Brayton cycle: namely compression by ram, combustion in the high-pressure flow and expansion via the nozzle.

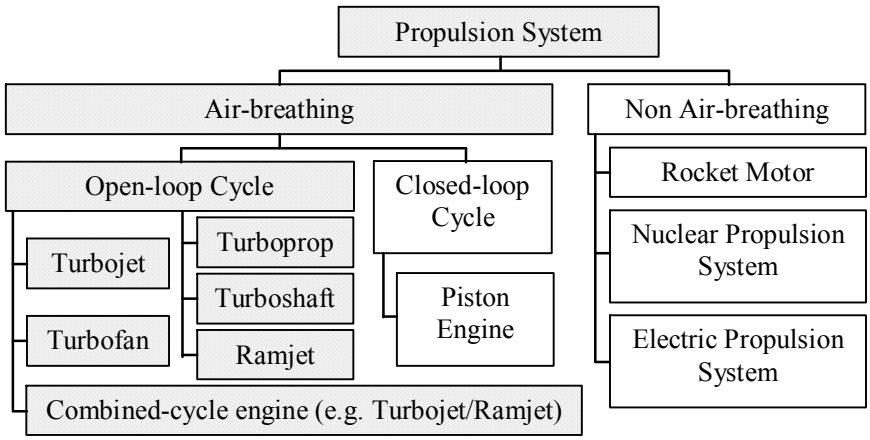

Figure 2.5. Propulsion systems for aero-applications.

Over the last sixty years, the performances of engines have been greatly improved (see Figure 2.6 and Figure 2.7). One of the contributing factors is that the designers now have better understandings of the engines' thermodynamics cycles and its complex internal-flow physics, which enable components of higher performance to be designed and manufactured [46]. Improvements in material properties, manufacturing processes and cooling technologies have led to increases in the turbine's entry-temperature (TET) (see Figure 2.8). The rise in TET enables the engine to produce a higher maximum achievable specific thrust (see Figure 2.6). The increase in TET coupled with an increase in overall pressure-ratio (OPR) (see Figure 2.9) lead to a rise in the engine's thermal-efficiency (see Figure 2.10). Hence the decreasing trend in the engine's specific fuel-consumption rate (SFC) (see Figure 2.7).

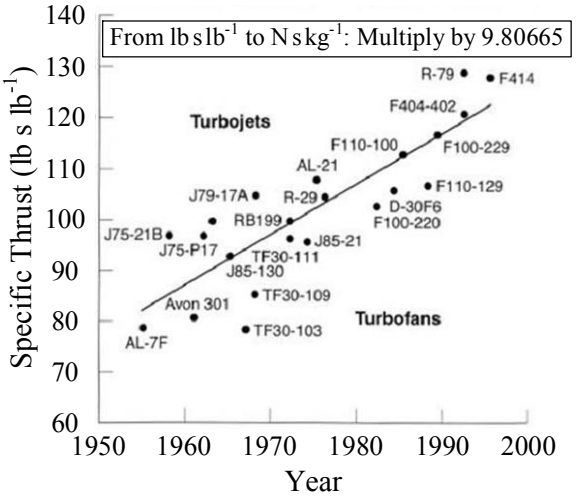

Figure 2.6. Trend of engine's specific-thrust versus time [48].

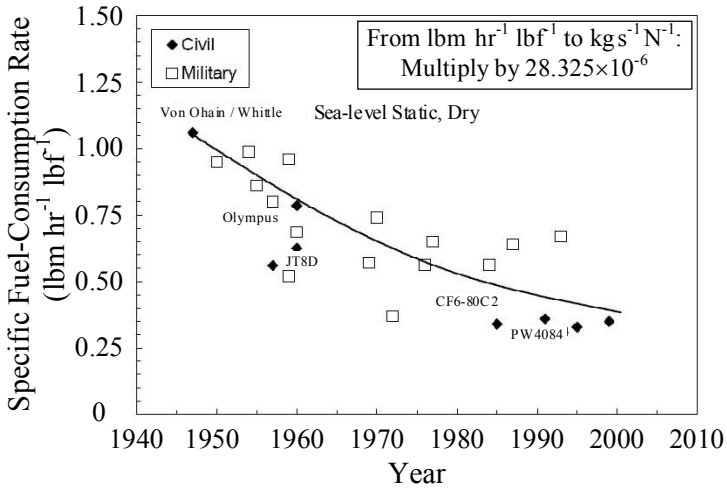

Figure 2.7. Trend of engine's specific fuel-consumption rate versus time [49].

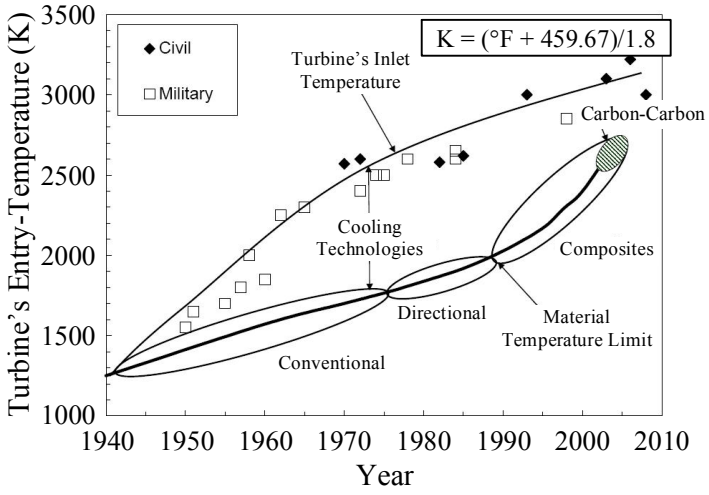

Figure 2.8. Trend of engine's turbine's entry-temperature versus time [49].

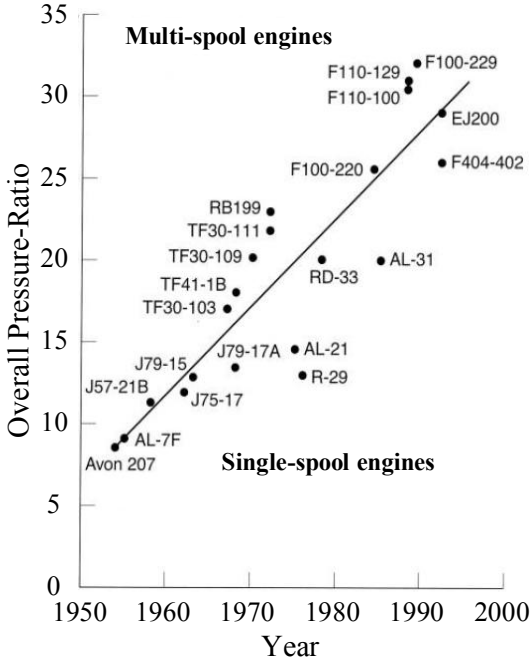

Figure 2.9. Trend of engine's overall pressure-ratio versus time [48].

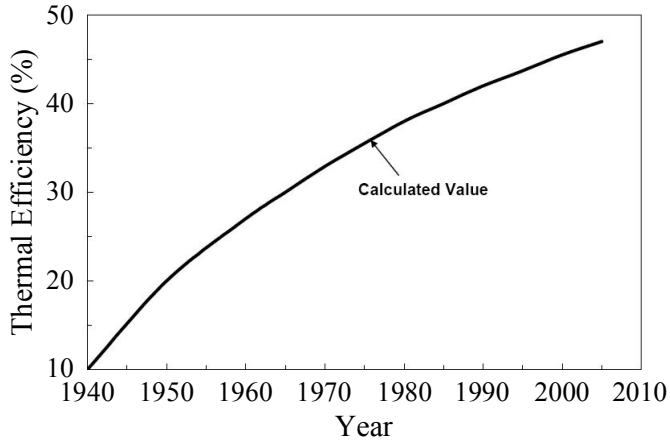

Figure 2.10. Trend of engine's thermal efficiency versus time [49].

The thrust-to-weight (F_{net}/Wt) ratio of an engine is also a crucial consideration in aero-engine's design. The improvements in components to achieve higher performances (e.g. an increase in pressure-ratio per compressor stage – see Figure 2.11) have enabled smaller and lighter components to be manufactured. The ability to achieve higher allowable values of the TET has increased the engine's specific thrust and hence produce a rise in the engine's F_{net}/Wt ratio (Figure 2.12).

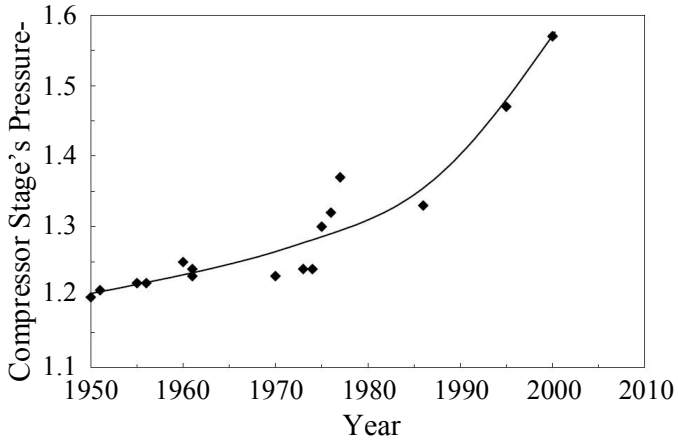

Figure 2.11. Trend of the compressor's pressure-ratio per stage versus time [49].

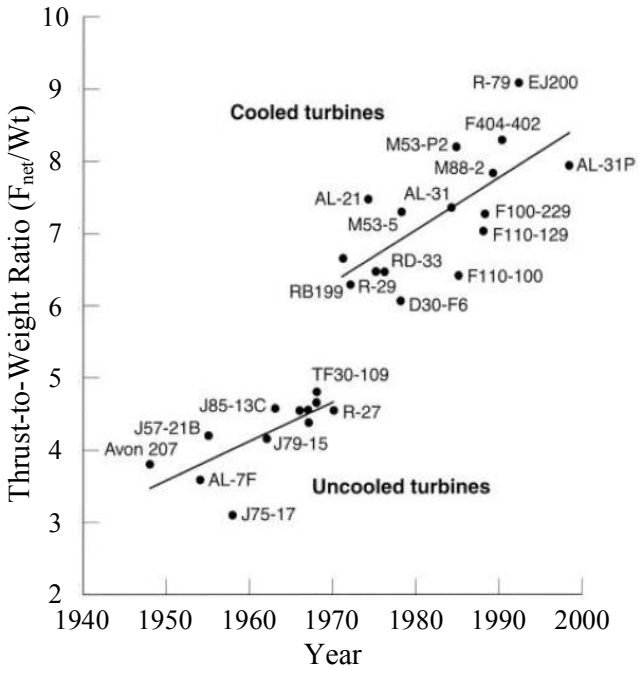

Figure 2.12. Trend of engine thrust-to-weight ratio versus time [48].

2.4 Requirements for Future Propulsion System

Quantitatively, the requirements on the future aircraft (see Section 1.4) are directly imposed on its propulsion system [7, 8, 24-29]. The demands for propulsion systems with better aerothermodynamics performance and lower infrared-energy signature are the concerns here. Improvements in the engine's aerothermodynamics performance will reduce the aircraft size (see Figure 2.13) [7] and so the cost of an aircraft can be reduced and its capability improved. The engine's tail-pipe and exhaust-plume are the main sources of the infrared signature; thus it is important to design the propulsion system so that it has a low infrared signature.

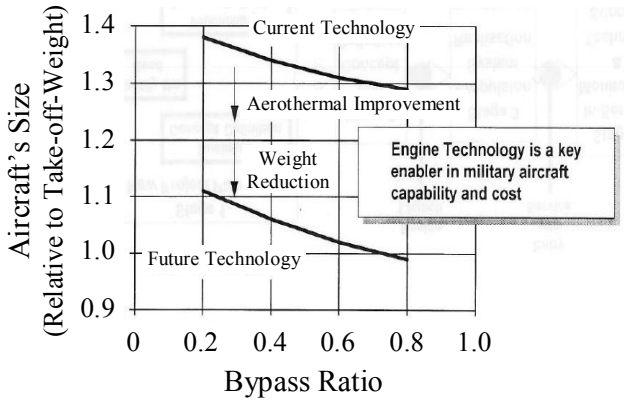

Figure 2.13. Trends with respect to the improvements in the engine's aerothermodynamics performance and reductions in engine's weight on the size of the aircraft [7].

2.5 Motivation for Research into Novel Engine Cycles: Possible Limitations in the Performance of the Gas Turbines

Figure 2.14 shows the trends of specific thrust versus flight Mach-number for the various types of engine. The turbojet has a higher specific thrust when compared with that of the turbofan engine. However, the latter operates with high propulsive (see Figure 2.15) and overall efficiencies, thus reduced SFC when compared with that of the turbojet engine (see Figure 2.16). Although the turbofan's SFC decreases with increase in the bypass-ratio, the corresponding reduction in the specific thrust will require a larger engine to produce a comparable thrust with lower bypass turbofan and turbojet engines. The turboprop has a high propulsive efficiency with low SFC. However, the limitations in the maximum achievable specific thrust and flight Mach-number make it unsuitable for fighter aircraft.

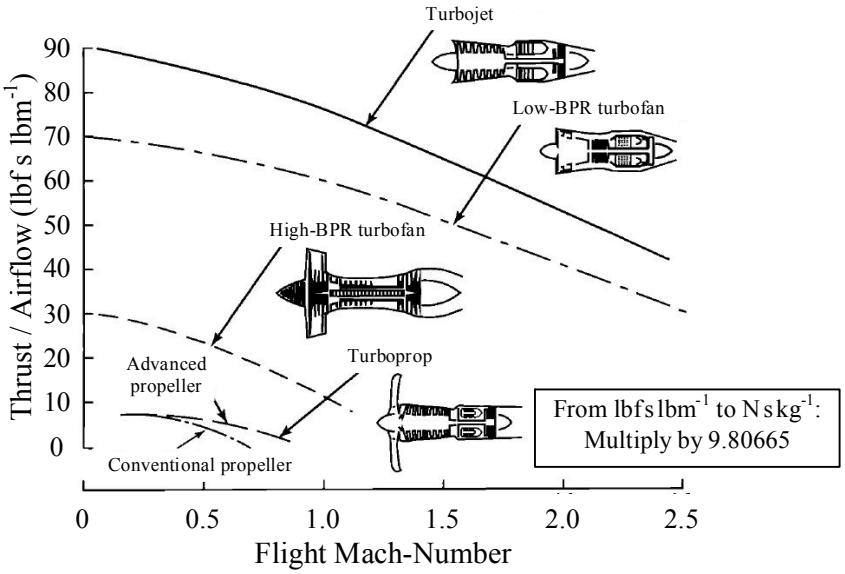

Figure 2.14. Specific thrust characteristics of aero-engines [46].

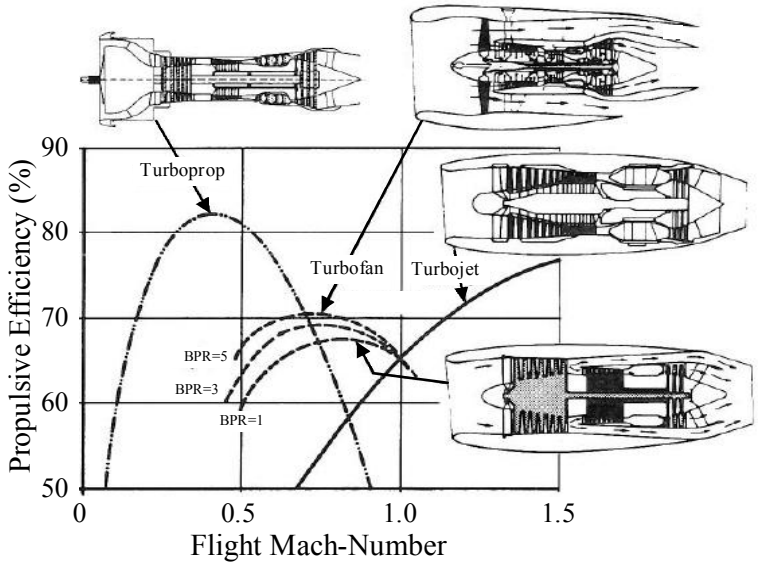

Figure 2.15. Propulsive efficiency characteristics of aero-engines [47].

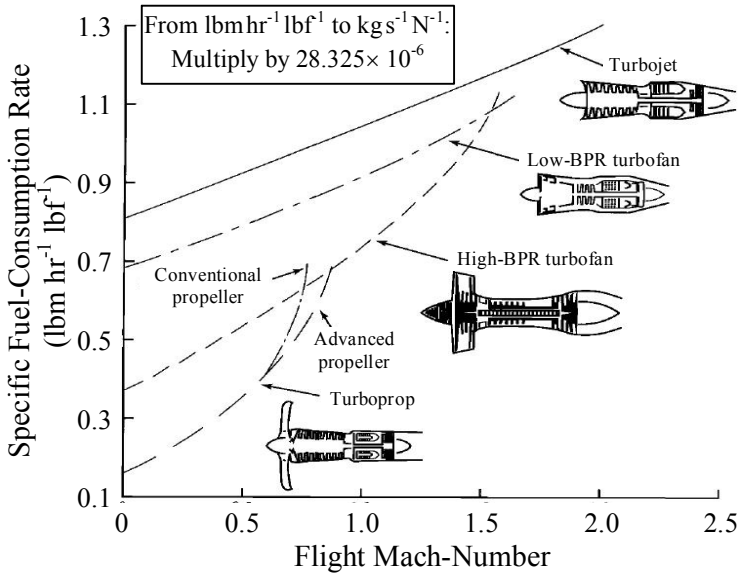

Figure 2.16. The characteristics of specific fuel-consumption rate of aero-engines [46].

Figure 2.17 shows the operating envelopes of typical turbojet and turbofan engines. The turbofan has a lower SFC, but due to it larger mass-flow rate and frontal area, the drag at high flight-speeds is tremendous. Thus the turbofan, especially with a high bypass-ratio, is not recommended for high-speed flight when compared with the turbojet engine. An afterburner can be added to both the turbojet and turbofan engines in order to provide extra thrust thereby achieving higher flight Mach-numbers. However, combustion in the afterburner results in a low cycle-efficiency due to its low inlet pressure and temperature: for instance a typical increase in 50% thrust is achieved at the expense of approximately three times the normal rate of fuel consumption [44].

Figure 2.18 shows the relation between specific thrust and SFC, with respect to the TET and OPR. Depending on the application, there is probably no single-engine that can satisfy a wide range of applications.

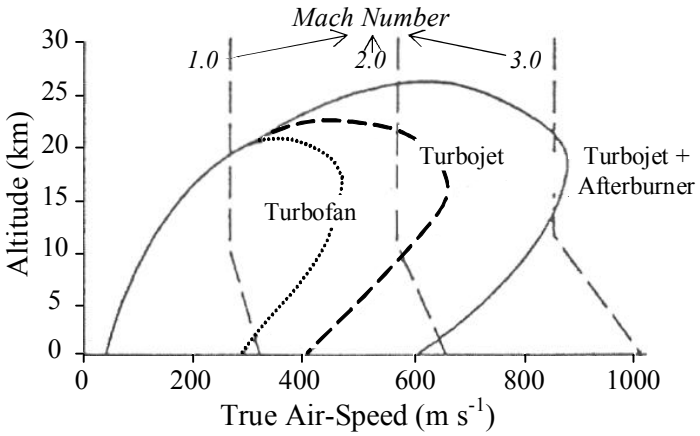

Figure 2.17. Typical flight envelopes for both turbofan and turbojet engines [50].

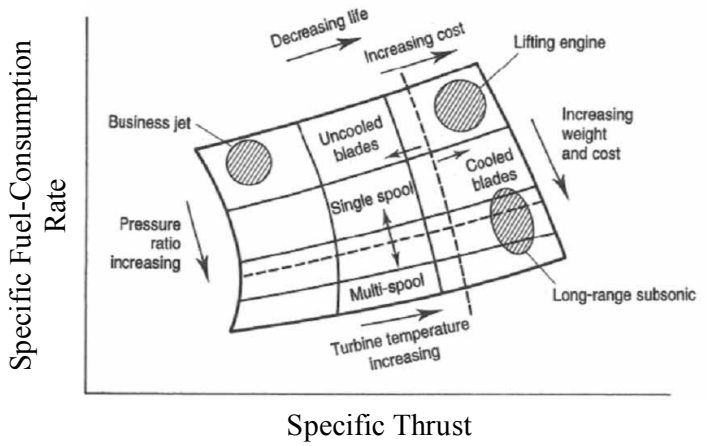

Figure 2.18. Performance and design considerations for aero-engines to satisfy various applications [51].

2.6 Novel Engine Cycle: Combustion in the Expansion Passage

Conventional thermodynamic-cycle propulsion-systems appear to be reaching their performance limits. Therefore novel engine-cycles (e.g. variable-cycle engines [7, 8, 50, 52, 53]) with the prospects of better performances and/or larger operating-envelopes are investigated. The concept of "heat addition (i.e. combustion) in the expansion process" is a relatively new novel engine-cycle, in

particular in aero-engine applications. The two means for implementing this concept are the "constant-temperature" and the "constant-pressure" combustion processes. In the former [30, 31, 54-57], fuel is added and burnt in the turbine passage simultaneously, while work is extracted to drive the compressors and other auxiliary systems. Balancing the rates of heat input and energy extraction serves to maintain a constant maximum-temperature during the expansion phase. In the "constant-pressure" combustion [30-43, 58, 59] process, fuel is burnt at (approximately) constant pressure in an additional combustor between the turbine stages. The latter is the focus for this study.

Various terminologies are used, by researchers, to refer to an engine implemented with "heat-addition in the expansion process". In this thesis, the turbine, whereby fuel is burnt at "constant-temperature" is designated as a constant-temperature turbine (CTT), and the corresponding engine cycle is referred to as the CTT engine-cycle. The combustor for "constant-pressure" combustion in the expansion-turbine will be designated as an inter-stage turbine burner (ITB). Technically, the performance of an engine with a sufficient number of ITBs will tend to that of the CTT engine [32, 33]. Therefore, the performance of the CTT engine is considered to be the maximum achievable for that of the ITB engine. For ease of expression, the engine with installation of ITB(s) will be termed as the ITB engine; specifically, for an engine with installation of a single ITB, it is also designated as two-combustor engine. Literature reviews concerning the ITB concept in aero-applications are presented here. Information concerning the CTT engine is presented in Appendix A. Recent findings concerning the CTT concept in industrial applications are discussed in Appendix B.

In 1948, BBC Brown Boveri developed the first industrial gas-turbine including an ITB (see Figure 2.19) [60, 61], which was designated as a sequential-combustion cycle (SCC). In 1990s, ABB Power Generation Ltd introduced a new class of ITB gas-turbine, i.e. namely the GT24 (see Figure 2.20) and GT26 [60-63]. The introduction of the ITB gas-turbine will enable an improvement in the combined-cycle efficiency to be achieved [60-63].

The implementation of the ITB in an aero application at present does not occur. In the presently-considered aero-engine, an afterburner is installed to achieve higher specific thrust at the expenses of a lower cycle efficiency: this increases the SFC appreciably. The current interest is to investigate the performance of the ITB engine for a military fighter application. This concept enables extra fuel to be burnt in the gas of higher pressures and temperatures, hence achieving a higher cycle efficiency when compared with that accomplishable with the incorporation of an afterburner for an conventional engine.

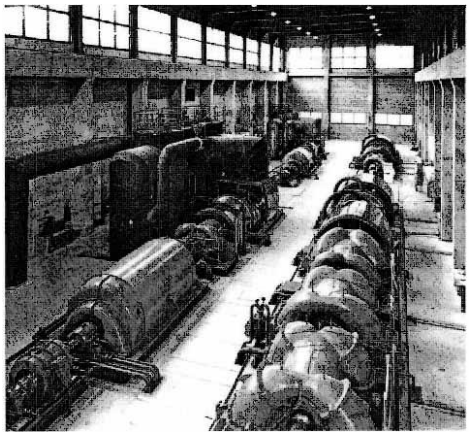

Figure 2.19. The first industrial gas-turbine implemented with sequential combustion [60].

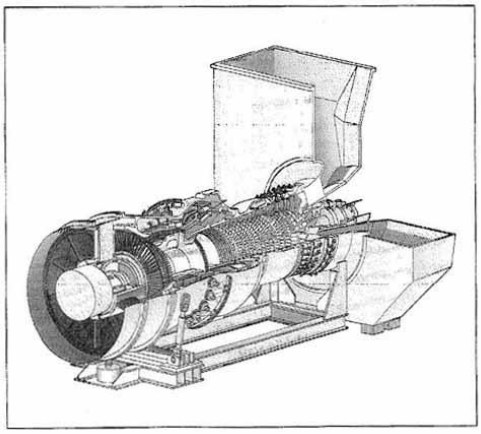

Figure 2.20. Cutaway view of the GT24 industrial gas-turbine [61].

2.7 Inter-stage Turbine Burner (ITB) Engines

The performance analysis for the CTT engine has shown great prospects [30, 31, 54-57]. However, the realization of a CTT engine is deemed to be too difficult to be achieved with existing technology [30-34]. However, a feasible configuration, with a potential performance that lies between those of a conventional engine and a CTT engine, is the ITB engine.

Figure 2.21 shows the thermodynamics-cycles for both conventional and the ITB engines. In the conventional engine, the energy in the combustion's exit-gas is extracted at the turbine stages to power the compressors; and the remaining energy in the high-temperature flow is converted to thrust. In an ITB engine, the temperature of the gas entering the low-pressure turbine (LPT) is further raised; this increases the entropy of the nozzle's flow and so achieves a higher thrust.

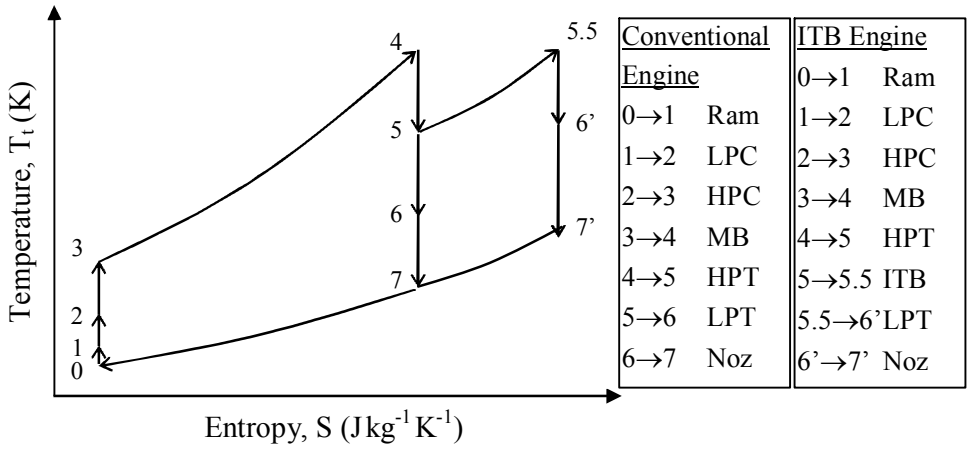

Figure 2.21. Thermodynamics cycles for the conventional turbojet engine and the inter-stage turbine burner (ITB) engine.

2.7.1 Aero-Engine

The performance of the ITB engine has been studied by Andriani et al [30, 31], Liu et al [32, 33], Liew et al [34-39], Vogeler [40] and members of Cranfield University [41-43]. In particular, the present investigation challenges the peculiar trends published by Liew et al and Vogeler: the conclusions presented in Chapter 4.

- **Andriani et al**

The on-design performance of an ITB turbojet-engine has been investigated by Andriani et al [30, 31] (see Figure 2.22). Apart from the increase in the flexibility of the engine operation, the ITB engine can also achieve a higher maximum specific thrust, for approximately the same SFC when compared with that of a conventional engine. Nevertheless, the amount of increase in the specific thrust was not explicitly stated. Also, the simplistic approach adopted by Andriani et al is unlikely to reveal accurately the benefits of the ITB engine.

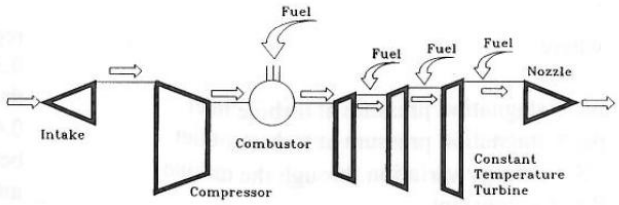

(a) Layout of ITB-engine

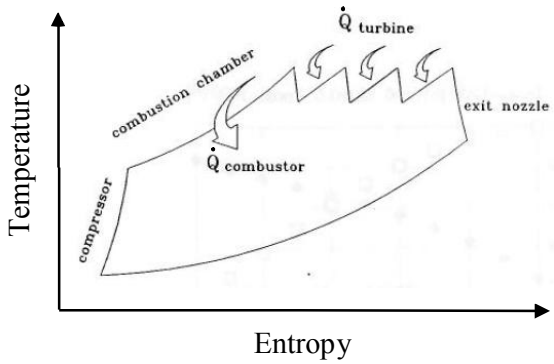

(b) Thermodynamics cycle

Figure 2.22. Layout of a turbojet engine with three-ITB and its corresponding thermodynamics cycle [31].

- **Liu and Sirignano**

Liu and Sirignano [32, 33] conducted parametric studies to investigate the effects of incorporating ITB (see Figure 2.23) on the performances of both the turbojet and turbofan engines under design-point conditions. The performances were compared with that of the conventional version of the engine. Apart from the parameter of interest, the values of the remaining design-parameters were kept

identical in both the conventional and ITB engines. The observations on the influence of ITB on the turbojet engine's on-design performance are summarized as follows: -

- ✓ Overall pressure-ratio (OPR): The ITB-engine's performance is enhanced with higher values of the OPR when compared with those of the baseline engine. Nevertheless, the corresponding increase in the engine's thermal-efficiency was lower than the decrease in its propulsive efficiency: this results in a higher SFC.
- ✓ Flight Mach-number (M_0): With the ability to burn extra fuel in the ITB, the engine is capable of operating at higher flight Mach-numbers with higher specific thrusts.
- ✓ Turbine's entry-temperature (TET): The increase in the TET will benefit both the ITB and conventional engines in achieving higher specific thrusts.
- ✓ Turbine's power-ratio: At a low turbine's power-ratio, the ITB's performance is nearer to that of the main combustor: then the ITB engine behaves like a conventional engine. At high turbine's power-ratio, the characteristics of the ITB tends to be those of the afterburner. Thus the ITB engine performance resembles that of a conventional engine in afterburner mode.

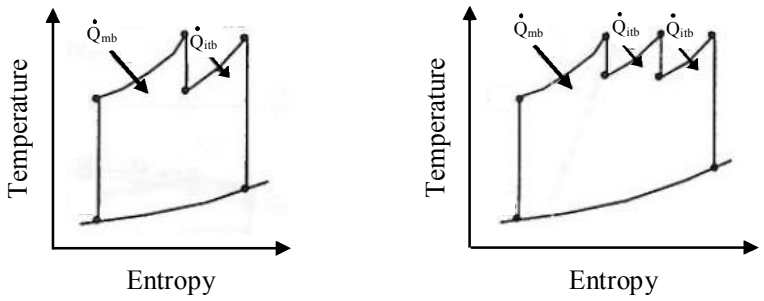

(a) One-ITB engine (b) Two-ITB engine

Figure 2.23. Thermodynamic cycles of the ITB-engines [32].

The above findings were also observed when the ITB was introduced into a turbofan engine [32, 33]. In addition, the implementation of the ITB enables more

power extraction to be achieved at the LPT. Hence the ITB turbofan-engine has a better performance at higher values of the bypass-ratio (BPR) and fan pressure-ratio (FPR) when compared with that of a corresponding conventional turbofan-engine. Comparing the ITB engine, with its higher values of OPR, FPR and BPR, against the conventional engine, the improvement in the performance associated with the implementation of the ITB engine becomes obvious.

The influences of the presence of the ITB on the performances of the turbofan and turbojet engines have been compared. The presence of an ITB in the turbofan engine produces a larger increase in specific thrust with only a minimal increase in SFC when compared with the implementation of ITB in the turbojet engine. Thus the former is a better configuration for extracting the "extra" power generated in the ITB.

The methodology used by Liu and Sirignano [32, 33] are relatively simplified. The exact cooling-flow requirement has not been explicitly accounted for in the analytical model. Although the results predicted by Liu and Sirignano might not be absolutely reliable, the promising findings provide the motivation for more detailed studies.

- **Liew et al**

The results published by Liu and Sirignano [32, 33] motivated Liew et al to investigate the performance of an ITB engine using a more refined methodology [34-39]. The selected baseline conventional engine is a two-spool separate-exhaust turbofan engine. The results show that the ITB engine produces a higher thrust with only a minimal increase in SFC when compared with that of the conventional engine. Studies were also conducted to ascertain the effects of various parameters (e.g. OPR, FPR, BPR, M_0) on the performance of ITB engine relative to that of the conventional engine [34]. The findings are consistent with those published by Liu and Sirignano [32, 33].

Given the same level of technological sophiscation, the ITB engine requires increased turbine's cooling-flow, which will off-set the benefit of achieving a higher achievable thrust by the introduction of the ITB. Therefore Liew et al [37,

39] suggested keeping the ITB's exit gas-temperature below the maximum allowable temperature that the material can withstand over prolonged periods, i.e. 1300K. For a specific low-pressure turbine's entry-temperature (LPTET), the benefit associated with the implementation of the ITB is enhanced for configurations with low high-pressure turbine's inlet temperature (HPTET) (see Figure 2.24) and high flight Mach-number (see Figure 2.24). However, the engine's maximum achievable specific thrust will be sufficiently lower than that obtainable by engine with the implementation of maximum allowable TETs.

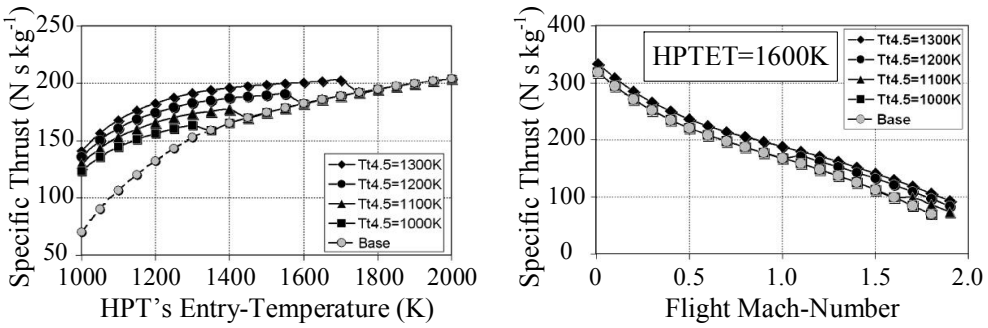

Figure 2.24. The effects of the LPTET (i.e. $T_{t4.5}$) on the engine's specific-thrust with respect to the variations in the HPTET and flight Mach-number [37].

Figure 2.25 shows the behaviour of the two-combustor engine under off-design conditions predicted by Liew et al [35, 38]. When the LPTET was reduced but with the HPTET held constant, the reduction in the engine's thrust is almost linear to that of its SFC. Also the quantitative "fish-hook" trend was observed when the HPTET was reduced with ITB turned-off (see Figure 2.25). The constant specific-heat (CSH) [38] and modified specific-heat (MSH) [35] models were used to calculate the gas-properties at the various engine-stations. The use of the CSH model predicted an increase in the engine's thrust with a corresponding decrease in the SFC when the ITB was turned on (see Figure 2.25(a)). However, the prediction using the MSH model indicates an increase, instead of a decrease, in the SFC (see Figure 2.25(b)).

The engines' design-point conditions in both references [36] and [38] are identical, but the predicted off-design performance obviously different (see Figure 2.26). In reference [36], the SFC of the ITB engine (with the ITB turned-off) is

higher than that of the conventional engine producing a comparable thrust (see Figure 2.26(a)). However, in reference [38], the performance of the ITB engine (with the ITB turned-off) resembles that of the conventional engine (see Figure 2.26(b)).

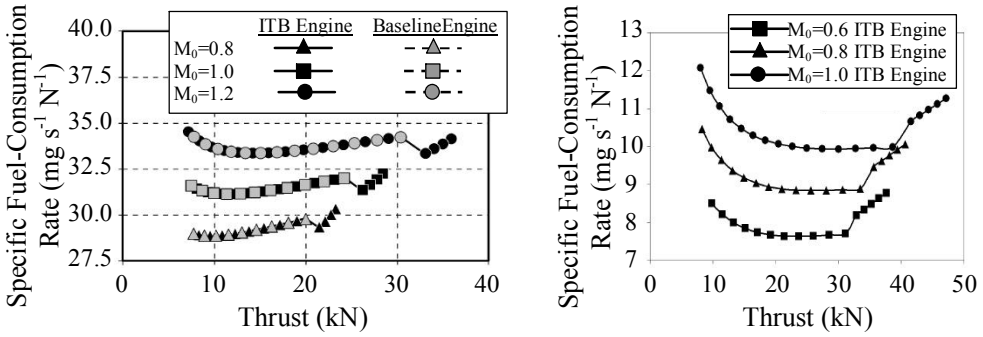

(a) CSH model [38] (b) MSH model [35]

Figure 2.25. The performance of ITB-engine under partial-throttle conditions as predicted using the CSH [38] and MSH [35] models.

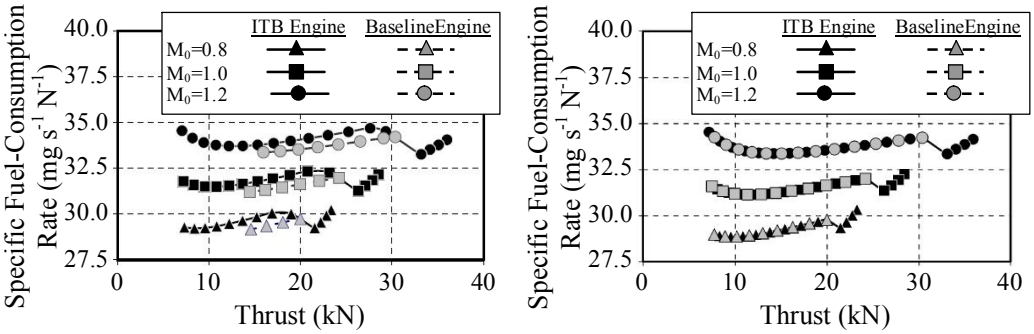

(a) Reference [36] (b) Reference [38]

Figure 2.26. The performance of the baseline and ITB engines under partial-throttle conditions as predicted using the CSH model [36, 38].

The above peculiar findings motivated the present author to conduct more detailed studies to investigate the reliability of Liew et al's publications: the outcomes of the present investigation are presented in Chapter 4. In addition, although the engine performance-simulation program, adopted by Liew et al, is of higher fidelity than that used by Liu and Sirignano, it can be further improved

especially for off-design performance-simulation. With the majority of Liew et al's studies not considering the exact turbine's cooling-flow requirement, the benefit associated with the ITB engine are likely to be over-predicted.

- **Vogeler**

Vogeler also conducted a study to investigate the performance of an ITB aero-engines [40]. The considered baseline engine was a two-spool turbofan engine with a bypass-ratio of five: the exact turbine's cooling-flow rate was considered in the engine-bahaviour modelling. Two configurations were considered, namely a twin-spool and a single-spool ITB gas-turbine. The ITB is located between the high-pressure and low-pressure turbines (HPT and LPT). The maximum achievable thrust of the two-spool ITB-engine is increased but at the expense of a higher SFC when compared with that of the baseline engine. The single-spool ITB-engine has a higher OPR and also possesses the flexibility of independently selecting the value of the HPT's pressure-ratio. Thus it has a higher achievable thrust with a lower SFC when compared with that of the baseline engine. The present author has conducted an investigation based on the data in reference [40]. The results, shown in Chapter 4, reveal that the Vogeler's findings are questionable.

- **Cranfield University**

Researches were conducted in Cranfield University to ascertain the performance of an ITB engine in both military and commercial aero-applications [41-43]. Although an in-house developed engine performance-simulation program (TURBOMATCH – see Chapter 3) was used, the requirement for extra turbine's cooling-flow rate, with the incorporating of an ITB, was not addressed.

Eady's study shows that the ITB engine can produce a higher thrust than that achievable by the conventional engine [41]; also its performance can be further enhanced with the implementation of variable turbine's nozzle-guiding vanes. However, Eady employed the fuel-consumption rate as the engine's control-parameter, which lead to an increase in the TET above its maximum allowable value. This observation is not presented in Eady's thesis.

Kristiansen [42] and Yannakoulis [43] researches were on the application of ITB engine for a civil airliner. The analyses show that the performance of the ITB engine is enhanced with higher FPR and BPR incorporated, which is consistent with that published in references [32-34]. The ITB engine provides a significant increase in the specific thrust with only a minimal increase in SFC when compared with that of the convection engine. With respect to emission and economic issues, the ITB engine is superior to that of the conventional engine. However, there is a potential weight increase of 20-25% when compared with the conventional engine [42].

2.8 Ultra-compact Combustor

Sirignano et al [55, 56] and Liu et al [32] have shown promising benefits of the CTT and ITB engines over a conventional engine, respectively. This motivated Zelinak et al [64, 65] to conduct experimental studies to investigate the feasibility of combustion in the turbine's vanes, i.e. the ultra-compact combustor (UCC) (see Figure 2.27). Concurrently, Mawid et al [66] conducted numerical analyses to study the process of combustion in the UCC using computational fluid dynamics (CFD). The combined results show that the combustion in the UCC is feasible and that a combustion efficiency of 99% is achievable.

The ITB proposed by Siow and Yang [67] was situated in the transition-duct, between the HPT and LPT. Using CFD, Siow and Yang revealed that the Reynolds number has a strong influence on the flow-field and flame stability of the ITB.

In the above-discussed configurations, the flow through both the UCC and ITB will experiences a high swirl; also the time taken is significantly shorter than the residue-time for complete combustion. These two factors are unfavourable for the combustion process. Although the analyses have shown promising results, more investigations will have to be conducted before the implementation of UCC.

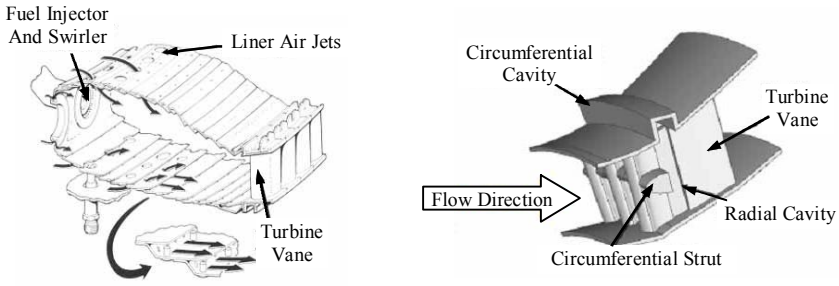

(a) Conventional combustor (a) Ultra-compact combustor

Figure 2.27. Comparison between the conventional combustion-system and the ultra-compact combustor (UCC) [64, 65].

2.9 Conclusions

The performance of a conventional gas-turbine might be reaching its limits. The continuous requirements imposed on the engine to achieve better performances and capabilities have motivated researchers to investigate the performance of novel engine cycle. The inter-stage turbine burner (ITB) is a relatively new concept proposed for aero-applications. Researches on the ITB engine also show a higher specific thrust is achievable with manageable or no increase in specific fuel-consumption rate (SFC). However, the adopted engine performance-simulation programs of lower fidelity [30-40] and hence the predictions could be of lower order of accuracy. Also, most of the studies did not consider the exact turbine's cooling-flow requirements for the ITB engine. In addition, there exist peculiar trends in the results in some publications. Nevertheless, the present author concluded that the ITB engine has the following potential characteristics; hence selected this concept for further study.

- ✓ The gas enters the ITB is at a higher pressure and temperature when compared with that at the afterburner. Hence the ITB engine is expected to be more efficient than a conventional engine with an afterburner.
- ✓ By optimizing the rates of fuel-consumption rate in both the combustors, the engine's transient-performance could be improved.

- ✓ The two-combustor engine's exhaust-temperature can be lower than that of the corresponding conventional engine with an afterburner. Thus the former possesses the possibility of emitting a less intense infrared-energy signature [31, 32].

In the publications concerning the ITB engine, except for references [42] and [43], the ITB is incorporated at either the transition-duct between high-pressure and low-pressure turbines (HPT and LPT) or the turbine's stator. The high swirling flows in these engine parts will have significant effects on the combustion stability and efficiency, which has not been addressed by the respective authors. The present author has assumed that the ITB to be of conventional combustor design: the entire analysis has been based purely on available technologies.

Chapter 3. Analytical Approaches Adopted and Tools Used

3.1 Introduction

The topic of two-combustor engine (TCE) for military fighter applications is described in this thesis. This research topic has been broken-down into various smaller tasks (see Section 3.2), and the approaches briefly described in this chapter.

The engine performance-simulation program, TURBOMATCH [68], is the main software used in this study. The author has implemented various sub-modules, interfaced (externally) with TURBOMATCH to perform various specific tasks (e.g. transient-performance prediction) for a wide range of studies. The methodologies of these sub-modules are described.

To try to understand the conflicting findings published by Liew et al [35, 36, 38] and Vogeler [40] (see Section 2.7.1), their engine performance-prediction methodologies have been studied and their programs re-produced. The present author's findings are described in Chapter 4.

3.2 Numerical-Prediction Approach

Figure 3.1 shows the analytical approach for this research project. Extensive surveys are conducted to appreciate the nature of the military (air) operations and threats to which the military aircraft are subjected. Hence the requirements imposed on the present and future aircraft and their propulsion systems have been deduced. The present prime focus is to investigate the performance of a novel (i.e. two-combustor) engine, for meeting future military-aircraft requirements, with respect to achieving high performance and low infrared-signature.

In the development of an aircraft, its propulsion system can be selected from the existing aero-engines that match the requirements. Alternatively, an

"customized" aero-engine could be developed (almost) simultaneously, and both the designs of aircraft and engine optimised concurrently to meet/optimize the aircraft's overall requirements. The present approach is slightly different: the author studied a two-combustor engine that would replace an existing-engine (i.e. the F100-PW229 engine, based on "open-publication") for an aircraft with aerodynamics-characteristic that resemble those of the F16 Falcon aircraft.

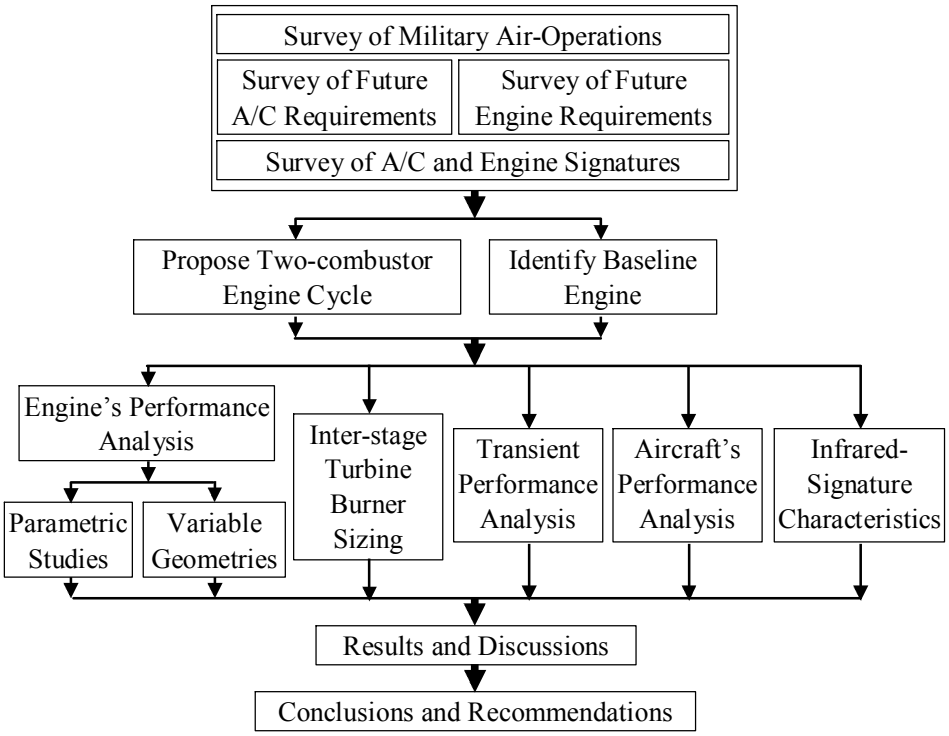

Figure 3.1. Stages in the numerical prediction.

The two-combustor engine's primary requirements continue to be high specific thrust and low specific fuel-consumption rate (SFC). The analysis begins by analyzing the two-combustor engine's steady-state performances under both on-design and off-design conditions. The influences of variable low-pressure turbine's nozzle-guiding-vanes (LPT's NGV) and variable turbine's cooling-flow requirements on the two-combustor engine's steady-state performance have been separately studied and included here. The size of the inter-stage turbine burner (ITB) has been estimated through the use of empirical correlations, thereby addressing the physical effects of the incorporation of ITB on the overall size of

the engine. Due to the possessing insufficient data on the aircraft's aerodynamic characteristics, the conduct of a full-mission performance analysis is not feasible. Nevertheless, the effects of the two-combustor engine on the aircraft's flight-envelopes and performances (under selected conditions) have been investigated. The transient performance of the engine is important with respect to the manoeuvrability of the aircraft; while the infrared signature of the engine (including its exhaust plume) is crucial to its survivability. Therefore these two subjects have also been studied. A baseline (i.e. conventional) engine is required for benchmarking (i.e. comparison) purposes, thereby more easily identifying any operational improvements that can be achieved by adopting the two-combustor engine. The selected baseline engine (F100-EQ, in abbreviation) has a performance equivalent to that of an F100-PW229 engine (see Chapter 5). The considered aircraft has the aerodynamic characteristic equivalent to those of the F16 Falcon aircraft. It is designed as F16-EQ aircraft for this thesis.

The F100-PW229 engine is (probably) optimized based on a set of specific requirements for selected flight-missions. However, with only limited available data, the author was unable to optimize the two-combustor engine in the way that was done for the F100-PW229 engine. Although parametric studies were conducted (see Chapter 6), the present studies (e.g. transient-performance analyses) have been conducted using the two-combustor engine under the "basic" design-point conditions. The "basic" design-point condition is identical to that for the baseline engine, except that the low-pressure turbine's entry-temperature (LPTET) is included (see Section 6.3). Although the design-point condition is not optimized, the present key objective remains achievable, i.e. to identify and demonstrate the potentials and design-alternatives associated with the two-combustor engine for military applications.

3.3 Analytical Tools

3.3.1 Propulsion-System's Performance-Simulation

TURBOMATCH is a software package developed by the late J. R. Palmer and used frequently at Cranfield University to simulate engine behaviour [68]. It

is used in the present study to predict the performances of both the baseline and corresponding two-combustor engines under both design and off-design conditions.

In a high-performance engine, cooling flow is required for the high-pressure turbine (HPT) and (sometimes) the low-pressure turbine (LPT) in order to ensure an acceptably long-life for the engine. A good estimation of the turbines' cooling-flow rate is essential, in order to achieve a more accurate prediction of the engine's performance. The cooling-flow rate for the turbine's stators and rotors are calculated using the adopted methodology. The baseline (i.e. F100-EQ) engine has two-stage turbine for both its HPT and LPT. In TURBOMATCH, the two-stage turbine is modelled as an equivalent single-stage turbine.

- **Prediction of Turbine's Cooling-Flow Requirements**

Three methods for predicting the turbine's cooling-flow rate have been considered, namely those introduced by Walsh et al [69], Kurzke [70] and Young et al [71], respectively. The author has chosen the methodology adopted by Young et al due to its flexibility for the current applications and future studies. For completeness of presentation, the methodologies for the former two methods are described in Appendix C.

Young and Wilock [71] extended the method, originally introduced by Holland and Thake [72], to include the effects of temperature-drops across metal components and thermal-barrier coatings (TBC). The cooling-flow rates for each row of blades or vanes can be calculated using Equations (3.1) to (3.4). The accuracy of the prediction depends on the values of K_{cool}, ε_{film}, η_{int}, Bi_{tbc} and Bi_{metal}. The values of these parameters, can at present only be obtained from simulations and experiments. The values depend heavily on the cooling technologies and turbine design. Among the publications surveyed, reference [73] provides the most comprehensive data on the stated parameters (see Table 3.1). The present author assumes that the "current" technology corresponds to the time at which reference [73] was published, i.e. AD 2005. Since the F100-PW229 engine was developed in the 1980s, the present author assumes that the

corresponding cooling technology is "two-generations" prior to the "current" technology (see Table 3.1).

$$\varepsilon_0 = \frac{T_{t/gas} - T_{metal}}{T_{t/gas} - T_{t/cl}} \tag{3.1}$$

$$Bi_{total} = Bi_{tbc} - Bi_{metal}\,\frac{\varepsilon_0 - \varepsilon_{film}}{1-\varepsilon_0} \tag{3.2}$$

$$\varsigma = \frac{\varepsilon_0 - \varepsilon_{film}\left[1-\eta_{\text{int}}\left(1-\varepsilon_0\right)\right]}{\eta_{\text{int}}\left(1-\varepsilon_0\right)} \tag{3.3}$$

$$\phi_{cl} = \frac{W_{cl}}{W_{gas}} = \frac{K_{cool}\varsigma}{1+Bi_{total}} \tag{3.4}$$

Table 3.1. Values of parameters for calculating turbine's cooling-flow rates.

	$\mathbf{K_{cool}}$	$\boldsymbol{\eta_{int}}$	$\boldsymbol{\varepsilon_{film}}$	$\mathbf{Bi_{metal}}$	$\mathbf{Bi_{tbc}}$
F100-EQ engine	0.045	0.60	0.30	0.15	0.1
Current technology *	0.045	0.70	0.40	0.15	0.3
Advanced technology *	0.045	0.75	0.45	0.15	0.4
Super advanced technology *	0.045	0.80	0.50	0.15	0.5

* Time frame with respect to Reference [73]

- **Modelling of the Single-Stage Equivalent Turbine**

Theoretically, the behaviour of a multi-stage turbine could mathematically be modelled as the integration of the behaviours for each individual stage. However the map of the individual turbine stage is unavailable even from test measurements, due to the limitations in the present instrumentation [74]. Moreover, the performance of the downstream stage(s) is often affected by swirling flow from upstream stage(s). Therefore the present practice is to model the behaviour of a multi-stage turbine by an equivalent single-stage turbine [69, 74].

Figure 3.2 shows a schematic of the cooling-flow into single and two-stage turbines. For simplicity, only the cooling-flows for the vanes and blades are considered here. Figure 3.3(a) shows the model of a two-stage turbine. The cooling-flow for the 1st row of nozzle-guiding-vanes (NGVs) will do work on both of the turbine stages; while the cooling-flow for the 2nd row of NGVs only does work on the 2nd stage of the turbine. The cooling flow for the 1st rotor will do work in the 2nd stage of the turbine, while the cooling flow for the 2nd rotor will not produce any useful work across the two-stage turbine.

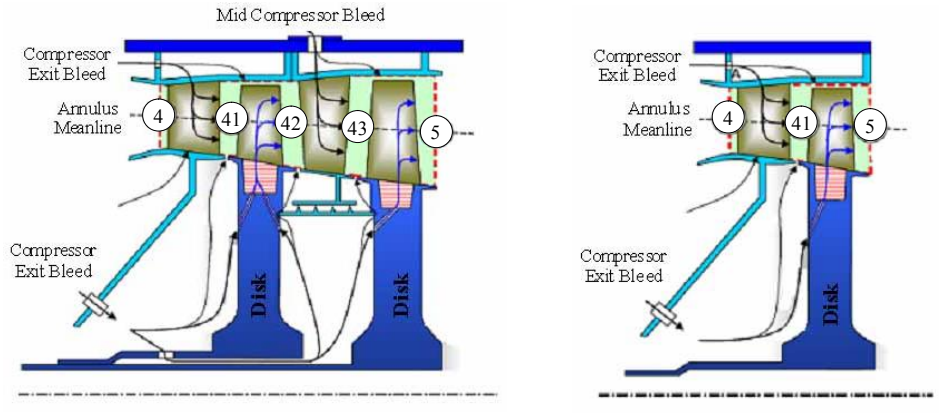

(a) Two-stage turbine (b) Single-stage turbine

Figure 3.2. Schematics of cooling flows for single-stage and two-stage turbines [74].

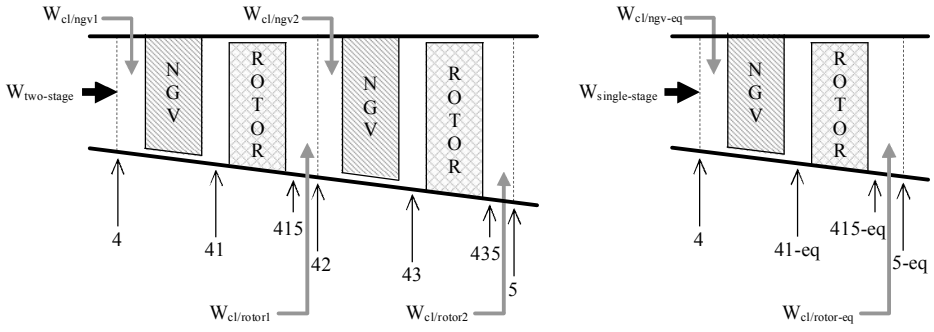

(a) Two-stage turbine (b) Single-stage turbine

Figure 3.3. Schematic of a two-stage turbine and a equivalent single-stage turbine.

Figure 3.4 shows the process of modelling the cooling-flow rate for the equivalent single-stage turbine (see Figure 3.3(b)). Equations (3.5) and (3.6) relate the cooling-flow rate for the two-stage turbine to that for the equivalent single stage turbine. The work-distribution (ξ) describes the ratio of work produces at the 1st stage to that of the whole turbine, which does not change significantly under off-design conditions. This term would enable the calculation of temperature drops across the turbine and thus is used in the prediction of vanes' and rotors' cooling-flow rates. The work-potential (Φ) is adjusted so that the exit

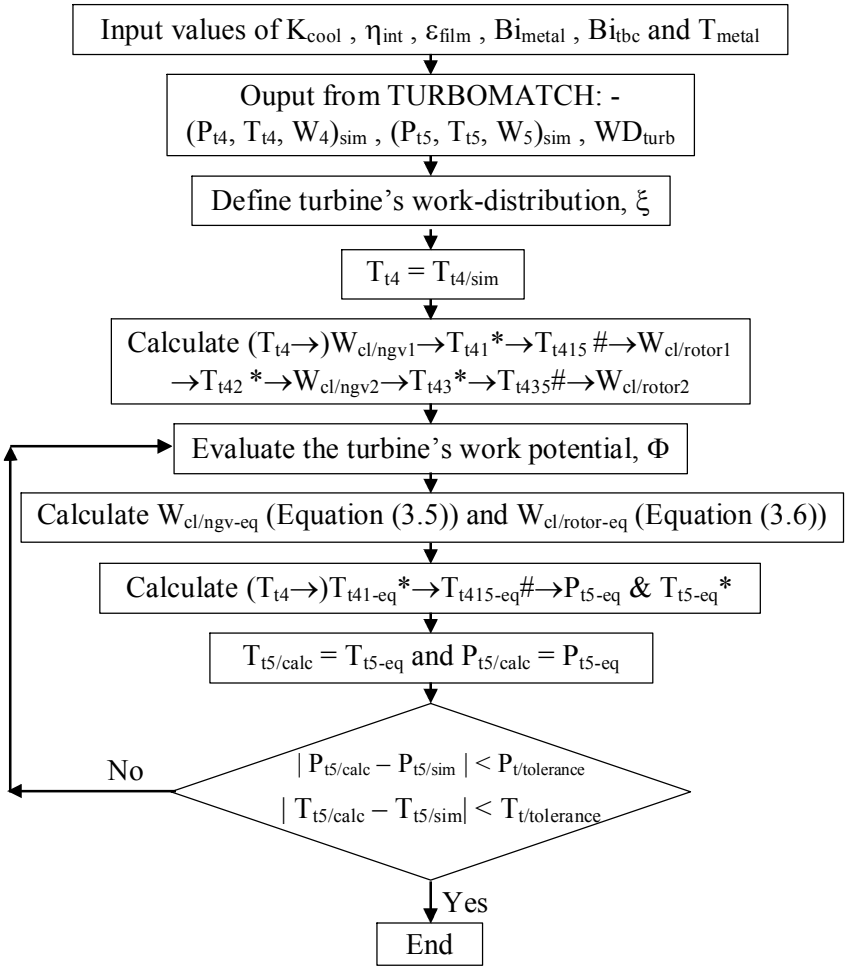

* Calculation based on an energy-balance of the flow

\# Calculation based on an work extraction from the turbine

Figure 3.4. Flow chart for the calculation of the cooling-flow rate in an equivalent single-stage turbine (Refer to Figure 3.3 for station numbers).

pressures and temperatures of the two-stage turbine and the single-stage equivalent turbine are respectively identical. Figure 3.5 shows the flow chart for the engine performance-prediction, incorporating the turbine's cooling-flow rate calculation, for a two-spool engine. Iteration is necessary to ensure that the calculated turbine's cooling-flow rate converged.

$$W_{cl/ngv-eq} = W_{cl/ngv1} + \Phi\left(W_{cl/rotor1} + W_{cl/ngv2}\right) \tag{3.5}$$

$$W_{cl/rotor-eq} = (1-\Phi)\left(W_{cl/rotor1} + W_{cl/ngv2}\right) + W_{cl/rotor2} \tag{3.6}$$

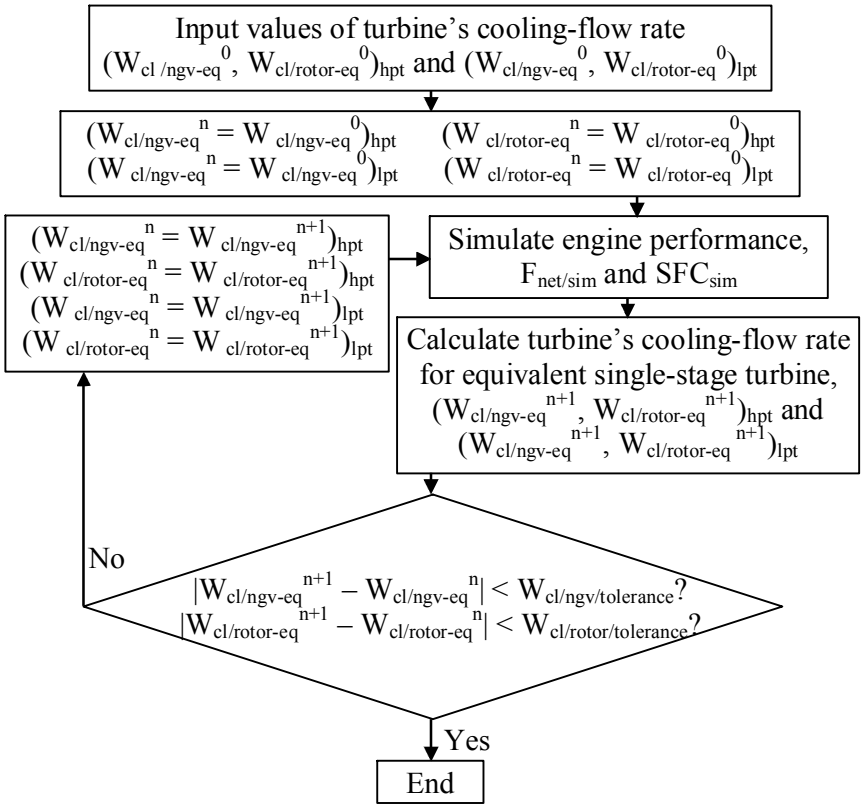

Figure 3.5. Flow chart for the engine performance-prediction taking into consideration the prediction of the cooling-flow rate.

- **Engine's Performance-Parameters**

The primary parameters used to describe the performances of the engines are: -

- ✓ Specific thrust (ST) is the thrust per unit mass-flow (see Equation (3.7)) [69]. A higher specific thrust would mean a higher thrust for a given mass-flow rate or a smaller engine could be developed to produce the required thrust.

$$ST = {F_{net}}/{W} \tag{3.7}$$

- ✓ Specific fuel-consumption rate (SFC) is the fuel-consumption rate needed for the engine to produce per unit of thrust (see Equation (3.8)) [69]. For the same thrust requirement, an engine requiring a lower SFC would have a longer endurance durations when compared with the use of an engine with a higher SFC.

$$SFC = {W_{fuel}}/{F_{net}} \tag{3.8}$$

- ✓ Thermal efficiency (η_{th}) indicates the engine's overall thermodynamic efficiency. It is the ratio of the rate of change in the propellant's kinetic energy to the rate of heat input (see Equation (3.9)) [69].

$$\eta_{th} = \frac{W_J V_J^2 - W_0 V_0^2}{2 W_{fuel} Q_{fuel}} \tag{3.9}$$

- ✓ Propulsive efficiency (η_{prop}) indicates the rate of energy emerging from the engine that is converted to useful power. Propulsive efficiency can be evaluated using Equation (3.10) [69].

$$\eta_{prop} = \frac{2 F_{net} V_0}{W_J V_J^2 - W_0 V_0^2} \tag{3.10}$$

- ✓ The overall efficiency of an engine is the product of its thermal and propulsive efficiencies (see Equation (3.11)) [69]. An increase in the engine's exhaust-velocity (V_J) would raise the thermal efficiency, but decrease the propulsive efficiency. To achieve a high propulsive efficiency, the value of V_J must tend to the engine's inlet velocity (V_0) and hence the

specific thrust will very low. Trade-offs are often necessary in the design of an engine and are chosen according to its application.

$$SFC = fn\left(\frac{1}{\eta_{th}\eta_{prop}}\right) \tag{3.11}$$

3.3.2 Variable Turbine's Cooling-Flow Requirement

The process for calculating the turbine's cooling-flow rate for the engine under specific off-design conditions is identical to that shown in Figure 3.5. Iterations are required by updating the turbine's cooling-flow rate in the simulation model until the calculated turbine's cooling-flow rate between consecutive iterations is within the specified tolerance, i.e. 0.01 kg s^{-1}. The following are assumptions made: -

- ✓ The maximum allowed material temperature is assumed constant, i.e. 1150K.
- ✓ The turbine's cooling-flow temperature is also equal to the compressor's bleed-air temperature, i.e. the effects of pre-swirl and radiant heat-transfer are not considered.
- ✓ The maps of the compressors' and turbines' characteristics are unaffected by the rate of cooling-flow.

3.3.3 Combustor Sizing

The combustor for an aero-engine must have a sufficient volume to ensure the altitude relight capability and also to achieve an acceptable combustion-efficiency over its operating envelope. Altitude relight at the highest altitude and lowest flight Mach-number is one of the critical design-conditions. To size the combustor for altitude relight, the combustor's inlet-flow condition under windmilling is required. The approaches for calculating the combustor's inlet-flow condition under windmilling and sizing of both combustor and afterburner are described below.

- **Calculation of Combustor's Inlet-Flow Condition under Windmilling Conditions**

The two methods, introduced by Walsh and Fletcher [69] and Jone [75], to calculate the combustor's inlet-flow condition under windmilling condition have been evaluated. For easy reference, the two methods are designated as WindMilling-Method-A and WindMilling-Method-B, respectively. The methodology for WindMilling-Method-A is adopted and described here. For completeness, the methodology for WindMilling-Method-B is included in Appendix D. Based on the results from WindMilling-Method-B, the calculated combustor size is appreciably larger than required (see Appendix E).

WindMilling-Method-A [69]

The compressor's pressure-ratio and temperature-ratio under windmilling condition can be estimated using Figure 3.6. The data for the compressor with design-point pressure-ratios of 5:1 and 20:1 are given in reference [69]. The present author, with no other information available, linearly-extrapolated using the available data to estimate the data for compressor at a design-point pressure-ratio of 32.4.

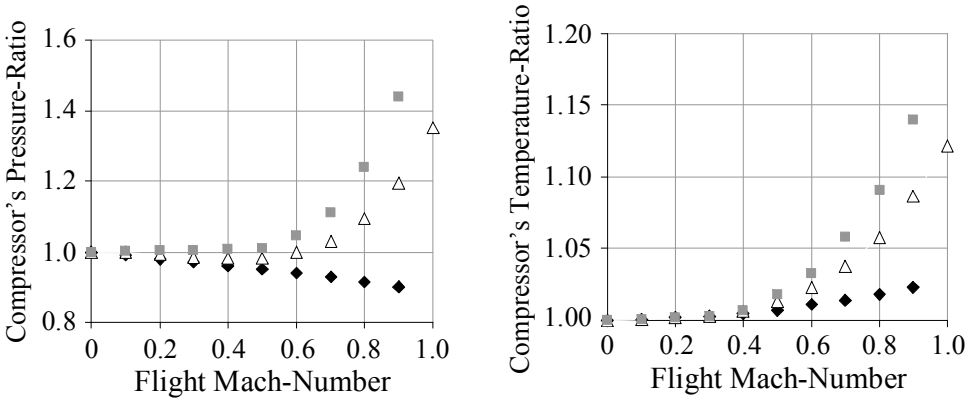

Figure 3.6. Compressor's pressure-ratio and temperature-ratio for the free windmilling condition [◆ PR_{dp}=5:1[69] △ PR_{dp}=20:1[69] ■ PR_{dp}=32.4:1].

The data in Figure 3.6 are for a turbojet under free-windmilling condition. Reference [69] states that the free-windmilling pressure-ratio of a turbofan engine

will be lower than for a turbojet with the same design-point pressure-ratio. Equation (3.12) enables a correction to be made, to first-order accuracy, for a turbofan with the same design-point pressure-ratio as that of the turbojet.

$$\Pi_{wm/TF} = 1 + (\Pi_{wm/TJ} - 1)(1 - 0.08\alpha_{dp}) \tag{3.12}$$

With a known engine's specific-thrust at sea-level static conditions and the free windmilling flight Mach-number, the free windmilling mass-flow function (MFF) can be read off from Figure 3.7 [76]. The engine's mass-flow rate can then be calculated using equations (3.13) and (3.14) [69], whereby subscripts "1" and "2" correspond to the engine's inlet and compressor faces, respectively.

$$W = \frac{MFF * A_2 * P_{t1} * fn(M_0)}{\sqrt{R * T_{t1}}} \tag{3.13}$$

$$fn(M_0) = \frac{M_0\sqrt{\gamma}}{\left(1 + \frac{\gamma - 1}{2} M_0^{\,2}\right)^{\frac{\gamma+1}{2(\gamma-1)}}} \tag{3.14}$$

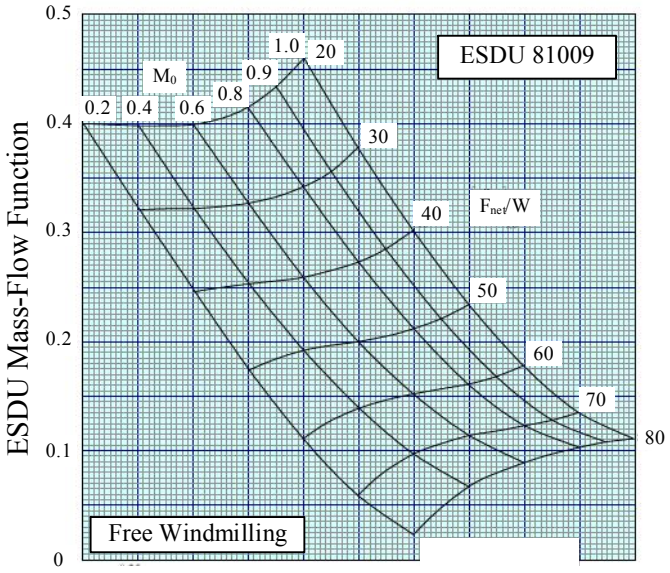

Figure 3.7. Engine inlet's mass-flow function (MFF) for a given engine's specific thrust (at the sea-level static condition) and free windmilling Mach-number [76].

For a turbofan engine with a bypass-ratio equal to five at the design-point condition, its free-windmilling bypass-ratio could be as high as eighty [69]. For first-order accuracy, the free-windmilling bypass-ratio for other design-point bypass-ratios is assumed to vary linearly as shown in equation (3.15).

$$\alpha_{wm} = 16\alpha_{dp} \tag{3.15}$$

- **Sizing of Combustor**

Two methodologies employed for sizing the combustor are designated as CombSizing-Method-A [77] and CombSizing-Method-B [69], which are evaluated using the size of the combustor for the F100-PW229 engine. The combustor size predicted using CombSizing-Method-A is close to that of the F100-PW229 engine's combustor: thus it was used in this study. The methodology for CombSizing-Method-B and the evaluation results are included in Appendices F and G, respectively. CombSizing-Method-A consists of the combustion and pressure-loss approaches: the larger combustor-size obtained from these two approaches is selected.

Combustion Approach [77]

Figure 3.8 shows the variation of η_{comb} with θ_{comb} for the sizing of the combustor. For the same combustor's inlet-flow condition, a large combustor is required to obtain a high θ-value (see Equation (3.16) [77]) so achieving a high combustion efficiency.

$$\theta_{comb} = \frac{P_t^{1.75} A_{comb} D_{comb}^{0.75} \exp\left(T_t/300\right)}{W} \tag{3.16}$$

In this study, an annular combustor is assumed for both the baseline and two-combustor engines. The combustion efficiencies of both the main-combustor and ITB are assumed to be 98% under normal operating conditions. With limited available information, the present author selects a corresponding θ_{comb}-value of 4×10^8 $Pa^{1.75}m^{2.75}kg^{-1}s$ (see Figure 3.8). To ensure that, at altitude, relight can

ensue, then a significantly lower combustion-efficiency (70%→80%) has to be accepted in order to reduce the combustor size: therefore the corresponding θ_{comb}-value of 1.5×10^7 $Pa^{1.75}m^{2.75}kg^{-1}s$ is assumed. Relight only occurs over a short time period. The penalty of a high SFC associated with a low combustion efficiency is acceptable.

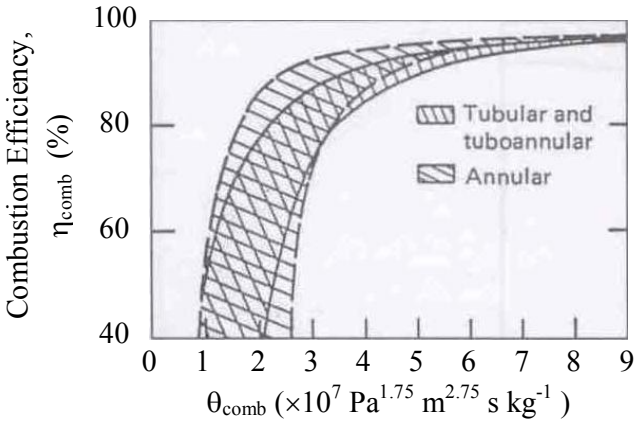

Figure 3.8. Combustion efficiency versus θ [77]

Pressure-Loss Approach [77]

Figure 3.9 shows the chart of combustor pressure-loss versus mass-flow function ($\Delta P_t/P_t$ versus MFF) for the sizing of combustor. For an annular combustor with a 5% pressure loss, the corresponding mass-flow function is ~0.006 (see Figure 3.9).

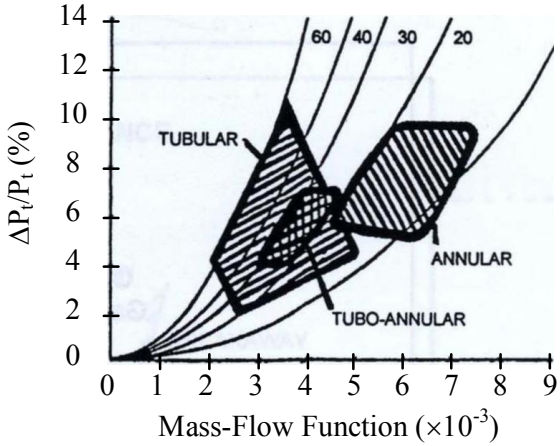

Figure 3.9. Combustion pressure-loss versus combustor inlet mass-flow function [77]

Sizing the Combustor's Length [77]

The depth of the flame-tube ($D_{flametube}$) is 65% of that of the combustor (D_{comb}). The flame-tube can be broken into primary, secondary/intermediate and dilution zones in the axial flow direction. The recommended ratios of lengths (L_{zone}) of the respective zones to the depth of the flame-tube ($D_{flametube}$) are shown in Table 3.2. The entire combustor length also includes the injector and the distance between the diffuser exit and injector (see Figure 3.10). The "length" of the injector (L_{inj}) is estimated to be ~50mm, which is assumed to be invariant. The distance between the diffuser exit and injector is assumed to be of the same magnitude as the depth of the annulus (D_{ann}) (see Figure 3.10).

Table 3.2. Recommended length of flame-tube with respect to its diameter [77].

	$L_{zone}/D_{flametube}$
Primary Zone	0.5
Secondary/Intermediate Zone	0.625
Dilution Zone	1.5→2.0

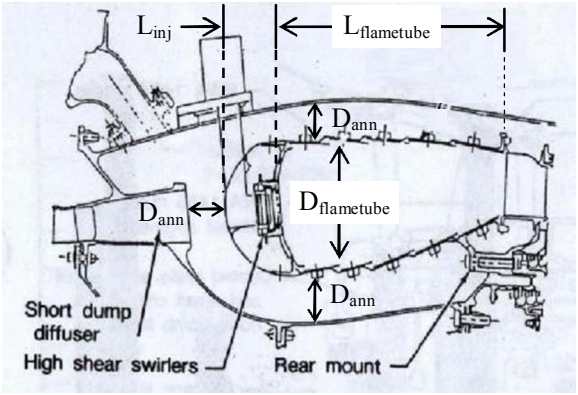

Figure 3.10. Schematic diagram of the F100-PW229 engine's diffuser and main combustor [78].

- **Sizing of Afterburner [77]**

Two methods for sizing the afterburner have been evaluated: Afterburner-Method-A is based on the correlation of the reheat combustion-efficiency and

Afterburner-Method-B is an extension of the loading-approaches (see Appendix F). In the latter method, a loading of lower than 100 kg s^{-1} atm^{-1} m^{-3} is recommended [69], which results in a small combustor size: therefore this method is not adopted here. In the use of Afterburner-Method-A, the θ_{ab}–value is estimated for the required afterburner's combustion efficiency and inlet-flow temperature [77]. With a known afterburner's inlet-flow condition, the afterburner volume ($A_{ab}L_{ab}$) can be calculated (see Equation (3.17)). With the limited relevant data available, interpolation and extrapolation are conducted in order to devise the curves of η_{ab} versus θ_{ab} for various afterburner's inlet temperatures (see Figure 3.11).

$$\theta_{ab} = \frac{P_t^{1.4} A_{ab} L_{ab} \exp(T_t/1000)}{W} \tag{3.17}$$

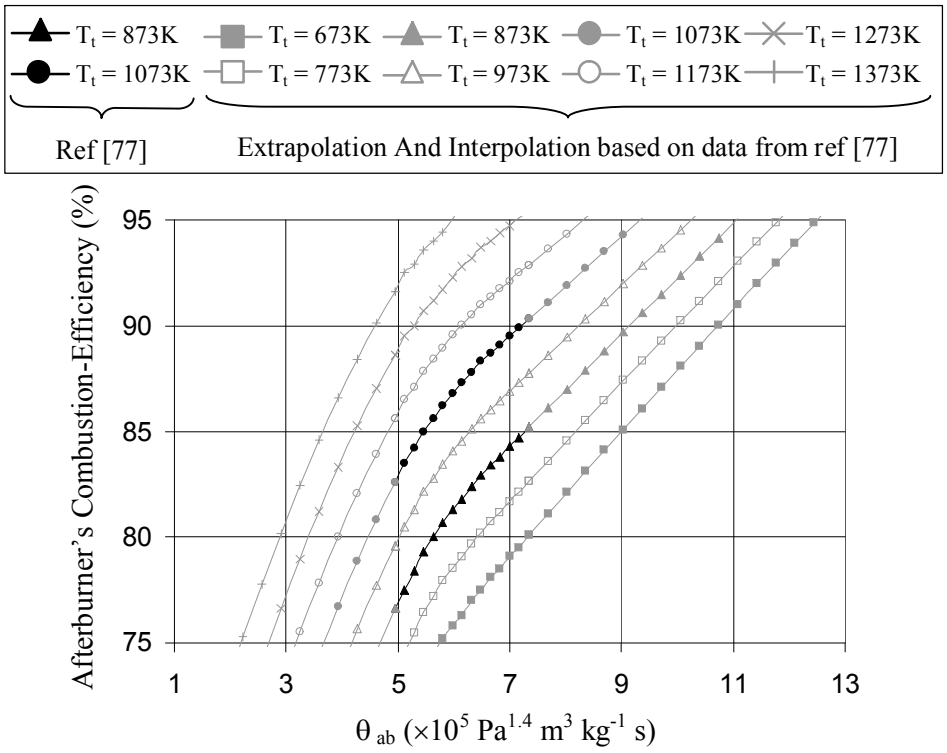

Figure 3.11. Correlation of afterburner's combustion-efficiency versus θ.

3.3.4 Transient-Performance Analysis

There are two common methods for predicting the engine's transient-behaviours, namely the method of Constant Mass-Flow and the Inter-component Volume Method [79]. Both methods are relatively straight-forward, but their implementation would be time consuming and a significant amount of addition data would be required. Therefore, a simpler approach is adopted in this study.

In the transient process, there is a work imbalance between the turbine and compressor (mounted on the same spool). Newton's second law of motion relates the rate-of-change of spool's rotational-speed to this imbalance of work [69, 80] – see Equation (3.18). To account for the effects of the variation in the components' inlet-flow conditions, a corrected version of Equation (3.18) is used - see Equation (3.19) [80].

$$\dot{N} = \frac{\Delta WD}{N \times J \times \left(2\pi/60\right)^2} \tag{3.18}$$

$$\frac{\dot{N}}{\delta} = \frac{\frac{\Delta WD}{\delta\sqrt{\theta}}}{\frac{N}{\sqrt{\theta}} \times J \times \left(2\pi/60\right)^2} \tag{3.19}$$

Figure 3.12 shows the methodology for analyzing the engine's transient-behaviour. The parameters that are commonly used to control the engine are the turbine's entry-temperature (TET) and fuel-flow rate (W_{fuel}): the former is used in this investigation. The TET-schedule is divided into M intervals each with an equal time-step, Δt (see Figure 3.13). The TET-schedule is also assumed to be of a step-function instead of a continuous-function. Another two parameters required are the spool's polar moment of inertia and its rotational speed: these are strongly dependent on the design of and materials for, the engine and its components. Hence exact values for these two parameters are difficult to obtain from the generalized literature in the public domain, and estimations have to be made. It is expected that there will be discrepancies in the estimated values. Nevertheless, by being consistent with respect to both the baseline and two-

combustor engines, such discrepancies should have minimal impact upon the findings of this study.

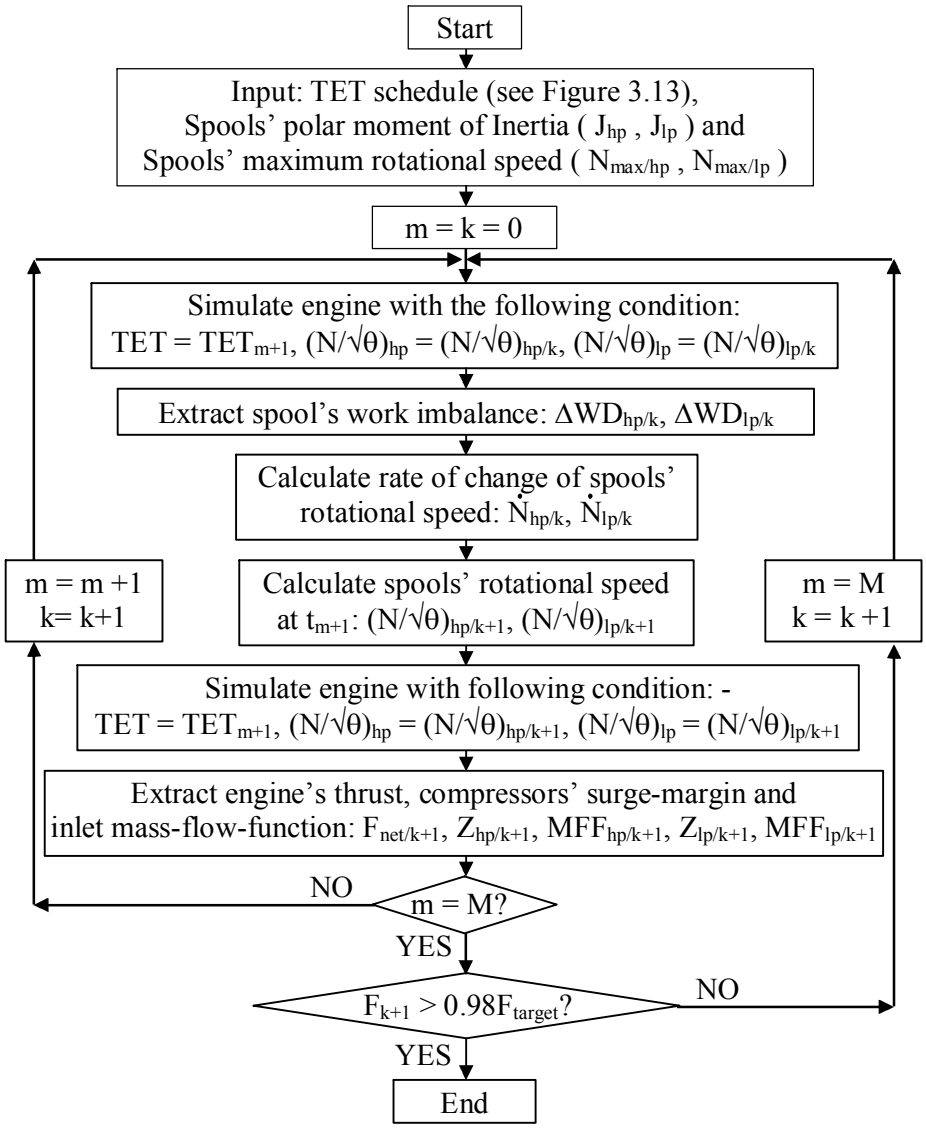

Figure 3.12. Flow chart for engine's transient-performance analysis.

At the beginning of each time-step, the engine operates with an instantaneous change in TET, but no change to the spools' corrected-speed. Hence, there is a work imbalance between the compressor and turbine mounted on the same spool (see Figure 3.14). The rate of change of spool's rotational speed can be calculated using Equation (3.19). The spool's rotational speed, at the end

of each time step, can be calculated using Equation (3.20). With known values for the TET and rotational speed, the engine behaviour at the end of the time step can be simulated (see Figure 3.14).

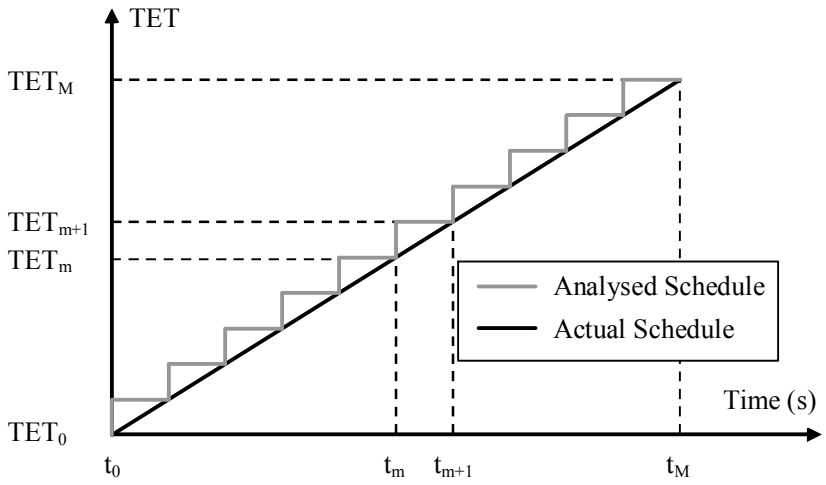

Figure 3.13. Schematic schedule of the engine turbine's entry-temperature.

$$\left(\frac{N}{\delta}\right)_{m+1} = \left(\frac{N}{\delta}\right)_{m} + \left(t_{m+1} - t_{m}\right)\left(\frac{\dot{N}}{\delta}\right) \tag{3.20}$$

Beyond the TET's scheduled time, the calculation of the spool's rotational-speed for each respective time step remains the same, except that the TET remains invariant. The work imbalance will gradually reduce to zero, i.e. the engine reaches its steady-state condition. Nevertheless, the computation will end when a preordained specific criterion has been achieved, e.g. 98% of the targeted spool's rotational-speed [69].

This method is simple: it does not include the influences of time-dependent factors, such as heat soakage, tip clearance, volume dynamics and delays in the combustion and control processes. Although there are these limitations in this approach, it is nevertheless sufficient to provide a preliminary assessment on the transient performance of the two-combustor engine relative to that of the baseline (i.e. conventional) engine.

The main equation (see equation (3.19)) in this approach is identical to that used in GasTurb [80]. As the GasTurb manual does not describe the complete methodology for the transient-performance prediction, the present author is uncertain if the proposed methodology is identical to that coded in GasTurb.

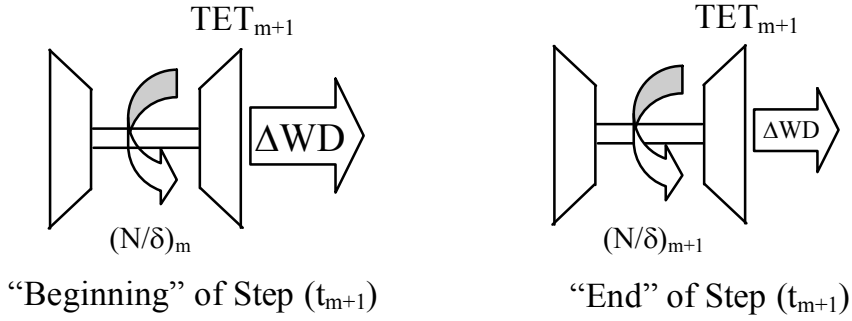

Figure 3.14. Schematic of the spool's behaviour at the beginning and end of each respective time-step.

- **Spools' Polar Moment of Inertia**

The spools are assumed to be constructed of several cylindrical parts. The dimensions are estimated from the diagram in Figure 3.15. Typical materials for the respective parts are assumed. Using Equation (3.21), the polar moment of inertia of the spools can be calculated. The estimated polar moments of inertia for the low-pressure (LP) and high-pressure (HP) spools of the F100-EQ engine are 2.2 kg m^2 and 3.0 kg m^2, respectively. Although the HP spool is shorter, there are more compressor stages and so result in a higher polar moment of inertia when compared with that for the LP spool. For the two-combustor engine with longer LP spool, a polar moment of inertia of 2.4 kg m^2 is assumed.

$$J = \Sigma m\left(\frac{R_o^2}{2} - \frac{R_i^2}{2}\right) \tag{3.21}$$

- **Spools' Maximum Rotational Speed**

The maximum rotational speeds of the LP and HP spools of the F100-PW220 engine are 10,400 RPM and 13,450 RPM, respectively [81]. Without

exact information concerning the F100-PW229 engine, the author assumed that the F100-EQ engine has LP and HP spools' maximum rotation speed of 11,000 RPM and 14,000 RPM, respectively.

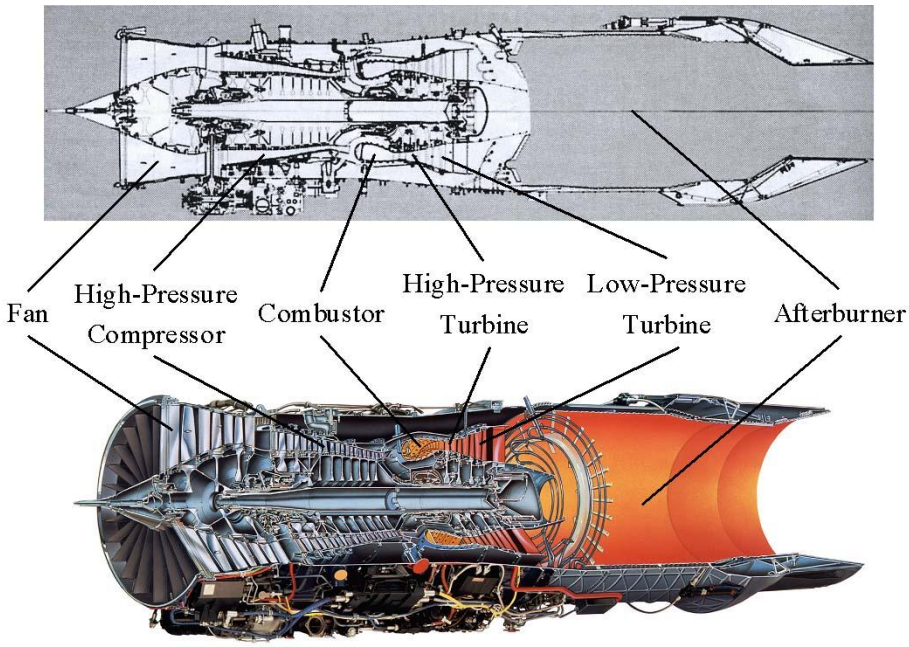

Figure 3.15. Sectional view of the F100-PW229 engine [81, 82].

3.3.5 Infrared-Signature Prediction

The propulsion system is the main source of the aircraft's infrared-signature when viewed from the aft and side of aircraft [14, 17-20]. In this study, the infrared-signatures from the engine's exhaust-cavity (i.e. turbine, tail-pipe and exhaust-nozzle) and the exhaust-plume are calculated and analyzed.

Computation programs are available to calculate the infrared-energy of an object with high accuracy. However, such programs are unavailable at relatively affordable cost. Theoretically, users could implement a prediction-code based on the fundamental radiation equations [17]. However, the process is time consuming and validation is difficult without experiment data. Empirical equations are available for user to make a quick estimation of the infrared-energy

of an object [12, 14, 83]. However, the results calculated using empirical approaches are expected to be of low accuracy.

The objective here is to investigate the infrared signature of the two-combustor engine relative to that of the baseline (i.e. conventional) engine. Therefore, given the considerations concerning the availability of an infrared-signature prediction code, the author chose the simple approach for calculating the infrared energies of the engine's exhaust-cavity and exhaust-plume using empirical equations.

- **Engine Exhaust-Cavity**

Figure 3.16 shows a typical engine tail-pipe with a convergent-divergent (CD) nozzle. The infrared detector is shown at angle, θ, with respect to the nozzle centreline. For the ratio of tail-pipe's length-to-radius ($L_{exh\text{-}sys}/R_{noz\text{-}throat}$) that falls in the range of three to eight, the nozzle could be treated as a blackbody-type source. Conservatively, the entire exhaust-cavity is assumed to be a thermally grey body (i.e. a continuum radiator whereby it emits radiation across the whole bandwidth) with an effective emissivity of 0.9 [83]. The radiance of the exhaust cavity can be calculated using equation (3.22) provided the total temperature at the nozzle's exit is known. With a known value for the nozzle's exit area, the radiant-intensity of the exhaust-cavity can be calculated using equation (3.23) [12].

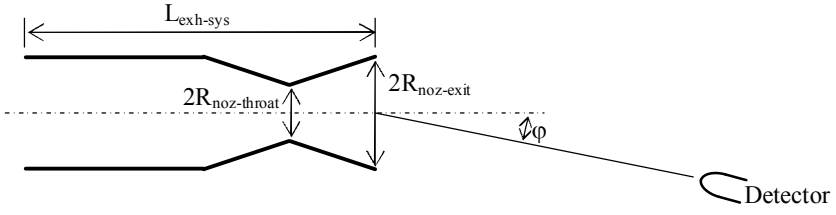

Figure 3.16. Sketch of engine's tail-pipe and convergent-divergent nozzle.

$$N = \frac{\varepsilon_e \sigma T_t^4 \cos\varphi}{\pi} \tag{3.22}$$

$$J = N\pi R_{noz-exit}^2 \tag{3.23}$$

Attenuation of the transmission of the infrared energy occurs due to absorption of the energy by the various gases in the atmosphere, i.e. mainly carbon dioxide (CO_2) and water vapour (H_2O). Generally, there are three wavebands (also known as windows) throughout which attenuation is minimal (see Figure 3.17), namely 1-3μm, 3-5μm and 8-14μm [14, 16]. According to reference [14], there is no official standard for the wavebands for the respective windows.

The spectral radiance of the target can be calculated using Planck's Law (see equation (3.24)). In order to calculate the radiance and radiant-intensity of a target over a selected waveband, the σT^4 term in equation (3.22) is replaced by equations (3.24) and (3.25) [14].

$$M_\lambda = \frac{\varepsilon_\lambda B_1}{\lambda^5 \left\{ \exp\left[B_2 \Big/ (\lambda T_t) \right] - 1 \right\}} \tag{3.24}$$

$$M(\lambda_1 \le \lambda \le \lambda_2) = \int_{\lambda_1}^{\lambda_2} M_\lambda d\lambda \tag{3.25}$$

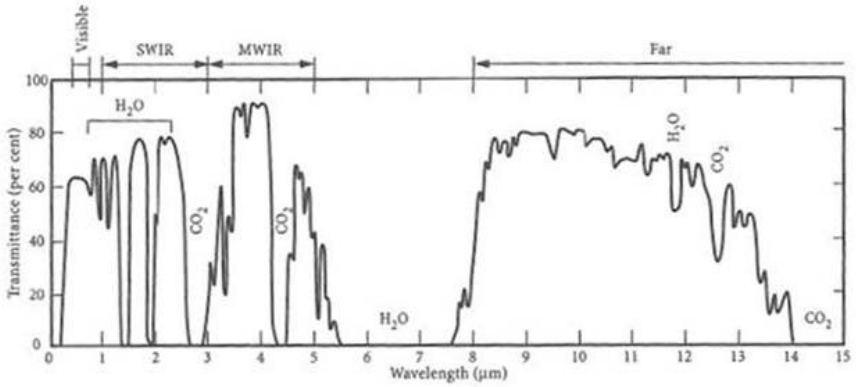

Figure 3.17. Atmospheric attenuation of infrared signature [14].

- **Exhaust Plume**

Most of the plume's infrared-energy is caused by presence of the CO_2 at the wavelengths of ~2.7μm and ~4.3μm; therefore this source of infrared radiation is known as line radiator [14]. The intensity of the radiation at a wavelength of

~2.7μm is significantly lower than that for the ~4.3μm wavelength radiation [14]; thus only the latter is considered here. The radiation from the plume's CO_2 experiences higher absorption at the same wavelengths (i.e. ~2.7μm and ~4.3μm) as it propagates through the atmosphere (see Figure 3.18). The radiations at the wavelengths correspond to the two-peaks (see Figure 3.18) are not absorbed during the propagation of the infrared energy. "Equivalent" radiations over the wavelengths from 4.10μm→4.15μm and from 4.45μm→4.55μm are arbitrarily selected for this study.

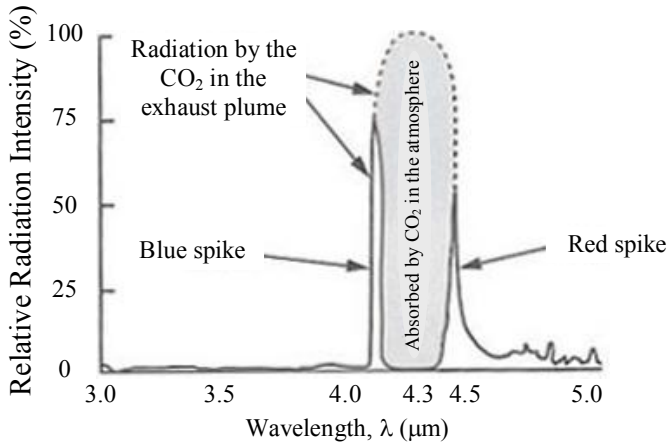

Figure 3.18. The radiation, from the exhaust plume at a wavelength of 4.3mm, absorption by atmosphere [14].

To calculate the exhaust-plume's radiant-intensity, reference [12] suggests that the plume can be modelled as a solid cone geometry with uniform surface temperature and emissivity. If the exhaust is subsonic, the gases' static temperature is used; whereas if the exhaust is supersonic with diamond-shock, the gases' stagnation temperature is used. There is ambiguity concerning the selection of the value of the plume's temperature when the exhaust flow consists of weak shocks. Reference [83] suggests the temperature of the plume for calculating its radiance can be obtained from Equation (3.26). Also, effective emissivities of 0.5 and 0.8 are assumed for the plume's temperatures of 643K and 1804K, respectively [83].

$$T_{t/plume} = 0.85 T_{t/noz-exit} \tag{3.26}$$

The present author proposes to use the computational fluid dynamics (CFD) software, FLUENT, to simulate the extent of the exhaust plume. The boundary contour for the total temperature, corresponding to that calculated using Equation (3.26), will be identified. Assuming the plume to be conical in shape, the plume's radiant-intensity can be calculated as stated in reference [12].

3.3.6 Aircraft's Performance-Analysis

Approaches to the prediction of the aircraft's flight-envelope, calculation of the aircraft's rate-of turn and SFC under specific flight conditions are described here. In addition to the engine's performance data, the aircraft's drag versus lift (i.e. drag-polar, C_L versus C_D) and weight characteristics are required. The method for predicting the drag-polar and weight characteristic, of selected aircraft configuration, are presented. Technically, the conduct of a mission analysis for the selected aircraft configuration should reflect more accurately the potential of the two-combustor engine. However, due to both commercial and military confidentiality constraints, there is insufficient exact data to conduct a fruitful mission-analysis here. Nevertheless, the findings from the present investigation will provide adequate preliminary results to ascertain the potential of the two-combustor engine.

- **F16-EQ Aircraft's Drag-polar**

The relationship of the aircraft's lift coefficient (C_L) to drag coefficient (C_D) is known as its drag polar, which can be described by Equation (3.27) [84]. In this thesis, the F16 Falcon and generic fighter aircraft's drag-polars available in the public domain [84, 85] are surveyed, tabulated and compared (see Appendix H). It is commonly accepted that test-data are more reliable: thus interpolations and extrapolations have to be conducted, based on data from reference [84], in order to tabulated the parasitic drag (C_{Do}) and drag-due-to-lift (k_1 and k_2) for the F16-EQ aircraft (see Table 3.3).

$$C_D = C_{Do} + k_1 C_L^2 + k_2 C_L \tag{3.27}$$

Table 3.3. The parasitic drag (C_{Do}) and drag-due-to-lift factors (k_1 and k_2) for the F16-EQ aircraft.

M_0	C_{Do}	k_1	k_2
0.2	0.01835	0.1170	-0.0070
0.4	0.01835	0.1166	-0.0065
0.6	0.01835	0.1159	-0.0054
0.8	0.01835	0.1152	-0.0043
0.86	0.01835	0.1150	-0.0040
0.9	0.01900	0.1245	-0.0034
0.95	0.02900	0.1363	-0.0026
1	0.04080	0.1482	-0.0018

M_0	C_{Do}	k_1	k_2
1.05	0.04380	0.1600	-0.0010
1.1	0.04360	0.1733	-0.0009
1.15	0.04300	0.1867	-0.0008
1.2	0.04280	0.2000	-0.0007
1.4	0.04280	0.2533	-0.0002
1.6	0.04280	0.2980	0.0000
1.8	0.04280	0.3340	0.0000
2	0.04280	0.3700	0.0000

The values of C_{Do}, k_1 and k_2 are for F16-EQ with Aim-9 missiles mounted on the wing-tips, is subsequently referred to as the F16-EQ "clean" configuration. For the F16-EQ configuration with extra externally mounted weapon-systems, the additional parasitic drag must be estimated and added to that of the "clean" configuration. Figure 3.19 shows the ratio of drag to dynamic-pressure (also known as the drag-area, D/q) of a typical weapon-system and its suspension. Depending on the mounting position relative to the aircraft, a correction factor (Q) is employed to account for interference effects (see Table 3.4) [86]. The parasitic drag of the considered F16-EQ configurations can be calculated using equation (3.28).

Table 3.4. Interference correction factor [86].

Position of Stores	**Q values**
Directly mounted	1.5
Mounted at < 0.5 diameter	1.3
Mounted at > 0.5 diameter	1.0

$$C_{Do} = C_{D/clean-cfg} + \sum\left(\frac{D}{q}\frac{Q}{S_{ref}}\right) \tag{3.28}$$

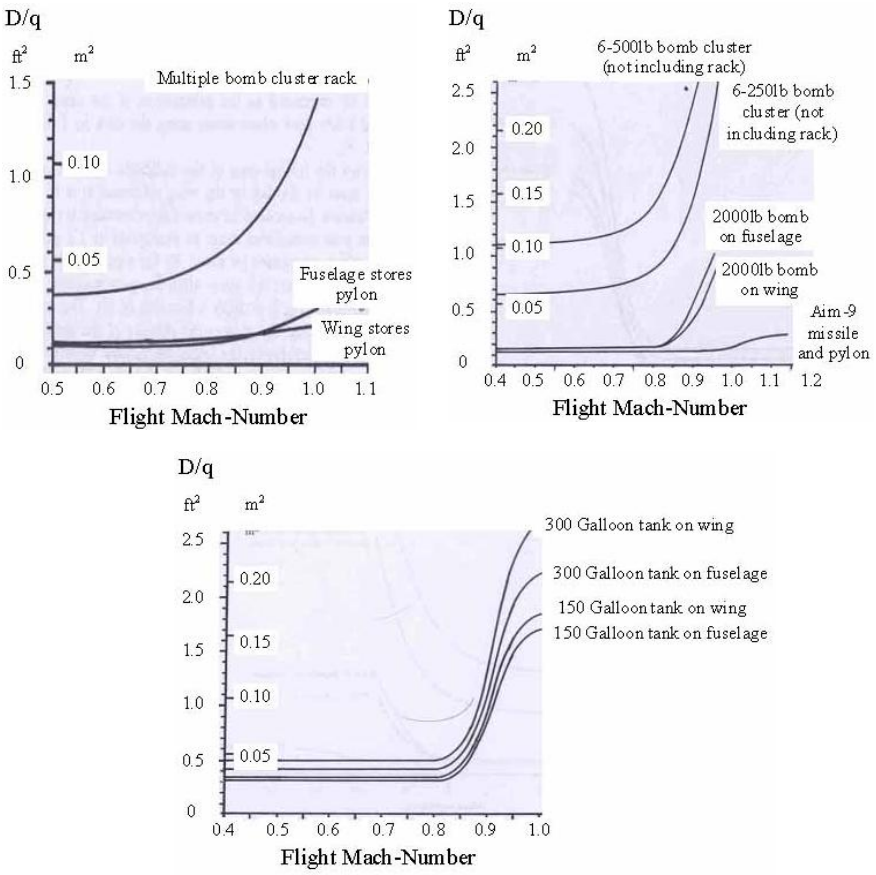

Figure 3.19. Drag-area curves for selected stores and suspensions/pylon [86].

Based on the Oswald Span Efficiency Method, the k_1 value is independent of aircraft configurations (see equations (3.29) and (3.30)). The influence of the k_2 value, on the tabulated drag polar, is minimal (see Figure 3.20). With limited available data and also based on the previous arguments, the author has assumed that the k_1 and k_2 values remain invariant for the various F16-EQ aircraft configuration.

In reality, the control surfaces are adjusted to trim (i.e. the drag equal to the thrust and lift equal to weight) the aircraft during the flight; thus the aircraft's drag-polar will be altered. In addition, the drag-polar also varies with the change

in the flight altitude. Due to the lack of precise data and prediction tools, the above two influential factors are also not take into consideration in the present analysis, i.e. the tabulation of the F16-EQ aircraft drag-polar is assumed to be dependent on the configuration and the flight Mach-number only.

Subsonic & Transonic $k_1 = \frac{1}{\pi e AR}$

$$e = 4.61\left(1 - 0.045AR^{0.68}\right)\left(\cos\Lambda_{LE}\right)^{0.15} - 3.1 \tag{3.29}$$

Supersonic

$$k_1 = \frac{AR\left(M_0^2 - 1\right)\cos\Lambda_{LE}}{4AR\sqrt{M_0^2 - 1} - 2} \tag{3.30}$$

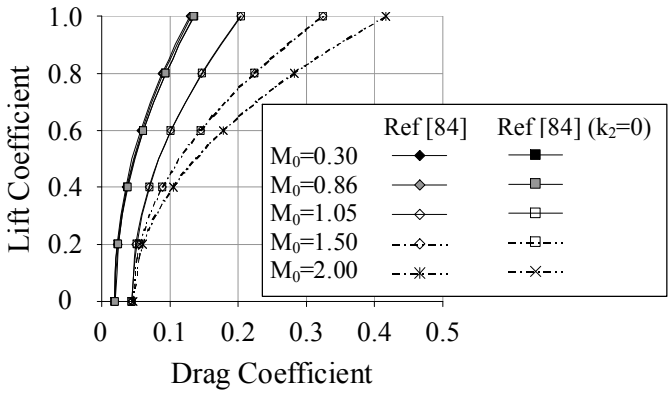

Figure 3.20. The effects of k_2 on the tabulation of drag polar for the F16-EQ aircraft "clean" configuration.

- **Weight of the F16 Falcon Aircraft and Associated Stores**

Table 3.5 shows the weights of F16 Falcon aircraft and various weapon systems [87-91]. In the literature, it is not clear whether the stated weight of the weapon system included the weight of the suspensions and/or pylons. Conservatively, the author assumed that the weight of the suspension and pylon is 20% of that of the respective weapon system. For the fuel tank, there is both the fuel weight and the weight of the empty tank. To calculate the weight of the fuel, a typical fuel density of 800kg/m^3 is assumed. The ratio of weight of the fuel to

that of the empty tank is calculated for the conformal fuel-tank (CFT) [87, 91]: the weight ratio is used to tabulate the weight of the empty tank for the 300G and 370G tanks.

It is not surprising that there are differences in the weight of the F16 listed in the various references. Partially, it is because the respective authors might not be able to assess the official aircraft data. In addition, there could discrepancies in the definition for the corresponding configurations for the "empty" weight and maximum take-off (T/O) weight. Therefore without knowing the exact configuration, it is impossible to give error limits for the weights of the aircraft and components in Table 3.5. For the purpose of this study, the empty weight of the F16 "clean" configuration and the total internal fuel are assumed to be 8910kg and 3228kg, respectively.

Table 3.5. Tabulation of weight of the F16 aircraft and its weight-systems.

	Reference				**Estimated Value**
	[87]	**[88]**	**[89]**	**[90]**	
F16 Empty Weight (kg)	8910	8670	8495	-	-
F16 Max T/O Weight (kg)	12723	19200	19185	-	-
Internal Fuel (kg)	3228	-	3250	-	-
300G Tank (Empty) (kg)	-	-	-	-	299
300G Tank (Fuel) (kg)	-	-	-	-	908
370G Tank (Empty) (kg)	-	-	-	-	368
370G Tank (Fuel) (kg)	-	-	-	-	1120
CFT (Empty) (kg)	-	-	-	-	224 [87]
CFT (Fuel) (kg)	-	-	-	-	681 [91]
Aim-9 Sidewinder (kg)	-	-	-	76	-
Aim-7 Sparrow (kg)	-	-	-	227	-

3.3.7 Operating Envelope Prediction

Figure 3.21 shows the operating envelope of a typical fighter-aircraft. The aircraft envelopes shown are for zero rate-of-climb (i.e. Ps=0) with the engine operating at either maximum dry (military thrust) or wet (maximum thrust)

conditions. These envelopes are dictated by three primary-factors: the aircraft's stall-limit, the structural-limit and the engine's capabilities. The drag and weight characteristics of the aircraft will also affect its achievable envelope.

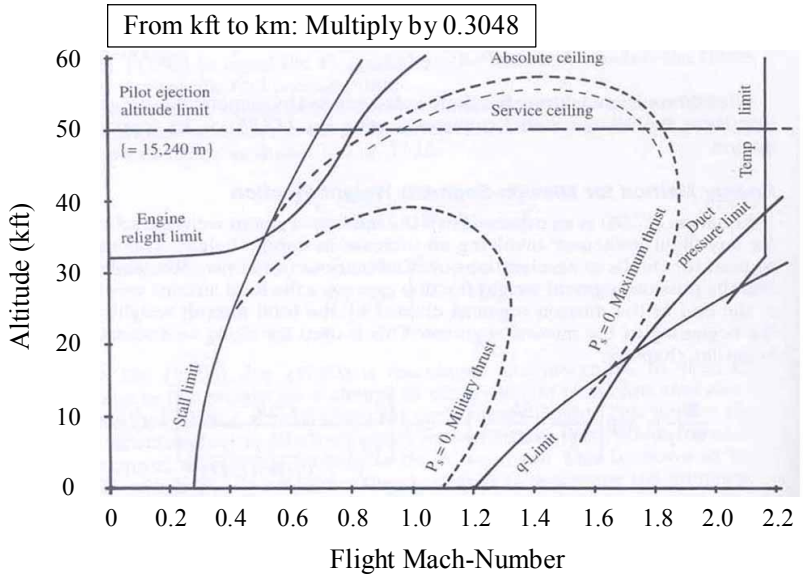

Figure 3.21. Operating envelope of typical fighter [86].

The author is unable to acquire the F16's stall-limits and its upper flight Mach-number limiting characteristics. Therefore it is assumed that the F16-EQ's stall-limit is at an equivalent airspeed of 110 knots [69]. In this analysis, the main concern is on the effects of the engine on the operating envelope at dry-thrust (military thrust) conditions. Therefore the author further assumes the engine performance is the limiting influential factor with respect to the aircraft's maximum achievable flight Mach-number.

Figure 3.22 shows the forces acting on an F16 aircraft under its flight condition. For a given configuration to stay airborne, the aircraft's angle-of-attack (AoA) is higher at low flight Mach-numbers than that at higher flight Mach-numbers. To be precise, the engine's thrust needs to be resolved into components along and perpendicular to the flight direction based on the flight's AoA. However, the data for the F16's lift versus AoA relation is not available. Therefore, the thrust is assumed to be acting purely in the flight direction. The

uncertainty due to this assumption has a higher impact at a lower flight Mach-number than at a higher flight Mach-number. Since the lowest boundary of the flight envelope is mainly governed by the aircraft's stall-limit, the above assumption would have minimal impact on the conclusions of the present study.

Equation (3.31) enables one to calculate the aircraft's rate-of-climb [86]: the aircraft's rate-of-climb is positive if the engine's thrust exceeds the aircraft's drag. At each flight altitude, there is a range of flight Mach-numbers at which the aircraft's rate-of-climb is greater than or equal to zero. Tabulating the range of flight Mach-numbers for a specific range of flight altitude will provide the operating envelope for that aircraft.

$$\dot{H} = V\left(F_{net} - D\right)/Wt \tag{3.31}$$

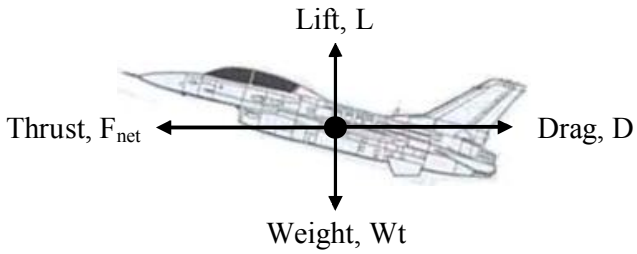

Figure 3.22. Forces acting on an aircraft in flight.

- **The Aircraft's Rate-of-Turn**

Figure 3.23 shows a sketch illustrating the turning of an aircraft and the lift force acting on the aircraft. Equations (3.32) and (3.33) are used to compute the aircraft's load-factor and rate-of-turn, respectively [86].

$$n = \left(F_{net}/Wt\right)\left(L/D\right) \tag{3.32}$$

$$\dot{\psi} = g\sqrt{n^2 - 1}/V \tag{3.33}$$

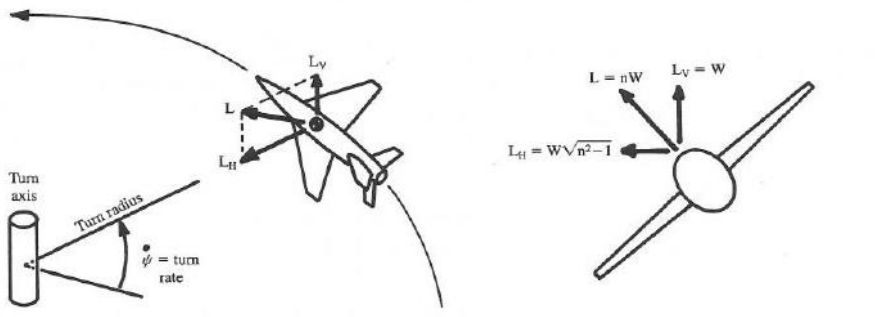

Figure 3.23. Sketch illustrating the aircraft's level rate-of-turn [86].

- **Assumptions and Limitations**

The engine's control-parameter in this analysis is the TETs. The engine is a complex system: the characteristics of the various components could become the limiters to the engine's maximum achievable thrust at off-design condition. In this analysis, the engine's TET is kept at its respective maximum value with the components' (e.g. the fan) operating envelope as its limiter.

In addition, the author does not have the schedule of the afterburner temperature at off-design condition. In general, the engine's mass-flow rate reduces with increase in altitude. Therefore, it is probably necessary to reduce the afterburner temperature with altitude to give the afterburner a reasonable life-span. Hence the author makes the assumptions that the afterburner temperature reduces at the rate of 50K per 10kft (i.e. 3.048km) increase in flight altitude.

3.4 Conclusions

The analytical approaches to the investigation on the potential of a two-combustor engine for military fighter applications has been finalized; whereby the research topic is sub-divided into various areas of interests. The analytical tools to be used for the wide range of analyses have been identified. In addition, assumptions are made in areas in which the required data and/or information are lacking.

Chapter 4. Review of Knowledge Pertinent to Two-combustor Engines

4.1 Introduction

In a two-combustor engine, the combustion in the inter-stage turbine burner (i.e. ITB) occurs in a lower-pressure environment; therefore the two-combustor engine is expected to have lower cycle-efficiency. However, Liew et al [35-39] and Vogeler [40] have reported that the two-combustor engine can achieve a higher specific thrust at lower specific fuel-consumption rates (SFCs) than that of the baseline (i.e. conventional) engine. Also, there are inconsistent trends in the publications – see Section 2.7. The "unexpected" findings and the inconsistency predictions have been investigated by the present author, and the reasons for the discrepancies are discussed. For this, the engine performance-prediction methodologies adopted by both Liew et al and Vogeler have been studied.

4.2 Liew et al's Publications

The engine performance-prediction methodologies, introduced in references [46] and [92], were developed for a conventional engine. Liew et al [34-39] extended the methodologies to predict the performances of both the baseline (i.e. conventional) and two-combustor engines. Liew et al had also incorporated two gas-properties models, namely the "Constant Specific-Heat" (CSH) and "Modified Specific-Heat" (MSH) models, in the engine's performance-prediction. However, the effects of the gas-properties model on the engine's performance were not addressed.

The present author has further incorporated the "Improved Specific Heat" (ISH) model into the engine performance-prediction. The effects of the selected gas-properties model on the engines' performances are illustrated for a baseline (i.e. conventional) engine (CE) and a two-combustor engine (TCE): thereby the reasons behind Liew et al's "unexpected" findings and inconsistency predictions are revealed.

4.2.1 Engine Performance-Prediction Methodology

The modelling of the thermodynamics of the gas properties using the ISH model is more comprehensive than those achieved with the CSH and MSH models. Therefore the methodology formatted for the ISH model has been applied for the CSH and MSH models; the methodology being elaborated in Appendices I to L.

4.2.2 Engine Configurations

Figure 4.1 shows schematically the layout of the two-combustor separate-exhaust turbofan engine, where the ITB is installed between the high-pressure and low-pressure turbines (HPT and LPT). The same layout is applicable to the baseline engine; whereby the gas properties at Station 7 are identical to those at Station 6 in the absence of the ITB.

The design-point conditions of both the baseline and two-combustor separate-exhaust turbofan engines are shown in Table 4.1. The low-pressure turbine's entry-temperature (LPTET) is an additional design-point parameter for the two-combustor engine. The components' pressure-ratios and efficiencies, common to both engines, are shown in Table 4.2.

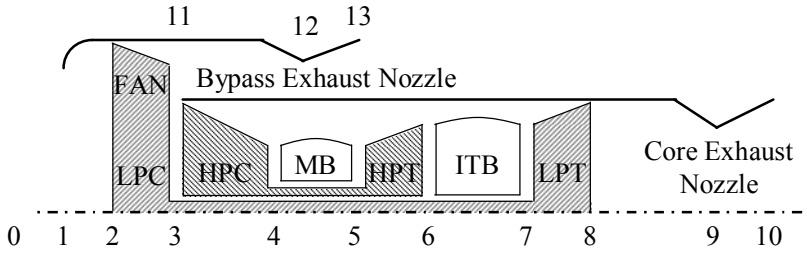

Figure 4.1. Schematic representations of the two-spool separate-exhaust two-combustor turbofan engine with station numbers indicating the locations at which measurements are taken.

Table 4.1. Engines' design-point conditions.

Parameters	**Baseline Engine**	**Two-combustor Engine**
Flight altitude, H (km)	0	0
Flight Mach-number, M_0	0	0
Fan's pressure-ratio, FPR	2.43	2.43
Overall pressure-ratio, OPR	20.0	20.0
Bypass ratio, BPR	0.73	0.73
Mass-flow rate, W (kg s^{-1})	118	118
HPT's entry-temperature, HPTET (K)	1450	1450
LPT's entry-temperature, LPTET (K)	N.A.	1350

Table 4.2. Engine components' design-parameters.

Parameter	**Value**
Total pressure-ratios	
Inlet, $\prod_{diff\text{-}max}$	0.99
Main burner, $\prod_{mb}$	0.95
ITB, $\prod_{itb}$	0.95
Nozzle, $\prod_{noz}$	0.99
Fan nozzle, $\prod_{fan\text{-}noz}$	0.98
Efficiencies	
Main burner, η_{mb}	0.99
ITB, η_{itb}	0.99
HP spool, $\eta_{mech/hp}$	0.92
LP spool, $\eta_{mech/lp}$	0.93

Parameter	**Value**
Polytropic efficiencies	
Fan, $\eta_{poly/fan}$	0.93
LPC, $\eta_{poly/lpc}$	0.8738
HPC, $\eta_{poly/hpc}$	0.9085
HPT, $\eta_{poly/hpt}$	0.8999
LPT, $\eta_{poly/lpt}$	0.9204
Fuel's low heating-value, Q_{fuel} (kJ kg^{-1})	43124

4.2.3 Gas-Properties Models

- **Constant specific-heat (CSH) model [39]**

The flows of both air and combustion gases through the engine are modelled as though they behaved as perfect gases. Three sets of gas properties are calculated and the assignments of the gas properties are as follows: -

- ✓ Cp_0, R_0 and γ_0, are computed based on the engine's inlet-temperature. The flow, upstream of the main-combustor exit, is assigned this set of constant values.
- ✓ Cp_{mb}, R_{mb} and γ_{mb}, are functions of the temperature and fuel-air-ratio at the main-combustor exit, the gas flow from which to the ITB exit has constant values of Cp_{mb}, R_{mb} and γ_{mb}.
- ✓ Cp_{itb}, R_{itb} and γ_{itb} are function of the temperature and fuel-air-ratio at the ITB's exit. Thereafter, constant values of Cp_{itb}, R_{itb} and γ_{itb} are used here.

Based on the calculated gas properties, the fuel-air-ratios of the main combustor and ITB are computed using Equations (4.1) and (4.2), respectively (please refer to Figure 4.1 for the respective stations number). When the ITB is turned-off, the gas properties downstream of the main-combustor exit will assume the same values as those of the exit (i.e. Cp_{mb}, R_{mb} and γ_{mb}). This assumption also applies in the prediction of the behaviour of the conventional engine.

$$FAR_{mb} = \frac{Cp_5 T_{t5} - Cp_4 T_{t4}}{Q_{fuel}\eta_{mb} - Cp_5 T_{t5}} \tag{4.1}$$

$$FAR_{itb} = \frac{Cp_7 T_{t7} - Cp_6 T_{t6}}{Q_{fuel}\eta_{itb} - Cp_7 T_{t7}} \tag{4.2}$$

- **Modified constant specific-heat (MSH) model [39]**

The modelling of the engine's performance is identical to that for the CSH model, except for the calculation of the combustors' fuel-air-ratios. In the MSH model, the gas properties at the combustors' inlets are calculated based on their inlet temperatures and fuel-air-ratios. The values of these gas properties are used in the calculation of fuel-air-ratio, but not directly in the prediction of the engine's overall-performance.

- **Improved constant specific-heat (ISH) model**

The flow in the engine is assumed to behave like perfect gas. Also, the gas properties at the respective components' inlets are calculated and used in the prediction of the engine's performance. The flows through the components, except for the combustor, are assumed to have the same values of the gas properties as at their inlets. For the combustors, the gas properties at its inlet and outlet are calculated and used to calculate the fuel-air-ratio using Equations 4.1 and 4.2.

This ISH model differs slightly from the "Variable Specific-Heat" (VSH) model [46, 92]. The latter calculates the gas properties at both the inlet and exit of each component, whereas the ISH model assumes each component, except the combustors, operates with same values of gas properties as at its inlet.

4.2.4 Validation of the Engine's Performance-Simulation Program

The reproduced engine-behaviour simulation program, based on the CSH model, was validated using results from reference [38]. Figure 4.2 shows that the predictions matched closely with the validation data and thus demonstrates the reliability of the reproduced program. The slight discrepancies, especially with respect to the thermal efficiencies, could be due to the following: -

- ✓ The approaches for calculating the values of both γ and R may be different.
- ✓ The possible errors incurred during the extraction of data from reference [38].
- ✓ The thermal efficiency is sensitive to the prediction accuracies for the engine's inlet and exhaust velocities.

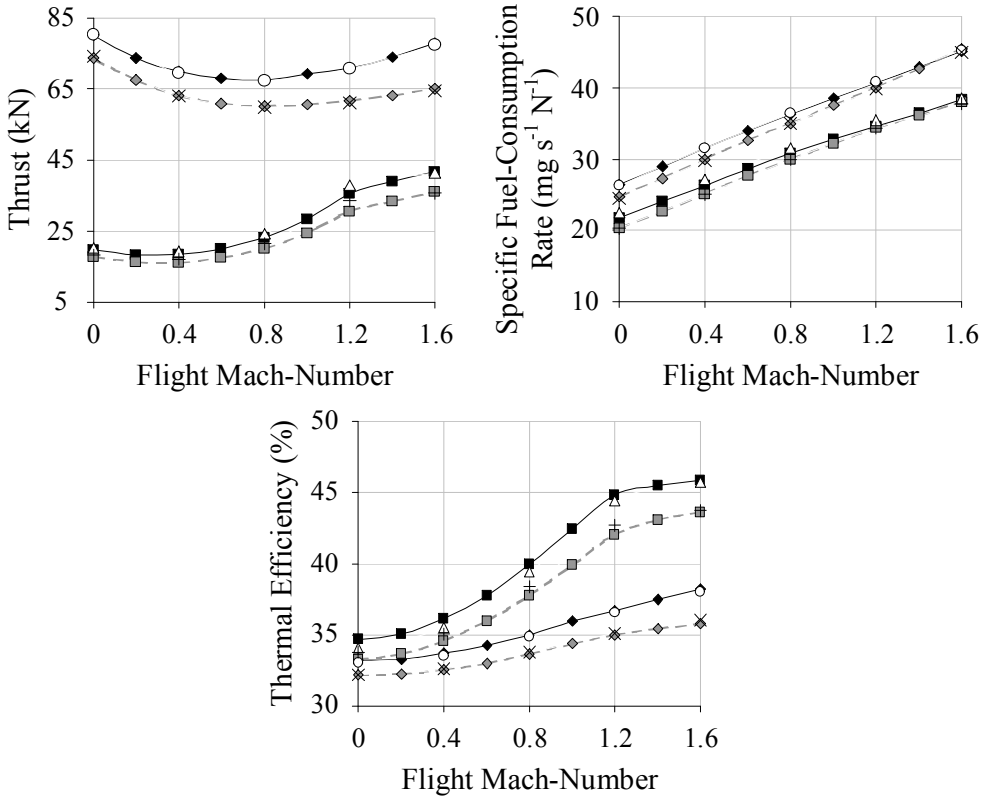

Figure 4.2. Validation of engine performance-prediction program
[TCE/0km[38] CE/0km[38] TCE/10km[38] CE/10km[38]
TCE/0km/CU CE/0km/CU TCE/10km/CU CE/10km/CU].

4.2.5 Clarifications concerning Liew et al's Publications

The design-point conditions for the two-combustor engine in references [36] and [38] are identical. However the behaviours of the above two-combustor engines under part-throttle conditions are different (see Figure 4.3). The present predictions are superimposed. The present author suggests that the results published in reference [38] are a combination of the performances of the two-combustor engine (with ITB turned-on) and the conventional engine. Also the curve, corresponds to the transition when the ITB is turned-on, has been smoothed (see Figure 4.3). As for the results published in reference [36], Liew et al could have smoothed the curve at the transition at which the ITB was turned-on (see Figure 4.3).

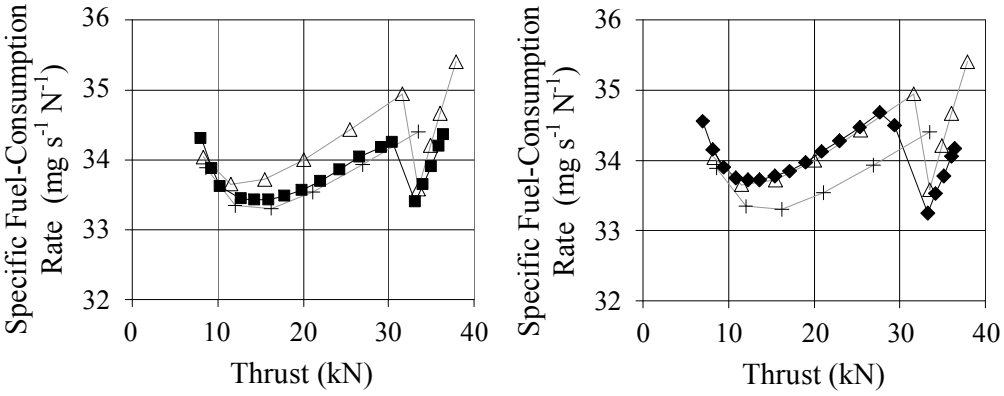

Figure 4.3. Results of two-combustor turbofan engine performance at part-throttle conditions at an altitude of 10km and flight Mach-number of 1.2 [TCE[38] TCE[36] TCE/CU CE/CU].

4.2.6 Suspected Errors in Liew et al's Modelling

Although the present author's prediction matches well with those in Liew et al publication (see Figure 4.2), further study reveals the following conflicting observations: -

- ✓ Liew et al assumed that there is no pressure-loss across the ITB when it is turned-off [39]. Technically, cold pressure-loss is always present regardless of the ITB's operating condition.
- ✓ In Liew et al's publications, the ITB's fuel-air-ratio (i.e. $FAR_{itb}=W_{fuel/itb}/W_6$) is used in the calculation of the Cp_{itb}, R_{itb} and γ_{itb}. For greater accuracy, the local fuel-air-ratio at the ITB's exit (see equation (4.3)) should be used.

$$FAR_6 = \left(W_{fuel/mb} + W_{fuel/itb}\right)/\left(W_6 - W_{fuel/mb}\right) \tag{4.3}$$

- ✓ The value of the bypass ratio (α) should be calculated via equation (4.4). But the terms T_0 and $T_{0/ref}$ are not present in the equation used by Liew et al (see equation (4.5)).

$$\alpha = \alpha_{ref}\frac{\left(\pi_{lpc}\pi_{hpc}/\pi_{fan}\right)_{ref}}{\pi_{lpc}\pi_{hpc}/\pi_{fan}}\sqrt{\left(\frac{T_{0/ref}}{T_0}\right)\left(\frac{T_{t4}}{\tau_{ram}\tau_{fan}}\right)\left(\frac{\tau_{ram}\tau_{fan}}{T_{t4}}\right)_{ref}}\frac{MFF\left(M_{12}\right)}{MFF\left(M_{12}\right)_{ref}} \tag{4.4}$$

$$\alpha = \alpha_{ref} \frac{\left(\pi_{lpc}\pi_{hpc}/\pi_{fan}\right)_{ref}}{\pi_{lpc}\pi_{hpc}/\pi_{fan}} \sqrt{\left(\frac{T_{t4}}{\tau_{ram}\tau_{fan}}\right)\left(\frac{\tau_{ram}\tau_{fan}}{T_{t4}}\right)_{ref}} \frac{MFF\left(M_{12}\right)}{MFF\left(M_{12}\right)_{ref}} \tag{4.5}$$

After the ITB is turned-off, omitting the effects of ITB's cold pressure-loss will result in over-predicting the engine's performance (see Figure 4.4). The miscalculations of the Cp_{itb} and bypass ratio have been corrected and the predicted results shown in Figure 4.5. The effects of the present prediction show that there is no indication that the two-combustor engine operates with a lower SFC when compared with that of the baseline engine producing a comparable thrust.

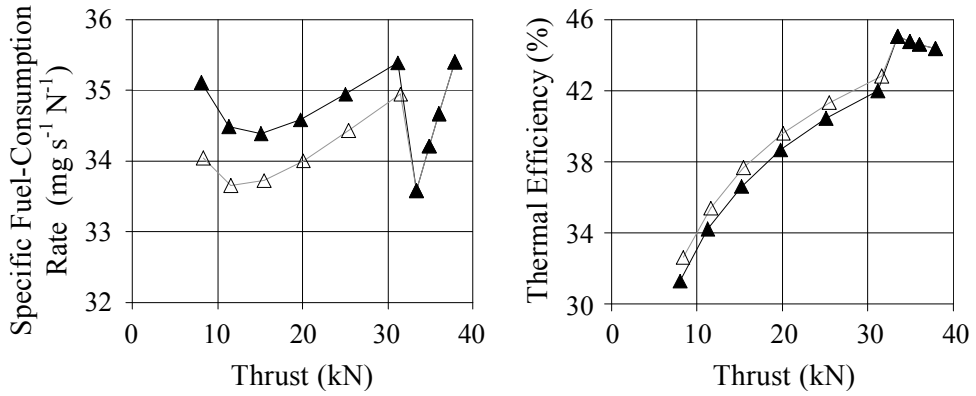

Figure 4.4. The effects of pressure-loss on the two-combustor turbofan engine's performance [—△— Π_{itb}=0% —▲— Π_{itb}=5%].

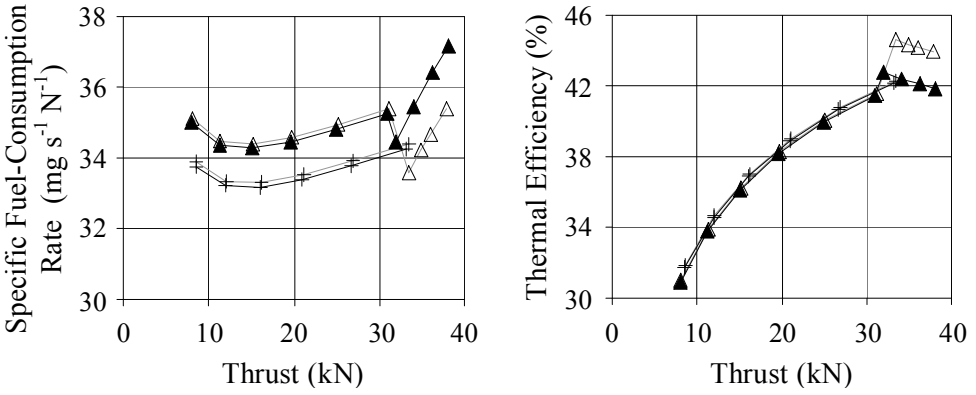

Figure 4.5. The performance of the two-combustor turbofan engine, under partial-throttle conditions, as predicted via the codes by Liew et al and that of the present author [—△— TCE[38] —+— CE[38] —▲— TCE/CU —+— CE/CU].

Nevertheless, the observation that an increase in the two-combustor engine thrust occurred with a reduction in the SFC remains; this peculiarity will be addressed in a later section.

4.2.7 Effects of the Choice of Gas-properties Model on the Engine Performance-Prediction

The off-design performances of both engines, at full and part-throttle, are simulated and analyzed. Under full-throttle condition, the analyses are conducted, for flight Mach-numbers of zero to 1.6, at both at sea-level and an altitude of 10km. For the analysis of the part-throttle performance, the flight condition for an altitude of 10km and flight Mach-number of 1.2 is selected. For the two-combustor engine, under part-throttle condition, the low-pressure turbine's entry-temperature (LPTET) is reduced with the high-pressure turbine's entry-temperature (HPTET) held at its maximum allowable value. The HPTET is reduced after the ITB is shut-down.

- **Conventional Engine**

Under full-throttle condition, the trends of the thrust, SFC and thermal efficiency versus flight Mach-number do not change appreciably even though different gas-properties models are used (Figure 4.6). The thrusts predicted by the three models have only marginal differences. However, the predicted values of the SFC and thermal efficiency differ significantly according to the model adopted.

In the CSH model, the Cp_4 value is equal to Cp_0, which is calculated based on the engine's inlet-temperature. However, in the MSH model, the Cp_4 value is calculated based on the main combustor's inlet-temperature, which is higher than the engine's inlet-temperature. Hence the value of the Cp_4 in the CSH model is lower than that for the MSH model. In the ISH model, the predicted main combustor's inlet-temperature is slightly lower than that predicted via the MSH model. Therefore the value of the Cp_4 in the ISH model is slightly lower than that for the MSH model, but appreciably higher than that for the CSH model. Because, the Cp_5 value is approximately the same for all three models, the fuel-air

ratio predicted via the CSH model is higher than both those for the ISH and MSH model (please refer to equation (4.1)) (see Figure 4.6). Generally, the use of the CSH model over-predicts the fuel-air-ratio (and hence the fuel-consumption rate) for the main combustor. The impacts of the differences in the fuel-consumption rates are reflected by the SFC and thermal efficiency curves.

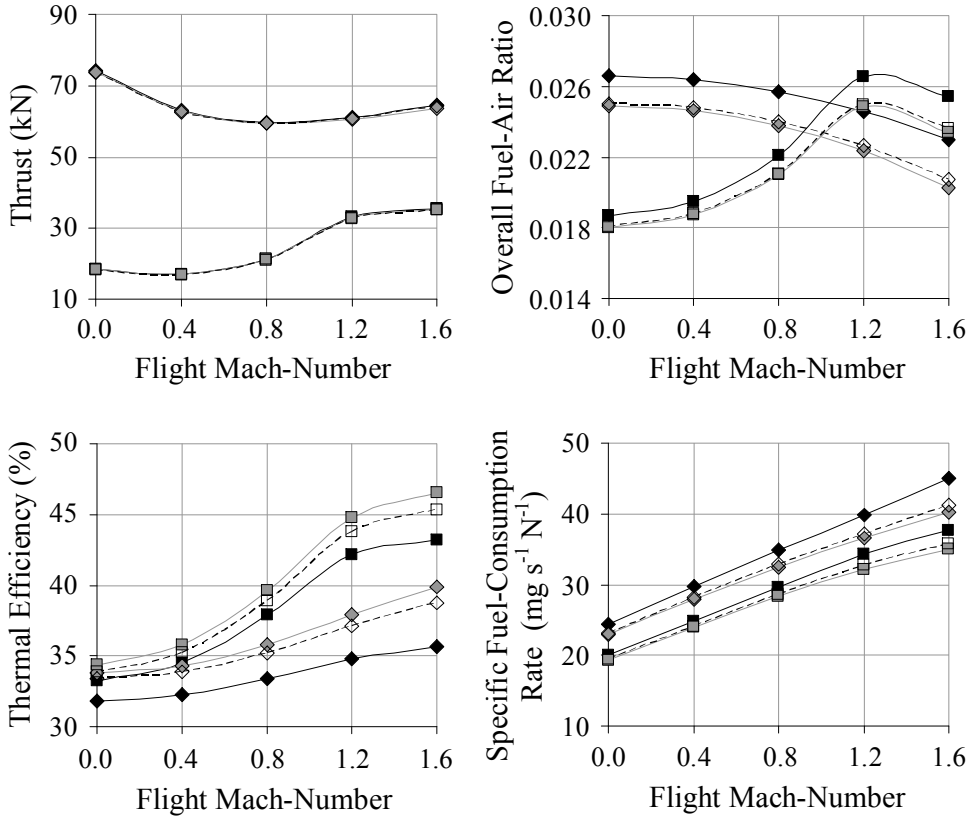

Figure 4.6. Predictions for the conventional engine under full-throttle conditions [CSH/0km, MSH/0km, ISH/0km, CSH/10km, MSH/10km, ISH/10km].

Figure 4.7 shows the conventional engine's performances under the part-throttle condition. For the higher TET range (i.e. above 1250K), both the thrust and SFC decrease; the loss in thrust is accompanied by an increase in SFC when the TET is further reduced. Although there are differences in the absolute values predicted by the different models, all three models predict the classical qualitative "fish-hook" trend for the SFC versus thrust curves. Similarly, the trends of the

thermal efficiency versus net thrust curves are predicted by all the three models to be qualitatively similar (see Figure 4.7).

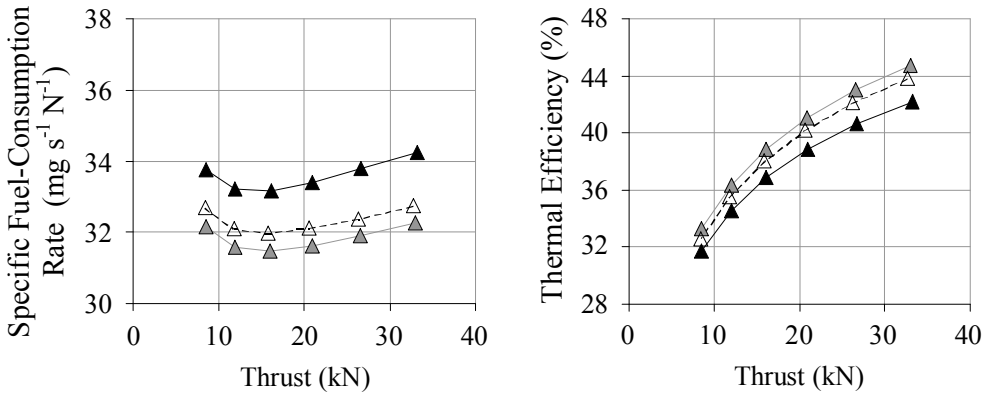

Figure 4.7. Predictions for the conventional engine under part-throttle conditions at an altitude of 10km and flight Mach-number of 1.2 [—▲— CSH —△— MSH - -△- - ISH].

- **Two-combustor Engine**

The study of the performance of the two-combustor engine under the full-throttle condition reveals qualitatively similar findings to those for the conventional engine (see Figure 4.8). In particular:-

✓ The trends of the performance parameters are similar, i.e. independent of the model employed in making the predictions.

✓ The thrust values predicted using the three models are approximately the same.

✓ Each gas-properties model has a significant influence on the absolute values of both the SFC and thermal efficiency due to the differences in the prediction of the fuel-consumption rate via each model.

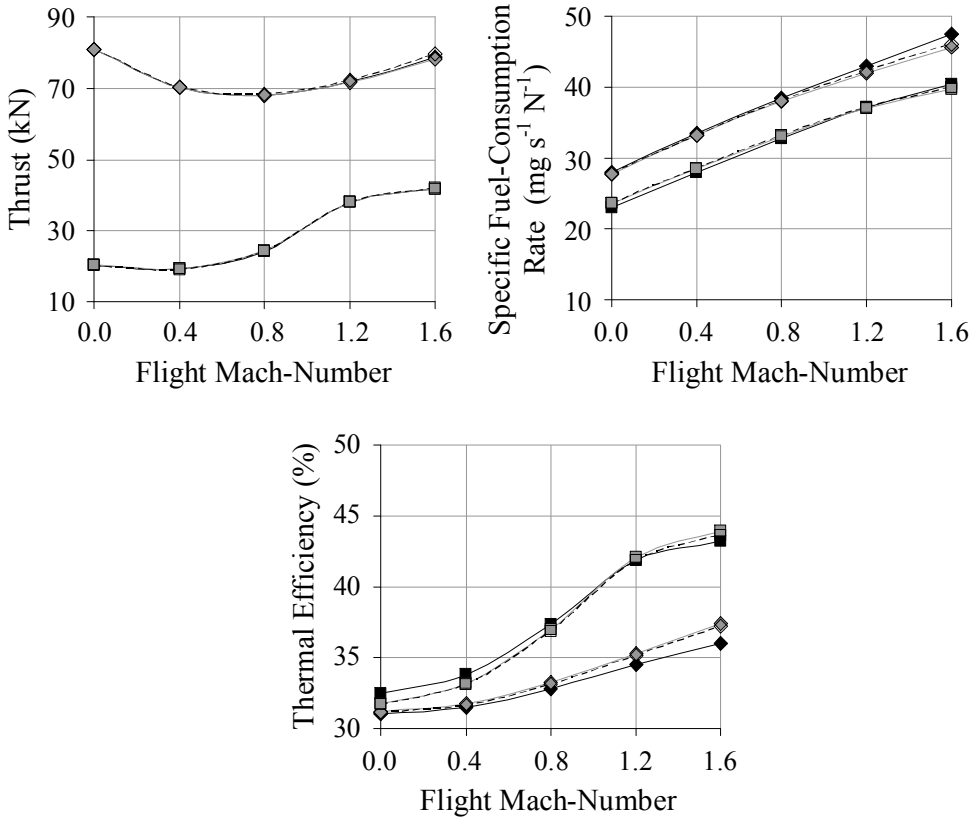

Figure 4.8. Predictions for the two-combustor engine under full-throttle conditions [—◆— CSH/0km —◇— MSH/0km - -◇- - ISH/0km —■— CSH/10km —□— MSH/10km - -⊟- - ISH/10km].

Nevertheless, the influence of the gas model is less significant on the predicted performance for the two-combustor engine than for the conventional engine. The use of the CSH model results in an over-prediction of the main combustor's fuel-air-ratio: this also occurs for the two-combustor engine. However, the use of the CSH model under-predicts the ITB's fuel-air-ratio: this is caused by the use of the higher value of the Cp at the ITB inlet (i.e. it is assumed that $Cp_6=Cp_5$). Therefore this reduces the impact of over-predicting the engine's fuel-air-ratio (see Figure 4.9); it also demonstrates that the net influence of the CSH model depends on the engine's configuration.

Figure 4.10 shows the two-combustor engine's performance under part-throttle conditions at an altitude of 10km and a flight Mach-number 1.2 condition. With the HPTET kept at its maximum allowable value, the net thrust and SFC

decrease with a reduction on LPTET value. The reduction in the SFC is almost linear with the decrease in the net thrust (see Figure 4.10). The "discontinuity" on the curve occurs when the ITB is turned-off. A further reduction in thrust is due to the reduction in the HPTET. After the ITB is turned-off, the trend of the SFC versus net thrust curve resembles that of the conventional engine, i.e. the classical "fish-hook" shape [79]. Generally, predictions obtained using the three models exhibit similar qualitative trends, but different transitions occur when the ITB is turned-off/on. The trends of the SFC and thermal efficiency versus net thrust as predicted using the CSH and MSH models resemble the appropriate trends in references [38] and [35], respectively.

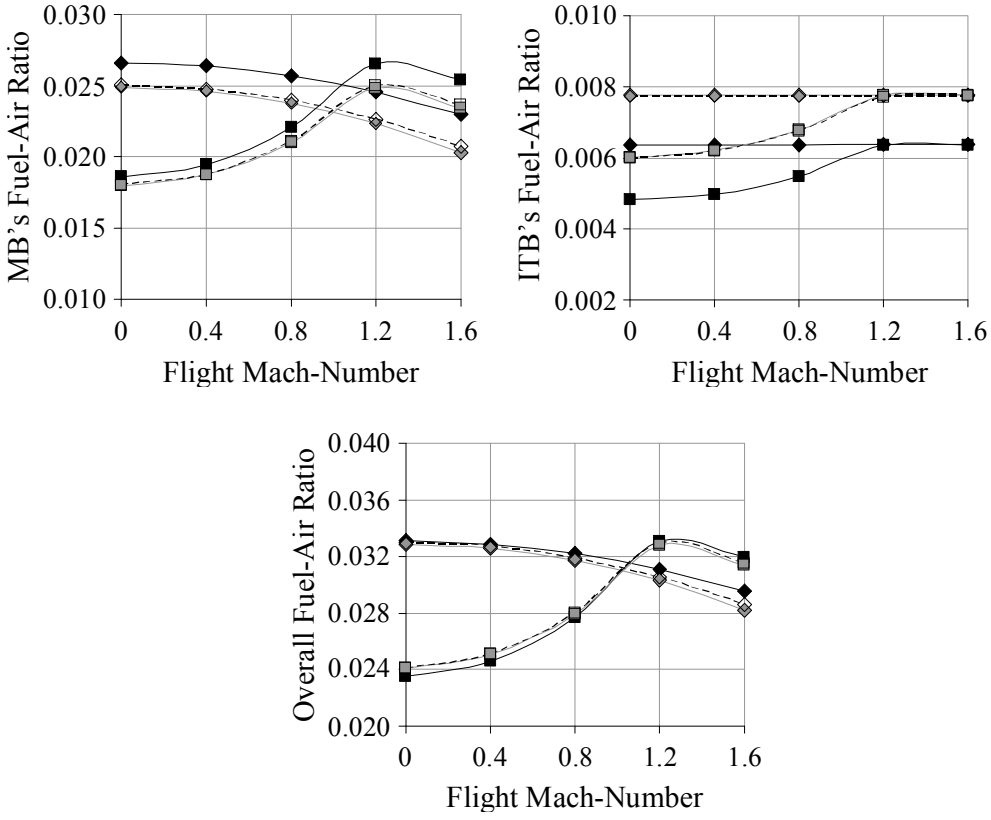

Figure 4.9. The two-combustor engine's fuel-air-ratio under full-throttle conditions [—◆— CSH/0km —◇— MSH/0km - -◇- - ISH/0km —■— CSH/10km —□— MSH/10km - -⊡- - ISH/10km].

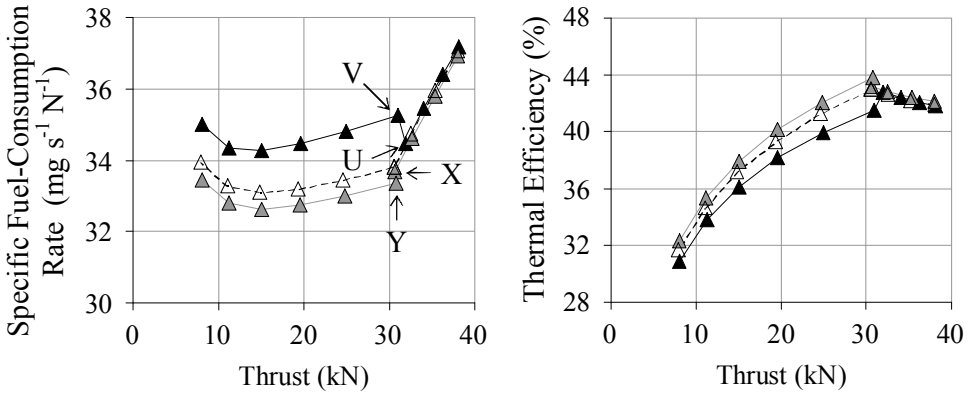

Figure 4.10. Predictions for the two-combustor engine under part-throttle condition at an altitude of 10km and flight Mach-number of 1.2 [—▲— CSH —△— MSH - - △ - - ISH].

In the curves predicted using the CSH model, there is a decrease in SFC with a corresponding increase in thermal efficiency when the ITB is turned-on. At point U (see Figure 4.10), the ITB's fuel-air-ratio is equal to zero, i.e. the CpT values at the ITB's inlet (station 6 – see Figure 4.1) and exit (station 7 – see Figure 4.1) are equal (see equation (4.2). In the CSH model, the Cp_6 value is assumed to be equal to Cp_5; thus it is higher than the Cp_7 value. In order for $(CpT)_6$ to be equal $(CpT)_7$, T_7 will need to exceed T_6. At point V (see Figure 4.10), the values of Cp_6 and Cp_7 are assumed to be equal to Cp_5 for the CSH model. Therefore for ITB with zero fuel-consumption rate, the value of T_7 is equal to T_6. At point U, the higher T_7 value results in a higher thrust, but the fuel-consumption rate required to achieve the T_7 is "under-predicted" when compared with those for point V (see Figure 4.10).

When the MSH model is used, the SFC increases and thermal efficiency decreases when the ITB is turned-on, i.e. the trend at the transition is opposite to that predicted using the CSH model. At point X (see Figure 4.10), the ITB is turned-on, so the Cp_6 value is calculated based on LPTET (T_6). For zero fuel-consumption rate in the ITB, the values of Cp_7 and T_7 are equal to Cp_6 and T_6, respectively. Whereas, at point Y (see Figure 4.10), the ITB is turned-off, and the Cp_7 value is set equal to the Cp_5 value. The Cp_7 value at point X is lower than at point Y, and this results in lower flow's temperature and pressure at the LPT's

exit (station 8 – see Figure 4.1). This in turn, corresponds to a lower thrust occurring at point X than at point Y. Therefore, the introduction of the ITB (point X) results in an increase in the SFC and a decrease in thermal efficiency.

When using the ISH model, the calculation is based on the gas properties at the inlet flows of respective components. Hence it is reasonable to assume this model predicts more accurate results than can be achieved with the CSH and MSH models. There is a discontinuity in the gradient of the curve when the ITB is turned-off. Nevertheless, there is no "jump" in the transition for the engine with ITB turned-on to ITB turned-off.

4.2.8 Summary

The present author has shown that the "unexpected" findings and the inconsistent trends published by Liew et al are caused by (i) the miscalculation of the values of the gas properties, (ii) the inappropriate assumptions and (iii) employment of different gas-properties models. At the full-throttle condition, the thrust produced by the two-combustor engine is higher at the expense of a higher SFC when compared with that of the baseline (i.e. conventional) engine. Similarly, under the part-throttle condition, there is no indication that there is a reduction in the two-combustor engine's SFC when the ITB is turned-on.

4.3 Review on Vogeler's Publication

The selected baseline engine, in Vogeler's publication [40], is a conventional two-spool separate-exhaust turbofan engine (see Figure 4.11(a)). Vogeler's results reveal that a two-combustor engine produces a higher achievable thrust when compared with that of the baseline (i.e. reference) engine. However, the two-combustor engine of two-spool configuration (see Figure 4.11(b)) will require a higher SFC, whereas the single-spool configuration (see Figure 4.11(c)) will require a lower SFC when compared with that of the baseline engine. The latter finding is doubtful: this motivated the present author to conduct the present investigation.

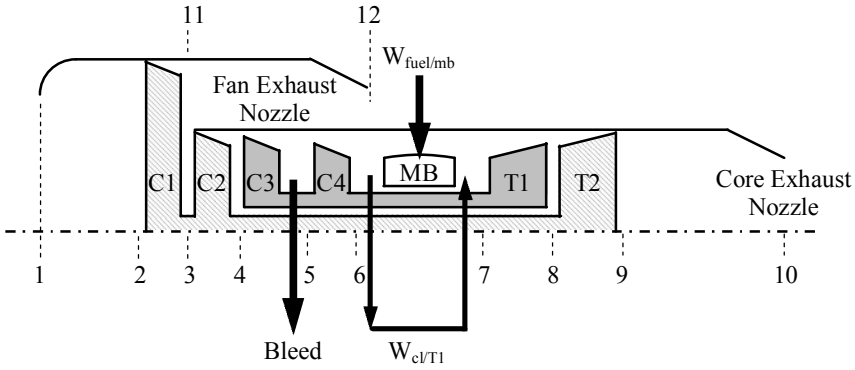

(a) Conventional two-spool engine

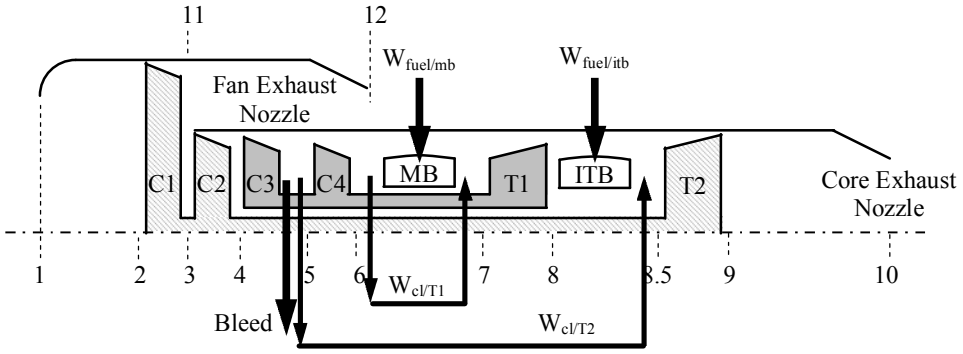

(b) Two-combustor two-spool engine

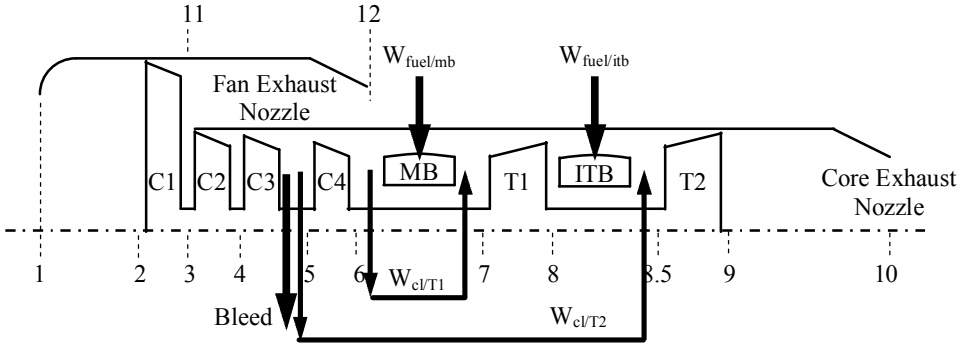

(c) Two-combustor single-spool engine

Figure 4.11. Conventional and two-combustor two-spool separate-exhaust turbofan engines.

- **Engine Performance-Prediction Program**

Vogeler adopted engine performance-prediction methodology [40] was studied and the code reproduced. The following assumptions were made by the present author due to the insufficient available information: -

- ✓ The pressure ratios for compressor C2, C3 and C4 were deduced from the temperature-entropy and/or pressure-entropy diagrams in reference [40].
- ✓ The approach to calculate the gas properties presented in reference [46] was adopted.
- ✓ The main combustor's pressure-loss and combustion-efficiency were assumed to be 5% and 99%, respectively [46].
- ✓ The cooling-flow rate was adjusted to match the T_{hg} of 1740K and TET of 1580K, respectively. However, this does not match the cooling-air percentage as specified in reference [40].

- **Engine Performance-Prediction Program Validations**

The validation is conducted using the baseline (i.e. conventional) engine under design-point conditions as in Table 4.3 and with the component characteristics listed in Table 4.4. The predicted results for the total-temperature, at respective stations, matches well with the published data (see Figure 4.12). However, the predicted thrust and fuel-consumption rate are significantly lower than the published data (see Table 4.5).

Table 4.6 shows the values of the parameters extracted or deduced from reference [40]: the thrust of the baseline engine is calculated using these values and included in Table 4.5 for comparison. The comparison reveals that the present author's predicted and calculated thrusts are approximately equal, but significantly lower than the pertinent published data. The effects of the uncertainty in the fuel-consumption rate on the calculated thrust are relatively small. This is because the amount of the fuel-consumption rate is significantly lower than the engine mass-flow rate.

Table 4.3. Engine's design-point conditions [40].

Parameter	**Value**
Total mass-flow rate, W (kg s^{-1})	800
Bypass ratio, BPR	5
Bypass-exit pressure (bars)	1.7
Overall pressure-ratio, OPR	36
Bleed mass-flow (% of HPC's exit)	10
TET=$T_{t/7}$ (K)	1580
$T_{t/hg}$ (K)	1740

Table 4.4. Components' efficiencies.

Parameter	**Value**
Compressor's polytropic efficiency (%) [40]	91
Turbine's polytropic efficiency (%) [40]	86
Combustor's efficiency (%)	99
Combustor's pressure-loss (%)	5

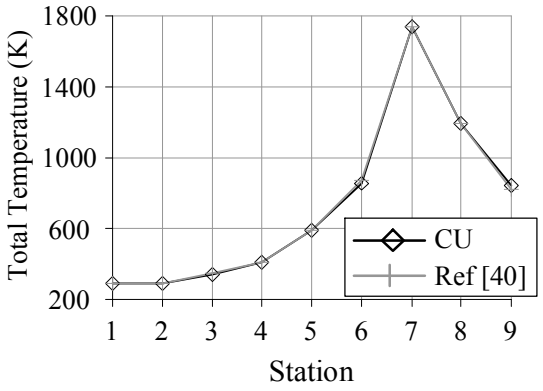

Figure 4.12. Comparison of the reference-engine's temperatures, at respective stations, as predicted by the present author and extracted from reference [40].

Table 4.5. Comparison of baseline engine's performance characteristics.

Parameter	**Reference [40]**	**Predicted (CU)**	**Calculated * (CU)**
Total thrust (kN)	289	263	260
MB's fuel-consumption rate (kg s^{-1})	2.92	2.49	2.92

* Calculated using the values in Table 4.6

Table 4.6. Baseline engine's parameters extracted/deduced from reference [40].

Parameter	**Magnitude**
Total mass-flow rate, W (kg s^{-1})	800
Fuel-consumption rate, W_{fuel} (kg s^{-1})	2.92
Bypass ratio, BPR	5
Bleed mass-flow (% of core inlet mass-flow rate)	10
Bypass-exit pressure (bars)	1.7
Bypass-exit temperature (K)	340
Core-exit pressure (bar)	1.4-1.5
Core exit temperature (K)	820

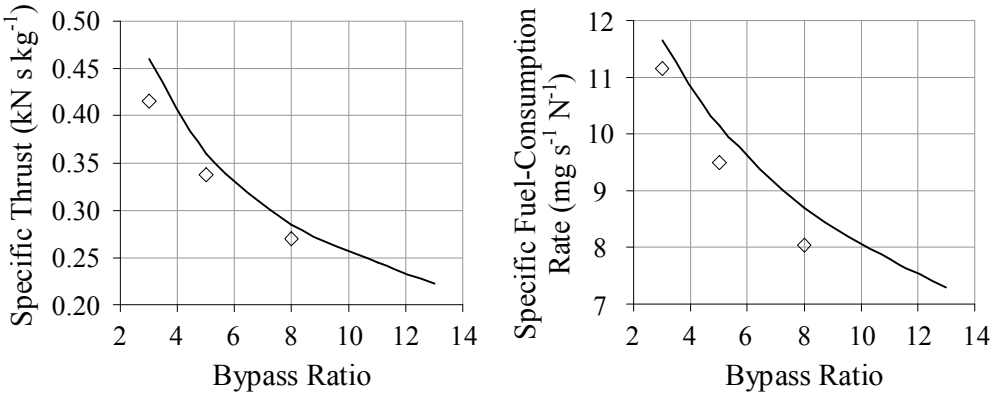

Figure 4.13. Comparison of engines' performances from present predictions and previously published results [—— Ref [40] ◇ CU].

The engine's performance is predicted for various bypass-ratios (BPR). The predicted trends for the specific thrust and SFC versus BPR match the published trends (see Figure 4.13). Therefore the author suspects that there are some "off-sets" in the published results. Based on the above discussion, the present author believes that the reproduced engine performance-prediction program is relatively reliable.

- **Two-combustor Engine Versus Conventional Engine**

Two configurations of the two-combustor two-spool separate-exhaust turbofan engine are considered in reference [40], namely a single-spool (see Figure 4.11(b)) and a two-spool configuration (see Figure 4.11(c)). The design-points of the baseline (i.e. conventional) engine and two-combustor engines are shown in Table 4.7: the components' characteristics are the same as in Table 4.4

Table 4.7. Design-point conditions for the baseline and two-combustor engines.

Parameter	**Conventional two-spool engine**	**Two-combustor two-spool engine**	**Two-combustor single-spool engine**
Mass-flow rate, W (kg s^{-1})	800	800	800
Bypass ratio, BPR	8	8	8
Overall pressure-ratio, OPR	32	32	53
C1's pressure-ratio	1.45	1.60	1.60
C2's pressure-ratio	1.80	1.95	2.25
C3's pressure-ratio	2.60	2.85	3.05
T1's pressure-ratio	N.A.	N.A.	2.5
$T_{t/hg/mb}$ (K)	1740	1740	1740
T_{t7} (K)	1580	1580	1580
$T_{t/hg/itb}$ (K)	N.A.	1740	1740
$T_{t8.5}$ (K)	N.A.	1580	1580

Further reviewing of Vogeler's methodology [40] reveals inconsistencies in the calculation of combustor's fuel-consumption rate and the mixing of the cooling-flow rate with the main stream's hot-gas. Equations (4.6) and (4.7) are used by Vogeler to calculate the main combustor's fuel-consumption rate and model the mixing of the cooling-flow and hot gases entering the HPT (i.e. T1) (see Figure 4.11 for the station numbers). Based on these equations, schematics of the flows are shown in Figure 4.14. However, there are inconsistencies in the two models. The present author has counter-proposed the system as shown in Figure 4.15 with corresponding Equation (4.8) replacing Equation (4.6).

$$\left(W_{fuel}Q_{fuel}\eta\right)_{mb} + W_6\left(CpT_t\right)_6 + W_{fuel/mb}\left(CpT_t\right)_{fuel/mb} = \left(W_6 + W_{fuel/mb}\right)\left(CpT_t\right)_7 \tag{4.6}$$

$$W_7\left(CpT_t\right)_7 = W_{cl/T1}\left(CpT_t\right)_6 + \left(W_7 - W_{cl/T1}\right)\left(CpT_t\right)_{hg} \tag{4.7}$$

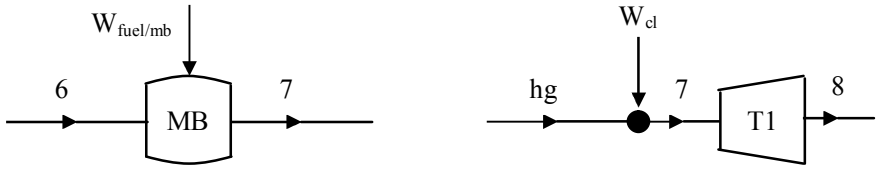

(a) Flows in and out of the main combustor.

(b) Mixing of the cooling flow and hot gases entering T1.

Figure 4.14. Schematic of (a) flows in and out of the main combustor and (b) mixing of the cooling flow and the hot gases entering T1.

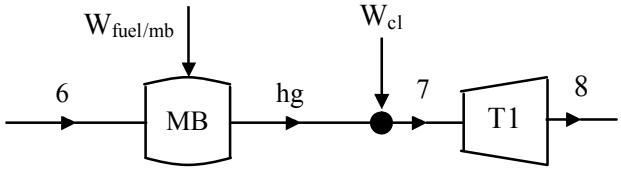

Figure 4.15. Schematic of flows in and out of the main combustor and the mixing of the cooling flow and the hot gases prior to entering T1.

$$\left(W_{fuel}Q_{fuel}\eta\right)_{mb} + W_6\left(CpT_t\right)_6 + W_{fuel/mb}\left(CpT_t\right)_{fuel/mb} = \left(W_6 + W_{fuel/mb}\right)\left(CpT_t\right)_{hg} \tag{4.8}$$

Similarly, the present author counter-proposed the modelling of the ITB's fuel-air-ratio calculation as shown in Figure 4.16 with corresponding equations (4.9) and (4.10).

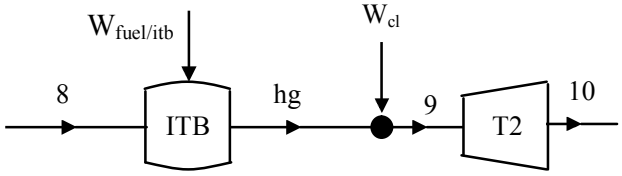

Figure 4.16. Schematic of flows in and out of the inter-stage turbine burner and the mixing of the cooling flow and hot gases prior to entering T2.

$$\left(W_{fuel}Q_{fuel}\eta\right)_{itb} + W_8\left(CpT_t\right)_8 + W_{fuel/itb}\left(CpT_t\right)_{fuel/itb} = \left(W_8 + W_{fuel/itb}\right)\left(CpT_t\right)_{hg} \tag{4.9}$$

$$W_9\left(CpT_t\right)_9 = W_{cl/T2}\left(CpT_t\right)_5 + \left(W_9 - W_{cl/T2}\right)\left(CpT_t\right)_{hg} \tag{4.10}$$

Based on the equations adopted by Vogelar [40], the fuel-consumption rate in both the main combustor and ITB are under-predicted. In the two-combustor engine, the under-prediction of the fuel-consumption rate in the single-spool configuration is significantly higher than that in the two-spool configuration; such that the former has a lower SFC and the latter has a higher SFC when compared with that of the baseline. When corrections are made, based on equations (4.8) to (4.10), the results show that the two-combustor engine (with either single or two spools) has a higher SFC when compared with that of the baseline engine (Table 4.8). Nevertheless, the trends of the two-combustor single-spool engine operate with a lower SFC when compared with that of the two-combustor two-spool engine. This is probably because the design-point conditions for the two-combustor single-spool engine are more optimized than those of the two-combustor two-spool engine. Further investigation on this issue is not part of this present investigation.

Table 4.8. Predictions based on updated methodology.

Parameter	**Conventional two-spool engine**	**Two-combustor two-spool engine**	**Two-combustor single-spool engine**
Total thrust (kN)	217954	249042	244462
Fuel-consumption rate (kg s^{-1})	2.16	3.28	2.65
Specific fuel consumption rate (mg s^{-1} N^{-1})	9.93	13.19	10.83

4.4 Conclusions

The reasons for the misleading deductions made by Liew et al [36, 38, 39] and Vogeler [40] have been identified. The two-combustor engine could produce a higher achievable thrust. However, there is no evidence that the two-combustor engine will operate with a lower specific fuel-consumption rate than the conventional engine.

Chapter 5. Simulations of Baseline (F100-EQ) Conventional Engine

5.1 Introduction

The performance of a conventional engine is necessary to provide a benchmark against which that of the two-combustor engine can be compared. The Pratt and Whitney F100-PW229 (see Figure 5.1) engine is a low-bypass two-spool turbofan engine, which was introduced into service in AD1989 [81]. It is used to power state-of-the-art fighter aircraft such as the F-15 Eagle and F-16 Falcon [81]. Thus with the aim of studying the capability of the two-combustor engine for military-aircraft applications, the F100-PW229 turbofan engine has been chosen to be suitable benchmark configuration.

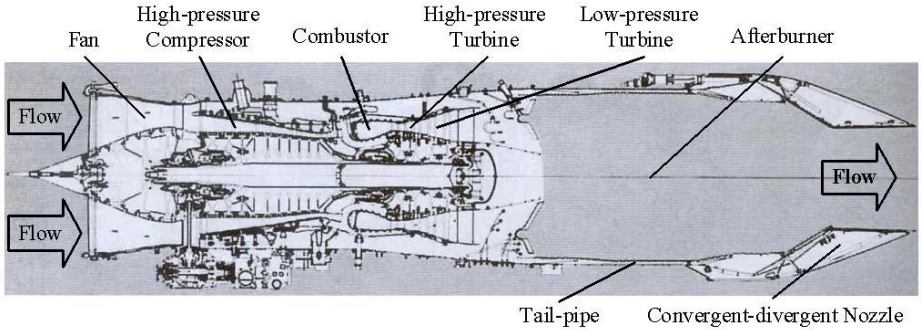

Figure 5.1. Cross-section of a F100-PW229 turbofan engine [81].

Due to the lack of comprehensive data because of commercial and military confidentiality considerations, the modelling of the exact behaviour of the F100-PW229 engine is not available for this research programme. Hence, the baseline engine is an engine of allegedly equivalent performance to that of the F100-PW229 engine. The abbreviation "F100-EQ engine" and the term "baseline engine" will be used synonymously to refer to the baseline engine whose performance is believed to be equivalent to that of the F100-PW229 engine.

The F100-EQ engine is modelled in TURBOMATCH using data from publications in the open literature. The modelling of the F100-EQ engine's

performance and the assumptions made are discussed in Section 5.2. To model the F100-EQ engine's behaviour, the F100-PW229 engine's characteristics and its components' characteristics are surveyed and tabulated; generic data are used where data for the F100-PW229 engine are not available (see section 5.3). The F100-PW229 engine's thrusts and fuel-consumption rates (see section 5.4) are used to validate the F100-EQ engine model. Engineering judgments have had to be made in the processes of using the above-stated data. Therefore the precise objective here is, through engineering judgments, to identify and model the F100-EQ engine with so that it possesses a performance very close, if not equal, to that of the F100-PW229 engine.

5.2 Modelling the Behaviour of the F100-EQ Turbofan Engine

Figure 5.2 shows the schematic layout of the F100-EQ engine model as used in TURBOMATCH. The compression system of the F100-PW229 engine consists of a three-stage fan and an eleven-stage high-pressure compressor (HPC). The air at the HPC's exit is drawn to cool the high-pressure turbine (HPT); and the air bleed from the mid-stage of the HPC is used to cool the low-pressure turbine (LPT). For modelling purposes, the HPC has been split into two compressors, namely HPC1 and HPC2. The cooling-flows for the HPT and LPT are drawn from the exits of the HPC2 and HPC1, respectively. Appendix M shows that the approach of representing the HPC by two compressors has minimal impact on the predicted engine's performance.

In the simulation of the off-design performance for the engine with mixed-exhaust nozzle, the total pressures at bypass's and core's exits are chosen to be (approximately) equal. This criterion resulted in poor convergence in the simulation when the engine's operating-point is further away from its design-point condition. Appendix N shows the differences in the performance of the engine with mixed and separate-exhaust nozzles. The results show that the nozzle type has minimal influence on the specific fuel-consumption rate versus thrust behaviour, except for low throttle position. However the behaviours of the

components, in particular the fan, are heavily dependent on the exhaust-nozzle configuration. Therefore, the modelling of the mixed-exhaust nozzle configuration is essential in order to simulate the F100-EQ engine's performance and behaviour more accurately.

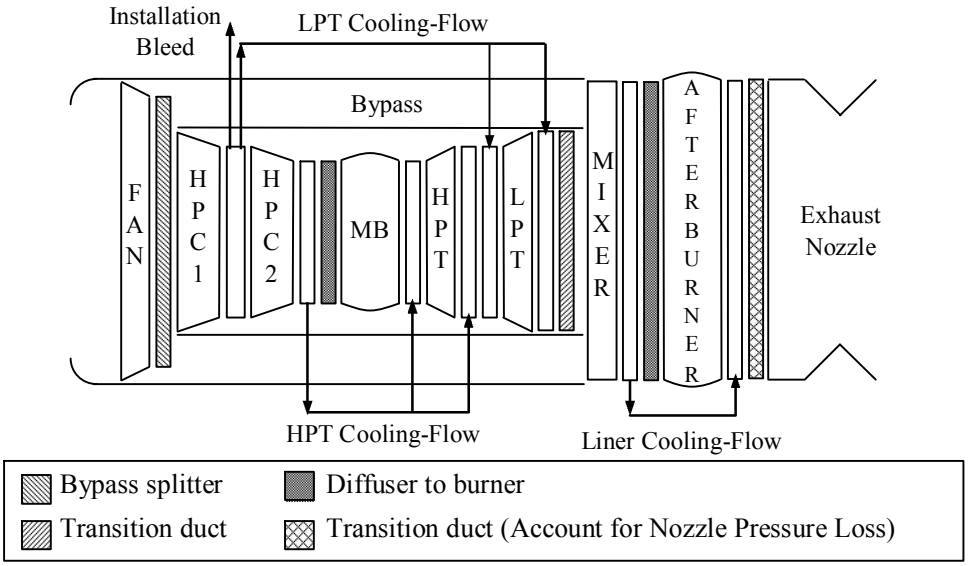

Figure 5.2. Schematic diagram of F100-EQ engine's layout.

5.2.1 Analytical Approach

The data on the F100-PW229 engine and its components' characteristics have been surveyed from the open literature. Due to the lack of availability of exactly pertinent data, generic data have had to be used. Further assumptions (see Section 5.2.2) have also been employed in order to obtain a preliminary model of the behaviour of the F100-EQ engine (see Section 5.5). Fine-tunings are made to the components' characteristics and design-parameters in attempt to produce a F100-EQ theoretical engine model with a performance as close as possible to that of the F100-PW229 engine.

5.2.2 Assumptions in the Modelling of F100-EQ engine

- The design point is set for the sea-level static condition.

- The HPC1's exit-pressure is ~5% higher than the pressure at the LPT's inlet.
- The combustor's pressure-losses are independent of the turbine's entry-temperature (TET).
- The afterburner's cold pressure-loss (i.e. cold-loss) is invariant with respect to the engine's operating-conditions. When the afterburner is turned-on, a constant value of hot pressure-loss (i.e. hot-loss) is considered to occur irrespective of the temperature-rise.
- The efficiencies of the main-combustor and afterburner are kept invariant throughout the flight condition.
- Generic values for components' characteristics are used when those of the F100-PW229 engine are not available.
- Generic component maps in TURBOMATCH are used for off-design performance simulation.

5.3 F100-PW229 Engine's and its Components' Characteristics

5.3.1 F100-PW229 Engine's Characteristics

These are tabulated from references [46], [81] and [93] (see Table 5.1). Jane's Aero-Engines [81] is a "reputable" source for information and hence it has been selected as the main data source. To narrow down the number of possible configurations for the F100-EQ engine, its overall pressure-ratio (OPR) and bypass-ratio (BPR) are fixed at 32.4 and 0.36, respectively.

The fan's pressure-ratio (FPR) has been selected, such that the F100-EQ engine will operate at its maximum specific thrust and/or thermal efficiency. The F100-EQ engine's TET has been determined by the fine-tuning of the simulation model. There is insufficient data to assess the reliability of the engine's mass-flow rate in reference [46]. For the engine's inlet Mach-number of 0.4 and 0.6 [69], the corresponding mass-flow rate is ~100 kg s^{-1} and ~150 kg s^{-1},

respectively. Therefore a mass-flow rate of 112.7 kg s^{-1} is within the ballpark of normal aero-engine operation. Hence the author used this value (i.e. 112.7 kg s^{-1}) as a guideline in the tuning of the F100-EQ engine-behaviour model.

Table 5.1. The characteristics of the F100-PW229 engine.

	Ref [46]	**Ref [81]**	**Ref [93]**
Mass-flow rate, W (kg s^{-1})	112.7	–	–
Overall pressure-ratio, OPR	32.0	32.4	32.0
Fan's pressure-ratio, FPR	3.8	$3.06 \rightarrow 4.05$	–
Bypass Ratio, BPR	0.40	0.36	0.36
Turbine's entry-temperature, TET (K)	1755	>1672	–

5.3.2 Components' Characteristics

Table 5.2 shows the values of the components' characteristics as obtained from the stated publications: reference [81] is the only available source of data specifically for the F100-PW229 engine. The following provides the rationale behind the selection of the component's characteristics for the preliminary modelling of the F100-EQ engine's behaviour.

- Intake and diffuser: The pressure recovery through the engine's intake and diffuser are modelled based on the U.S.A.F. standards for military aircraft [68] (see Equation (5.1)).

$$\begin{aligned} &\text{If} \quad M_0 \le 1, && \Pi_{intake} = 1 \\ &\text{If} \quad 1 < M_0 < 5, && \Pi_{intake} = 1 - 0.075(M_0 - 1)^{1.35} \\ &\text{Otherwise} && \Pi_{intake} = \frac{800}{M_0^{\,4} + 935} \end{aligned} \tag{5.1}$$

- Fan and high-pressure compressor (HPC): The isentropic efficiencies of these components for the F100-PW229 engine, under full-throttle condition (see Figure 5.3 and Figure 5.4) have been used.

Table 5.2. Behavioural characteristics of the engine's components.

	Ref [78]	Ref [46]		Ref [69]	Ref [85]
		1965-1985	1985-2005		
$\eta_{isen/fan}$ (%)	~79	82	86	----	----
$\eta_{isen/hpc}$ (%)	~85	----	----	----	----
$\eta_{poly/fan}$ (%)	----	82	86	----	----
$\eta_{poly/hpc}$ (%)	----	84	88	----	----
$\eta_{cooled\text{-}turb}$ (%)	----	83	87	----	----
$\eta_{uncooled\text{-}turb}$ (%)	----	85	89	----	----
η_{mb} (%)	----	94	99	----	----
η_{ab} (%)	----	91	96	90	----
Π_{bp}	----	----	----	0.96→0.975	----
$\Pi_{diff\text{-}mb}$	----	----	----	0.97→0.985	----
Π_{mb}	----	0.92	0.94	0.96→0.98	0.95
$\Pi_{ab/cold}$	----	0.92	0.94	0.93→0.95	----
$\Pi_{ab/hot}$	----	----	----	0.90→0.95	----
T_{ab} (K)	----	1670	2000	1850→2000	2200

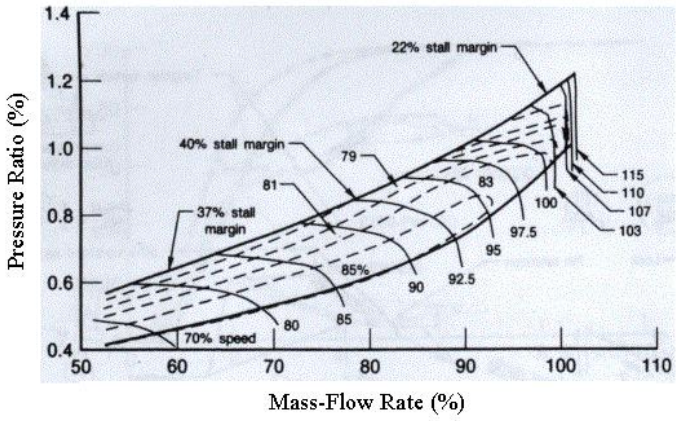

Figure 5.3. Fan map for the F100-PW-229 engine [78].

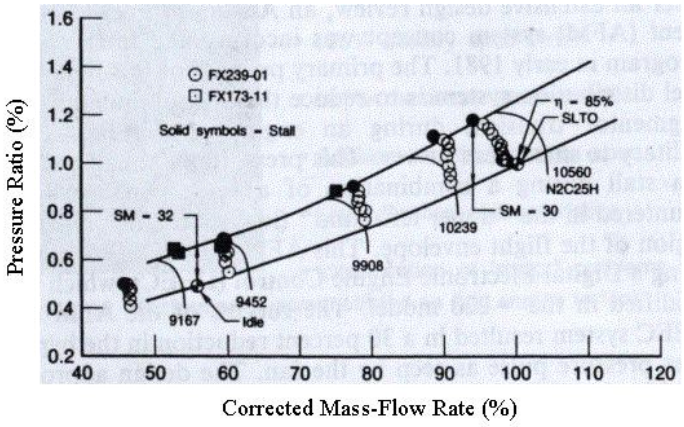

Figure 5.4. The high-pressure compressor map for the F100-PW-229 engine [78].

- Diffuser: A dump diffuser is used in the F100-PW229 engine to reduce the length and weight of the engine (see Figure 5.5), but this occurs at the expenses of achieving a higher pressure-loss (i.e. lower recovery pressure) when compared with that of a conventional faired diffuser. Therefore in this investigation, a diffuser with pressure-recovery factor of 97.5% was selected.

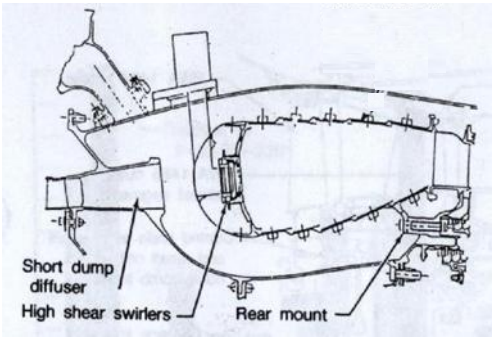

Figure 5.5. Schematic diagram of the F100-PW229 engine's diffuser and main combustor [78].

- Main combustor: Pressure losses and combustion efficiency are used to indicate the performance of the combustor: they are dependent on the type of combustor and the operating conditions. The combustor's pressure-losses consist of both cold and hot pressure-losses. For this investigation, a combustor's cold-loss of 5% was chosen as reasonable. Hot-losses of

0.05% and 0.15% are recommended for the combustor's temperature-ratios of two and four, respectively [69]. The main-combustor's hot-loss is one to two orders of magnitude lower than its cold-loss. To simplify the input parameters for the present predictions, a fixed total pressure-loss of 5% was used. The latest combustor can achieve a combustion efficiency as high as 99%. Because the F100-PW229 engine was developed during the 1980s, the main-combustor's combustion efficiency is assumed to be 98%.

- Turbine's entry-temperature (TET): The F100-PW229 engine's TET was modestly higher than that of the F100-PW220 engine (i.e. 1672K) [81]. The F100-EQ engine's TET was assumed to be 1700K for the preliminary engine-configuration.

- Turbine's cooling-flow rate: The basic requirement for the turbine's cooling-flow rate is a trade-off between the turbine's lifing requirement and the engine's performance. The author assumed that the turbine's cooling-flow rate lies within the range of 15% to 25% of the engine's core mass-flow [69, 85].

- Non-cooled turbine efficiency: The efficiency of an un-cooled turbine is ~2% higher than that of a cooled turbine [46]. In the F100-PW229 engine, only a minimal rate of air-flow is drawn from the mid-stage of the HPC in order to cool the LPT's blades [78]. Therefore for the present investigation, the efficiency for the LPT for the F100-EQ engine is assumed to be that of an uncooled turbine.

- Afterburner's performance: This is defined by its combustion efficiency and pressure-losses. The afterburner's combustion-efficiency (~90%) is significantly lower than that of the main combustor because of its low inlet-pressure and geometrical constraints. The afterburner's cold and hot pressure-losses are assumed to be 5% and 10%, respectively, of its inlet total-pressure. Two other parameters tie with the modelling of the afterburner are its liner cooling-flow rate and the temperature-rise. In the preliminary model, 10% of the total mass-flow is used for cooling the liner [69]. Theoretically, the afterburner's combustion temperature could reach a

stoichiometric value (i.e. all the available oxygen is burned), which corresponds to 2300 to 2500K [69]. The temperature of the gas entering the afterburner of the F100-EQ engine is ~870K. Assuming a stoichiometric temperature of 2500K and combustion efficiency of 90%, the maximum achievable afterburner temperature is ~2350K (see equation (5.2)). Conservatively, a temperature of 2250K was used in the preliminary model. The influence of dissociation has not been considered here.

$$T_{t/ab} = T_{t/ab-in} + \eta_{ab}\Delta T_{ab} \tag{5.2}$$

- Transmission losses: Reference [69] states that the losses in the transmission of power from the turbine to the compressor can be as high as 5%; whereas reference [51] states that the transmission losses are in the order of 1%. However, the corresponding class and/or type of gas-turbine are not indicated in these references. The transmission losses are contributed to by mechanical losses (e.g. at bearings), windage loss and engine auxiliaries (e.g. work extraction for the fuel pump). Large engines with long shafts supported by multiple bearings and engines with transmission gear-systems usually have higher transmission losses. In relatively small aero-engines, such as the F100-PW229, the power losses are expected to be relatively small. Nevertheless, the high manoeuvrability requirement for military engines is associated with high transmission losses. The low-pressure (LP) shaft for these engines are longer and heavier (especially is three-stage fan are involved) and thus expected to experience larger mechanical losses, while the high-pressure (HP) shaft drives the compressor, with more stages rotating at higher speeds and hence more windage losses are expected. The author has arbitrarily assumed that the power losses across the LP and HP spools are 3% and 2%, respectively.

5.3.3 Calculation of Turbine's Cooling-Flow Requirement

The methodology for the calculation of the turbine's cooling-flow rate has been discussed in Section 3.3.1. The corresponding values for K_{cool} , η_{int} , ε_{film} ,

Bi_{tbc} , and Bi_{metal} which are used to calculate the F100-EQ engine's turbine's cooling-flow rate are shown in Table 3.1.

In reality, the temperature profile at the combustor's exit is non-uniform. The gas temperature used in the calculation of the turbine's cooling-flow rate is arbitrary increased by the introduction of the "combustion pattern factor", i.e. K_{comb} (see equation (5.3)) [71]. This will increase the turbine's cooling-flow rate, so preventing damage occuring to the turbine, in particular to the nozzle-guiding-vanes, due to the non-uniform high-temperature gases.

$$T_{t/gas}^{\max} = T_{t/gas} + K_{comb}\Delta T_{comb} \tag{5.3}$$

However, to reduce the number of variables in the calculation of the turbine's cooling-flow requirement, the author has set the value of K_{comb} equal to unity. The maximum allowable material temperature is ~1300K in the mid 1980s (see Figure 2.8). To prevent damage occuring to the turbine due to the non-uniform temperature experienced, the value of the maximum allowable temperature for the turbine's material, i.e. T_{metal} , is arbitrarily selected to be 1150K.

5.4 Data for Validating the F100-EQ Engine's Behavioural Model

Table 5.3 shows the data for the F100-PW229 engine's performance [46, 81, 93] that has been used for validating the F100-EQ behavioural model. Being a "reputable" source of pertinent data, the data from Jane's Aero-Engines [81] has been selected to validate the F100-EQ engine's behavioural-model. The corresponding fuel-consumption rate under the dry-thrust condition was assumed to be the average of that published in references [46] and [93]. The engine mass-flow rate is tuned so that the predicted dry thrust matches the validation data. To account for uncertainties in the data, the author has allowed a margin of tolerance of 1% for the wet-thrust and 2% for the fuel-consumption rate under both dry-thrust and wet-thrust conditions.

Table 5.3. The F100-PW-229 engine's performance data.

	Ref [46]	Ref [81]	Ref [93]
Dry thrust (kN)	79.37	79.18	79.10
Dry-thrust's fuel-consumption rate (kg s^{-1})	1.663	-	1.703
Wet thrust (kN)	129.31	129.45	129.6
Wet-thrust's fuel-consumption rate (kg s^{-1})	7.51	7.11	7.12

5.5 Building and Validation of F100-EQ Engine' Behavioural Model

Based on the selected value for the engine's and components' characteristics, a preliminary F100-EQ engine performance-model has been built. The characteristics of this preliminary model will be described here. Fine-tunings are made to the engine's and components' characteristics in order to achieve the final model for F100-EQ engine's behaiour.

5.5.1 Preliminary Model for the F100-EQ Engine's Performance

The turbofan engine has three principal design-parameters, namely the OPR, BPR and TET. The selected values for these principal design-parameters are discussed in Section 5.3.2. The value for the FPR was selected based on the comparison between the F100-PW220 and PW229 engine. The layouts of F100-PW220 and F100-PW229 are identical. The fan's pressure-ratio of the F100-PW220 engine is ~3.06 [81]. The afterburner's flow-pressure of the F100-PW229 engine is 20% higher than that of the F100-PW220 [78]. Assuming that the pressure-losses across the F100-PW220 and PW229 engines are identical, the FPR of the F100-PW229 engine is ~3.65. Based on the data put-together and the assumptions made, design-point conditions for the preliminary model of the F100-EQ engine are as shown in Table 5.4 and the characteristics of the components are listed in Table 5.5.

- The Appropriateness of the Fan's Selected Pressure-Ratio

Figure 5.6 shows the influences of ratio of the pressures of the hot-stream to cold-stream on the engine's gross-thrust gain: the total-pressure ratio should be near unity in order to enable maximum thrust to be achieved. The selection of a FPR of 3.65 results in approximately the same total-pressure at the core and bypass exits (i.e. 332kPa relative to 356kPa). Therefore the FPR value of 3.65 is close to the optimal FPR in order to achieve maximum specific-thrust.

Table 5.4. F100-EQ engine's preliminary design-point condition.

Parameter	**Value**
Flight altitude, H (km)	0
Flight Mach-number, M_0	0
Mass-flow rate, W (kg s^{-1})	111.5
Overall pressure-ratio, OPR	32.4
Fan's pressure-ratio, FPR	3.65
Bypass ratio, BPR	0.36
Turbine's entry-temperature, TET (K)	1700

Table 5.5. Components' characteristics for the F100-EQ engine's preliminary-configuration.

Parameter	**Value**
$\eta_{poly/fan}$	0.825
$\eta_{poly/hpc}$	0.890
$\Pi_{mb\text{-}diff}$	0.975
Π_{mb}	0.96
η_{mb}	0.98
$\eta_{poly/hpt}$	0.87

Parameter	**Value**
$\eta_{poly/lpt}$	0.89
Π_{bp}	0.975
$\Pi_{ab/cold}$	0.95
$\Pi_{ab/hot}$	0.90
η_{ab}	0.90
AB's Cooling-Flow (%) *	10

* Percentage of mixer's exit flow rate.

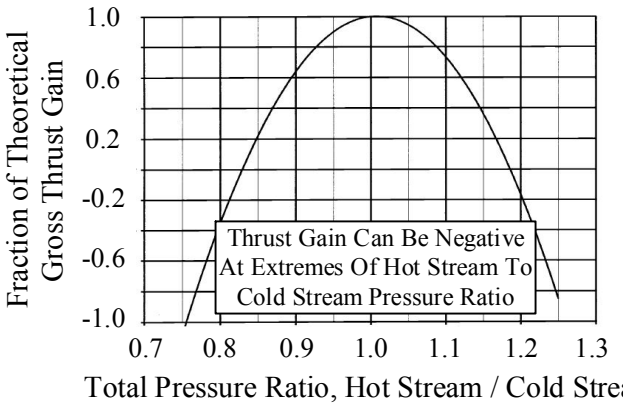

Figure 5.6. Effect of the hot-stream to cold-stream pressure-ratio on engine gross thrust gain [69].

- The Fan's Low Efficiency

The isentropic efficiencies of the fan and HPC are ~79% and ~85%, respectively [78]. For a given pressure-ratio (see Table 5.4), the fan's and HPC's polytropic efficiencies of the fan and HPC are ~82.5% and ~89%, respectively. Comparing these values with those recommended by Mattingly et al [46], for the period of 1985-2005, the HPC's polytrophic efficiency is ~1% higher than the maximum recommended value; whereas the fan's polytrophic efficiency is near the lowest recommended value. The fan's and HPC's pressure-ratios for the F100-EQ engine are plotted in Figure 5.7. Apart from the fact that a lower pressure-ratio is expected when this chart is used for the HPC, it is also apparent that the three-stage fan for the F100-PW229 engine could have achieved a high pressure-ratio at the expenses of a low efficiency. This provides an insight into the relation between the number of stages, pressure-ratios and efficiencies of both the fan and HPC for the F100-EQ engine.

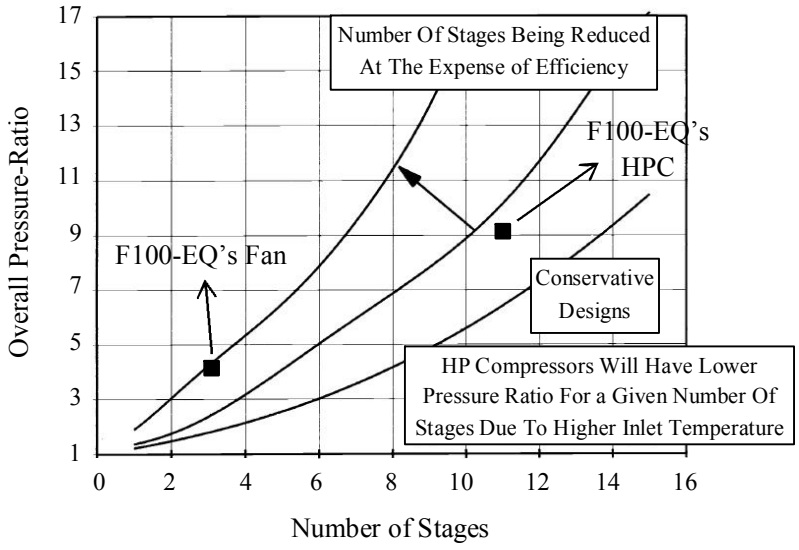

Figure 5.7. Pressure-ratio versus number of stages for the (low-pressure) axial compressor [69].

- Analyzing the Performance Predicyions

The predicted engine's thrust and fuel-consumption rate are shown in Table 5.6. The predicted dry-thrust and fuel-consumption rate match closely with those for the F100-PW229 engine. However, the predicted wet-thrust is considerably lower than that for the F100-PW229 engine. A series of fine-tuning operations, on the engine design-parameters and components efficiencies, have been conducted in order to match the predicted data with those acquired from the open-literature. Generally, the approach is to reduce the temperature of the gas entering the afterburner in order to increase the temperature-ratio across it (assuming the afterburner exit's temperature is fixed at 2250K).

Table 5.6. Comparison of present predictions with published data.

Parameter	**Prediction**	**Published**
Dry-thrust (kN)	79.18	79.18
Dry-thrust's fuel-consumption rate (kg s^{-1})	1.70	1.68
Wet-thrust (kN)	126.56	129.45
Wet-thrust's fuel consumption rate (kg s^{-1})	7.27	7.11

5.5.2 Finalized Version of the F100-EQ Engine's Performance Model

The effects of variations in the engine's design-point parameters and components' characteristics have been investigated. The updated model for the F100-EQ engine (see Table 5.7) has thermal efficiency of 39.5%, which is marginally higher than that achievable by the preliminary model, i.e. 38.9% (see Table 5.4). However, the predicted wet thrust and corresponding fuel-consumption rate still divert from the published data. Therefore it was necessary to tune the afterburner's characteristics in order for the predicted results to match those of the published data.

Reference [44] suggests that the use of the afterburner can achieve an approximately 50% increase in thrust to be obtained at the expense of at least three times the fuel-consumption rate. The F100-PW229 engine's thrust can be increased by ~62% but with corresponding ~4.3 times increases in fuel-consumption rate. Therefore the author believes that the wet thrust of the F100-EQ engine can be matched by adjusting the boundaries of the afterburner's temperature and/or afterburner's cooling-flow requirements. The cooling-flow is essential to maintain the liner's maximum temperature below an acceptable level to achieve an acceptable life duration and also to limit the exhaust-cavity's infrared-signature. Therefore the author suggests keeping the afterburner's cooling-flow rate at 10% of the total mass-flow rate. Because it is believed that afterburner temperature is pushed near to the maximum achievable temperature, there is no basis for reducing the afterburner's hot-loss (i.e. it was maintained at 10% of its inlet mass-flow rate). For an afterburner operating under sea-level static condition, its achievable combustion efficiency exceeds that operating under higher altitudes and flight Mach-numbers. Therefore the combustor efficiency for the afterburner is revised upwards from 90% to 92.5%. Another parameter that defines the afterburner's performance is the temperature rise: thus the author increased the originally selected temperature from 2250K to 2300K.

The updated design-point conditions and components' characteristics for the F100-EQ engine model are shown in Table 5.7 and Table 5.8, respectively. Table 5.9 shows that the predicted thrust and SFC match closely with the published data.

Table 5.7. F100-EQ engine's design-point condition.

Parameter	**Value**
Flight altitude, H (km)	0
Flight Mach-number, M_0	0
Mass-flow rate, W (kg s^{-1})	111.5
Overall pressure-ratio, OPR	32.4
Fan's pressure-ratio, FPR	3.55
Bypass ratio, BPR	0.36
Turbine's entry-temperature (K)	1700
Afterburner temperature (K)	2300

Table 5.8. Components' characteristics for the F100-EQ engine's configuration.

Parameter	**Value**
η_{fan}	0.830
η_{hpc}	0.895
$\Pi_{mb\text{-}diff}$	0.975
Π_{mb}	0.96
η_{mb}	0.98
η_{hpt}	0.875

Parameter	**Value**
η_{lpt}	0.895
Π_{bp}	0.975
$\Pi_{ab/cold}$	0.95
$\Pi_{ab/hot}$	0.91
η_{ab}	0.925
AB's Cooling-Flow (%) *	8.0

* Percentage of mixer's exit-flow rate.

Table 5.9. Comparison of present predictions with published data.

Parameter	**Prediction**	**Published**
Dry thrust (kN)	79.18	79.18
Dry thrust's fuel-consumption rate (kg s^{-1})	1.71	1.68
Wet thrust (kN)	128.9	129.45
Wet thrust's fuel-consumption rate (kg s^{-1})	7.17	7.11

- Effects of the Overall and Fan's Pressure-Ratios on the Selection of the F100-EQ Engine Configuration

The performances of the F100-EQ engine model with respect to the variations in the FPR and OPR have been studied. All the configurations considered have the turbines' cooling-flow rate re-calculated and updated.

Figure 5.8 shows the effects of varying the FPR on the F100-EQ engine at a chosen OPR of 32.4. The selected FPR of 3.55 enables the engine to operate near its maximum specific-thrust and thermal-efficiency conditions. This outcome is not surprising as the requirements for approximately the same bypass's and core's exits total-pressures have been considered in the fine-tuning process.

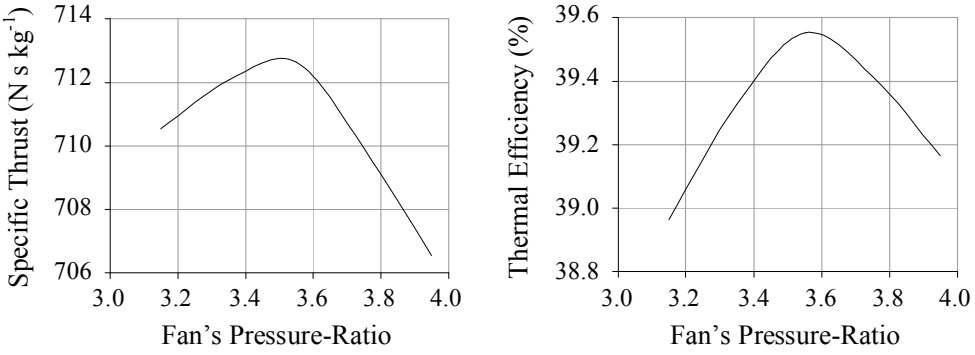

Figure 5.8. Effects of fan's pressure-ratio on the performance of the F100-EQ engine with an overall pressure-ratio of 32.4.

Figure 5.9 shows the influence of the OPR on the performance of the F100-EQ engine with an FPR of 3.55. It is interesting to reveal that the F100-EQ engine with an OPR of 32.4 corresponds to the maximum thermal-efficiency condition: also an OPR of ~16.0 enables the engine to operate at its maximum achievable specific-thrust. Qualitatively, this behaviour is similar to that of a typical conventional engine, i.e. the optimal OPR for the maximum specific thrust is significantly less than that for the maximum thermal-efficiency [69]. This is further evidence that the adapted approach to model the F100-EQ engine's behaviour is appropriate.

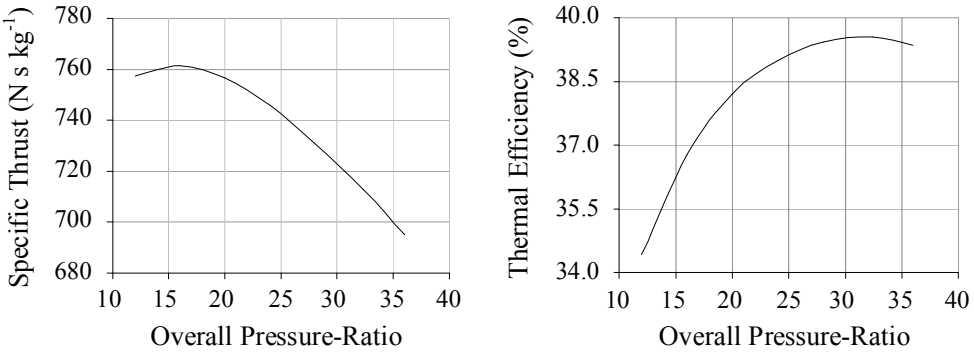

Figure 5.9. Effects of overall pressure-ratio on the performance of the F100-EQ engine with a fan pressure-ratio of 3.55.

- Off-design Performances of the F100-EQ Engine

Figure 5.10 reveals the trend of the SFC versus thrust for the F100-EQ engine. The typical "fish-hook" behaviour is shown with the throttling down of the engine [79]. Qualitatively, this correlates that the F100-EQ engine behaviour has been modelled correctly.

The F100-PW229 engine's fan and HPC behaviour are shown in reference [78]. The corresponding components' characteristics for the F100-EQ engine differ from those for the F100PW229 engine. Therefore, it is expected that the predicted behaviour is unlikely to match that of the published data [78]. Nevertheless, the comparison of the fan's and HPC's behaviours between the predicted results and published data will provide an indication on the reliability of the F100-EQ engine's behavioural model (see Figure 5.11). The results show fairly good correlations with respect to the trends for both the fan and HPC behaviours between the prediction and published data.

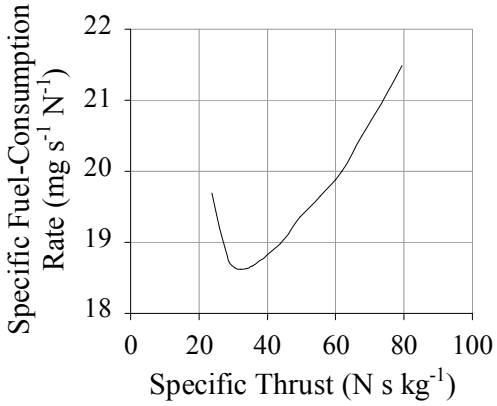

Figure 5.10. The specific fuel-consumption rate versus thrust for the F100-EQ engine.

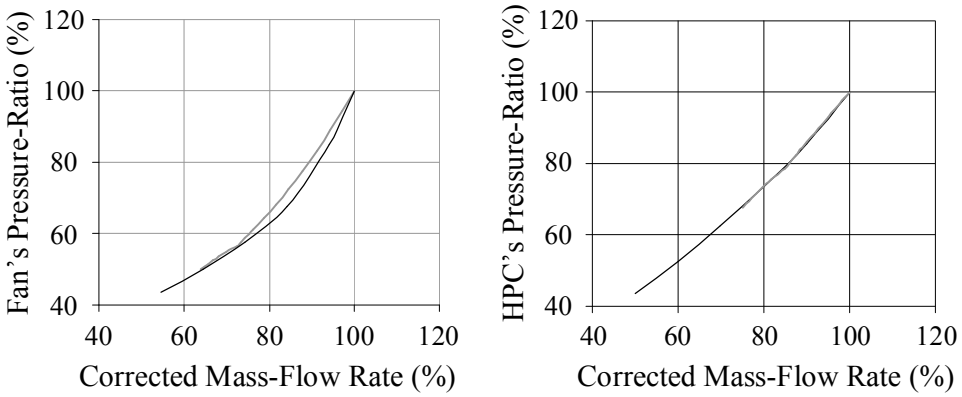

(a) Fan's working line (b) HPC's working line

Figure 5.11. The fan and high-pressure compressor behaviours for the F100-EQ engine when compared with that of the F100-PW229 engine [—— Ref [78] —— Prediction].

5.6 Conclusions

Truly representative baseline engine are desirable, in order to make more readily apparent the relative benefits as well as disadvantages of the two-combustor engine. The F100-PW229 low-bypass two-spool turbofan engine has been chosen as the baseline engine. The F100-EQ engine, with a performance equivalent to that of the F100-PW229 engine has been modelled, via

TURBOMATCH, using published data. Based on the limited available data, extra efforts could be invested in order to tune the behaviours of the model in an attempt to further match the behaviour of the fan and compressor. Nevertheless, the present behavioural model of the F100-EQ engine has already met the objective of modelling a representative engine for benchmarking the behaviour of the two-combustor engine. Therefore the author decided to channel his efforts in order preferentially to study the performance of the two-combustor engine, instead of improving the baseline engine model.

Chapter 6. Performances of the Two-combustor Engine versus the Conventional Engine under Design and Off-design Conditions

6.1 Introduction

The layout of the two-combustor engine is identical to that of the baseline (i.e. conventional) engine, except with respect to the installation of an inter-stage turbine burner (ITB) between the high-pressure and low-pressure turbines (HPT and LPT) (see Figure 6.1). The temperatures of the flows at the HPT's and LPT's inlets will be referred to as the high-pressure and low-pressure turbine's entry-temperatures, respectively (i.e. HPTET and LPTET).

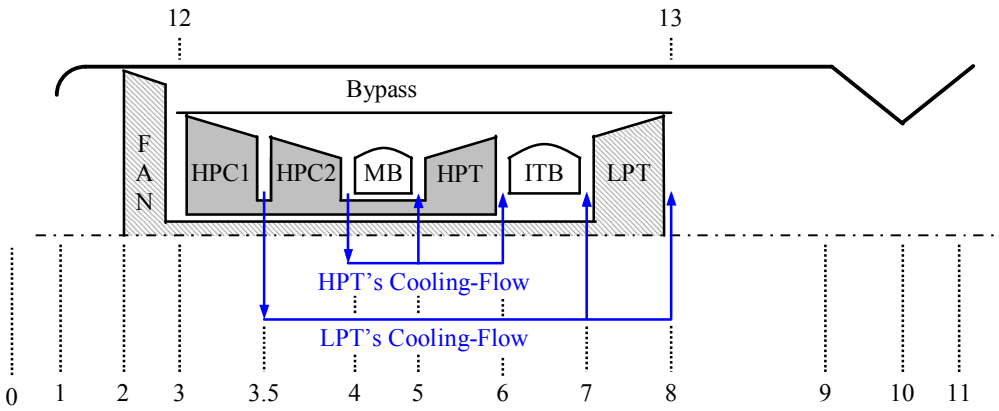

Figure 6.1. Schematic diagram of the two-spool two-combustor mixed-exhaust engine.

For the design-point conditions given in Section 6.2, the fundamental characteristics and behaviours of the two-combustor engine have been investigated and presented (see Section 6.3). For the conventional engine to match the maximum specific-thrust achievable by the two-combustor engine, its HPTET needs to be increased. In order to appreciate the behaviour resulting from increasing the maximum achievable specific-thrust, i.e. for the conventional engine with increased HPTET and two-combustor engine, their performances are compared (see Section 6.4).

The conventional turbofan engine has three prime design parameters, namely turbine's entry-temperature (TET), overall pressure-ratio (OPR) and bypass-ratio (BPR). Based on preliminary assessments, the design parameters for the two-combustor engine also include the LPTET and the HPT's pressure-ratio. The effects of the variations in these parameters on the two-combustor engine's performance have been investigated (see Section 6.5).

For completeness, the study was extended to investigate the off-design performances of the two-combustor engine with reference to that of the baseline engine (see Section 6.6). The performances of the engines under part-throttle condition have also been studied under sea-level static conditions, and the engines' off-design performances at full throttle have been revealed across a range of flight Mach-number at sea-level.

6.2 Design-Point Conditions for the Baseline (i.e. F100-EQ) and (Basic) Two-Combustor Engines (see Table 6.1)

The selection of the design-point condition is such that the engine operation has been optimized for selected flight profile(s)/requirement(s). With a lack of

Table 6.1. The design-point conditions for the baseline and (basic) two-combustor engines.

Parameter	**Baseline (F100-EQ) Engine**	**Two-combustor Engine**
Flight altitude, H (km)	0	0
Flight Mach-number, M_0	0	0
Fan's pressure-ratio, FPR	3.55	3.55
Overall pressure-ratio, OPR	32.4	32.4
Bypass ratio, BPR	0.36	0.36
Mass-flow rate, W (kg s^{-1})	111.5	111.5
HPT's entry-temperature, HPTET (K)	1700	1700
LPT's entry-temperature, LPTET (K)	N.A.	1700

real flight profile(s)/requirement(s) and also exact optimization criteria, the selection of optimal design-point conditions for the respective engines are not available. Therefore the design-point conditions for both the baseline and two-combustor engines have been specified for the sea-level static condition. For the present exercise, the values of the OPR, FPR and TETs of the baseline and two-combustor engines have been also kept identical. All the studies conducted, except for the transient-performance analysis, were made with reference to the two-combustor engine with layout shown in Figure 6.1 and corresponding design-point conditions in Table 6.1.

6.3 The Behaviour of the Two-combustor Engine

The two-combustor engine's specific thrust would be significantly over-predicted if the exact turbine's cooling-flow requirement is neglected in the performance simulation (see Figure 6.2). Hence it was necessary to incorporate the exact turbine's cooling-flow rate in the modelling of the behaviour of the two-combustor engine.

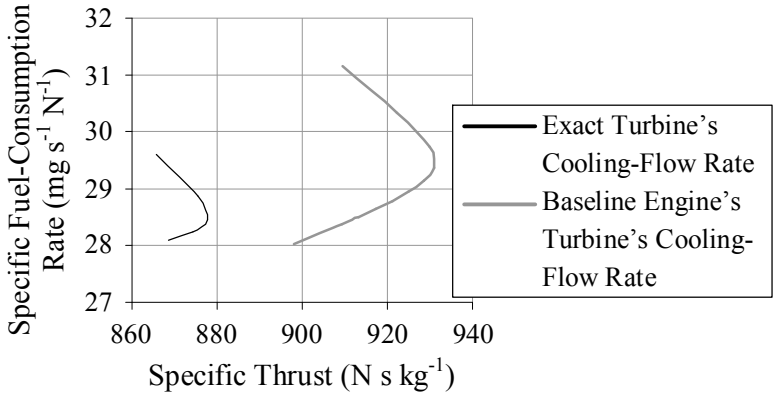

Figure 6.2. The effects of the turbine's cooling-flow rate on the two-combustor engine's performance.

Figure 6.3 shows the influences of fan's pressure-ratio (FPR) on the performance of the two-combustor engine. The temperature of the LPT's inlet-flow is raised by the introduction of the ITB, so enabling more work extraction at the LPT in order to increase the optimal FPR (i.e. FPR=~3.95) for maximum

achievable specific-thrust. Nevertheless, the improvement in the performance of the two-combustor engine with a FPR of ~3.95 is marginal (i.e. an increase by ~0.25% in thrust and a decrease by ~1% in SFC) when compared with that with a FPR of ~3.55. Based on Figure 5.7, a further increase in FPR of the three-stage fan can be seen to decrease its efficiency. Alternatively, a fourth-stage could be added at the expense of a heavier engine. Therefore, there may be a minimal or no incentive to increase the FPR from ~3.55 to ~3.95.

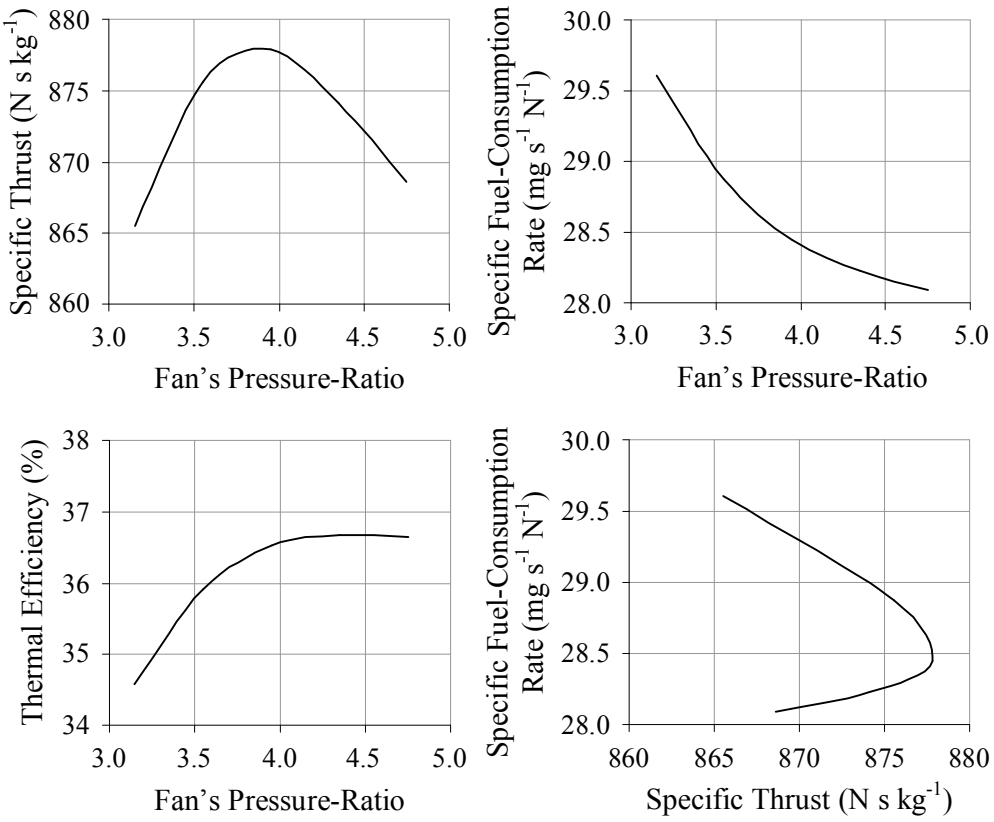

Figure 6.3. The influences of variations in the fan's pressure-ratio on the performance of the two-combustor engine.

Interestingly, the results also reveal that the optimal FPR for achieving maximum thermal-efficiency is higher than that for the maximum specific-thrust. This observation differs from that for a conventional engine, for which the optimal FPRs for maximum specific-thrust and thermal efficiency are approximately the same. In the two-combustor engine, the combustion process in the ITB will also influence the cycle efficiency. Further increases in the FPR (~3.95<FPR<~4.45)

will "bring" the ITB nearer to the main combustor, whereby the cycle efficiency is increased. Nevertheless, there is also a reduction in the amount of fuel to be burnt in the ITB, thus reducing the maximum achievable specific thrust of the engine. With a higher FPR (>~4.45), the demand for an increasing LPT's cooling-flow rate becomes predominant and therefore results in a drop in thermal efficiency. For increases in the value of the FPR, the reduction in the fuel-consumption rate in the ITB out-weights the reduction in engine's specific-thrust, thus reducing the engine's SFC. It is assumed that the maximum specific thrust would be more crucial than minimal SFC for the fighter applications. Therefore the study was not extended to identify the FPR for the corresponding minimum SFC.

6.4 Performances of the Baseline Engine (increase in TET) versus that of the Two-combustor Engine

Three configurations of the conventional engine with its TET of 1900K, 2100K and 2300K have been considered. The performances were compared with those of the baseline and two-combustor engines. To reduce the complexity, the flight conditions (H and M_0), OPR and BPR of the engines were kept identical. The FPR was selected for the engine operating at its maximum specific thrust. Although the considered configurations were not fully optimized, the predictions are still useful in as much as they provide an indication of the performance of the two-combustor engine relative to the corresponding conventional engines.

Given the same level of technological sophistication, the increase in the conventional engine's HPTET will require higher cooling-flow rate for both the HPT and LPT. The configurations of respective engines are listed in Table 6.2: the exact cooling-flow rate for the turbine is incorporated and selected FPRs correspond to that of maximum specific thrust. The design-point performances of these engine configurations are plotted in Figure 6.4. Even with a HPTET of 2300K (i.e. Configuration 4), the conventional engine's maximum achievable specific-thrust remains lower (by ~8%) than that achievable with the two-combustor engine. The effects of dissociation have not been considered in this study.

Table 6.2. Conventional engines' design-point conditions for respective engines with exact cooling-flow rate of the turbine incorporated.

Parameter	Conventional Engine				Two-combustor Engine
	Cfg1	Cfg2	Cfg3	Cfg4	
Flight altitude, H (km)	0	0	0	0	0
Flight Mach-number, M_0	0	0	0	0	0
Fan's pressure-ratio, FPR	3.55	3.75	3.95	4.05	3.55
Overall pressure-ratio, OPR	32.4	32.4	32.4	32.4	32.4
Bypass ratio, BPR	0.36	0.36	0.36	0.36	0.36
Mass-flow rate, W (kg s^{-1})	111.5	111.5	111.5	111.5	111.5
HPT's entry-temperature, HPTET (K)	1700	1900	2100	2300	1700
LPT's entry-temperature, LPTET (K)	N.A.	N.A.	N.A.	N.A.	1700

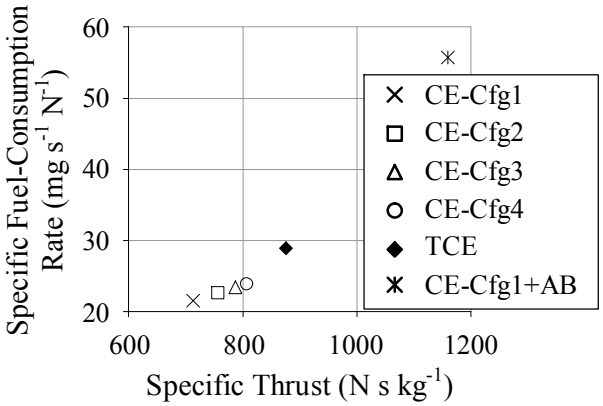

Figure 6.4. Performances of the conventional and two-combustor engines.

When comparing the performance of the baseline engine (i.e. Configuration 1) incorporating an afterburner, the two-combustor engine generates a significantly lower specific thrust. The two-combustor engine burns fuel at a higher pressure in the ITB, and hence achieves a more efficient engine-cycle when compared with that of the conventional engine incorporating an afterburner (see Table 6.3). It is clear that the performance of the two-combustor engine lies between that of the conventional engine with and without an afterburner.

Table 6.3. Performance of the baseline (i.e. F100-EQ = Cgf 1) engine with and without an afterburner (AB), relative to that of the two-combustor engine.

	Baseline Engine		**Two-combustor Engine**
	Without AB	**With AB**	
Specific thrust (N s kg^{-1})	713	1160	876
Specific fuel-consumption Rate, SFC (mg s^{-1} N^{-1})	21.5	55.4	28.6
Thermal Efficiency (%)	39.6	23.7	36.1

6.5 Effects of Design Parameters on the Performance of the Two-combustor Engine

In the parametric studies conducted, by Sirignano et al [32, 33] and Liew et al [34], the influences of variations in the values of specific parameters on the performances of the conventional and two-combustor engines were compared (see Section 2.7). The approach in this study was slightly different: the effects of the variation in a specific parameter on the performance of the two-combustor engine were studied and comparisons were made with the performance of a baseline (i.e. F100-EQ) engine. In addition, the presently adopted engine performance-simulation program is of higher fidelity and the engine model incorporates the exact turbine's cooling-flow rate. The following parametric studies have been conducted here, whereby the components' characteristics of the baseline (i.e. F100-EQ) and two-combustor engines are kept identical.

Apart from the variations in the OPR and BPR, the effects of the variations in the TETs on the performance of the two-combustor engine have also been investigated. The LPTET is kept the same as the HPTET in order for the two-combustor engine to achieve the maximum specific thrust. The effects of lower TETs, with corresponding reductions in the turbines' cooling-flow rate, on the performance of the two-combustor engine are compared with the performance of the baseline engine. Another influential parameter is the "position" of the ITB (i.e. HPT's pressure-ratio). An engine configuration with an additional intermediate-pressure compressor (IPC) is proposed. The variation in the IPC's

pressure-ratio will independently alter the HPT's pressure-ratio, in turn affecting the performance of the engine.

6.5.1 Effects of the Overall Pressure-ratio (OPR) on the Performance of the Two-combustor Engine

The effects of the variations in the OPR have been studied for the TETs equal to 1700K. For each OPR value, the performances of the two-combustor engine over a range of values of FPR have been simulated (see Figure 6.5). The results reveal that the performance of the two-combustor engine are weakly dependent on the range of OPR considered.

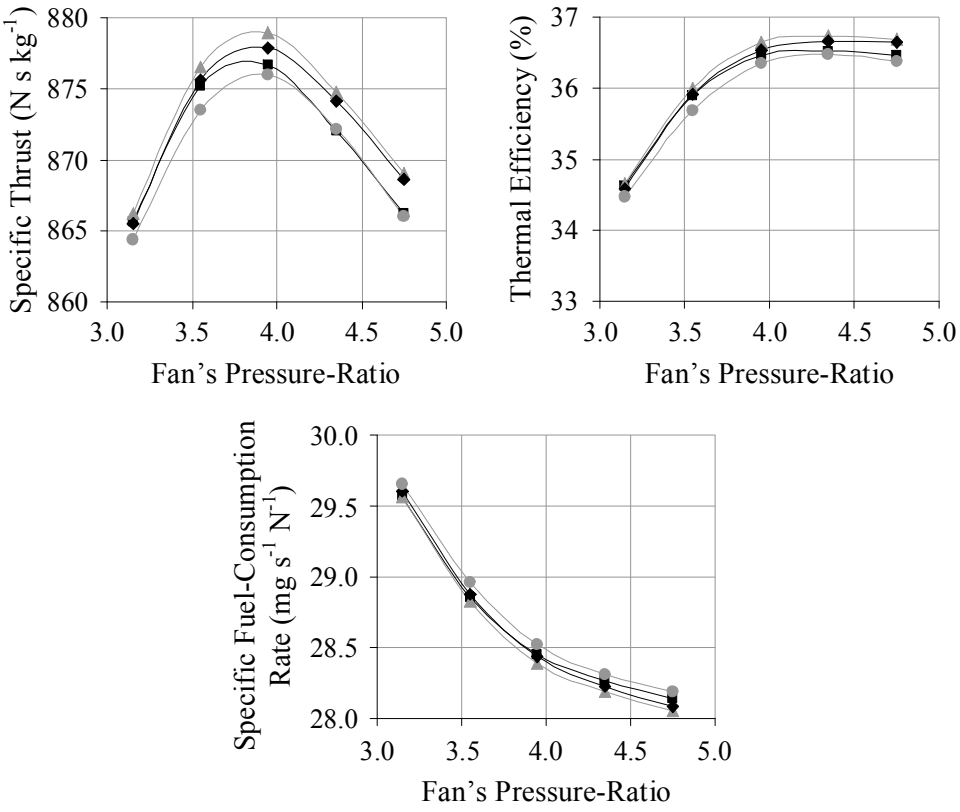

Figure 6.5. The influences of the variations in the fan's pressure-ratio on the performances of the two-combustor engine for selected overall pressure-ratio [—■— OPR=24.0 —▲— OPR=28.0 —◆— OPR=32.4 —●— OPR=36.0].

As that observed in Section 6.3, the optimal FPR for maximum specific thrust is lower than that for maximum thermal efficiency. In addition, it has been observed that the maximum specific thrust and thermal efficiency occur at approximately the same OPR (see Figure 6.6); unlike that of the conventional engine, whereby the OPR for maximum specific thrust is substantially lower than that for maximum thermal efficiency.

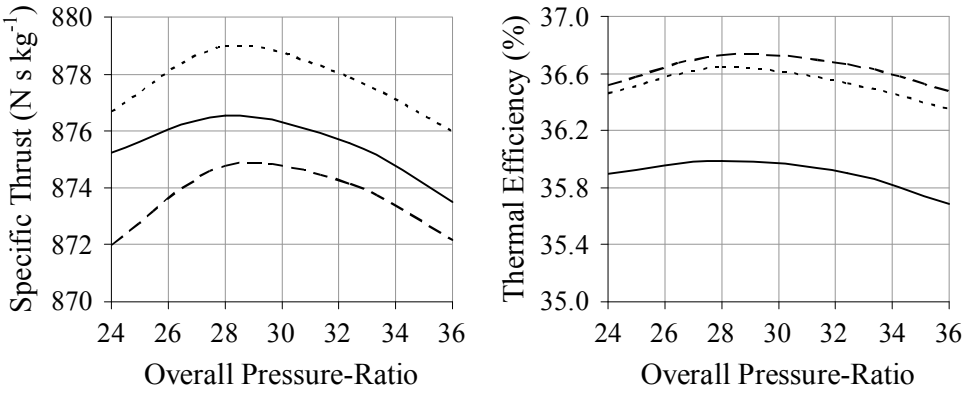

Figure 6.6. The effects of the variations in the overall pressure-ratio on the two-combustor engine's specific thrust and thermal efficiency for select fan's pressure-ratio [——— FPR=3.55 ····· FPR=3.95 - - - - FPR4.15].

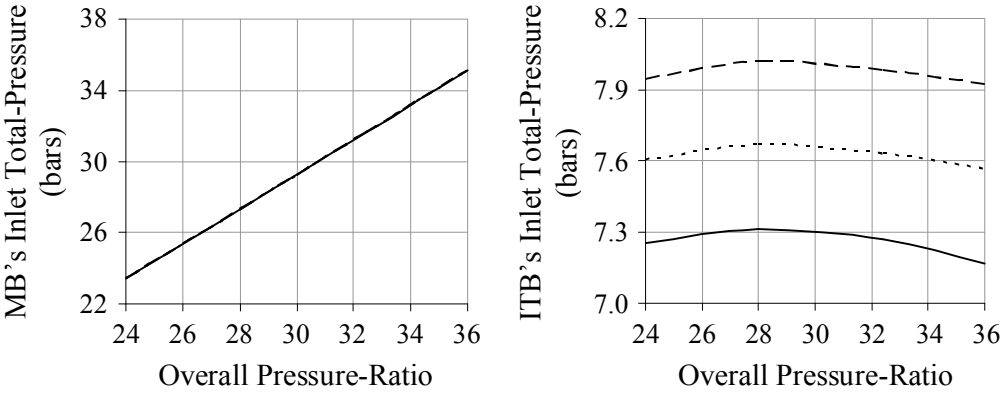

Figure 6.7. The effects of the variations in the overall pressure-ratio on the inlet total-pressure of the two-combustor engine's main-combustor and inter-stage turbine burner [——— FPR=3.55 ····· FPR3.95 - - - - FPR4.35].

The conventional engine's thermal efficiency increases with corresponding increases in OPR and TET. In the two-combustor engine, the engine's efficiency

depends on the total pressure and the TET in both the main-combustor and the ITB. Figure 6.7 also shows the inlet total-pressures of the two-combustor engine's main-combustor and ITB over a range of OPR. It appears that the trends for the specific thrust and thermal efficiency versus OPR are governed by the ITB's inlet-pressure. In addition, the thermal efficiency is strongly dependent on the ITB's inlet-pressure.

6.5.2 Effects of the Bypass Ratio (BPR) on the Performance of the Two-combustor Engine

The predictions for the effects of the BPR on the performance of the two-combustor engine are plotted in Figure 6.8. With a lower BPR, the maximum

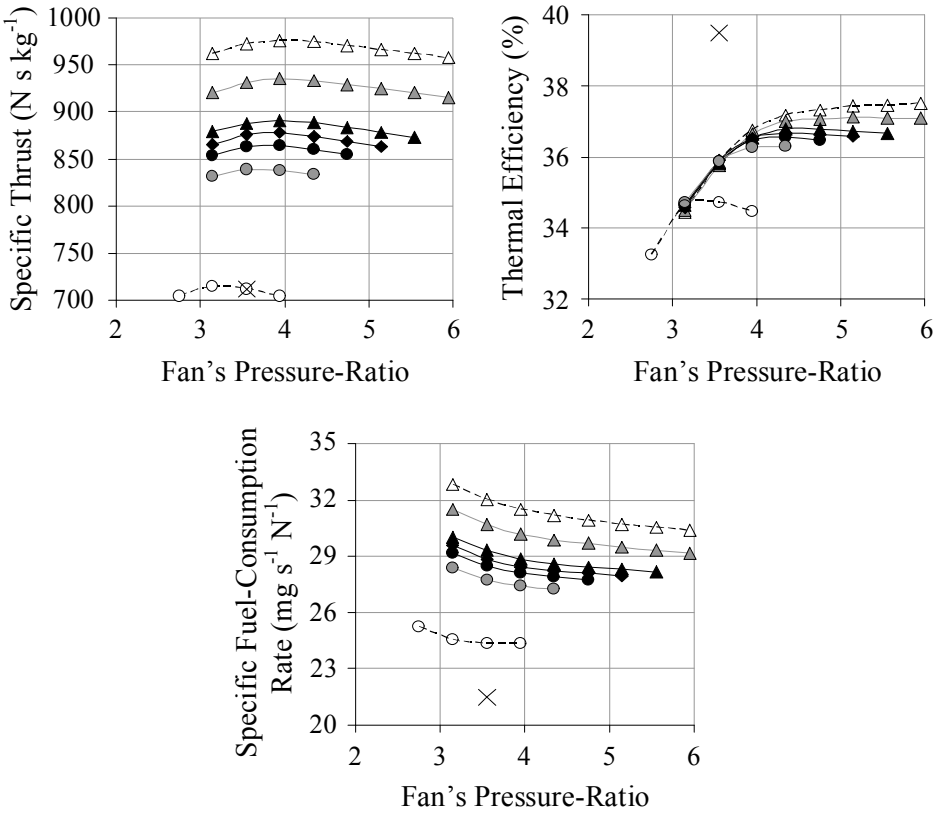

Figure 6.8. The effects of fan's pressure-ratio on the two-combustor engine's performance against that of the baseline (F100-EQ) engine for selected bypass-ratio [F100-EQ TCE(BPR=0.10) TCE(BPR=0.20) TCE(BPR=0.32) TCE(BPR=0.36) TCE(BPR=0.40) TCE(BPR=0.48) TCE(BPR=1.00)].

achievable specific thrust of the two-combustor engine is increased, but at the expense of a higher specific fuel-consumption rate. Also, the optimal FPR for maximum specific-thrust/thermal-efficiency increases with the implementation of an engine with a lower BPR. These observations are consistent with the behaviour of the conventional engine.

It has also been observed that the maximum achievable thermal efficiency increases with a decrease in the BPR. The main combustor's inlet total-pressure is invariant (i.e. ~32.4 bar), but the ITB's inlet total-pressure is mainly functions of FPR (see Figure 6.9). For respective configurations at maximum thermal efficiency, the configuration with the lower BPR (e.g. BPR=0.1) has a higher ITB's inlet total-pressure. Therefore its thermal efficiency is higher than that of the configuration with the higher BPR (e.g. BPR=1.0).

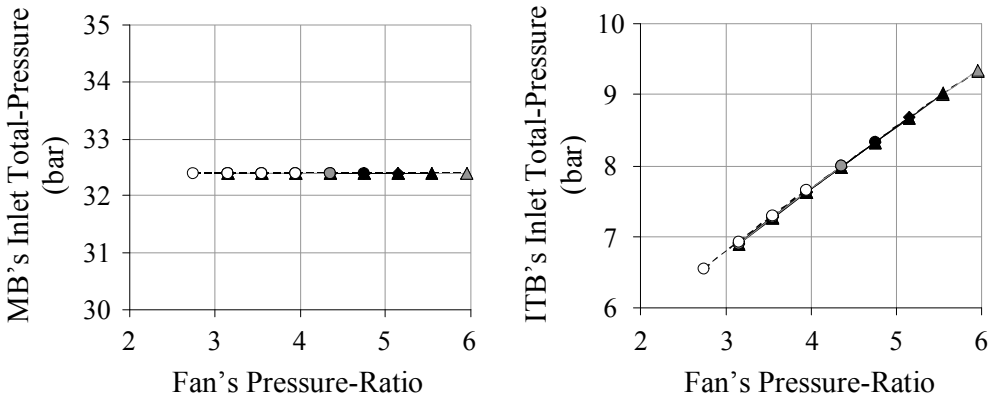

Figure 6.9. The effects of the fan's pressure-ratio on the two-combustor engine's main combustor's and inter-stage turbine burner's inlet total-pressure behaviour [TCE(BPR=0.10) TCE(BPR=0.20) TCE(BPR=0.32) TCE(BPR=0.36) TCE(BPR=0.40) TCE(BPR=0.48) TCE(BPR=1.00)].

6.5.3 Effects of the Turbine's Entry-Temperatures on the Performance of the Two-combustor Engine

Figure 6.10 shows the effects of the TETs on the performance of the two-combustor engine. With the lower values of the TETs, lower specific-thrust is generated at lower values of the thermal efficiencies and SFCs. Also the

corresponding optimal FPR has also to be reduced for the engine to operate at its maximum specific thrust. Liew et al [37] reported that a two-combustor engine with a relatively low TETs (i.e. low turbine's cooling-flow requirements) could produce higher a specific thrust at higher thermal efficiency when compared with that of the baseline engine with a higher TET. This claim is not corroborated in this investigation: the two-combustor engine, with TETs of 1300K, has a marginally lower specific thrust, but at a significantly higher SFC than that of the baseline engine (i.e. the F100-EQ engine).

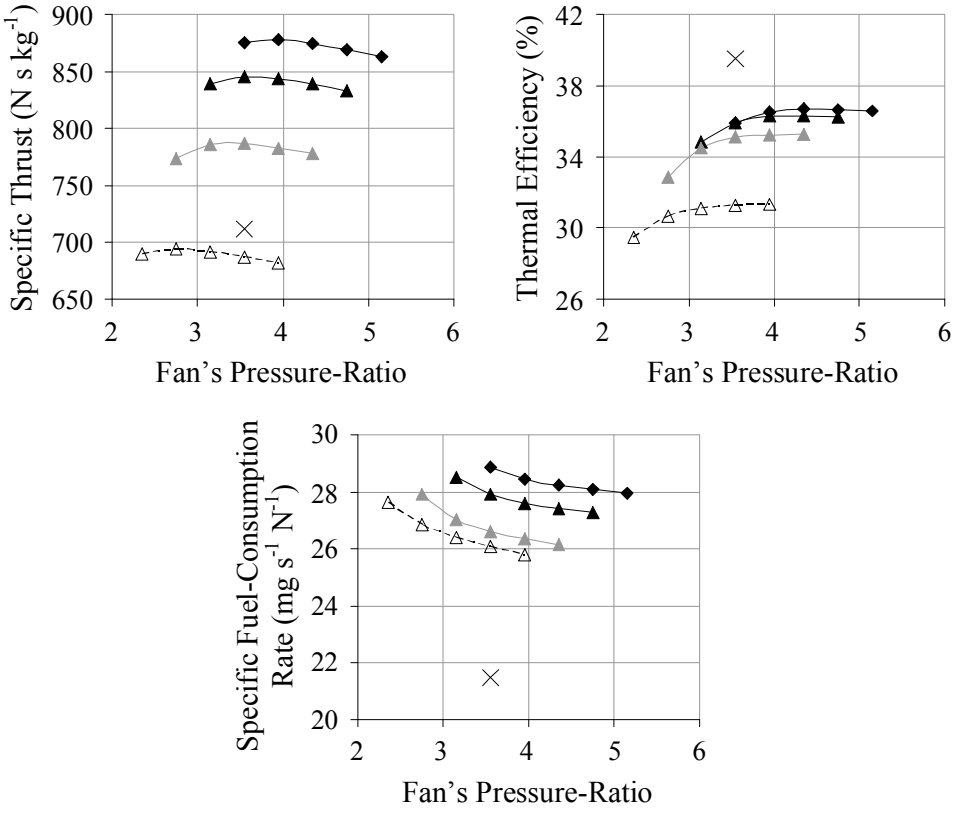

Figure 6.10. Effects of the values of the fan's pressure-ratio on the two-combustor engine's performance relative to those of the baseline (F100-EQ) engine for selected turbine's entry-temperature (OPR32.4)

[F100-EQ TCE(TETs=1700K) TCE(TETs=1600K) TCE(TETs=1450K) TCE(TETs=1300K)].

The FPR corresponding to the engine operating at its maximum achievable specific thrust is selected based on the predictions shown in Figure 6.10. The effects of the variation in the OPR are studied based on the above-selected FPRs (see Figure 6.11). The maximum achievable specific-thrust and thermal efficiency are increased by corresponding increases in the values of the OPR and TET: this is consistent with the behaviour of the conventional engine [69]. Nevertheless, there is no evidence that it could produce a higher specific thrust at a higher thermal efficiency than that of the comparable baseline engine (F100-EQ engine).

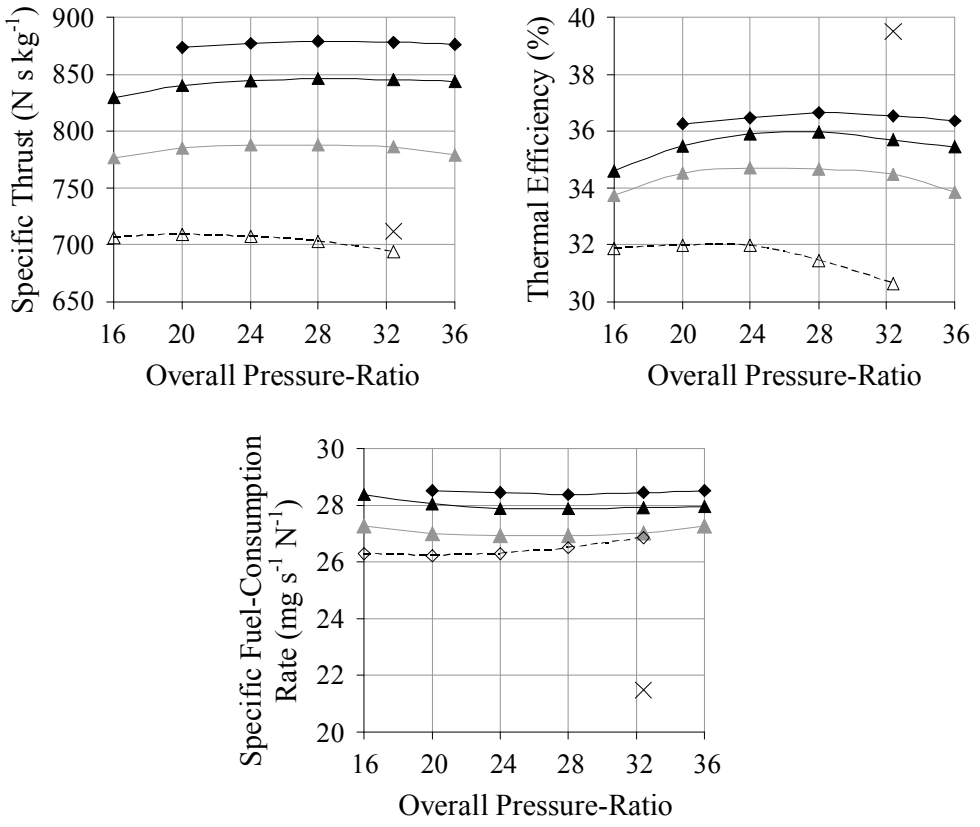

Figure 6.11. Effects of the values of the overall pressure-ratio on the two-combustor engine's performance relative to that of the baseline (F100-EQ) engine for selected turbine's entry-temperature

[F100-EQ TCE(TETs=1700K) TCE(TETs=1600K) TCE(TETs=1450K) TCE(TETs=1300K)].

6.5.4 Effects of the High-Pressure Turbine's Pressure-Ratio on the Performance of the Two-combustor Engine

Figure 6.12 shows the configuration of the proposed two-combustor engine, for which an IPC is added to the low-pressure (LP) spool. The variations in the IPC's pressure-ratio will change the HPC's pressure-ratio; thus altering the HPT's pressure-ratio. With an increase in IPC's pressure-ratio, the two-combustor engine's specific-thrust decreases, but thermal efficiency increases (see Figure 6.13). Increasing the IPC's pressure-ratio will decrease the HPC's pressure-ratio, i.e. HPT's pressure-ratio, thus shifting the ITB "toward" the main-combustor. This will enable the combustion in the ITB to occur at a higher pressure and temperature thereby raising the cycle's efficiency. Unavoidably, less fuel can be burnt in the ITB and this reduces the specific thrust of the engine. Therefore the maximum IPC's pressure-ratio is limited in order for the two-combustor engine to have adequate thrust-benefit over the conventional engine. Figure 6.14 shows the optimization of the FPR for an IPC's pressure-ratio of 4.5. Even at it optimal FPR, the two-combustor engine's thermal efficiency remains lower and its SFC remains higher than those of the baseline engine.

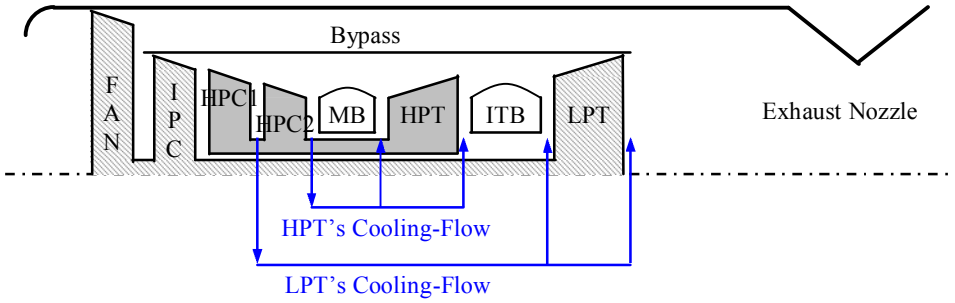

Figure 6.12. Schematic of the two-spool (with intermediate pressure compressor) two-combustor mixed-exhaust nozzle.

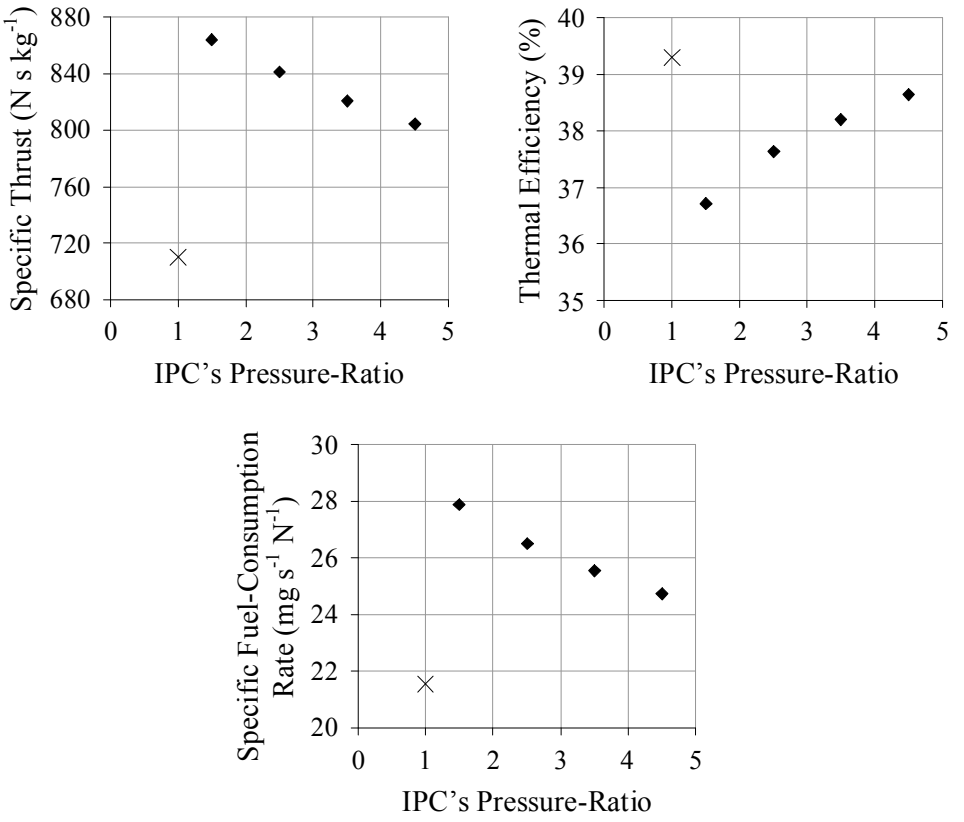

Figure 6.13. Effects of IPC's pressure-ratio on the performance of the two-combustor engines (FPR=3.55) against that of the baseline (F100-EQ) engine [× F100-EQ ◆ F100-TCE].

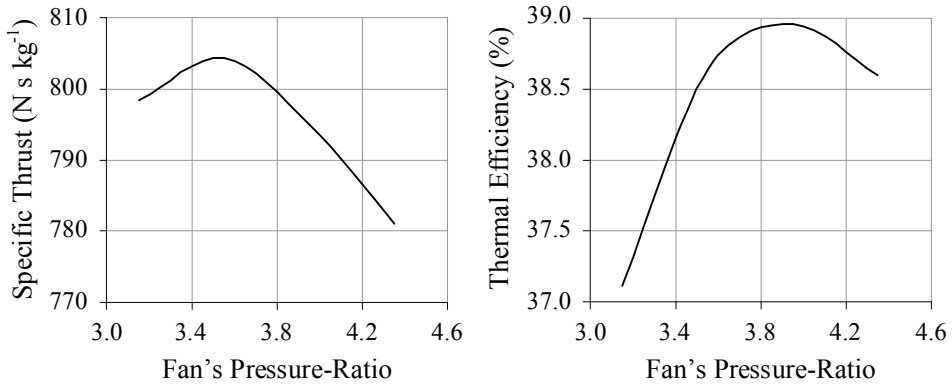

Figure 6.14. Effects of fan's pressure-ratio on the performance of the two-combustor engine (IPC's pressure-ratio=4.5) against that of the baseline (F100-EQ) engine.

6.6 Off-Design Performance of the Two-combustor Engine

The off-design performances of the baseline and two-combustor engines are studied (see Table 6.4). The configurations for the two-combustor engine are extracted from Section 6.5; whereby they are operating at maximum specific thrust condition.

6.6.1 Engines' Performance under Part-Throttle Conditions

The behaviour of the two-combustor engine has been compared with that of the baseline engine (see Figure 6.15). The behaviour of the baseline engine is controlled by its HPTET, whereas that of the two-combustor engine are controlled by its HPTET and LPTET. For the simulated results given in Figure 6.15, it is assumed that the HPTET and LPTET are simultaneously throttled-down at the same rate under part-throttle condition.

Table 6.4. Design-point conditions for the studies of baseline and two-combustor engines' performance under off-design conditions.

Parameter	Baseline Engine	Two-combustor Engine					
		Cfg1	Cfg2	Cfg3	Cfg4	Cfg5	Cfg6
H (km)	0	0	0	0	0	0	0
M_0	0	0	0	0	0	0	0
FPR	3.55	3.55	3.85	3.95	3.15	2.75	3.55
IPC's PR	N.A.	N.A.	N.A.	N.A.	N.A.	N.A.	4.5
OPR	32.4	32.4	28.0	32.4	32.4	20.0	32.4
BPR	0.36	0.36	0.36	0.10	1.00	0.36	0.36
W (kg s^{-1})	111.5	111.5	111.5	111.5	111.5	111.5	111.5
HPTET (K)	1700	1700	1700	1700	1700	1300	1700
LPTET (K)	N.A.	1700	1700	1700	1700	1300	1700

Under the design-point conditions, Cfg 2 of the two-combustor engine is operating at its optimal condition when compared with that of Cfg 1 (see Section

6.5.1). Nevertheless, under part-throttle conditions, the performance of Cfg 1 is only marginally different from that of Cfg 1, except at low throttle-settings.

Cfg 3 of the two-combustor engine, with a bypass-ratio of 0.1, has a maximum achievable thrust significantly higher, but also operates with a significantly higher SFC when compared with that of the baseline engine. The two-combustor engine with the higher BPR of 1.00 (i.e. Cfg 4) has also been considered. The maximum achievable thrust was approximately the same as that of the baseline engine, but the SFC remains higher than that of the baseline engine under both design and off-design conditions.

Under design-point conditions, Cfg 5 of the two-combustor engine has approximately the same specific thrust as that of the baseline engine. However, under both the design and off-design conditions, its SFC also remains significantly higher than that of the baseline engine. Similarly, with respect to Cfgs 1 to 5, the SFC of Cfg 6 of the two-combustor engine remains substantially higher than that of the baseline engine at the same thrust.

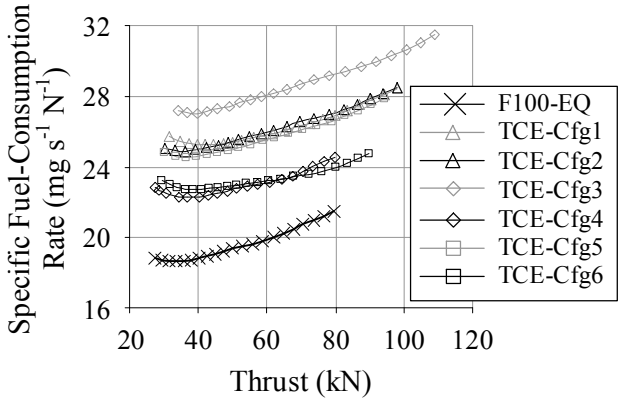

Figure 6.15. Comparisons of the off-design performances of the baseline (F100-EQ) engine and the two-combustor engines (see Table 6.4).

The influences of the TETs-schedule on the performances of the engines at part-throttle condition have also been investigated. An alternate possible TETs-schedule is to reduce the LPTET while the HPTET is kept at its maximum allowable value; subsequently reducing the HPTET after the ITB is shut-down.

To produce the same thrust, the engine's thermal efficiency is higher when "more" fuel is burnt in the main combustor than in the ITB: this results in a lower SFC (see Figure 6.16). Nevertheless, the SFCs of the two-combustor engines remain significantly higher than that of the baseline engine at comparable net-thrusts.

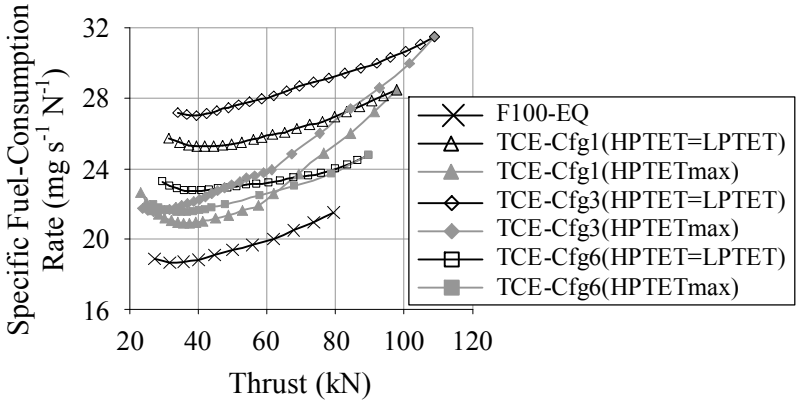

Figure 6.16. The effects of TETs-schedule on the off-design performances of the baseline (F100-EQ) engine and the two-combustor engines (see Table 6.4).

Further analysis was conducted on Cfg 1 of the two-combustor engine for various constant HPTET values (see Figure 6.17). At constant HPTET, the reduction in SFC versus net-thrust was approximately linear, and the gradients of SFC versus net-thrust for various HPTETs were approximately constant. After the shut-down of the ITB, the curves collapse into a single curve. To achieve the required thrust, it is often necessary to keep the HPTET at its highest possible value in order to achieve lowest SFC. This is further demonstrated when the other extreme of the TETs-schedule was studied; whereby the two-combustor engine's HPTET was reduced with the LPTET kept at its maximum allowable value (see Figure 6.18).

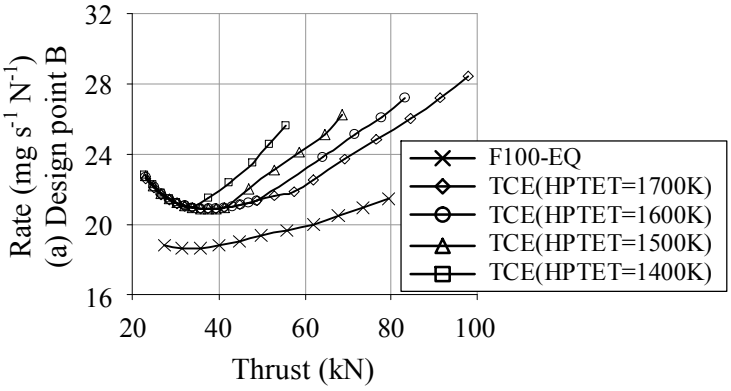

Figure 6.17. The effects of the TETs-schedule on the off-design performances of the baseline (F100-EQ) engine and the two-combustor engine configuration 1 (see Table 6.4).

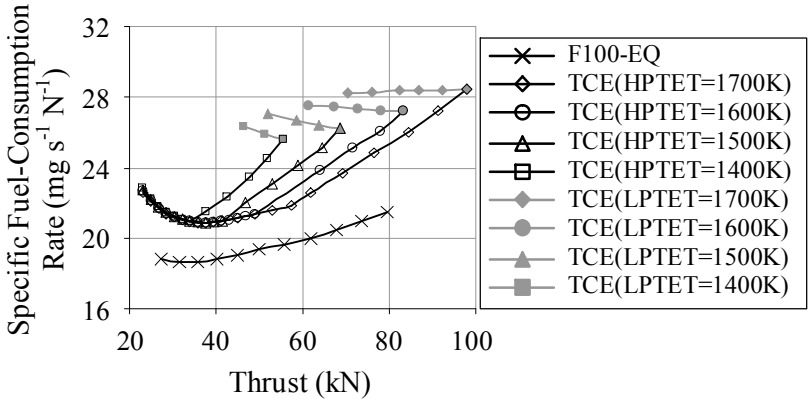

Figure 6.18. The effects of the TETs-schedule on the performances of the baseline (F100-EQ) engine and the two-combustor engine configuration 1 (see Table 6.4).

6.6.2 Engines' Performance under Full-Throttle Conditions

Figure 6.19 shows the performance of the baseline and two-combustor engines under full-throttle conditions over a range of flight Mach-numbers. Although the two-combustor engines are capable of producing higher net-thrusts, its SFCs are also higher than that of the baseline engine. The respective performance positioning of the engines remained invariant across the range of flight Mach-number considered. The corresponding engines' efficiencies are

shown in Figure 6.20. With the ITB operating at a lower pressure, the thermal efficiencies of the two-combustor engines was lower than that of the baseline engine. Also with a higher exhaust-gas velocity, the propulsive efficiency of the two-combustor engines was lower or approximately the same as that of the baseline engine. The engine's SFC was inversely proportional to its overall efficiency (i.e. the product of thermal and propulsive efficiencies). Therefore the two-combustor engine with a lower overall efficiency will operate with a higher SFC when compared with that of the baseline engine.

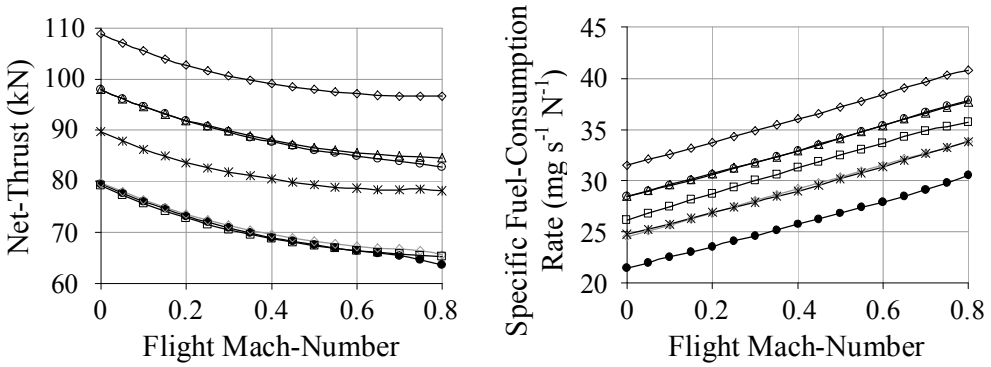

Figure 6.19. The effects of flight Mach-number on the net-thrust and specific fuel-consumption rate for the baseline and two-combustor engines (see Table 6.4)
[F100-EQ TCE-Cfg1 TCE-Cfg2 TCE-Cfg3 TCE-Cfg4 TCE-Cfg5 TCE-Cfg6].

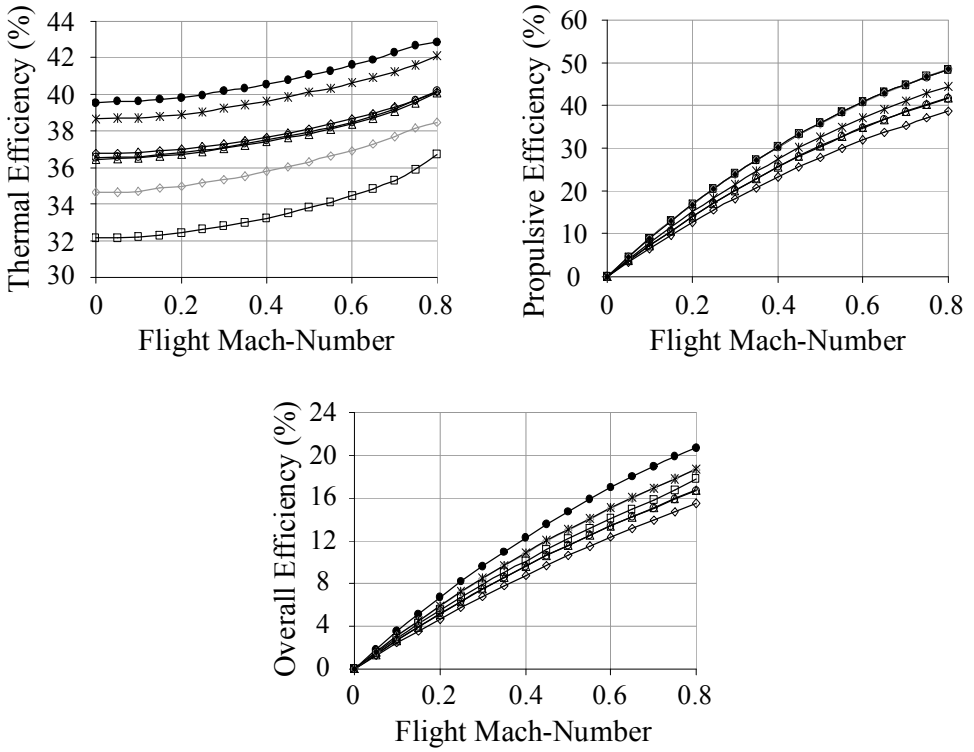

Figure 6.20. The variation in the efficiencies of the baseline and two-combustor engines (see Table 6.4) against flight Mach-number

[F100-EQ TCE-Cfg1 TCE-Cfg2 TCE-Cfg3 TCE-Cfg4 TCE-Cfg5 TCE-Cfg6].

6.7 Conclusions

The implementation of the two-combustor engine will require a higher turbine's cooling-flow rate than that for the baseline engine with the same turbine's entry-temperature. The potentials of the two-combustor engine, relative to the baseline engine, will be over-predicted when the exact turbine's cooling-flow requirement was not considered.

Parametric studies have also been conducted to investigate the influences of various design-parameters on the performance of the two-combustor engine. Generally, optimizing the use of the extra power from the ITB will improve the efficiency of the two-combustor engines. The two-combustor engine is capable of achieving a higher maximum specific thrust, but there is no evidence showing that its thermal efficiency could be higher than that of the baseline engine. Therefore

from the point of view of fuel economy, there is no incentive to the use of the two-combustor engine rather than the conventional engine. Nevertheless the benefit of the significant increase in specific thrust produced by the two-combustor engine might be worthwhile for other applications, in particular for engines in fighter jets.

The off-design performances of the two-combustor engines in comparison with that of the baseline engine have also been studied. The performances of the engines under part-throttle conditions under the sea-level static condition have been simulated. In addition, the effects of flight Mach-number have also been investigated for engines under full-throttle conditions at sea-level condition. Both sets of results reveal that the two-combustor engine requires a higher specific fuel-consumption rate when compared with that of the baseline engine for comparable thrust. There seems to be no incentive to move towards a lower design-point TETs from the aerothermodynamics performance point-of-view.

Chapter 7. Effects of Design-point and Variable Low-pressure Turbine's Nozzle-Guiding-Vanes under Off-design Conditions

7.1 Introduction

The effects of design-point's low-pressure turbine's entry-temperature (LPTET) on the two-combustor engine's off-design performance have been investigated here. Two design-point conditions are considered with different LPTET settings, whereby both design-point conditions have its high-pressure turbine's entry-temperature (HPTET) set at its maximum allowable value (i.e. 1700K). The analysis of the off-design performance is limited to the range of LPTET.

Eady [41] and Andriani et al [54] have reported the benefit of variable nozzle-guiding-vanes (NGVs) and exhaust-nozzle in enhancing the thrust produced by the two-combustor engine and the constant-temperature turbine engine, respectively. Quantitatively, the variations in the LPTET has similarity with that of an afterburner: a variable-geometry nozzle at downstream of the afterburner is required for optimum engine operation. Therefore, the effects of variable low-pressure turbine's nozzle-guiding-vanes (LPT's NGV) on the performance of the two-combustor engine are also investigated.

Contend similar to that discussed in this chapter has been published [94]. The present baseline engine model has been updated to better represent the performance of the F100-PW229 engine. Also, the two-combustor engine model has incorporated the exact turbine's cooling-flow rate, which is not considered in reference [94]. Therefore it is reasonable to presume that the findings describe in this chapter are of higher order of accuracy and reliability.

7.2 Analysis Approaches

The performances of the two-combustor engines are simulated, using TURBOMATCH, and compared with that of the baseline (i.e. F100-EQ) engine

when appropriate. The engine configurations, design points conditions and associated-assumptions are described in the following sub-sections. The relationships between the components, used to explain the trends of the engines' off-design performances, are also present.

7.2.1 Engine Configurations, Design Points and Assumptions

Table 7.1 shows the design-point conditions for both the baseline and two-combustor engine (see Figure 6.1 for layout of the two-combustor engine). Two two-combustor engines, with design-point A (DP-A) and design-point B (DP-B), are analysed. Under design-point A condition, the two-combustor engine operates fundamentally like the baseline engine, i.e. ITB turned-off. Under design-point B condition, the two-combustor engine operates at its maximum achievable thrust because both combustors burning at their maximum allowable temperatures. The conditions for design-point B, in present chapter, are identical to that for the "basic" two-combustor engine shown in Table 6.1.

The following are common assumptions made for both the baseline (i.e. F100-EQ engine) and the two-combustor engines: -

- ✓ Identical components' characteristics, under design-point condition, are applied to both engines.
- ✓ Common generic components' behavioural maps, from TURBOMATCH, are used.
- ✓ Both the engines are fitted with variable-area exhaust nozzles.
- ✓ The turbine's cooling-air distributions, for respective engine, are kept constant across on-design and off-design condition.

The turbine's cooling-flow rate for both the baseline engine and two-combustor engine (under design-point B) are calculated for respective design-point conditions. For two-combustor engine under design-point A condition, the turbines' cooling-flow rate is calculated based on its off-design condition with both the HPTET and LPTET at 1700K.

Table 7.1. Design-point conditions for the baseline (F100-EQ) and the two-combustor engines.

Parameter	**Baseline Engine**	**Two-combustor Engine**	
		DP-A	**DP-B**
Flight altitude, H (km)	0	0	0
Flight Mach-number, M_0	0	0	0
Mass-flow rate, W (kg s^{-1})	111.5	111.5	111.5
Bypass ratio, BPR	0.36	0.36	0.36
Overall pressure-ratio, OPR	32.4	32.4	32.4
Fan's pressure-ratio, FPR	3.55	3.55	3.55
HPT's Entry-Temperature, HPTET (K)	1700	1700	1700
LPT's Entry-Temperature, LPTET (K)	N.A.	ITB Off	1700

7.2.2 Components' Relationships

The relationships between the behaviours of the high-pressure turbine (HPT), low-pressure turbine (LPT) and the work-balances of the low-pressure (LP) and high-pressure (HP) spools are the main topics for discussion in accessing the two-combustor engines' off-design performances. Equation (7.1) shows the relationship between the mass-flow functions at the HPT's exit (station 6, see Figure 6.1) and LPT's inlet (station 7, see Figure 6.1) [94]. Assuming that the pressure losses across the ITB remain invariant and the LPT operates under choked conditions, Equation (7.1) becomes Equation (7.2). Equations (7.3) and (7.4) show the work-balance expressions for the HP and LP spools, respectively.

$$\left(\frac{W\sqrt{T_t}}{P_t}\right)_7 = \left(\frac{W\sqrt{T_t}}{P_t}\right)_6 \sqrt{\frac{T_{t7}}{T_{t6}}}\,\frac{P_{t6}}{P_{t7}} \tag{7.1}$$

$$\left(\frac{W\sqrt{T_t}}{P_t}\right)_6 \sqrt{\frac{T_{t7}}{T_{t6}}} = const \tag{7.2}$$

$$\left[WCp\frac{T_{t/in}}{\eta}\left(\Pi^{\frac{\gamma-1}{\gamma}}-1\right)\right]_{hpc1} + \left[WCp\frac{T_{t/in}}{\eta}\left(\Pi^{\frac{\gamma-1}{\gamma}}-1\right)\right]_{hpc2} = \left[WCpT_{t/in}\eta\left(1-\left(\frac{1}{\Pi}\right)^{\frac{\gamma-1}{\gamma}}\right)\right]_{hpt} \tag{7.3}$$

$$\left[WCp\frac{T_{t/in}}{\eta}\left(\Pi^{\frac{\gamma-1}{\gamma}} - 1 \right) \right]_{fan} = \left[WCpT_{t/in}\eta\left(1 - \left(\frac{1}{\Pi} \right)^{\frac{\gamma-1}{\gamma}} \right) \right]_{lpt} \tag{7.4}$$

The effects of varying the LPT's NGV on the two-combustor engine's off-design performances are determined. With the LPT's NGV operating at near-choked conditions (i.e. M=~1), the LPT's inlet mass-flow function is mainly governed by the LPT's NGV flow-area – see Equation (7.5) [94]. The convention adopted in this presentation is that the flow-area (and hence the mass-flow function) increases with the LPT's NGV angle.

$$\frac{W\sqrt{T_t}}{P_t} = \left(1 + \frac{\gamma-1}{2}M^2 \right)^{\frac{3\gamma-1}{2(1-\gamma)}} AM\sqrt{\frac{\gamma}{R}} \tag{7.5}$$

7.3 Performance of the Baseline Engine and the Two-combustor Engine under Design and Off-design Conditions

In the operation of the two-combustor engine, there are pressure-losses across the ITB and also higher turbine's cooling-flow rate than that for the baseline engine. Therefore the specific thrust of the two-combustor engine, under design-point A condition, is significantly lower than that achievable with the baseline engine (see Table 7.2). Also with lower combustor mass-flow rate, the fuel-consumption rate for the two-combustor engine is also lower. For two-combustor engine, under design-point B, extra fuel is burnt in the ITB to rise the flow temperature. Therefore the specific thrust and fuel-consumption rate is also higher than that of the baseline engine.

With the HPTET maintained at 1700K, the analyses for the two-combustor engines' off-design performances are conducted from ITB at turn-off condition to ITB at maximum operating condition (i.e. LPTET = 1700K) (see Figure 7.1). For design-point A, the maximum thrust achievable with the two-combustor engine is marginally higher than that of the baseline engine under design-point condition (i.e. 79.18kN). For the two-combustor engine, at design-point B, the thrust achievable with a low LPTET (i.e. below 1450K) is poorer than the baseline

engine's design-point performance (i.e. 79.18kN). Generally, the additional thrust produced by the two-combustor engine is achieved by burning more fuel in the ITB, so resulting in a higher fuel-consumption rate when compared with that of the baseline engine. In summary, the two-combustor engine under design-point A is not recommended; whereas two-combustor engine under design-point B condition is not recommended for operating at low LPTET regime.

Table 7.2. Engines' specific-thrusts and specific fuel-consumption rates under design-point conditions.

	Baseline Engine	**Two-combustor Engine**	
		DP-A	**DP-B**
Specific thrust (N s kg^{-1})	713	653	876
Fuel-consumption rate (kg s^{-1})	1.71	1.54	2.79

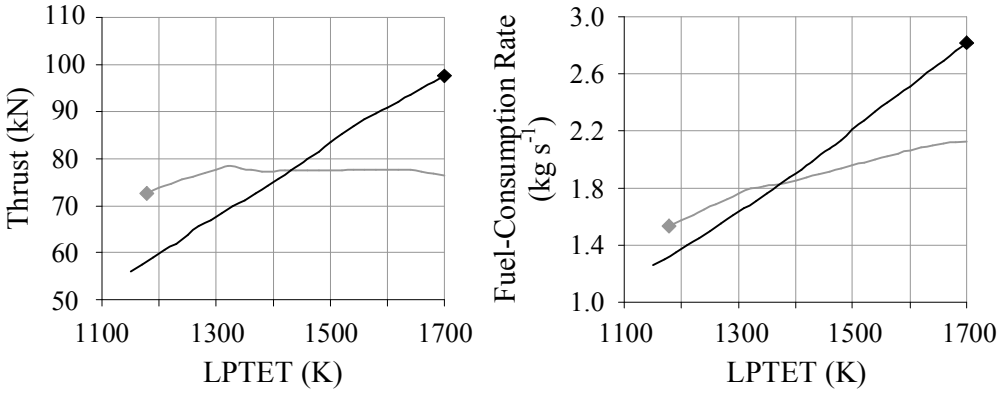

Figure 7.1. The two-combustor engine's thrusts and fuel-consumption rates versus variations in the LPTET [◆ DP-A(DP) ◆ DP-B(DP) —— DP-A(OD) —— DP-B (OD)].

7.3.1 Two-Combustor Engine under Design-Point A Condition

The increase in LPTET (T_{t7}) will increase the ITB's temperature-ratio (T_{t7}/T_{t6}) in Equation (7.2): thus the value of HPT's outlet mass-flow function (MFF_6) will decrease and lead to a fall in the HPT's pressure-ratio (see Figure 7.2). Due to the dominating effects of the decrease in the HPT's pressure-ratio,

the HPC's pressure-ratio experience a similar decreasing trend as the HPT's pressure-ratio (see Equation (7.3) and Figure 7.3).

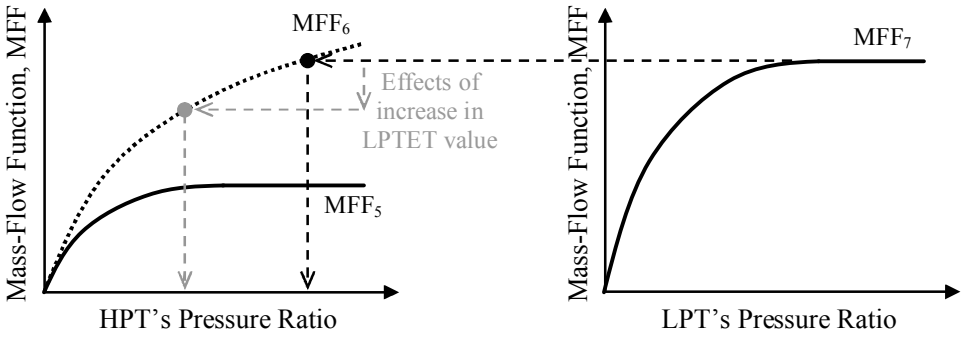

Figure 7.2. Sketch illustrating the relation between the behaviours of the low-pressure and high-pressure turbines.

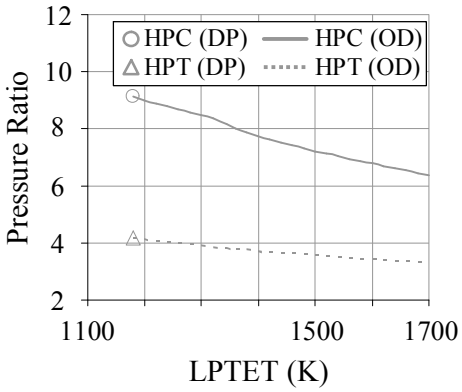

Figure 7.3. Variations of the pressure-ratios of the HPC and HPT versus the LPTET for the two-combustor engine under design-point A condition.

With the LPT operating at (near) choked condition, the LPT's inlet mass-flow function (MFF_7) is held approximately constant. Therefore the increase in LPTET (T_{t7}) will couple with a decrease in W_7/P_{t7}. With marginal variation in the LPT's inlet-pressure, there is a decrease in the LPT's mass-flow rate (see equation (7.4) and Figure 7.4); whereby the effect of an increase in the LPTET in producing a higher LPT's work is diminished. At LPTET higher than 1400K, there is a drastic decrease in the fan efficiency, which further degrades the rate of increase in the FPR with increase in LPTET (see equation (7.4) and Figure 7.5).

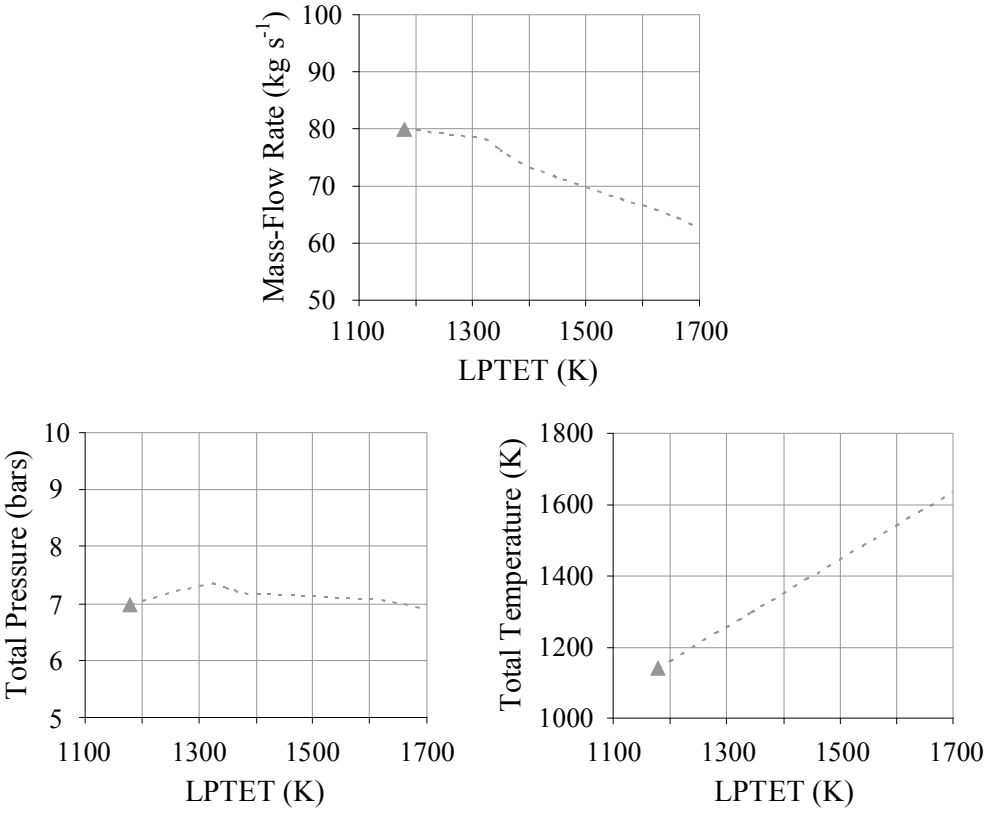

Figure 7.4. Variations of LPT's inlet flow conditions of the two-combustor engine under design-point A condition [▲ DP ····· OD].

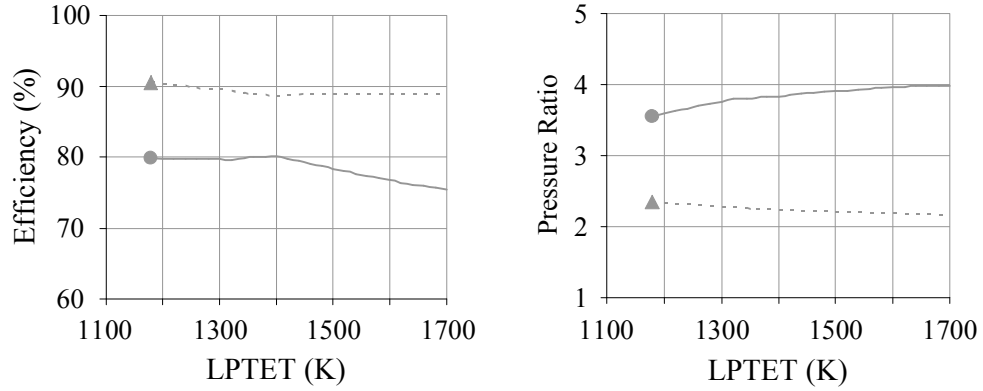

Figure 7.5. Variations in the efficiencies and pressure-ratios of the fan and LPT against LPTET for the two-combustor engine under design-point A condition [● Fan(DP) ▲ LPT(DP) —— Fan(OD) ····· LPT(OD)].

Figure 7.6 shows the variations in the nozzle's exit flow condition. At LPTET below ~1325K, the increase in nozzle's exit temperature and pressure are predominant factors, thus there is an increase in the engine's thrust (see Figure 7.1). At higher values of the LPTET (>1325K), the variations in nozzle's exit-pressure is marginal. With the influences of the decreasing mass-flow rate and increasing temperature approximately even-out, the variations in the thrust is also marginal (see Figure 7.1).

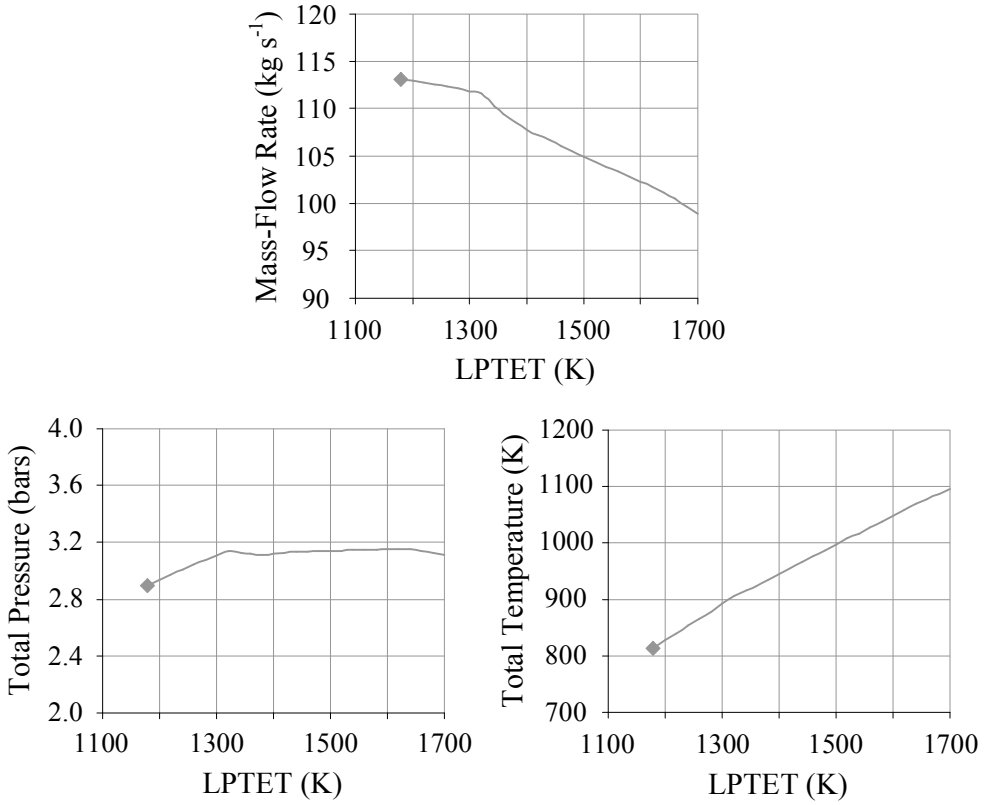

Figure 7.6. Variations of the nozzle's exit flow conditions of the two-combustor engine under design-point A condition [◆ DP —— OD].

7.3.2 Two-Combustor Engine under Design-Point B Conditions

With the LPTET (T_{t7}) decreasing, the ratio of T_{t7}/T_{t6} decreases; thus the LPT's inlet mass-flow function (MFF_7, i.e. HPT's pressure-ratio) has to increase in accordance with Equation (7.2) (see Figure 7.7). With increase in HPT's pressure-ratio as the dominating factor, the HPC's pressure-ratio is increased with reduction in the LPTET (see Equation (7.3) and Figure 7.8). Also, the LPT's

work decreases as the LPTET decreases: This result in the fan's pressure-ratio falling (see Figure 7.8).

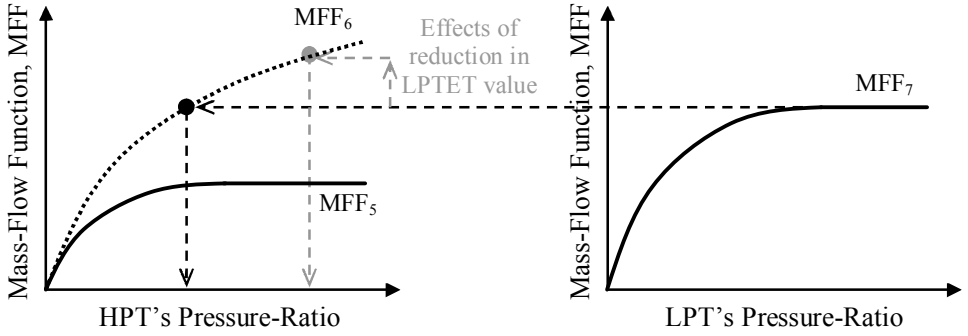

Figure 7.7. Sketch illustrating the relation between the behaviours of the low-pressure and high-pressure turbines.

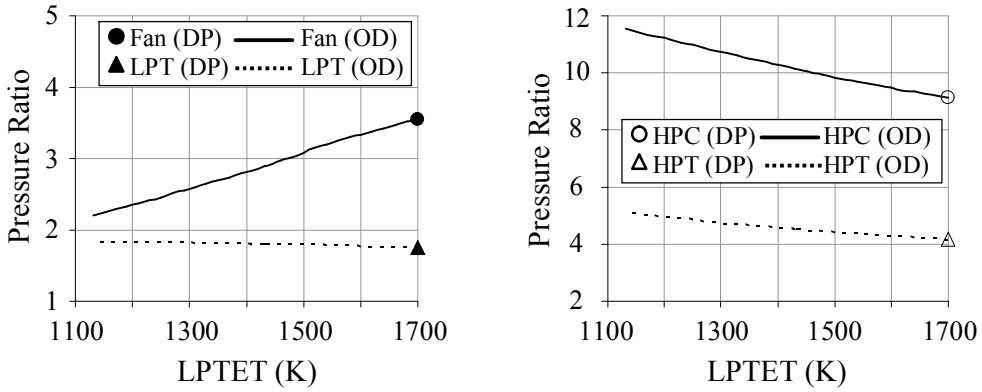

Figure 7.8. Variations in the pressure-ratios for the fan, compressor and turbines versus the LPTET for the two-combustor engine under design-point B condition.

The reduction in the FPR surpassed the increase in the HPC's pressure-ratio, hence resulting in a reduction in the mass-flow rate. Together with the reduction in the engine's nozzle temperature and pressure, the engine's thrust decreases when the LPTET decreases (see Figure 7.1 and Figure 7.9).

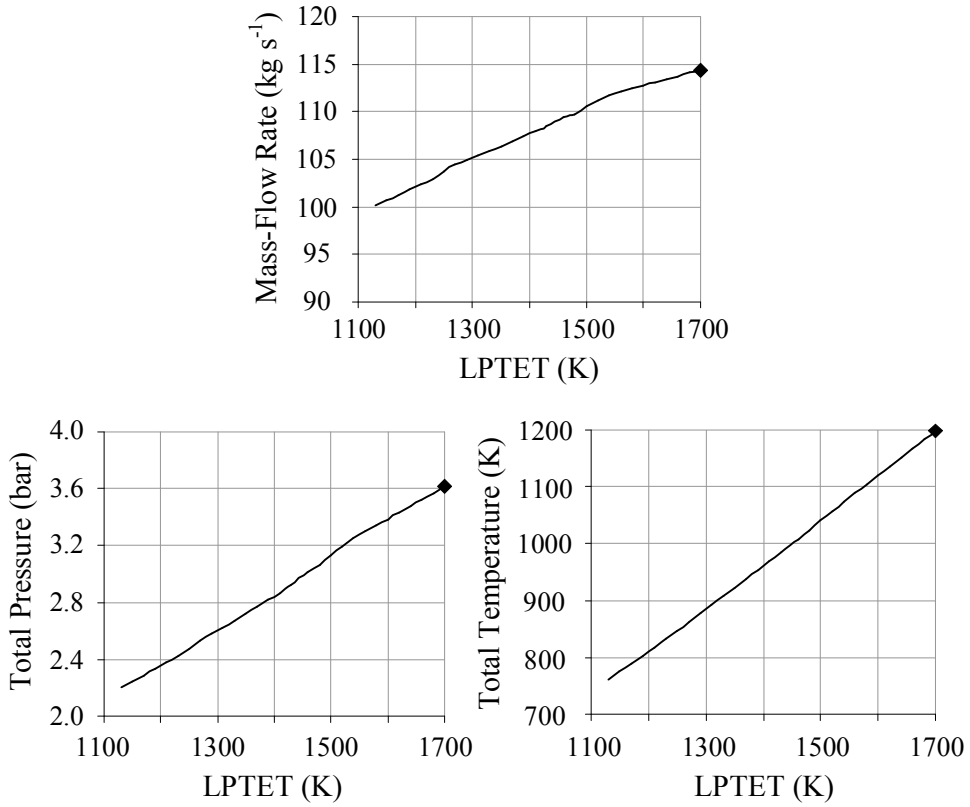

Figure 7.9. Variations of the nozzle's exit flow condition of the two-combustor engine under design-point B conditions [◆ DP —— OD].

7.4 Effects of Varying the Nozzle-Guiding-Vanes

For two-combustor engine with fixed LPT's NGV, the HPT's exit mass-flow function (MFF_6) is dependent on the LPTET value (see Figure 7.2 and Figure 7.7). In this analysis, the LPT's NGV is altered to vary its flow-area such that the HPT's exit mass-flow function (MFF_6) remains invariant at off-design conditions. With the implementation of variable LPT's NGV, the thrust of the two-combustor engine under off-design conditions is significantly higher when compared with that achievable with fixed LPT's NGV (see Figure 7.10). Similar observation was made by Eady [41] and Andriani et al [54].

Unfortunately, the improve in the thrust of the engine is achieved at the expenses of higher fuel-consumption rate (see Figure 7.10). In addition, the variations in the LPT's NGV are also limited in TURBOMATCH. Under design-

point A, the LPT's NGV of the two-combustor engine reaches it maximum limit of +20° for LPTET above 1500K (see Figure 7.11(a)). And the LPT's NGV of the two-combustor engine, under design-point B, reaches its minimum limit of -5° for LPTET below 1400K (see Figure 7.11(b)).

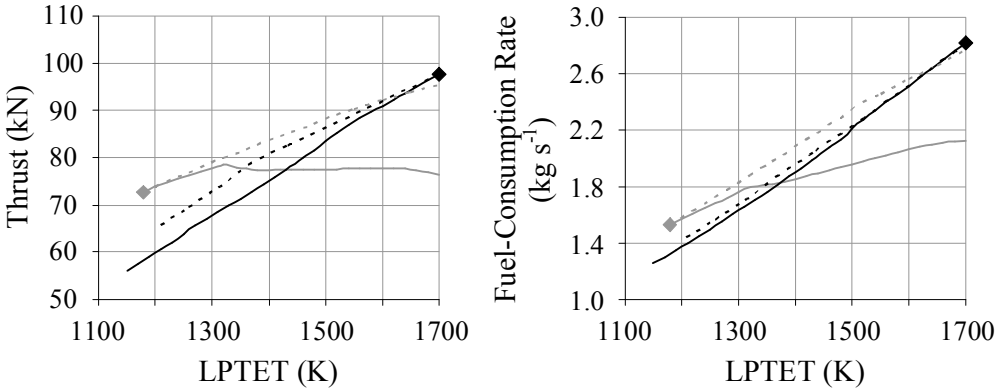

Figure 7.10. Variations in the two-combustor engine's thrusts and fuel-consumption rates for configurations with fixed and variable LPT's NGV
[◆ DP-A(DP) —— DP-A(OD)(FLPTNGV) ····· DP-A(OD)(VLPTNGV)
◆ DP-B(DP) —— DP-B(OD)(FLPTNGV) ····· DP-B (OD)(VLPTNGV)].

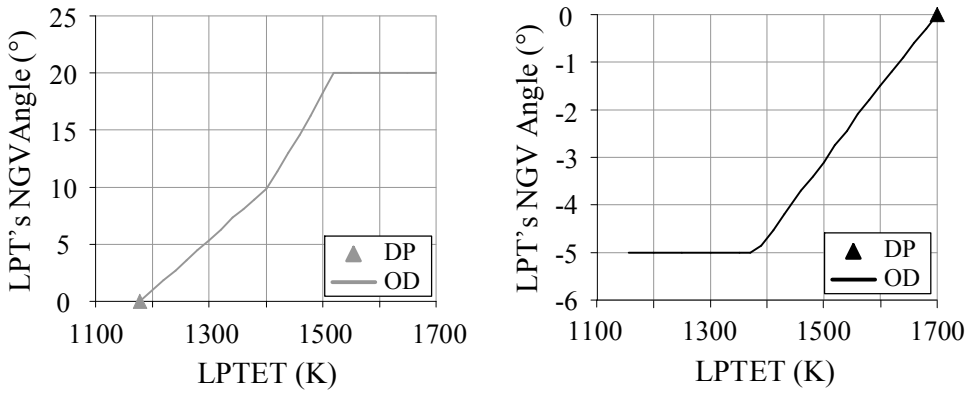

(a) Design point A Specific Fuel-Consumption

Figure 7.11. Variations of the LPT's NGV angle versus the LPTET for two-combustor engine under design-point A and B conditions.

Figure 7.12 shows the fan's surge-characteristics of the two-combustor engine. Under design-point A condition, the two-combustor engine with variable LPT's NGV has a higher surge margin. However, for the two-combustor engine under design-point B condition, the implementation of variable LPT's NGV decreases the fan's surge-margin. Nevertheless, for the considered range of LPTET, the two-combustor engine under design-point B condition always have a larger fan's surge-margin when compared with that under design-point A. In the adopted approach, the HPC is represented by two compressors; thus the HPC's surge-margin is not available.

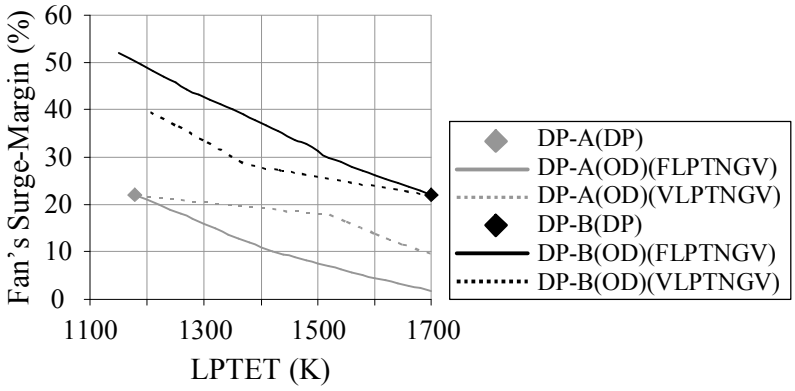

Figure 7.12. Variations of the fan's surge-margin for two-combustor engines with fixed and variable LPT's NGV.

- **<u>Two-Combustor Engine under Design-Point A Conditions</u>**

To keep the HPT's outlet mass-flow function (MFF_6) invariant, the LPT's inlet mass-flow function (MFF_7 i.e. the HPT's pressure-ratio) has to be increased appropriately with an increase of the LPTET (T_{t7}) (see Figure 7.13). The variable LPT's NGV reaches its limit of +20° at LPTET above ~1500K (see Figure 7.11(a)); thus the value of MFF_6 cannot be maintenance thereafter.

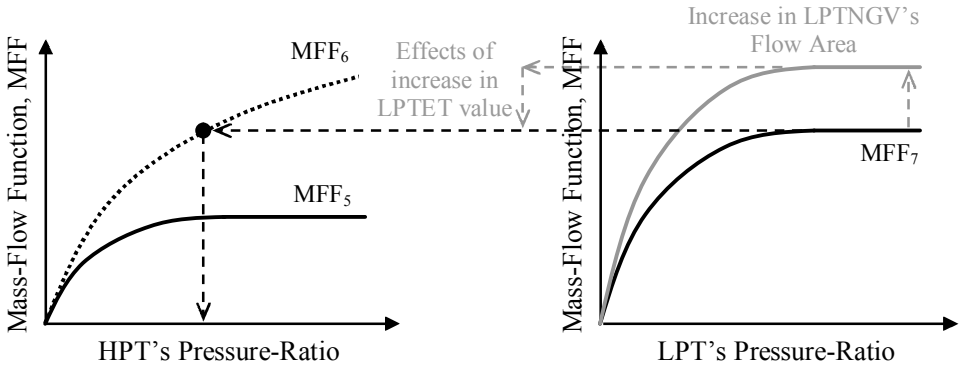

Figure 7.13. Sketch illustrating the relation between the behaviours of the low-pressure and high-pressure turbines.

With a variable LPT's NGV, to keep MFF_6 approximately constant, the FPR with variations in LPTET is marginally lower than that with a fixed LPT's NGV. However, the rate of decrease in the HPC's pressure-ratio with increase in LPTET is greatly reduced (see Figure 7.14). With the increase in the LPT's NGV angle, there is an corresponding increase in the core mass-flow rate and reduction in the engine's BPR (see Figure 7.15). However, the increase in the LPT's NGV angle reduces the LPT efficiency considerably; thus off-set the positive effects of reduced in BPR and increase in core mass-flow rate in increasing the FPR (see equation (7.4) and Figure 7.16).

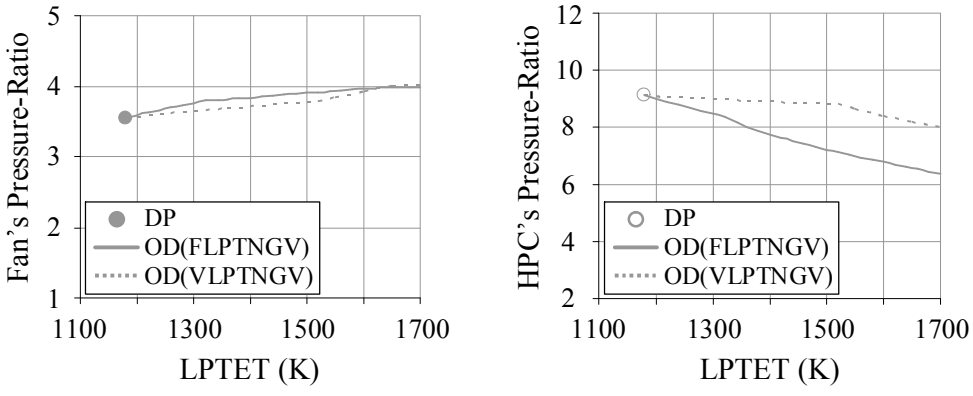

Figure 7.14. Variations in the fan's and HPC's pressure-ratios for the two-combustor engine, under the design-point A conditions, with a fixed or variable LPT's NGV.

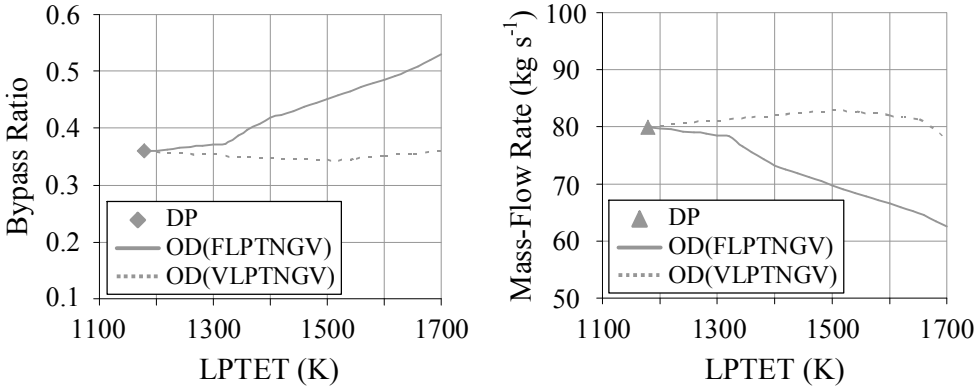

Figure 7.15. Variations of the engine's bypass-ratio and LPT's inlet mass-flow rate for the two-combustor engine, under design-point A conditions, with fixed and variable LPT's NGV.

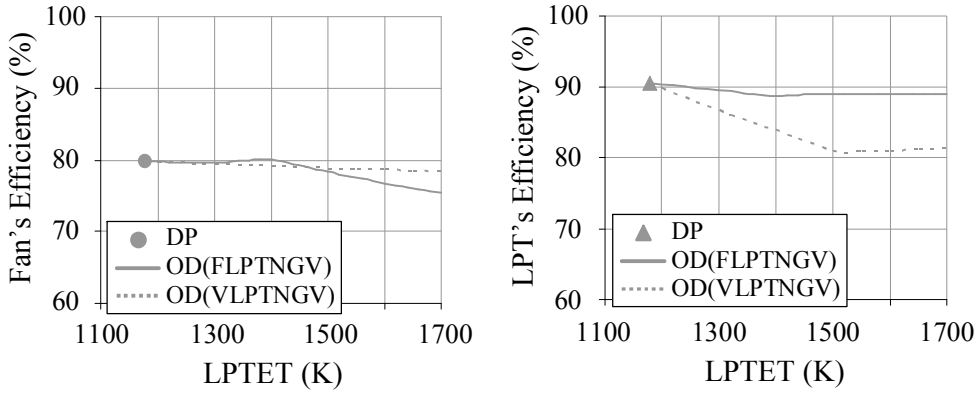

Figure 7.16. Variations of the efficiencies of the fan and LPT for the two-combustor engine, under design-point A conditions, with fixed and variable LPT's NGV.

With variable LPT's NGV, the engine mass-flow rate is significantly higher than that achievable with fixed LPT's NGV; also the reduction in BPR (with variable LPT's NGV) increases the nozzle's exit temperature (see Figure 7.17). However, the configuration with variable LPT's NGV suffers a lower nozzle's exit-pressure for LPTET below ~1420K (see Figure 7.17). Nevertheless, the former two characteristics dominated and thus result in a considerably higher thrust when compared with that achievable with fixed LPT's NGV.

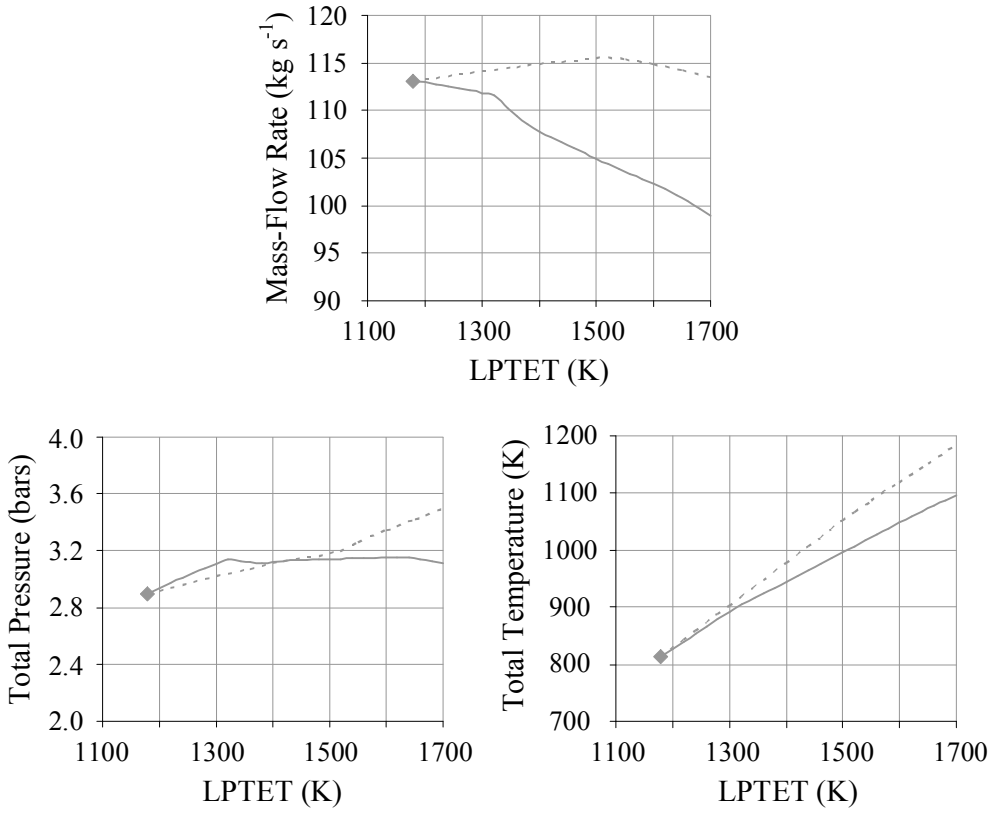

Figure 7.17. Variations in the nozzle's flow conditions over the range of LPTET for the two-combustor engine, under the design-point A conditions, with fixed and variable LPT's NGV [◆ DP ——— OD(FLPTNGV) ····· OD(VLPTNGV)].

- **<u>Two-Combustor Engine under Design-Point B conditions</u>**

With the decrease in LPTET (T_{t7}), the LPT's NGV is reduced (see Figure 7.11(b)) such that the HPT's inlet mass-flow function (MFF_6 i.e. with the HPT's pressure-ratio) remains the same as under the design-point conditions (see Figure 7.18).

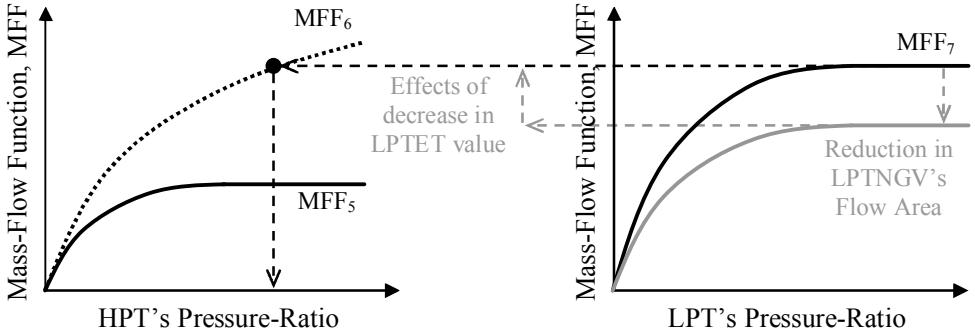

Figure 7.18. Sketch illustrating the relation between the behaviours of the low-pressure and high-pressure turbines.

The two-combustor engine under design-point B condition, with variable LPT's NGV, has lower bypass-ratio and higher core mass-flow rate when compared with that achievable with fixed LPT's NGV(see Figure 7.19). In turn, these two effects contribute to a higher FPR (see Figure 7.20). The higher core mass-flow rate and FPR are reflected in the enhanced nozzle's exit mass-flow rate and pressure, respectively (see Figure 7.21). Benefit from these two factors, the two-combustor engine with variable LPT's NGV produces higher thrust when compared with to that achievable with fixed LPT's NGV (see Figure 7.1).

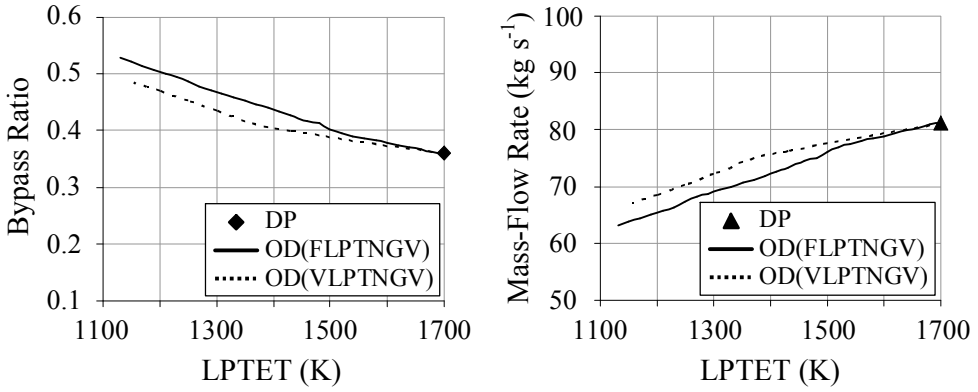

Figure 7.19. Variations of the engine's bypass-ratio and LPT's inlet mass-flow rate for the two-combustor engine, under design-point B condition, with fixed and variable LPT's NGV.

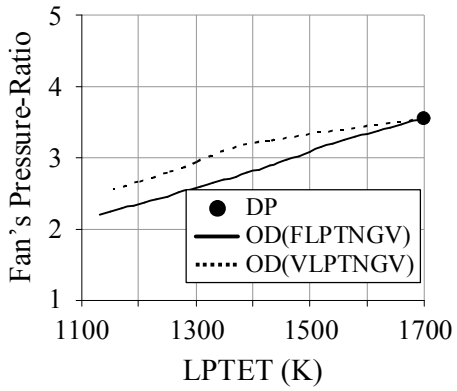

Figure 7.20. Variations of the fan's pressure-ratio over the range of LPTET for the two-combustor engine, under the design-point B condition, with fixed and variable LPTNGV.

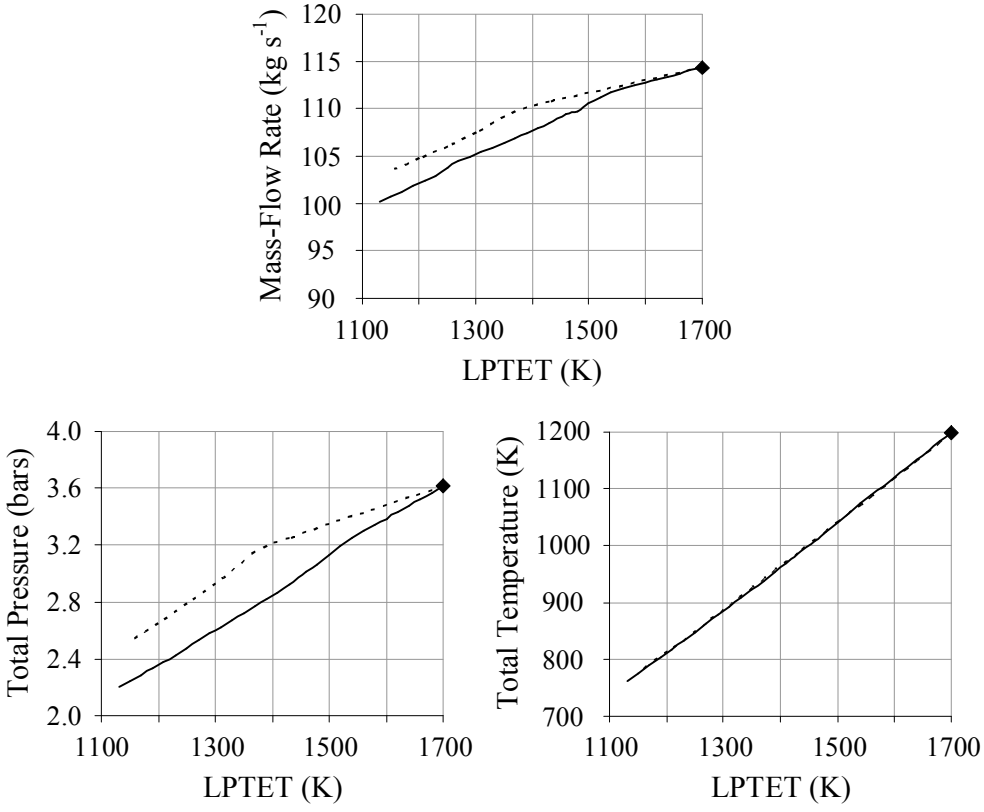

Figure 7.21. Variations of the nozzle's flow conditions over the range of LPTET for the two-combustor engine, under the design-point B condition, with fixed and variable LPT's NGV [◆ DP ——OD(FLPTNGV) ····· OD(VLPTNGV)].

7.5 Conclusions

The predictions indicate that two-combustor engines enable an extended operating envelope to be achieved compared with using a conventional engine without an afterburner. However, the potential of the two-combustor engine in generating high thrust is constrained when the LPT's NGVs' inclinations are non-variable. Further analyses have been conducted on the two-combustor engine with variable LPT's NGVs: this has produced significantly higher thrust, especially for the two-combustor engine under design-point A, when compared with that of a fixed LPT's NGV. When comparing the performance of the two-combustor engine with variable LPT's NGV under design-points A and B, the former generates higher thrust but at the expenses of higher fuel-consumption rate. However, prior to the development of variable nozzle-guiding-vanes for high temperature flow, two-combustor engine with design-point B would be a better option in achieving higher thrust when compared to design-point A.

Chapter 8. The Effects of Variable Turbine's Cooling-Flow Requirements on the Engine's Performance

8.1 Introduction

The thrust of an engine can be increased by having a higher turbine's entry-temperature (TET). However, the full-potential releasable from the increase in TET is offset by the requirements for turbine's cooling-flow [69]. Typically, the turbine's cooling-flow rate is calculated at engine's full-throttle condition, which will be over-specified under part-throttle condition. The ability to vary the turbine's cooling-flow requirement according to the engine operating-condition will enable a more efficiency engine-cycle.

Conventionally, in the simulation of the engine's performance, the ratio of the cooling-flow rate to the core mass-flow rate (bleed-air ratio) is kept invariant under both the design and off-design conditions. Precisely, this topic should be the study on the effects of variable bleed-air ratio on the engine's performance. Nevertheless, the term "variable turbine's cooling-flow requirement" is used for the ease of associating to the subject of present study.

Studies [95-97] have shown that the implementation of variable turbine's cooling-flow requirement will improve the conventional engine's performance. The influences of variable turbine's cooling-flow requirement on the aerothermodynamics performances of both the baseline (i.e. F100-EQ) engine and two-combustor engine have been investigated here; the analyses on the lifing of the turbines' vanes and blades are not included here. The adopted approach to simulate the performance of the engine with variable turbine's cooling-flow requirements is provided in Section 3.3.2.

8.2 Engines' On-design And Off-design Conditions

The design-point conditions for the baseline (F100-EQ) and two-combustor engines are as shown in Table 6.1. For the baseline engine, the off-design

performances over the range of TET are simulated. The throttling of the two-combustor engine can be controlled by varying the high-pressure and low-pressure turbines' entry-temperatures (HPTET and LPTET, respectively). The throttling-down of the two-combustor engine via two different paths are studied, i.e. configuration 1 (Cfg1) throttles-down the LPTET with HPTET kept at it maximum allowable temperature, subsequently throttles-down the HPTET after the ITB is turned-off, and configuration 2 (Cfg2) throttles-down both HPTET and LPTET at the same rate simultaneously.

8.3 Influences of Varying the Cooling-Flow Requirement on the Performance of the Baseline (F100-EQ) Engine

For the same TET, the engine with variable turbine's cooling-flow requirement is capable of producing higher thrust when compared with that achievable with a fixed turbine's cooling-flow requirement (see Figure 8.1); which is inline with the findings in references [95-97]. For comparable thrust, the engine with variable turbine's cooling-flow requirement operates with a lower TET; also achieving an increase in its thermal efficiency and a reduction in the SFC (see Figure 8.1).

With variable turbine's cooling-flow rate, there is an increase in LPT work-output to drive the fan to a higher pressure-ratio when compared with that achievable with fixed turbine's cooling-flow requirement for identical TET setting. With the engine's mass-flow rate constraints by the flow-area of the turbine's nozzle-guiding-vane, the fan for the engine with variable turbine's cooling-flow moves toward the surge line (see Figure 8.2(a)). Nevertheless, for comparable thrust, the fan for the engine with variable cooling-flow requirement has a larger surge margin when compared with that for the engine with fixed turbine's cooling-flow requirement (see Figure 8.2(b)). Since the high-pressure compressor (HPC) is modelled as two-separate compressors, its surge-margin is not available here.

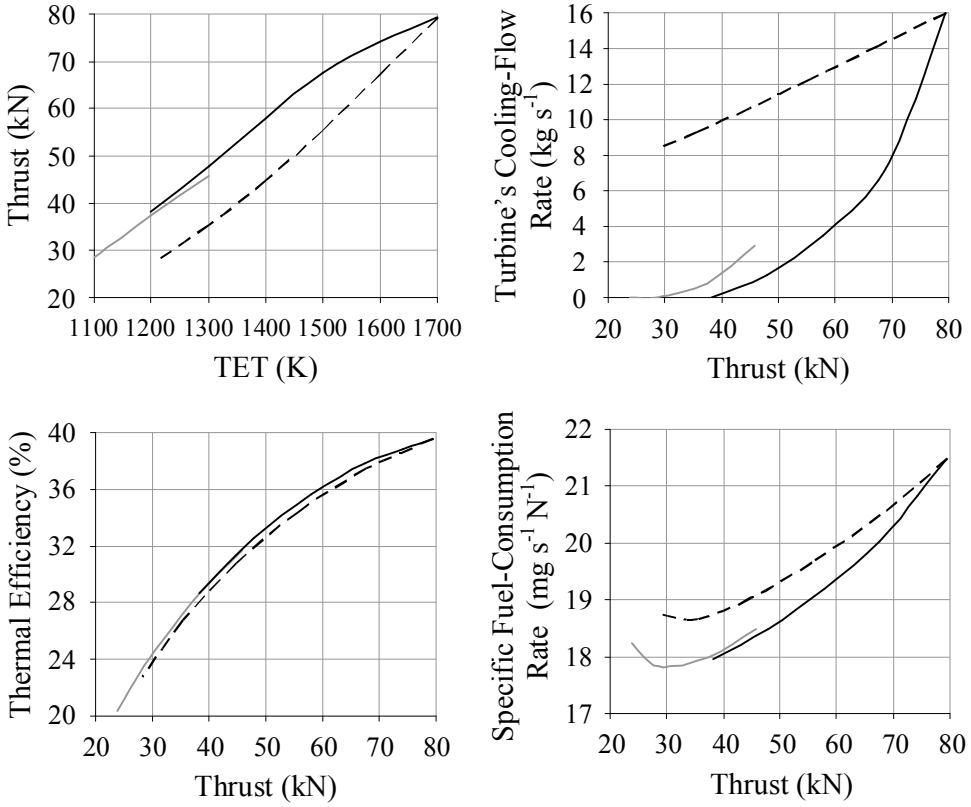

Figure 8.1. Performances of the baseline engine with fixed and variable turbine's cooling-flow requirement [---- Fixed —— Variable(ε_{film}=0.3) —— Variable(ε_{film}=0.0)].

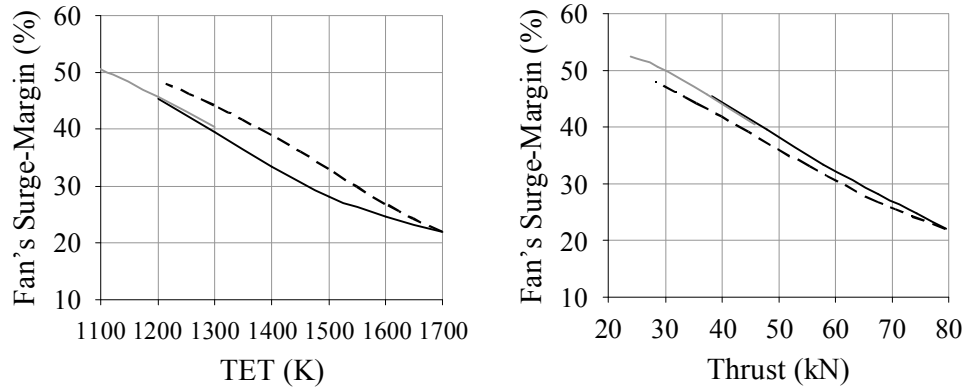

(a) Surge margin versus TET (b) Surge margin versus thrust

Figure 8.2. The fan's surge-margin for the baseline engine with fixed and variable turbine's cooling-flow requirement [---- Fixed —— Variable(ε_{film}=0.3) —— Variable(ε_{film}=0.0)].

Sensitivity study was also conducted assuming that the film-cooling effectiveness (ε_{film}) is reduced to zero for TET below 1300K. With lower value of ε_{film}, higher turbine's cooling-flow rate is required; thus penalizes on the engine's performance (see Figure 8.1 and Figure 8.2). The components' behaviours and engine's performances, for the configuration with lower value of ε_{film}, tend to that of the configuration with fixed turbine's cooling-flow requirement.

8.4 Influences of Variable Cooling-Flow Requirement on the Performance of the Two-combustor Engine

8.4.1 Two-combustor Engine - Configuration 1

For the same TETs setting, the incorporating of variable turbine's cooling-flow requirement enables the engine to achieve higher thrust (see Figure 8.3). Also, the fan of the two-combustor engine with variable turbine's cooling-flow requirement has a lower surge-margin when compared with that with fixed turbine's cooling-flow rate with identical TETs setting (see Figure 8.4). These two observations are identical to those made for the baseline engine.

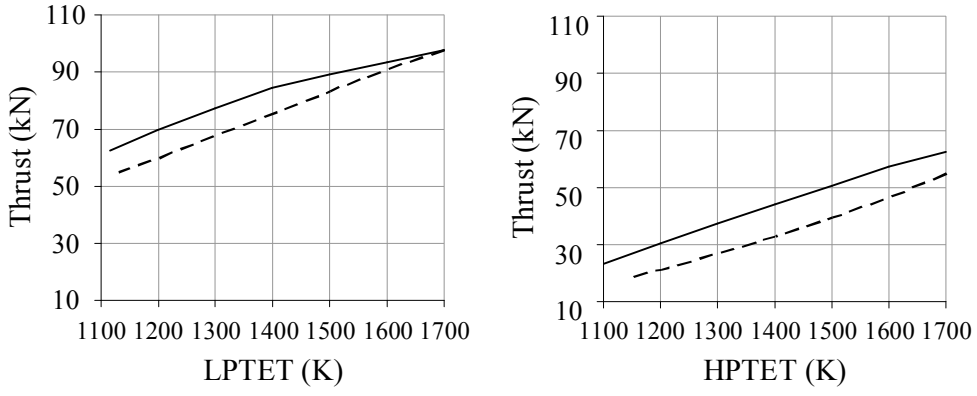

(a) HPTET keeps at 1700K (b) ITB turned-off

Figure 8.3. Thrusts of two-combustor engine (configuration 1) with fixed and variable turbine's cooling-flow requirement
[- - - - Fixed —— Variable($\varepsilon_{film/hpt}=\varepsilon_{film/lpt}=0.3$)].

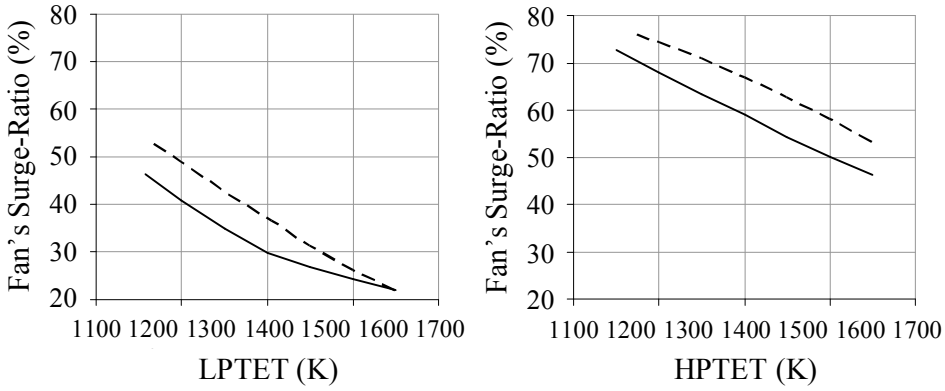

(a) HPTET keeps at 1700K (b) ITB turned-off

Figure 8.4. The fan's surge-margin for the two-combustor engine (configuration 1) with fixed and variable turbine's cooling-flow requirement [- - - - Fixed —— Variable($\varepsilon_{film/hpt}=\varepsilon_{film/lpt}=0.3$)].

During operation, the thrust of the engine is the parameter of concern, rather than the TET value. Therefore comparison is made for two-combustor engine producing comparable thrusts: the configuration with variable turbine's cooling-flow requirement has a lower SFC and a higher thermal efficiency than those of the configuration with fixed turbine's cooling-flow requirement (see Figure 8.5). This observation is also inline with that shown for that baseline engine. Similarly, the fan's surge-characteristics for two-combustor engines with fixed and variable turbine's cooling-flow requirement are compared. The latter reveals marginal difference in the fan's surge-margin when compared with that of the engine with fixed turbine's cooling-flow requirement (see Figure 8.6).

The influence of varying the film-cooling effectiveness (ε_{film}) is also investigated. Similar to the observation make for the baseline engine: the enhance in the engine's performance with implementation of variable turbine's cooling-flow rate is reduced when the film-cooling effectiveness, ε_{film}, is degraded (see Figure 8.5 and Figure 8.6).

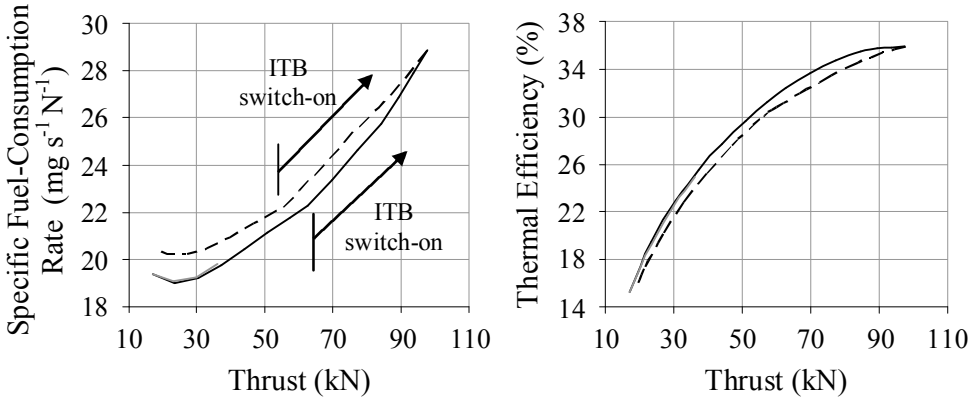

Figure 8.5. Specific fuel-consumption rates and thermal efficiencies of two-combustor engine (configuration 1) with fixed and variable cooling-flow requirement [---- Fixed —— Variable($\varepsilon_{film/hpt}=\varepsilon_{film/lpt}=0.3$) —— Variable($\varepsilon_{film/hpt}=\varepsilon_{film/lpt}=0.0$)].

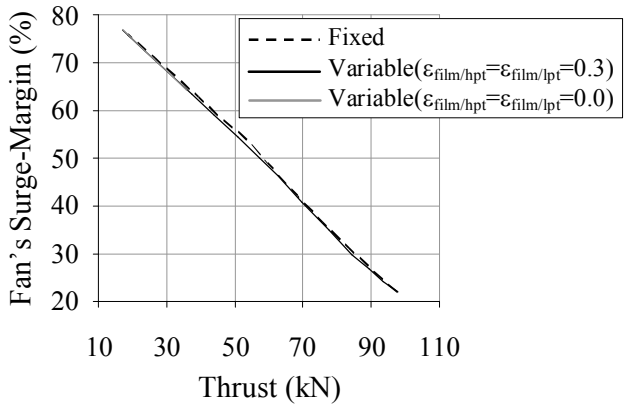

Figure 8.6. The fan's surge-margin for two-combustor engine (configuration 1) with fixed and variable turbine's cooling-flow requirement.

8.4.2 Two-combustor Engine Configuration 2

Generally, the trends associate with the implementation of variable turbine's cooling-flow requirement, on configuration 2, is identical to those for configuration 1. For comparable thrust, the two-combustor engine with variable turbine's cooling-flow requirement operates with higher thermal efficiency and lower SFC when compared with those for the same engine with fixed turbine's cooling-flow requirement (see Figure 8.7). The fan for the two-combustor engine with variable turbine's cooling-flow rate has marginally higher surge margin

when compared with that for the same engine with fixed turbine's cooling-flow requirement (see Figure 8.8).

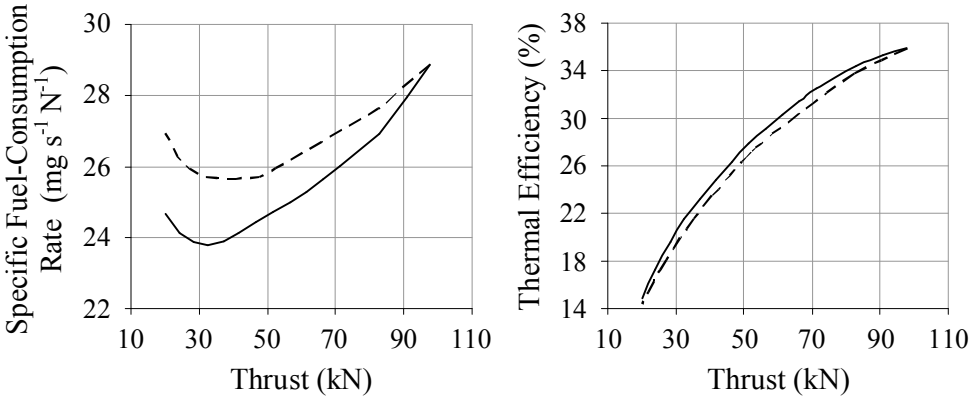

Figure 8.7. Specific fuel-consumption rates and thermal efficiencies of two-combustor engine (configuration 2) with fixed and variable turbine's cooling-flow requirement [- - - - Fixed ——— Variable($\varepsilon_{film/hpt}=\varepsilon_{film/lpt}=0.3$)].

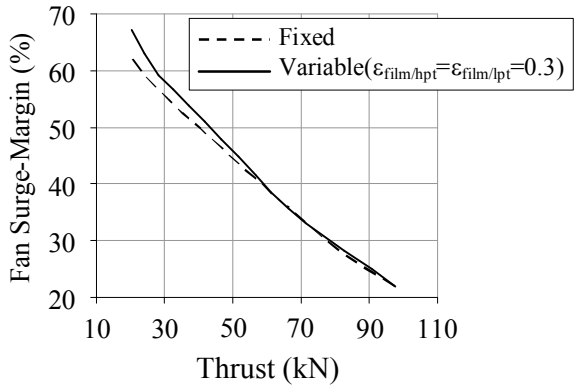

Figure 8.8. The fan's surge-margins for the two-combustor engine (configuration 2) with fixed and variable turbine's cooling-flow requirement.

8.5 Comparison of the Performances of Baseline (F100-EQ) Versus Two-combustor Engines

The present investigation has shown that both the baseline and two-combustor engines benefit from the implementation of variable turbine's cooling-flow rate i.e. lower SFC and higher thermal efficiency at comparable thrust (see Figure 8.9). Also, the reduction in SFC of the two-combustor engine is higher

than that of the baseline engine (see Figure 8.10). Generally, the amount of reduction in the SFC increases with the throttling-down of the engine. The dip in the curve for two-combustor engine at thrust of ~45kN to ~65kN is due to the increase in the HPT's cooling-flow rate with minimal reduction in LPT's cooling-flow rate. Therefore "degrading" the improvement in the reduction in SFC with the implementation of variable turbine's cooling-flow rate.

The two-combustor engine gains more benefit from the implementation of variable turbine's cooling-flow requirement than the baseline engine. Nevertheless, it does not change the respective positions of the two type of engines, i.e. the two-combustor engine operates with a larger thrust envelope (see Figure 8.9) at the expenses of higher SFC and lower thermal efficiency when compared with those of the baseline engine. It is also shown that the throttling-down of the two-combustor engine, by keeping the HPTET at it maximum allowable value, requires a lower SFC than that with both HPTET and LPTET throttle-down simultaneously; similar observation was made in Section 6.6.1). Therefore, with either the fixed or the variable cooling-flow requirement, the two-combustor engine operates more efficiently with more fuel consumed in the main combustor.

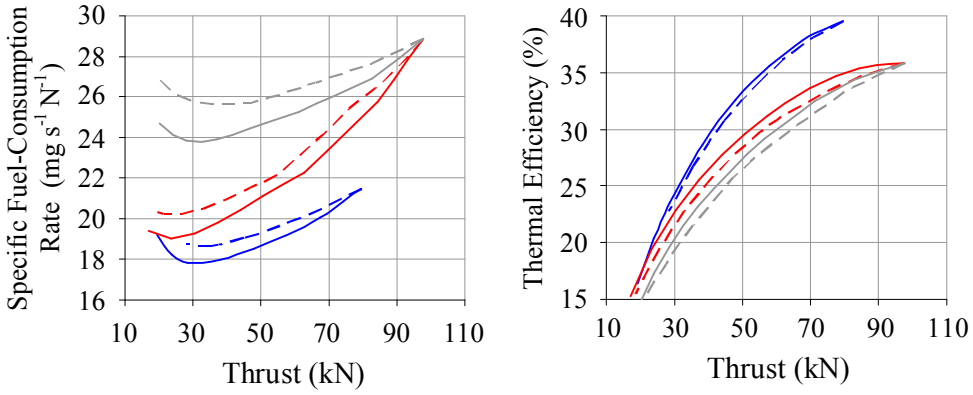

Figure 8.9. Predictions of baseline and two-combustor engines' performances with fixed and variable cooling-flow requirements
[BLE-Fixed TCE-Cfg1-Fixed TCE-Cfg2-Fixed
BLE-Variable TCE-Cgf1-Variable TCE-Cgf2-Variable].

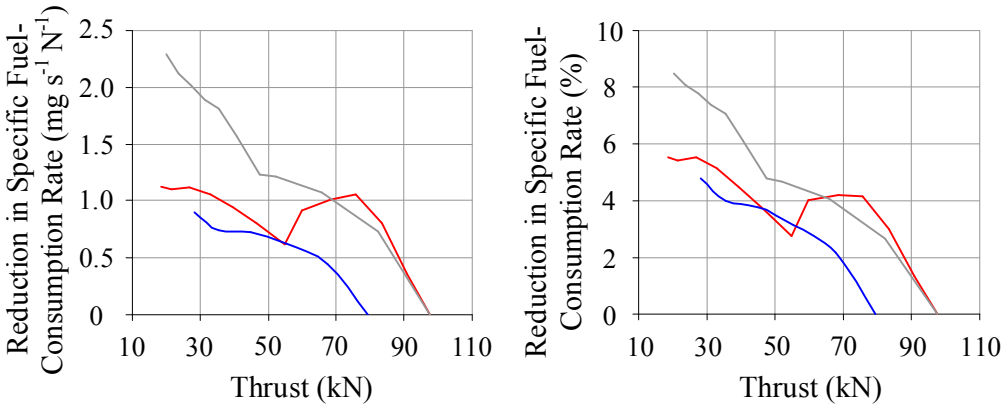

Figure 8.10. Reduction in the specific fuel-consumption rates for the engines with variable turbine's cooling-flow requirements relative to that with fixed turbines' cooling-flow requirements [BLE TCE-Cgf1 TCE-Cfg2].

Figure 8.11 shows the relationship of the fan's surge-margins versus the variations in the thrust for the baseline and two-combustor engines. The fan's surge-margins of the baseline and two-combustor engines are identical at design-point conditions. Regardless of fixed or variable turbine's cooling-flow requirement, the surge margin of the fan for the two-combustor engine is always higher than that for the baseline engine.

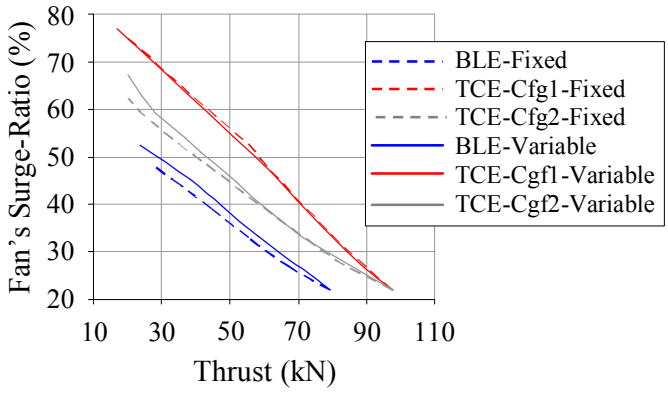

Figure 8.11. The fan's surge-margins versus variations of the thrusts for engines with fixed and variable turbine's cooling-flow requirements.

8.6 Conclusions

The implementation of variable turbine's cooling-flow requirement improves the performances of both the baseline (F100-EQ) and two-combustor engines. However, the respective positions of the engines remained i.e. the two-combustor engine produces higher maximum achievable thrust at the expenses of higher specific fuel-consumption rate when compared with those of the baseline engine. In addition, the investigation also reveals that the two-combustor engine is more efficient when more fuel is burnt in the main combustor than in the ITB.

In this analysis, a simple parametric study is also conducted by varying the value of the film-cooling effectiveness (ε_{film}); while the values of other parameters and components' characteristics are held constant. The decrease in film-cooling effectiveness increases the turbine's cooling-flow requirement, thus moving the performances of the engines towards that with fixed turbine's cooling-flow requirement. Although the accuracy of the predictions is limited, the results reveal the benefit of the incorporation of the variable turbine's cooling-flow requirement in the two-combustor engine when compared with that for the baseline engine.

Chapter 9. Sizing of the Inter-stage Turbine Burner for the Two-combustor Engine

9.1 Introduction

There are typically three types of combustor, namely the can-type, annular-type and can-annular type [98]. It is assumed that the inter-stage turbine burner (ITB), which is the same as the main combustor, is an annular-type of design (see Figure 9.1). There is limited experience of the sizing and design of the ITB, except for the sequential combustor (namely the environmental combustor) in the industrial gas-turbine GT24/26 [60-63]. Apart from the differences in the design of the environmental-combustor and that of the conventional annular-combustor, the requirements imposed on the combustor for an aero-engine and that for an industrial gas-turbine are also not identical. Nevertheless, in order to provide an initial gauge of the effects of the ITB on the overall length of the engine, existing empirical approaches for the sizing of the conventional main-combustor and afterburner have been used to estimate the ITB's size (see Section 3.3.3).

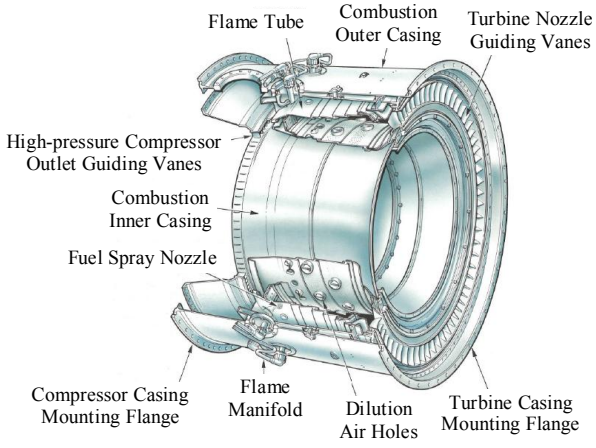

Figure 9.1. Sketch of a typical annular-type combustor [98].

9.2 Sizing of the Baseline Engine's Main-Combustor and Afterburner

9.2.1 Sizing of Main Combustor

For this assessment, the three crucial flight-conditions [69] considered are (i) the engine operating at maximum rating under sea-level static conditions; (ii) the engine idling at maximum altitude and lowest flight Mach-number; and (iii) the combustor relight at maximum required altitude and lowest flight Mach-number. The lowest achievable flight Mach-number is normally limited by the aircraft's stall-limits, which is assumed to occur at equivalent air-speed (VEAS) of 110knots [69]. Therefore the author has identified seven flight conditions for the sizing of the main-combustor (see Table 9.1).

Table 9.1. List of flight conditions for sizing of the main combustor.

Condition	Flight altitude (kft/km)	Flight Mach-number
1	0 / 0	0
2	30 / 9.144	0.305 *
3	40 / 12.192	0.390 *
4	50 / 15.240	0.500 *
5 #	30 / 9.144	0.305 *
6 #	40 / 12.192	0.390 *
7 #	50 / 15.240	0.500 *

* Equal to an equivalent air-speed (EVAS) of 110 knots.

Windmilling conditions.

The mean centerline of the main combustor, from the centreline of the engine, has been estimated to be approximately 0.246m (see Figure 5.1). The dimensions of the main combustor, for the flight condition in Table 9.1, were calculated and shown in Figure 9.2. It is obvious that the worst case, i.e. largest combustor, occurs under windmilling at the highest altitude considered (i.e 50kft / 15.24km).

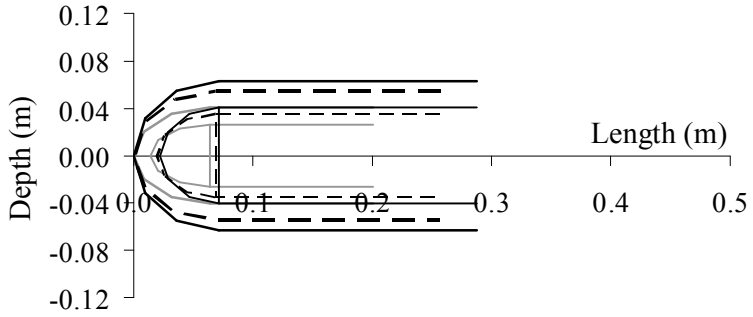

(a) Flame-on operating condition

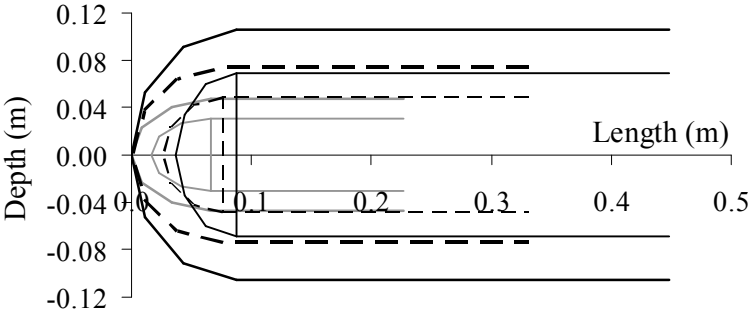

(b) Windmilling condition

Figure 9.2. Sketches for the size of the main-combustor's flame-tube (thin line) and casing (thick line) for the engine under selected flight condition (see Table 9.1) [30kft/9.144km 40kft/12.192km 50 kft/15.240km].

The size of the main combustor for the F100-PW229 engine has been estimated from Figure 3.10 and Figure 5.1. The comparison of the calculated and estimated dimensions for the main-combustor is shown Figure 9.3. At an altitude of 50kft (15.24km) and flight Mach-number of 0.5, under the windmilling condition, the calculated combustor's depth matches well with the estimated dimension. However, the calculated length of the combustor is significantly longer than the estimated dimensions. Figure 9.4 shows the variations of the combustor's length-to-depth ratio for the developed engine: the ratio decreases as more research has been undertaken. The recommended length-to-depth ratio (see Table 3.2) of various sections in the flame-tube could be for the combustor developed in the 1950s to 1970s. In the primary zone, its length should be half the flame-tube's diameter to ensure the circulation of the air. Therefore the

primary-zone's length-to-depth ratio of 0.5 is retained. In certain engine developments, the intermediate zone is omitted so as to reduce the size of the combustor. Also, with a better understanding of the combustion process and associated flow phenomena, it is likely that both the intermediate and dilution zones could also be shortened. Therefore the author applied an arbitrary correction factor on the length-to-depth ratios, for the combined intermediate and dilution zones, such that the calculated length of the flame-tube is the same as the estimated values. The combustor and pressure-loss approaches, with the above-selected correction factor, are also used in the sizing of the ITB.

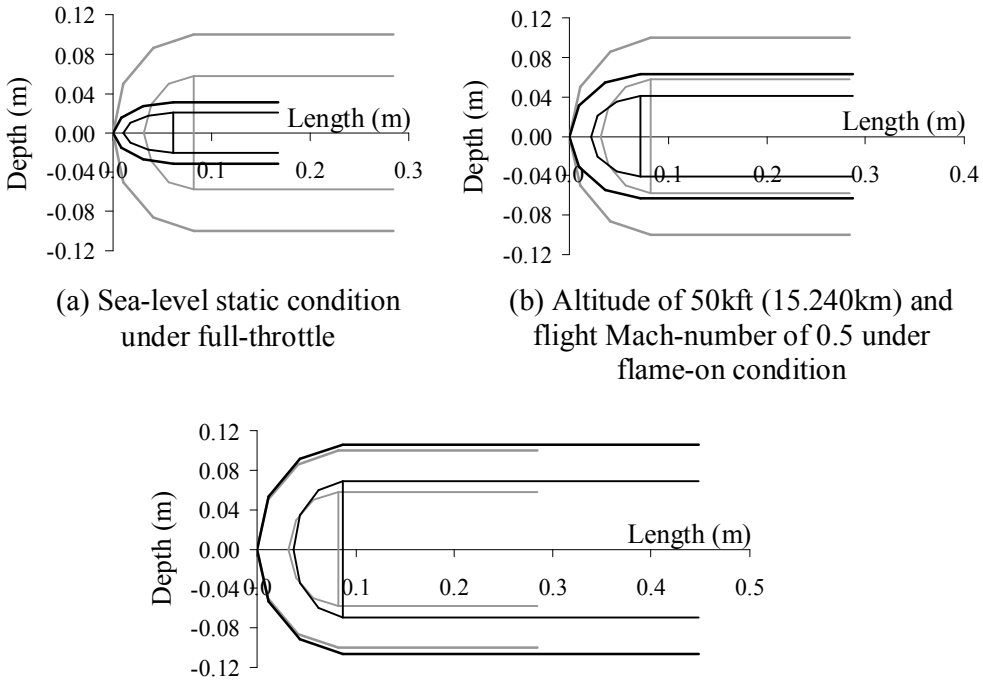

(a) Sea-level static condition under full-throttle

(b) Altitude of 50kft (15.240km) and flight Mach-number of 0.5 under flame-on condition

(c) Altitude of 50kft (15.240km) and flight Mach-number of 0.5 under the windmilling condition

Figure 9.3. Sketches of the size of the main-combustor's flame-tube (thin line) and casing (thick line) for the F100-EQ engine in comparison with those for the F100-PW229 engine [F100-PW229 F100-EQ].

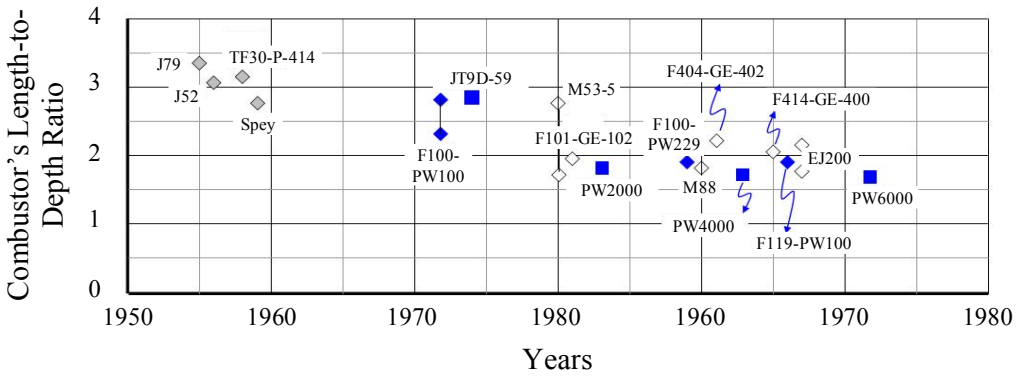

Figure 9.4. The combustor's length-to-diameter ratio relative to the year of development.

9.2.2 Sizing of the Afterburner

Using Figure 5.1, the estimated afterburner's radius (R_{ab}) and length (L_{ab}) for the F100-PW229 engine are ~0.5m and ~1.5m, respectively. For sizing the afterburner for the F100-EQ engine, a combustion efficiency of 90% and an inlet Mach-number of 0.2 are assumed [69]. The selected flight condition with corresponding afterburner dimensions are shown in Table 9.2. The radiuses of the afterburner are relatively close to 0.5m; and its length increases with the reduction in the flight Mach-number. Reference [69] states that the typical combustion-efficiency of 90% for the afterburner is for high altitude supersonic flight Mach-

Table 9.2. List of flight conditions with corresponding afterburner dimensions for the baseline (F100-EQ) engine.

Flight Condition	Flight Altitude (kft/km)	Flight Mach-number	$A_{ab}L_{ab}$ (m^2)	R_{ab} (m)	L_{ab} (m)
1	40 / 12.192	0.9	1.47	0.51	1.84
2	40 / 12.192	1.1	1.27	0.49	1.65
3	40 / 12.192	1.3	1.09	0.48	1.48
4	50 / 15.240	0.9	1.82	0.51	2.26
5	50 / 15.240	1.1	1.57	0.5	2.03
6	50 / 15.240	1.3	1.34	0.49	1.81
7	50 / 15.240	1.5	1.03	0.46	1.54

numbers. Together with the estimated afterburner dimensions of ~1.5m, the author assumed that the afterburner for the F100-PW229 engine is sized for equivalent flight conditions of 40kft/Mach1.3 and 50kft/Mach1.5. The length of the afterburner is chosen to be the longer of the two lengths calculated from these two flight-conditions.

9.3 Sizing of the Two-combustor Engine's Main-Combustor, Inter-stage Turbine Burner and Afterburner

9.3.1 Sizing of Main Combustor

The two-combustor engine's main-combustor is sized for the same flight conditions as for the baseline engine (i.e. F100-EQ engine). The worst case is expected to occur at the highest altitude and lowest flight Mach-number for the two-combustor engine under the windmilling conditions. The design-point conditions of the baseline and two-combustor engines are similar (see Table 6.1). Therefore, based on the adopted approach, the main-combustor's inlet pressure and temperature for the two-combustor engine should be identical to those of the baseline engine for both engines under the windmilling condition. Under the design-point conditions, the specific thrust of the two-combustor engine is higher than that of the baseline engine. Therefore its mass-flow function is greater than that of the baseline engine under the identical windmilling condition (see Figure 3.7). Based on Equation (3.13) and the above information, a smaller main-combustor is required for the two-combustor engine when compared with that for the baseline engine. Nevertheless to be conservative, the size of the main combustor for the two-combustor engine is assumed to be the same as that of the baseline engine.

9.3.2 Sizing of the Inter-stage Turbine Burner

The effects of the variations of various parameters (e.g. flight altitude and Mach-number) on the size of the ITB have been investigated in order to identify the largest ITB-size required. The ability for the ITB to relight with the engine

under the windmilling condition might not be necessary: the main combustor can be re-lighted prior to the ITB.

The approaches of CombSizing-Method-A and Afterburner-Method-A have been developed for sizing the main-combustor and afterburner for a conventional engine. A similar approach is not available for sizing the inter-stage turbine burner (ITB). The author has employed both the CombSizing-Method-A and Afterburner-Method-A approaches to size the ITB. And the ITB's centerline is assumed to be identical to that of the main-combustor, i.e. approximately 0.246m from the engine's centerline. For the Afterburner-Method-A, the cross-sectional area of the ITB, i.e. its depth, was calculated assuming an inlet flow Mach-number of 0.1 for acceptable pressure-losses across the ITB. This "combined-approach" would provide estimated limits on the size of the ITB for the various flight conditions.

- **Sea-level Static Conditions for Achieving Maximum Thrust**

The size of the ITB is significantly larger than that of the main-combustor (see Table 9.3). This is because the ITB is operating with a significantly lower inlet-pressure and higher mass-flow rate; therefore the combustor has to be larger to meet the requirement for combustion efficiency, i.e. 98%. Also, the required size for the ITB increases with the throttling-down of the engine. However, there is no requirement to operate at a low throttle-setting for a prolonged duration. Therefore a lower combustion efficiency could be tolerated in exchange for a combustor of smaller size. Nevertheless, the size of the ITB at sea-level static conditions is not expected to be the worst case, i.e. the largest size.

Two main observations are made concerning the predictions from this "combined-approach". First, the size of the main combustor calculated using the combustor approach is larger than that calculated using the pressure-loss approach; whereas for the sizing of the ITB, the size calculated using the pressure-loss approach exceeds that calculated using the combustor approach. Secondly, the CombSizing-Method-A predicts a larger ITB-size than the Afterburner-Method-A when the engine is at full-throttle. However the CombSizing-Method-A predicts a smaller ITB-size than the Afterburner-Method-A when the engine is

at part-throttle. These observations are due to the difference in the "weightings" given for the various parameters in the respective approaches.

Table 9.3. The size of the inter-stage turbine burner for engine operating under the sea-level static condition.

H (kft/km)	M_0	CombSizing-Method-A			Afterburner-Method-A			Remarks
		D_{itb} (m)	L_{itb} (m)	Vol_{itb} (m^3)	D_{itb} (m)	L_{itb} (m)	Vol_{itb} (m^3)	
0 / 0	0	0.36	0.46	0.25	0.26	0. 31	0.14	Full-throttle
0 / 0	0	0.44	0.55	0.38	0.27	1.14	0.51	TETs=1100K

- **Effects of Flight Altitude**

Table 9.4 shows the effects of flight altitude on the size of the ITB for the two-combustor engine operating at a flight Mach-number of 0.9 under full-throttle condition. The size of the ITB calculated using CombSizing-Method-A is nearly independent of the flight altitude; whereas using the Afterburner-Method-A, the calculated ITB-size is the largest at the highest altitude considered, i.e. 50kft (15.240km).

Table 9.4. Effects of flight altitude on the size of the required inter-stage turbine burner.

H (kft/km)	M_0	CombSizing-Method-A			Afterburner-Method-A		
		D_{itb} (m)	L_{itb} (m)	Vol_{itb} (m^3)	D_{itb} (m)	L_{itb} (m)	Vol_{itb} (m^3)
30/9.144	0.90	0.36	0.46	0.25	0.31	0.33	0.17
40/12.192	0.90	0.36	0.46	0.25	0.31	0.39	0.20
50/15.240	0.90	0.36	0.46	0.25	0.31	0.48	0.25

- **Effects of Flight Mach-Number**

The study has been extended to investigate the effects of flight Mach-number at an altitude of 50kft, i.e. 15.24km. The size of the ITB, calculated using the CombSizing-Method-A, is approximately the same across the flight Mach-numbers considered (see Table 9.5). When the Afterburner-Method-A is used, the required ITB-size is larger at lower flight Mach-numbers.

Table 9.5. Effects of flight Mach-number on the size of the inter-stage turbine burner.

H (kft/km)	M_0	CombSizing-Method-A			Afterburner-Method-A		
		D_{itb} (m)	L_{itb} (m)	Vol_{itb} (m^3)	D_{itb} (m)	L_{itb} (m)	Vol_{itb} (m^3)
50/15.240	0.50	0.36	0.46	0.26	0.31	0.71	0.37
50/15.240	0.70	0.36	0.46	0.26	0.31	0.59	0.31
50/15.240	0.90	0.36	0.46	0.25	0.31	0.48	0.25
50/15.240	1.10	0.36	0.46	0.25	0.31	0.45	0.23
50/15.240	1.30	0.36	0.46	0.25	0.31	0.42	0.22

- **Effects of Lowest Flight Mach-number at Various Altitudes**

Based on the results from the studies on the effects of altitude and flight Mach-number, the ITB is sized for altitudes of 30kft, 40ft and 50kft for the engine operating at the aircraft stall-limits, i.e. VEAS of 110knots (see Table 9.6). Using the CombSizing-Method-A, the size of the ITB is nearly independent of the flight conditions; whereas using Afterburner-Method-A, the required size of the ITB increases with the flight altitude.

Table 9.6. The size of the inter-stage turbine burner at high altitudes and lowest flight Mach-numbers under full-throttle conditions.

H (kft/km)	M_0	CombSizing-Method-A			Afterburner-Method-A		
		D_{itb} (m)	L_{itb} (m)	Vol_{itb} (m^3)	D_{itb} (m)	L_{itb} (m)	Vol_{itb} (m^3)
30/9.144	0.30	0.36	0.46	0.26	0.31	0.47	0.24
40/12.192	0.39	0.36	0.46	0.26	0.31	0.65	0.34
50/15.240	0.50	0.36	0.46	0.26	0.31	0.71	0.37

- **Effects of Part Throttle**

The effects of part-throttle condition on the size of the ITB have been studied for an altitude of 50kft (i.e. 15.24km) and flight Mach-number of 0.90 (see Table 9.7). The sizes of the ITB calculated by the two approaches are significantly different, but both approaches show that the worst case (i.e. the largest ITB size) occurs when both the HPTET and LPTET are set at the lowest considered values.

Table 9.7. Effects of various combinations of high-pressure and low-pressure turbine's entry-temperature (HPTET and LPTET) on the size of inter-stage turbine burner.

H (kft/km)	M_0	CombSizing-Method-A			Afterburner-Method-A			HPTET (K)	LPTET (K)
		D_{itb} (m)	L_{itb} (m)	Vol_{itb} (m^3)	D_{itb} (m)	L_{itb} (m)	Vol_{itb} (m^3)		
50/15.24	0.90	0.36	0.46	0.25	0.31	0.48	0.25	1700	1700
50/15.24	0.90	0.36	0.46	0.26	0.31	0.60	0.31	1600	1600
50/15.24	0.90	0.36	0.46	0.26	0.31	0.76	0.39	1500	1500
50/15.24	0.90	0.41	0.51	0.32	0.31	0.96	0.49	1400	1400
50/15.24	0.90	0.51	0.63	0.45	0.31	1.21	0.61	1300	1300

The ITB is sized at lowest flight Mach-number for TETs of 1300K (see Table 9.8). The calculated size of the ITB exceeds that calculated for flight Mach-number of 0.9 at the same altitude and TETs setting. The "increase" in the ITB length with the "reduction" in the flight's Mach-number is ~9%. Conservatively, the worst case (i.e. largest ITB size) occurs at the highest altitude, lowest flight Mach-number and lowest TETs considered. However, at an altitude of 50kft (i.e. 15.240kft) with the TETs of 1300K, the ITB's mean diameter would have to be shifted to accommodate the depth of the ITB (see Table 9.8) or a lower combustion efficiency would have to be accepted for a smaller ITB-size.

Table 9.8. The effects of various combinations of HPTET and LPTET on the size of the inter-stage turbine burner.

H (kft/km)	M_0	CombSizing-Method-A			Afterburner-Method-A			Remarks	
		D_{itb} (m)	L_{itb} (m)	Vol_{itb} (m^3)	D_{itb} (m)	L_{itb} (m)	Vol_{itb} (m^3)	HPTET (K)	LPTET (K)
30/9.144	0.305	0.40	0.50	0.31	0.31	0.95	0.49	1300	1300
40/12.192	0.39	0.46	0.57	0.41	0.31	1.10	0.56	1300	1300
50/15.240	0.50	**0.56**	**0.69**	**0.60**	0.31	1.32	0.68	1300	1300
50/15.240	0.50	**0.50***	**0.69**	**0.60**	**0.31**	**1.32**	**0.68**	1300	1300

* ITB's mean diameter shift from 0.246m to 0.300m.

The alternate TETs-schedules for the two-combustor engine are (i) engine operating with maximum allowable HPTET and (ii) engine operating with

maximum allowable LPTET. The latter results in an engine with low cycle efficiency, thus it is not considered here. The former is considered as part of the study for the relighting of the ITB in next section.

- **Relighting of Inter-stage Turbine Burner**

For the ITB under relight condition, a lower combustion-efficiency was accepted in order to reduce the size of the ITB. For the combustor approach, a combustion efficiency of 75% is selected with a corresponding θ-value of 1.5×10^{7} $Pa^{1.8}m^{2.75}kg^{-1}s$. The calculated ITB-size using CombSizing-Method-A is approximately the same for the conditions considered (see Table 9.9); whereas using Afterburner-Method-A, the calculated ITB size is largest at the lowest HPTET considered (see Table 9.9). Generally, the size of the ITB can be reduced by limiting its relight envelope to a higher HPTET value.

Table 9.9. Effects of the high-pressure turbine's entry-temperature on the size of inter-stage turbine burner under relight condition.

H (kft/km)	M_0	CombSizing-Method-A			Afterburner-Method-A			HPTET (K)
		D_{itb} (m)	L_{itb} (m)	Vol_{itb} (m^3)	D_{itb} (m)	L_{itb} (m)	Vol_{itb} (m^3)	
30/9.144	0.30	0.441	0.548	0.373	0.377	0.595	0.372	1200
30/9.144	0.30	0.441	0.548	0.374	0.375	0.984	0.612	1000
30/9.144	0.30	0.437	0.543	0.367	0.370	1.599	0.981	800
40/12.192	0.39	0.446	0.553	0.381	0.381	0.703	0.444	1200
40/12.192	0.39	0.446	0.553	0.381	0.379	1.157	0.727	1000
40/12.192	0.39	0.440	0.547	0.373	0.372	1.975	1.220	800
50/15.240	0.50	0.445	0.552	0.380	0.380	0.835	0.527	1200
50/15.240	0.50	0.445	0.552	0.380	0.378	1.376	0.863	1000
50/15.240	0.50	0.439	0.546	0.370	0.371	2.352	1.449	800

- **Summary**

Combining the results from the above investigations, the following conclusions can be drawn.

✓ CombSizing-Method-A: The worst case (i.e. largest ITB size) is with the two-combustor engine operating at the highest flight altitude and lowest

flight Mach-number under TETs of 1300K. For any TETs lower than 1300K, the thrust produced by the two-combustor engine would (probably) not be sufficient to overcome the drag of the aircraft. The calculated ITB diameter is ~0.56m and length of ~0.69m. The mean diameter of the ITB would have to be higher (i.e. a shift from 0.246m to 0.300m) or a lower combustion efficiency has to be accepted for a smaller ITB size. Another case considered is for the sea-level static condition, whereby the size of the ITB increases with the engine at lower throttle position. Considering start-up progress, the main-combustor might have to be lighted prior to the ITB in order to keep the ITB size at an acceptable level.

- ✓ Afterburner-Method-A: Generally, assuming an inlet flow Mach-number of 0.1, this approach would suggest a thinner, but longer ITB shape compared with that calculated using CombSizing-Method-A. The worst scenario occurs for altitude-relight of the ITB (with the main combustor lighted). The largest ITB size required occurs for the maximum flight altitude with lowest allowable HPTET. Therefore the lowest allowable HPTET to relight the ITB will have to be limited in order to have an ITB of acceptable size.

9.3.3 Sizing of the Afterburner

The afterburner for the two-combustor engine is sized using the same approach as for the conventional engine. To meet the requirement of 90% and also to have a like-for-like comparison, the two flight conditions identified for the sizing of the baseline engine's afterburner are used here (see Section 9.2.2). Based on the length of the afterburner, the worst case occurs at an altitude of 50kft (i.e. 15.24km) and flight Mach-number of 1.5 (see Table 9.10). The corresponding calculated length of the afterburner for the two-combustor engine is ~0.59m, which is significantly shorter than that for the baseline engine. This is because the afterburner's inlet gas temperature for the two-combustor engine is significantly higher than that for the baseline engine.

Table 9.10. Afterburner volume ($A_{ab}L_{ab}$) and length for the two-combustor engine.

Flight Condition	Flight Altitude (kft/km)	Flight Mach-number	$A_{ab}L_{ab}$ (m^2)	R_{ab} (m)	L_{ab} (m)
1	40 / 12.192	1.3	0.46	0.51	0.57
2	50 / 15.240	1.5	0.44	0.49	0.59

9.4 Sizing of the Diffuser

The diffuser is installed at the inlet of the combustor to reduce the combustor's pressure-loss to an acceptable level. The author assumes that the dump diffuser will be used for the ITB, in which a lower efficiency is accepted for a shorter diffuser. The flow velocity is reduced by 30% [98] as it flows through the diffuser.

Generally, the dimensions of the diffuser are independent of the flight altitude and Mach-number when the two-combustor engine is operating at its full throttle condition (see Table 9.11 to Table 9.13). Similarly when the TETs (i.e. HPTET and LPTET) are throttled-down at the same rate simultaneously, the dimensions of the diffuser remain nearly the same (see Table 9.13). Another set of conditions investigated is to relight the ITB with the main combustor operating with various HPTET values (see Table 9.14). Generally, the diffuser size is weakly dependent on the HPTET value. Conservatively, the diffuser's inlet and outlet depths are 0.13m and 0.20m, respectively. With an included angle of 11° [77], the length of the diffuser is 0.34m.

Table 9.11. Dimensions of the diffuser at the lowest allowable flight Mach-number for the engine being used at full throttle.

H (ft/km)	M_0	$D_{diff\text{-}in}$ (m)	$D_{diff\text{-}out}$ (m)	L_{diff} (m)
0 / 0	0	0.106	0.158	0.273
30 / 9.144	0.30	0.106	0.159	0.275
40 / 12.192	0.39	0.106	0.159	0.275
50 / 15.240	0.50	0.106	0.159	0.275

Table 9.12. Dimensions of the diffuser at an altitude of 15.24km, the engine being used at full throttle.

H (kft/km)	M_0	$D_{diff\text{-}in}$ (m)	$D_{diff\text{-}out}$ (m)	L_{diff} (m)
50 / 15.240	0.5	0.106	0.159	0.275
50 / 15.240	0.7	0.106	0.159	0.275
50 / 15.240	0.9	0.106	0.158	0.274
50 / 15.240	1.1	0.105	0.158	0.273
50 / 15.240	1.3	0.106	0.158	0.274

Table 9.13. Dimensions of the diffuser at a flight Mach-number of 0.9.

H (kft/km)	M_0	$D_{diff\text{-}in}$ (m)	$D_{diff\text{-}out}$ (m)	L_{diff} (m)	Remarks
30 / 9.144	0.9	0.105	0.158	0.273	Full-throttle
40 / 12.192	0.9	0.105	0.158	0.273	Full-throttle
50 / 15.240	0.9	0.106	0.158	0.274	Full-throttle
50 / 15.240	0.9	0.106	0.158	0.274	TETs=1600K
50 / 15.240	0.9	0.106	0.159	0.274	TETs=1500K

Table 9.14. Dimensions of the diffuser at the lowest allowable flight Mach-number under ITB relight condition.

H (kft/km)	M_0	$D_{diff\text{-}in}$ (m)	$D_{diff\text{-}out}$ (m)	L_{diff} (m)	Remarks
30 / 9.144	0.3	0.106	0.159	0.275	Full-throttle
30 / 9.144	0.3	0.129	0.194	0.335	HPTET 1200K
30 / 9.144	0.3	0.129	0.194	0.336	HPTET 1000K
30 / 9.144	0.3	0.128	0.192	0.332	HPTET 800K
40 / 12.192	0.39	0.106	0.159	0.275	Full-throttle
40 / 12.192	0.39	0.131	0.196	0.339	HPTET 1200K
40 / 12.192	0.39	0.131	0.196	0.339	HPTET 1000K
40 / 12.192	0.39	0.129	0.194	0.335	HPTET 800K
50 / 15.240	0.50	0.106	0.159	0.275	Full-throttle
50 / 15.240	0.50	0.130	0.196	0.338	HPTET 1200K
50 / 15.240	0.50	0.130	0.196	0.338	HPTET 1000K
50 / 15.240	0.50	0.129	0.193	0.334	HPTET 800K

9.5 Overall Length of the Two-combustor Engine relative to that for the Baseline Engine

It is assumed that the depth of the ITB could be contained within the diameter of the F100-EQ engine. It is further assumed that the length of the diffuser (to the ITB) is 0.34m (see Section 9.4). The length of the afterburner for the two-combustor engine is ~0.96m (i.e. 1.54m minus 0.59m) shorter than that for the baseline engine. The maximum length of the ITB calculated using CombSizing-Method-A is ~0.69m. Therefore, considering both the baseline and two-combustor engines installed with afterburners, the latter would be marginally longer than the baseline engine. On the other hand, for the ITB calculated using Afterburner-Method-A, the two-combustor engine could be substantially longer than the baseline engine. Nevertheless, the length of the ITB (i.e. thus the overall length of the engine) can be "controlled" by limiting lowest values of TETs or accepting a lower combustion efficiency for engine at low throttle setting.

9.6 Conclusions

Due to the limited practical experience available concerning the sizing and design of the inter-stage turbine burner (ITB), the author has adopted an approach that combines the methods for sizing both the conventional combustor and afterburner. Generally, the installation of an ITB will increase the length of the engine. However, both the baseline and two-combustor engines each with the installation of an afterburner of comparable combustor efficiency, the latter could be marginally or substantially longer than the baseline engine. This is because the two methods within the "combined-approach" calculate significantly different length for the ITB. Unfortunately, the reliability and accuracy of this "combined-approach" for sizing of the ITB could not be verified without experimental data.

Nevertheless, this study reveals certain operation limitations experienced by the two-combustor engine, especially at low throttle-settlings. For example, the ITB has to be relighted when the HPTET is at a sufficiently high temperature in

order to contain the size of the ITB. This approach would probably impact on the transient behaviour of the engine, a problem which is not addressed here.

Chapter 10. Transient Performance of the Two-combustor Engine

10.1 Introduction

The transient performance measures the responses of the engine to change in its control parameters, e.g. the fuel-consumption rate (W_{fuel}) or turbine's entry-temperature (TET). Propulsion system with an excellent transient performance is a desirable requirement, in particular, for a military fighter aircraft in which manoeuvrability is crucial to its survival.

The available version of the TURBOMACTH is used to perform steady-state analysis for both design and off-design conditions. The GasTurb, engine performance-simulation software, developed by Kurzke [80], is capable of simulating both steady-state and transient performances. However, it does not permit the simulation of a multi-spool two-combustor engine. Therefore, a simple transient-prediction methodology (see Section 3.3.4) has been adopted to coalesce (externally) with TURBOMATCH in order to be able to conduct transient-performance study for both the baseline and two-combustor engines. Predictions from the GasTurb program for the transient behaviour of a conventional turbofan-engine were used for validating the proposed methodology.

The objective of this study is to try to demonstrate that the two-combustor engine exhibits a more desirable transient behaviour than that of the baseline engine. Therefore there was not attempt made to identify the optimal acceleration or deceleration paths for the two-combustor engine.

10.2 Validations of Transient-Prediction Methodology

Predictions from the GasTurb program for the transient behaviour of a simple conventional turbofan-engine were used for validating the proposed methodology of the present investigation. However, there are differences in the engine-components' characteristics and (probably) the methodologies adopted in the TURBOMATCH and GasTurb. Therefore, to achieve a closer match between

the predictions from these two programs, a simple, yet representative, configuration is used for validating the proposed approach (see Table 10.1). The cooling-flow rate is set to zero and a fixed convergent nozzle is used to further reduce any uncertainties arising in the validation process. The fuel-consumption rate is selected as the engine control-parameter because the GasTurb does not permit the use of turbine's entry-temperature (TET). The validation is conducted for both acceleration and deceleration of the engine for fuel-consumption rate of 0.3 kg s^{-1} to 1.1 kg s^{-1} and 1.1 kg s^{-1} to 0.3 kg s^{-1}, respectively. The rate of change of the fuel-consumption rate is selected at 1 kg s^{-2}.

Table 10.1. Engine's design point for validation of the transient-performance prediction methodology.

Parameter	**Value**
Mass-flow rate, W (kg s^{-1})	100
Fan's pressure-ratio, FPR	3.1
Overall pressure-ratio, OPR	30
Bypass ratio, BPR	0.36
Fuel flow rate, W_{fuel} (kg s^{-1})	1.1
Cooling air, W_{cl} (kg s^{-1})	0
Convergent nozzle	Fixed
LP spool polar moment of inertia, J_{lp} (kg m^2)	2.2
HP spool polar moment of inertia, J_{hp} (kg m^2)	3.0

10.2.1 Steady-state Performance

The steady-state behaviour of the engine is studied in order to appreciate the conclusion drawn for the validation of the proposed transient-performance methodology. The relationship of the engine's specific fuel-consumption rate (SFC) versus thrust, predicted by both the TURBOMATCH and GasTurn, matches closely (see Figure 10.1). The author suggested that the slight discrepancy at the design-point condition is due to the difference(s) in the approaches of fuel-air-ratio calculation.

The engine's off-design performance depends on the respective components' characteristics. Given the differences in the components' characteristic between that in the TURBOMATCH and GasTurb, the fan's and high-pressure compressor's (HPC's) behaviours predicted by the two programs diverged from each other when the engine operating-condition moves further away from its design-point condition (see Figure 10.2).

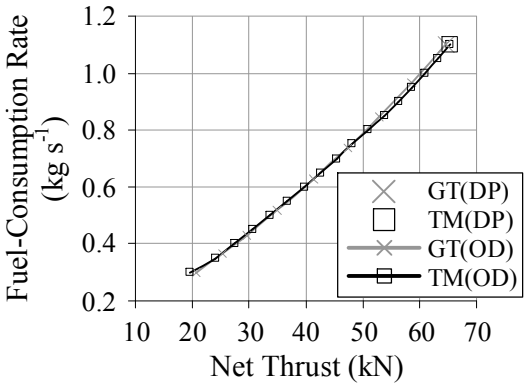

Figure 10.1. The engine's fuel-consumption rate versus net-thrust predicted via the TURBOMATCH (TM) and GasTurb (GT) programs.

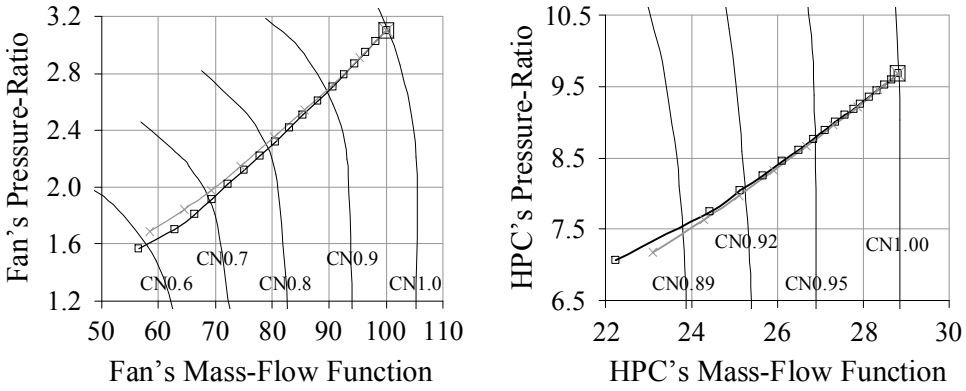

(a) Fan's working line (b) HPC's working line

Figure 10.2. The behaviours of the fan and HPC as predicted by the TURBOMATCH (TM) and GasTurb (GT) programs [□GT-DP × TM-DP —×— GT-OD —□— TM-OD].

10.2.2 Transient - Accelerations

Figure 10.3 shows the variations in the engine's thrust with time. The predictions by both the TURBOMATCH and GasTurb programs match closely. Figure 10.4 shows the steady-state and transient behaviours of the fan and HPC, as the fuel-consumption rate increases. The differences in the absolute values are due to differences in the components' characteristics and also (maybe) the prediction methodologies employed. As far as the validation of the present methodology is concerned, the predictions by the two codes match well.

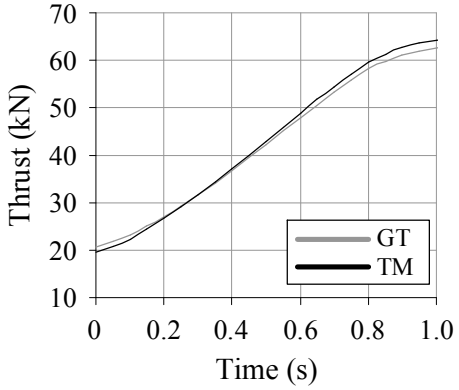

Figure 10.3. Engine's transient-behaviour predicted by the TURBOMATCH (TM) and GasTurb (GT) programs.

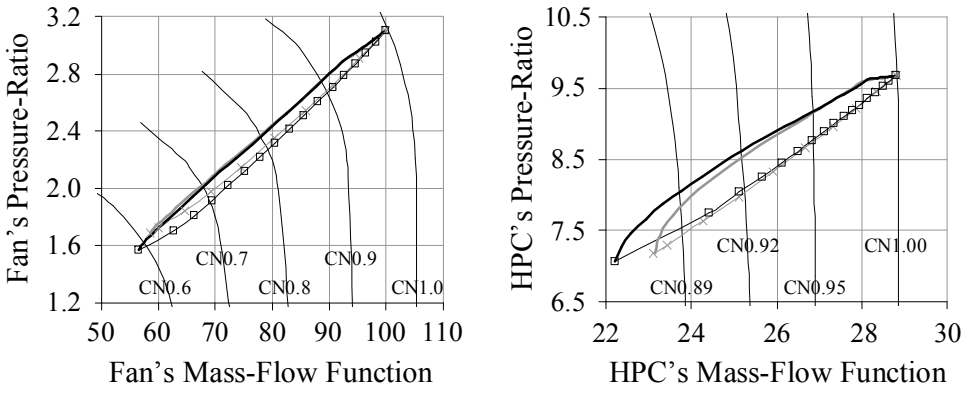

(a) Fan's working line (b) HPC's working line

Figure 10.4. The steady-state and transient behaviours of the fan and HPC as predicted using the TURBOMATCH (TM) and GasTurb (GT) programs [GT(Steady-State) GT(Transient) TM(Steady-State) TM(Transient)].

10.2.3 Transient - Decelerations

Figure 10.5 and Figure 10.6 shows the engine's steady-state and transient behaviours during its throttling-down process. The results reveal that the predictions, using the proposed methodology, match closely with those predictions from GasTurb.

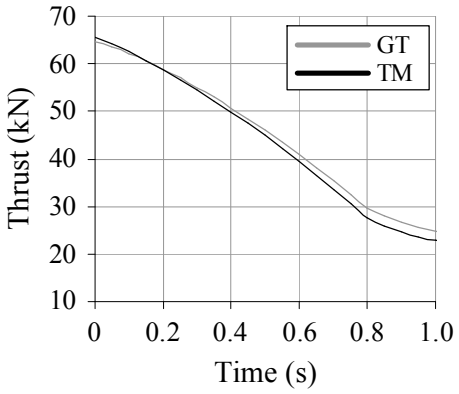

Figure 10.5. Engine's transient-behaviour predicted by the TURBOMATCH (TM) and GasTurb (GT) programs.

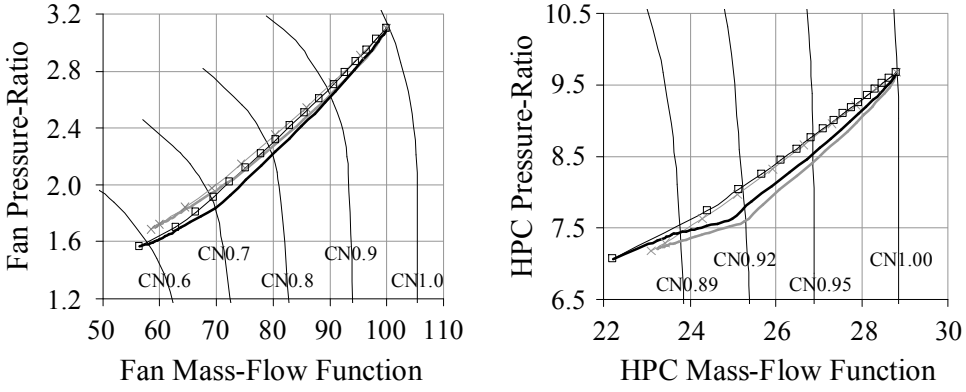

(a) Fan's working line (b) HPC's working line

Figure 10.6. The steady-state and transient behaviours of the fan and HPC as predicted using the TURBOMATCH (TM) and GasTurb (GT) programs [GT(Steady-State) GT(Transient) TM(Steady-State) TM(Transient)].

10.2.4 Remarks

The validation procedure, using a simple conventional engine, has shown the reliability of the proposed transient-prediction methodology. The methodology is extended to predict the transient behaviour of a two-combustor engine. Although there are shortfalls in the proposed methodology, it is sufficient to demonstrate the differences between the behaviours of the two-combustor engine relative to that of the baseline engine.

10.3 Baseline Engine versus Two-combustor Engine

In view of the complexity of the engine transient-behaviour prediction, the configurations for both the baseline and two-combustor engines are simplified. The HPC is modelled as a single component and the cooling-flow for the low-pressure turbine's (LPT's) is jointly drawn from the exits of the fan and HPC. Table 10.2 shows the design-point conditions for the baseline and two-combustor engines. To be consistent with previous analyses on two-combustor engine, the TET is selected as the engines' control-parameter.

Table 10.2. Design-point conditions for the baseline (F100-EQ) and the two-combustor engines.

Parameter	**Baseline Engine**	**Two-combustor Engine**
Flight altitude, H (km)	0	0
Flight Mach-number, M_0	0	0
Mass-flow rate, W (kg s^{-1})	111.5	111.5
Bypass ratio, BPR	0.36	0.36
Overall pressure-ratio, OPR	32.4	32.4
Fan's pressure-ratio, FPR	3.55	3.55
HPT's Entry-Temperature, HPTET (K)	1700	1700
LPT's Entry-Temperature, LPTET (K)	-	1700

10.3.1 Steady-state Performance

Figure 10.7 shows the fan's and HPC's working-lines for the baseline engine, which are unique to the engine operation. The two-combustor engine could have multiple working-lines depending on the distribution of fuel-consumption rate in the two combustors, i.e. the high-pressure and low-pressure turbines' entry-temperatures (HPTET and LPTET, respectively) (see Figure 10.8).

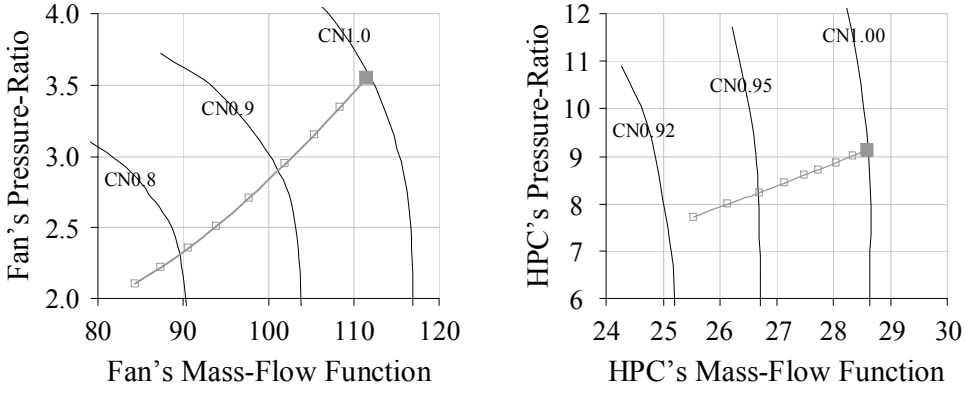

(a) Fan's working line (b) HPC's working line

Figure 10.7. The steady-state behaviours of the fan and HPC for the baseline (F100-EQ) engine [■ DP —□— OD].

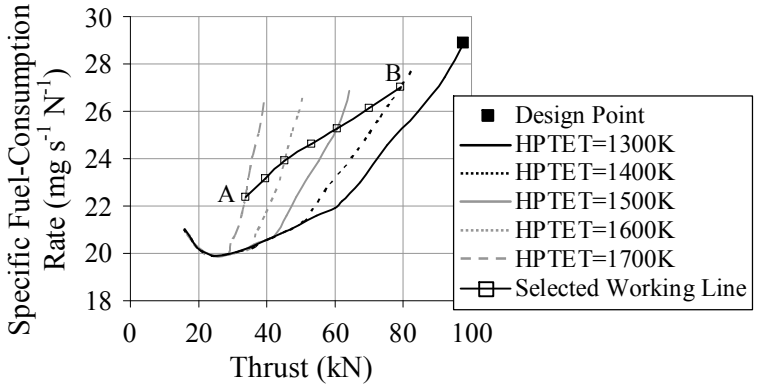

Figure 10.8. The performance of the two-combustor engine for constant high-pressure turbine's entry-temperatures.

The transient behavior of the baseline engine has been studied for engine acceleration(deceleration) with TET from 1300K(1700K) to 1700K(1300K). For

the two-combustor engine with corresponding increase in its thrust values, an arbitrary working-line is selected (Point A to B) (see Figure 10.8). The combination of HPTET and LPTET at Point A is 1300K and 1030K, respectively; and that at Point B is 1600K and 1545K, respectively. Both the values of HPTET and LPTET are varied linearly and simultaneously along the selected working-line. The corresponding steady-state working-lines for the fan and HPC for the two-combustor engine are shown in Figure 10.9.

In the prediction of the engines' transient-behaviour, the rate of change of the HPTET is fixed at 1000K per second for both the baseline and two-combustor engines. For the selected working-line of the two-combustor engine, the LPTET is operating slightly further from its maximum allowance temperature (1700K). Therefore the LPT has a higher tolerance for fluctuation in the gas-temperature associates with the higher rate of change LPTET, which is fixed at 1800K per second.

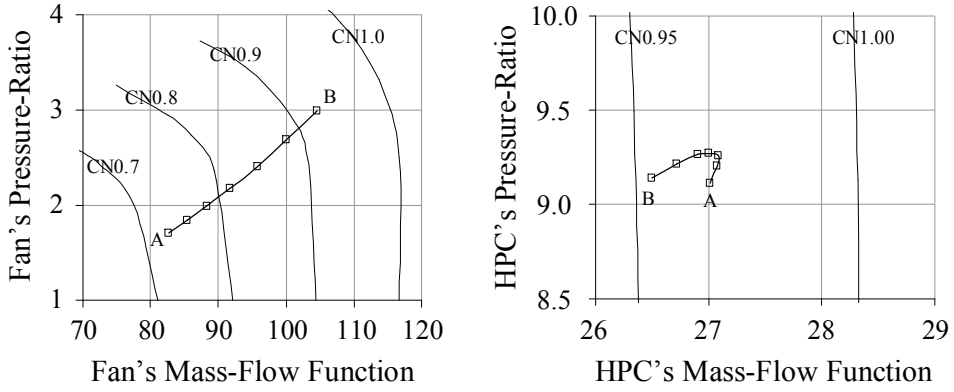

(a) Fan's working line (b) HPC's working line

Figure 10.9. The steady-state behaviours of the fan and HPC for the two-combustor engine operating along the arbitrary selected working-line.

10.3.2 Transient - Acceleration

Figure 10.10 shows the steady-state and transient behaviours of the baseline engine during acceleration. The pressure-ratios and the mass-flow functions of both the fan and HPC increase with the TET. The transient working-line of the fan is marginally above its steady-state working-line; whereas that of the HPC is

appreciably nearer to its surge line. The spool inertia "prevents" the increase of the both the mass-flow rate and the spool rotational speed at the rate corresponding to that of the increase in the TET. In particular for the high-pressure (HP) spool, with the HPT's nozzle-guiding-vanes operating at choked condition, a corresponding increase in the HPC's pressure-ratio is necessary. Therefore the transient working-line is moved further away from the steady-state line toward the surge line.

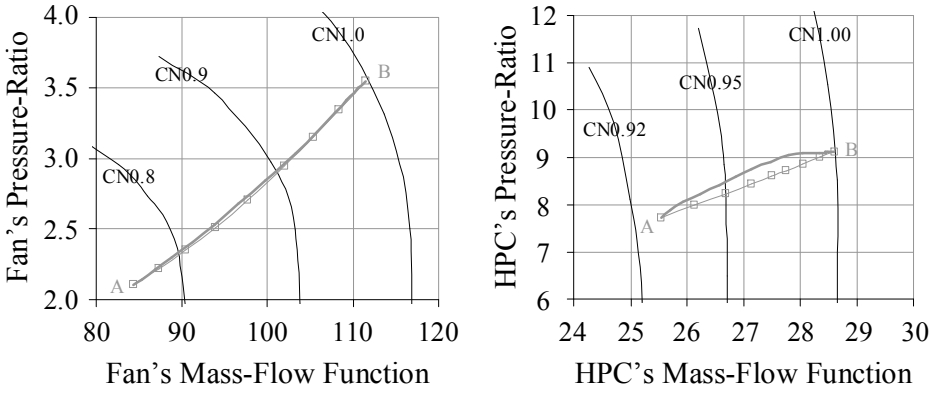

(a) Fan (b) High-pressure Compressor

Figure 10.10. Steady-state and transient behaviours of the baseline engine during acceleration from a HPTET of 1300K to 1700K (Point A→Point B) [—⊟— Steady-state ——— Transient].

Figure 10.11 shows the steady-state and transient behaviours of the two-combustor engine during acceleration from a HPTET of 1300K to 1700K and the corresponding increase in LPTET is from 1030K to 1545K. The pressure-ratios and mass-flow functions of both the fan and HPC increase with the TETs (Point A→B_1). At Point B_1, the TETs reach the designated maximum values and there is nearly zero work imbalance in the HP-spool. Corresponding, the LPT work is substantially higher than the amount of work requires to drive the fan; thus there is considerably amount of work imbalance in the low-pressure (LP) spool. From Point B_1→B_2, the work imbalance in the LP-spool continues to drive the fan to a high pressure-ratio. However, with the TETs kept invariant, the work imbalance in the LP-spool diminished. With the corresponding increase in the pressure and

temperature of the HPC's inlet-flow, the work requires to drive the HPC exceeds the available HPT's work; thus reducing the HPC's pressure-ratio and mass-flow function. Because of the spool inertia, the reduction in the HPC's pressure-ratio is faster than that of its mass-flow function; thus explain the steep drop in the curve of HPC's pressure-ratio versus mass-flow function. At Point B_2, there is near zero work imbalance in the LP-spool and a negative work imbalance (HPC's work < HPT's work) in the HP spool. With the corresponding operating pressure-ratios of both the fan and HPC higher than the respective steady-state pressure-ratios, it is nature that both LP-spool and HP-spool will gradually spool-down to it steady-state condition (i.e. Point $B_2 \rightarrow B$).

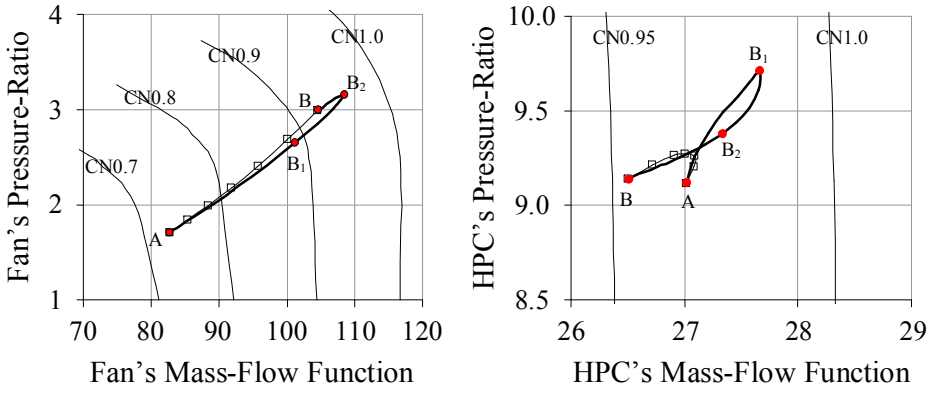

(a) Fan's running line (b) HPC's running line

Figure 10.11. Steady-state and transient behaviours of the two-combustor engine during acceleration from a HPTET(LPTET) of 1300K(1030K) to 1600K(1545K) (Point A→Point B) [—□— Steady-state ——— Transient].

Figure 10.12 shows the surge characteristics of the fan and HPC at both steady-state and transient processes. At respective thrust value, the surge margin of the fan for the two-combustor engine exceeds that of the baseline engine in both steady-state and transient processes; also the surge margin of the fan at the transient process is appreciably higher than that at the steady-state process, in particularly for the two-combustor engine. With regard to the surge margin of the HPC, the baseline engine has a slightly larger margin than the two-combustor engine at steady-state condition; whereas the minimum surge-margin of the HPC

for the baseline engine is slightly lower than that of the two-combustor engine. Nevertheless, the variations in the surge margin of the HPC are marginal when compared with that of the fan.

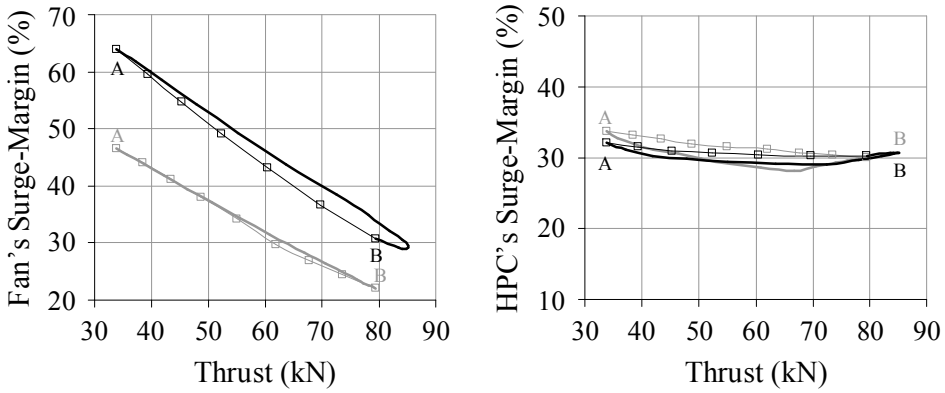

(a) Fan's working line (b) HPC's working line

Figure 10.12. The surge characteristics of the fan and HPC during both steady-state and transient processes for the baseline (BLE) and two-combustor (TCE) engines during acceleration [BLE(Steady-state) BLE(Transient) TCE(Steady-state) TCE(Transient)].

During operation, the fan is the prime component to experience disturbances due to the manoeuvres of the aircraft. Therefore the requirement for a large surge margin is more critical for the fan than for the HPC. Thus, the fan's surge-margin for the two-combustor engine at the design point could be reduced or the engine would withstand more extreme aircraft manoeuvres and/or higher acceleration rates.

For transient performance measurements, the transient time is measured from start of the acceleration process up to 98% of the targeted spool speed [69]. For this study, the author has decided to use 98% of the targeted thrust (i.e. 79.18kN) as the "end-point" of the transient process. It is obvious that the two-combustor engine requires a significantly shorter time (approximately 40%) to achieve the target thrust when compared with that required by the baseline engine (see Figure 10.13).

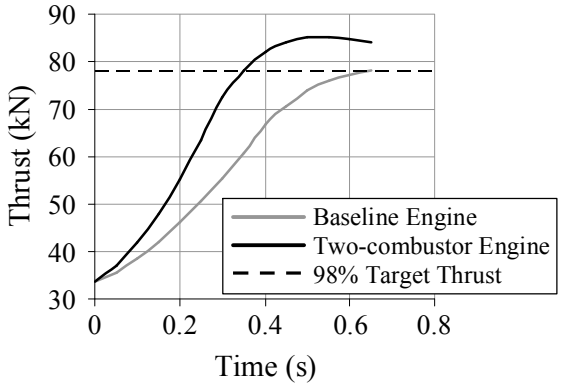

Figure 10.13. Engines' thrust during the transient process.

10.3.3 Transient - Deceleration

Figure 10.14 shows the baseline engine's fan and HPC behaviours during deceleration from HPTET of 1700K to 1300K. Quantitatively, the trends in the behaviours of the fan and HPC are simply the reverse of that during the engine acceleration. Similarly, for the two-combustor engine under deceleration, the trends in the behaviours of its fan and HPC are reverse of that observed during the engine acceleration (see Figure 10.15). The above observations are in particular obvious in the baseline engine and also in the fan's behaviour for the two-combustor engine. As for the HPC's behaviour of the two-combustor engine, the reverse in the trends at respective segments of Point A→Point B_1, Point B_1→Point B_2 and Point B_2→Point B are still present.

With regard to the fan's surge-characteristic, the surge margin during transient is lower than that at steady-state, in particular for the two-combustor engine. Nevertheless, given the characteristics of two-combustor engine, its fan's surge-margin is always higher than that of the baseline engine at comparable thrust. For the HPC, its surge-margin is increased in the deceleration process for both baseline and two-combustor engines. Nevertheless, the HPC's surge-margin of the two-combustor engine remains lower than that of the baseline engine at both steady-state and transient processes (see Figure 10.16).

Similar to that observe during the engine acceleration, the two-combustor engine has superior transient-performance over that achievable by the baseline engine: the rate of decrease of the thrust of the two-combustor engine is significantly higher than that achievable by the baseline (see Figure 10.17).

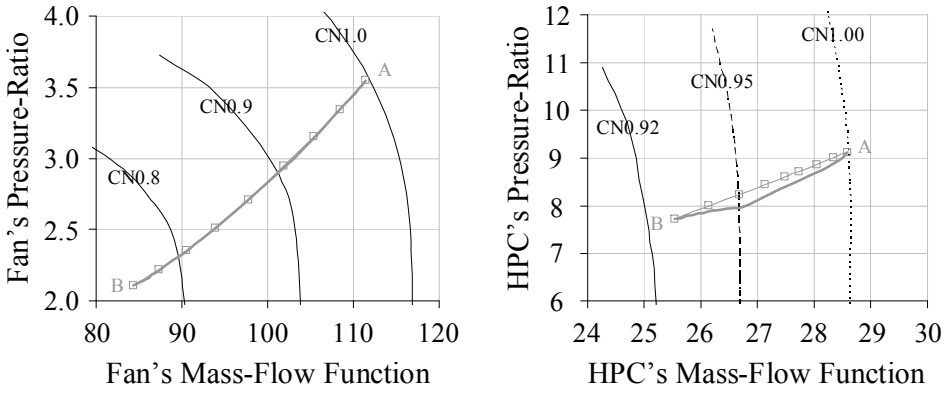

(a) Fan's working line (b) HPC's working line

Figure 10.14. Steady-state and transient behaviours of the baseline engine during deceleration from a TET of 1700K to 1300K (Point A→Point B)
[Steady-state Transient].

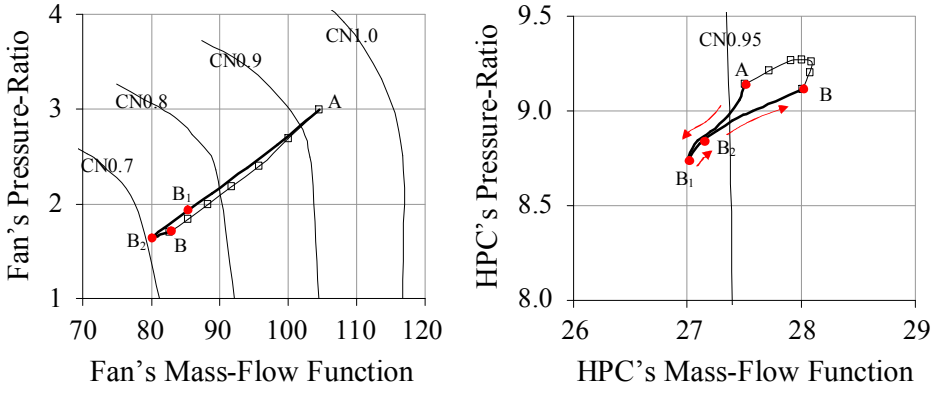

(a) Fan's working line (b) HPC's working line

Figure 10.15. Steady-state and transient behaviours of the two-combustor engine during deceleration from a HPTET(LPTET) of 1600K(1545K) to 1300K(1030K)
[Steady-state Transient].

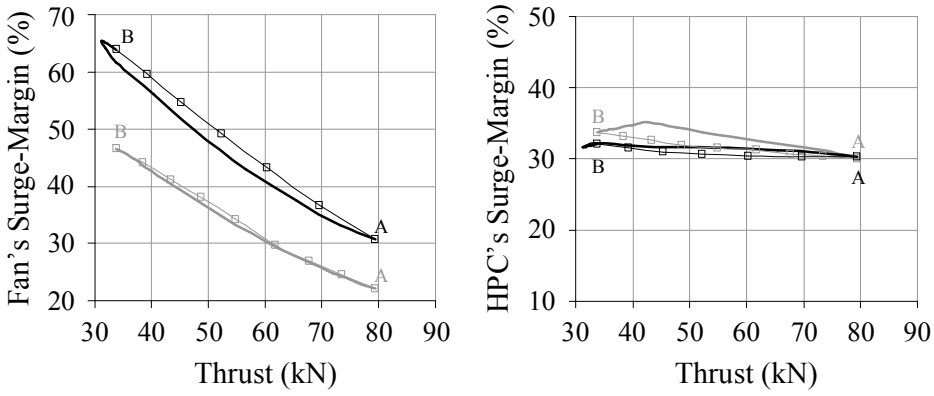

(a) Fan's surge-margin (b) HPC's surge-margin

Figure 10.16. The surge characteristics of the fan and HPC at both the steady-state and transient behaviours for the baseline (BLE) and two-combustor (TCE) engines during deceleration [BLE(Steady-state) BLE(Transient) TCE(Steady-state) TCE(Transient)].

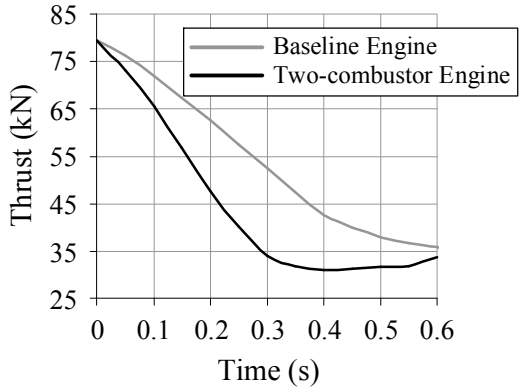

Figure 10.17. Engines' thrust during the transient process.

10.3.4 Transient – Acceleration to Maximum Achievable Thrust

Comparison is made for both baseline and two-combustor engines acceleration from ~33.8kN to 98% of respectively maximum achievable thrust, i.e. 79.18kN for the baseline engine and 100.63kN for the two-combustor engine. Figure 10.18 shows that two-combustor engine take around two-third of the time to reach 98% of its maximum achievable thrust when compared with that of the

baseline engine. Therefore demonstrates the superiority of the two-combustor engine in producing thrust at a faster rate than that achievable with a comparable conventional engine.

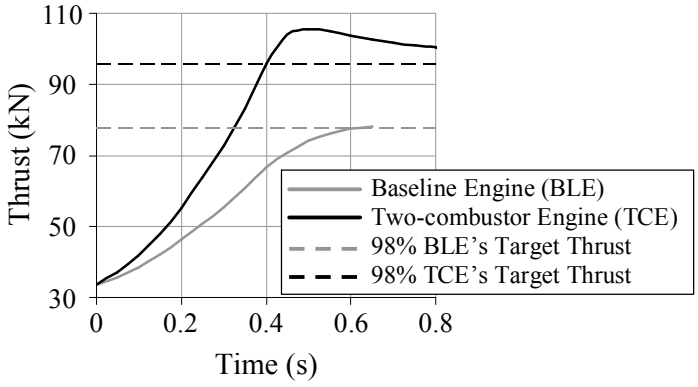

Figure 10.18. Engines' thrust during the transient process.

10.4 Conclusions

A methodology for the prediction of a conventional engine's transient-performance has been developed and validated, and subsequently extended to predicted a two-combustor engine's transient-performance.

Analysis has shown that the two-combustor engine requires substantially shorter time when compared with baseline engine for comparable increase or decrease in thrust. In addition, the fan of the two-combustor engine exhibits a larger surge margin than that of the baseline engine. Although the methodology neglects the effects of time-dependent factors, such heat soakage, it is nevertheless sufficient to meet the objective of understanding the transient behaviour of the two-combustor engine when compared with that of baseline (F100-EQ) engine.

Chapter 11. Impacts of the Performance of the Two-combustor Engine on the Aircraft's Performance

11.1 Introduction

Due to both commercial and military confidentiality restrictions, there is insufficient exact data for conducting a fruitful mission analysis. Therefore this investigation is limited to the study of the aircraft's flight envelope, rate-of-turn, specific fuel-consumption rate (SFC) and maximum achievable flight Mach-number. The analytical approaches and the estimations of the F16-EQ aircraft's characteristics (i.e. drag-polar and weight characteristics) are presented in Section 3.3. The baseline and two-combustor engines' design-point conditions are as shown in Table 6.1.

11.2 F16-EQ Aircraft Configurations

The considered configurations are shown in Table 11.1 with the weapon-systems are mounted at stations 1 to 9 (see Figure 11.1). Configurations 1 and 2 are equipped to perform Air-to-Air combat mission, thus also known as Air-to-Air configurations. Configuration 3 is mounted with weapon-system to conduct Air-to-Ground mission, therefore it is designated as Air-to-Ground configuration. All these configurations are assumed to have full internal-fuel.

Table 11.1. F16-EQ configurations for performance analysis.

Config	Stations										
	9	8	7	6	5R	5	5L	4	3	2	1
1 [84]	Aim9	-	-	-	-	-	-	-	-	-	Aim9
2	Aim9	Aim9	Aim7	Aim7	-	-	-	Aim7	Aim7	Aim9	Aim9
3 [84]	Aim9	ALQ-119-12	6x Mk82	370G Tank	-	300G Tank	-	370G Tank	6x Mk82	-	Aim9

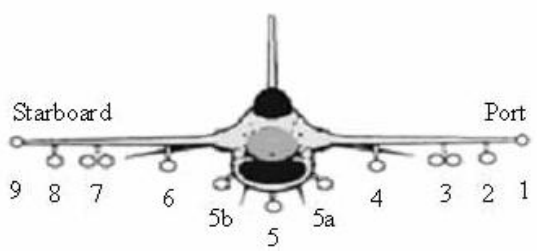

Figure 11.1. Label of station-numbers for the F16 aircraft where the weapon-systems are mounted [99].

11.3 Operating Envelope

11.3.1 Air-to-Air Configuration 1 (see Table 11.1)

Figure 11.2 shows the aircraft's drag and the engine's maximum available-thrust at an altitude of 30kft (i.e. 9.144km). At a lower flight Mach-number, the characteristics of the engine's components have limited the maximum allowable turbine's entry-temperature (TET); thus limiting the maximum achievable engine's thrust. For the two-combustor engine under low flight Mach-number conditions, there are numerous combinations of high-pressure and low-pressure turbines' entry-temperatures (HPTET and LPTET) to achieve maximum-thrust, without operating beyond the components' envelope. Nevertheless, to simplify the analysis, only combinations of identical HPTET and LPTET are considered.

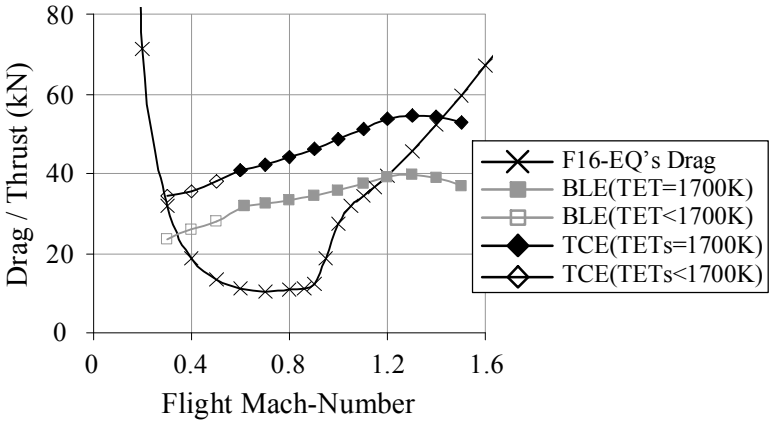

Figure 11.2. The variations of the F16-EQ aircraft's drag and engine's thrust at an altitude of 30kft (i.e. 9.144km).

The aircraft is permitted to operate over the range of flight Mach-number which the engine's thrust exceeds the aircraft's drag. Generally, the two-combustor engine can produce higher maximum achievable-thrust. Hence the aircraft powered by the two-combustor engine can operate over a larger flight Mach-number range when compared with that achievable with the baseline engine.

The range of flight Mach-number permissible for the aircraft operation is extracted for the various altitudes and plotted in Figure 11.3. The tabulated operating envelope resembles that in Figure 3.21. At lower flight altitude (<30kft, i.e. 9.144km), the lowest achievable flight Mach-number is limited by the aircraft's stall-limit (i.e. VEAS of 110knots). Generally, the F16-EQ aircraft with the two-combustor engine has a larger envelope than that achievable with the baseline engine, in particular at the higher altitude and flight Mach-number region (see Figure 11.3).

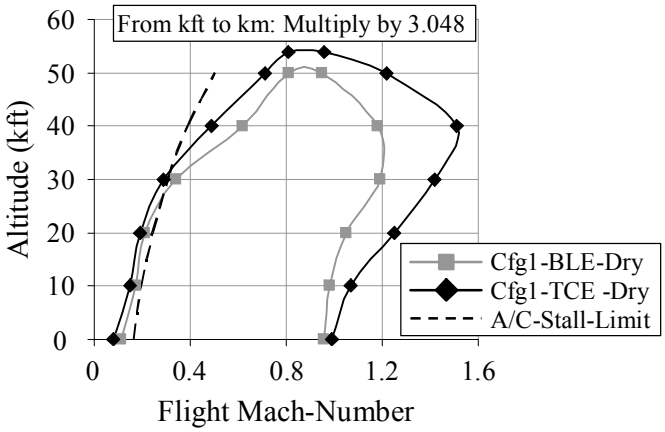

Figure 11.3. Operating envelope of the F16-EQ configuration 1 (see Table 11.1).

11.3.2 Air-to-Air Configuration 2 (see Table 11.1)

For F16-EQ aircraft powered by the two-combustor engine, the benefit of a larger envelope could be traded-off for heavier aircraft-configuration. Configuration 2 is heavier and has higher drag when compared with configuration 1. Nevertheless, the flight envelope of the configuration 2 (powered using two-combustor engine) is still larger than that of configuration 1 with the baseline engine (see Figure 11.4).

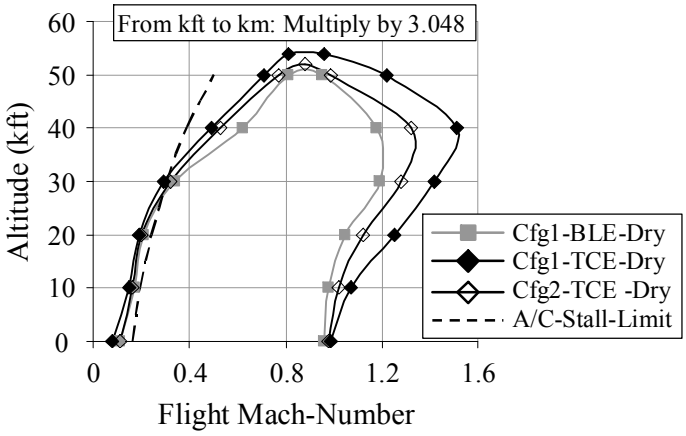

Figure 11.4. Operating envelope of the F16-EQ configurations (see Table 11.1).

11.3.3 Air-to-Ground Configuration 3 (see Table 11.1)

Figure 11.5 shows the operating envelope for the F16-EQ aircraft with Air-to-Ground configuration 3. Similar to the observation for configuration 1 (see Table 11.1), the F16-EQ aircraft with two-combustor engine has a larger operating envelope when compared with that achievable with the baseline engine.

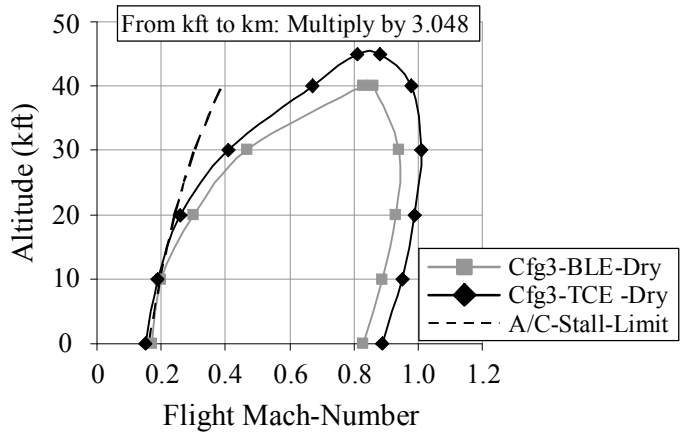

Figure 11.5. Operating envelope of the F16-EQ aircraft's Air-to-Ground configuration 3 (see Table 11.1).

11.4 Aircraft's Rate-of-Turn

The higher thrust produced by the two-combustor engine enables the aircraft to operate with higher load-factor and thus achieve a higher rate-of-turn (see

Figure 11.6). The increase in the rate-of-turn is typically around 1 to 1.5 degree-per-second, depending on the flight altitude and Mach-number (see Figure 11.7). Reference [86] states that an improvement of two degree-per-second in the rate-of-turn is significant to provide the aircraft its leading-edge in a dog-fight. However, without sufficient data to conduct a mission analysis, the exact benefit associates with the use of a two-combustor engine are not investigated.

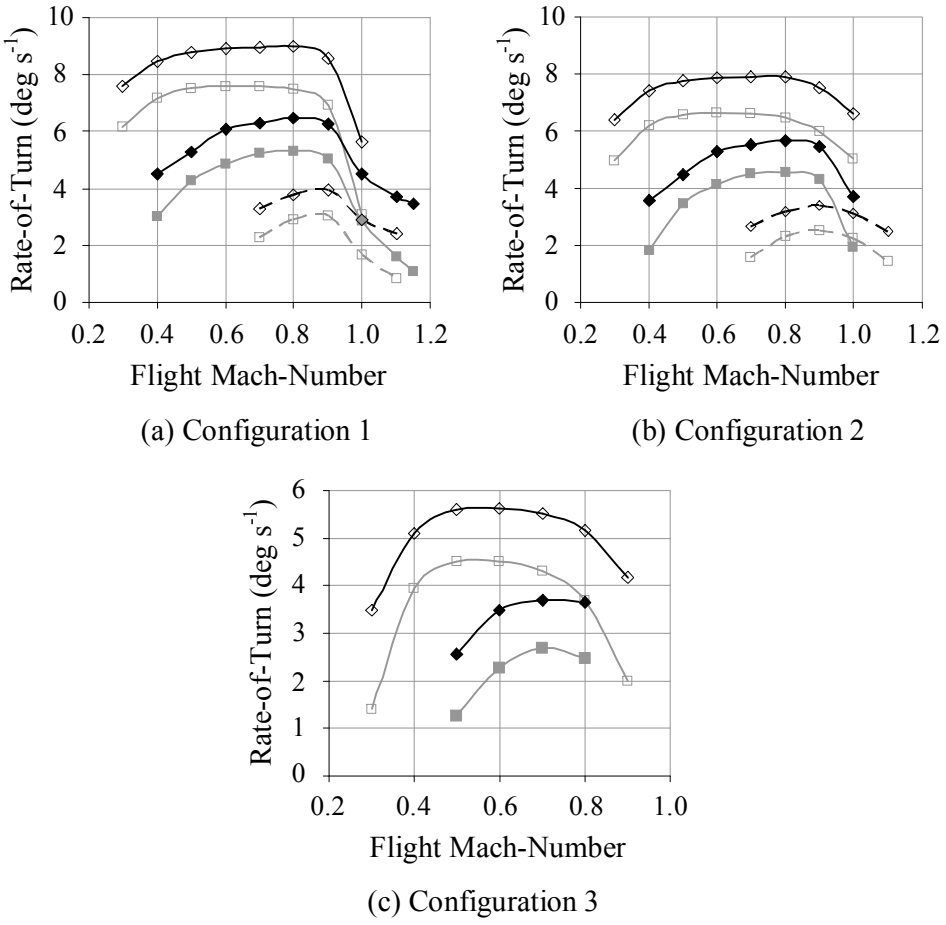

Figure 11.6. The F16-EQ aircraft's rate-of-turn for the F16-EQ aircraft (configuration 1) at selected altitudes
[BLE(20kft/6.096km) BLE(30kft/9.144km) BLE(40kft/12.192km)
TCE(20kft/6.096km) TCE(30kft/9.144km) TCE(40kft/12.192km)].

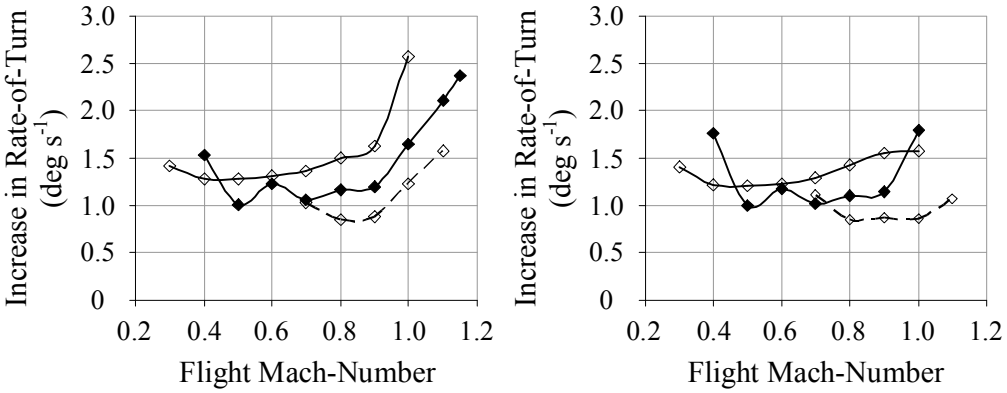

(a) Configuration 1

(b) Configuration 2

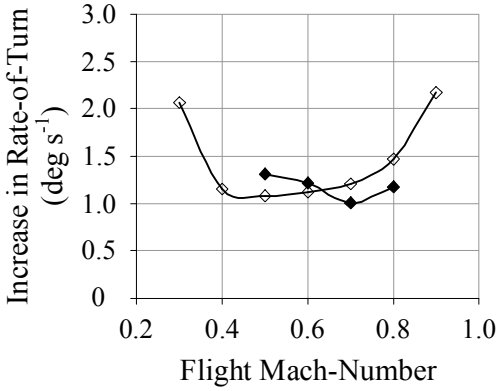

(c) Configuration 3

Figure 11.7. The improvement in the F16-EQ aircraft's rate-of-turn for two-combustor engine relative to that of the baseline engine [—◇— 20kft/6.098km —◆— 30kft/9.144km - -◇- · 40kft/12.192km].

11.5 Specific Fuel-Consumption Rate (SFC) at Selected Flight Conditions

11.5.1 Maximum Achievable Dry Thrust Conditions

Figure 11.8 shows the SFC for both the baseline and two-combustor engines operating at maximum achievable dry thrust for F16-EQ aircraft configuration 1 (see Table 11.1). The larger operating envelope and higher rate-of-turn of the two-combustor engine is achievable at the expenses of higher SFC when compared with that of the baseline engine (see Figure 11.8).

The baseline engine's afterburner is turned-on and adjusted such that its thrust is (approximately) the same as that of the two-combustor engine. Figure 11.8 shows that the SFC of the baseline engine with afterburner is significantly higher than that of the two-combustor engine. This is because with combustion in the afterburner occurs at low-pressure, the engine-cycle is less efficient. Again, it is demonstrated here that the two-combustor engine's performance is in between that of the baseline engine with and without afterburner.

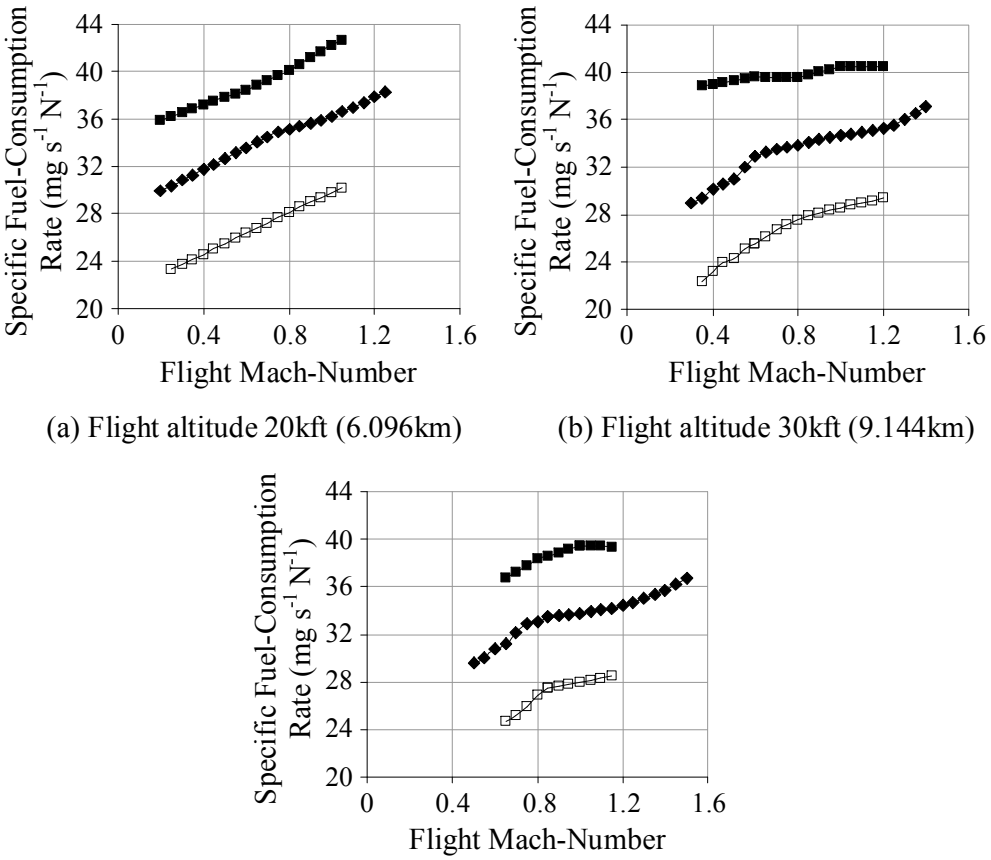

(a) Flight altitude 20kft (6.096km)

(b) Flight altitude 30kft (9.144km)

(c) Flight altitude 40kft (12.192km)

Figure 11.8. The engines' specific fuel-consumption rate at maximum dry thrust condition at various altitudes and flight Mach-numbers [BLE TCE BLE+AB].

11.5.2 Trim Flight Conditions

Figure 11.9 shows the SFC of F16-EQ aircraft configuration 1 (see Table 11.1) at trim condition, i.e. thrust equal drag and lift equal to weight. For the aircraft with the baseline engine, the HPTET is throttled-down to match the drag of the aircraft. For the aircraft powered using the two-combustor engine, the engine is throttled-down by having both HPTET and LPTET reduced at the same rate simultaneously; alternatively, the engine is throttled-down by reducing the LPTET with HPTET kept at its maximum allowable temperature. Regardless of the throttling-approaches, the SFC of the two-combustor engine is higher than that of the baseline engine for the same thrust produced.

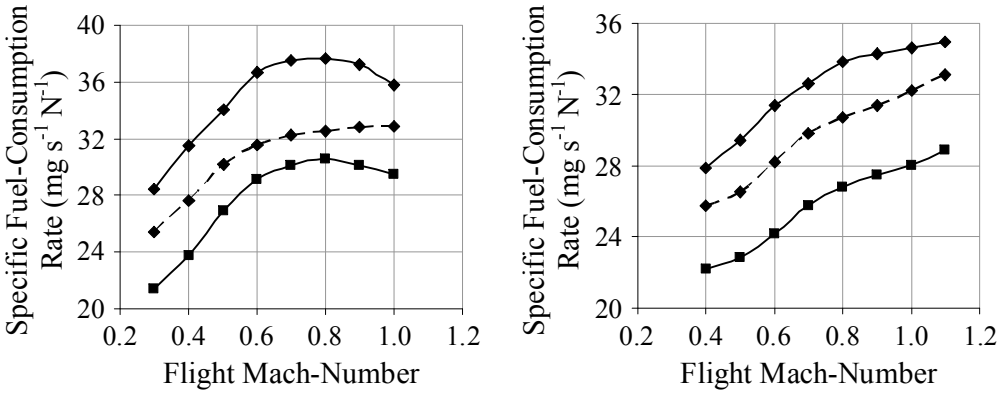

(a) Flight altitude 20kft (6.096km)

(b) Flight altitude 30kft (9.144km)

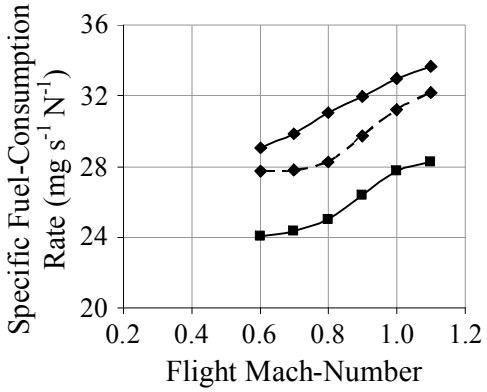

(c) Flight altitude 40kft (12.192km)

Figure 11.9. The engines' specific fuel-consumption rate for configuration 1 (see Table 11.1) operating at trim condition (drag = thrust)
[—■— BLE —◆— TCE(HPTET=LPTET) - -◆- - TCE(HPTET=max)].

11.5.3 Maximum Achievable Wet Thrust Conditions

Figure 11.10 shows that two-combustor engine with an afterburner produces higher thrust at a lower SFC when compared with that achievable by the baseline engine with an afterburner. However, the benefits of the two-combustor with afterburner, over that achievable by the baseline engine with an afterburner, are marginal. Taken into the considerations the assumptions made and the possible round-off errors, the observation might not be conclusive.

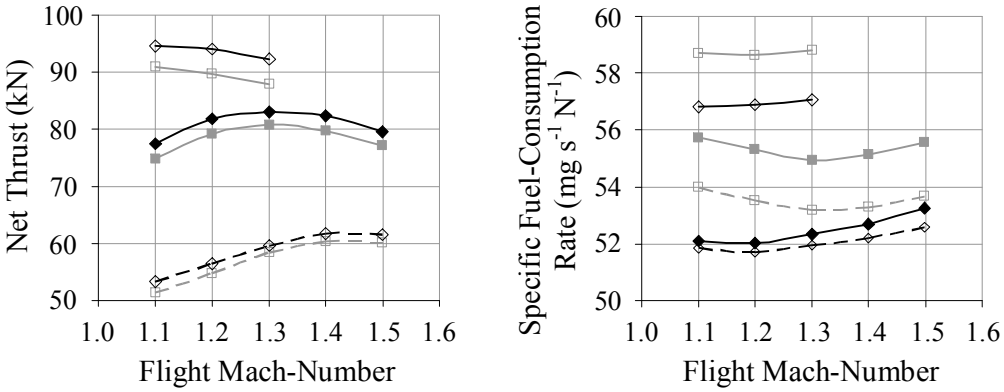

Figure 11.10. Performances of the baseline and two-combustor engines, both with afterburner, under full-thrust condition

[BLE-20kft(6.096km) BLE-30kft(9.144km) BLE-40kft(12.192km)
TCE-20kft(6.096km) TCE-30kft(9.144km) TCE-40kft(12.192km)].

11.6 Performance of Aircraft at Maximum Achievable Flight Speed

Upon detection of approaching hostile aircraft, the ground-based interceptor and/or combat-air patrol aircraft have to scramble to intercept. Also, the aircraft conducting strike mission might have to operate at high speed into the target area. Therefore there is a requirement for the aircraft to operate at its maximum achievable flight Mach-number for substantial duration. The effects of two-combustor engine, limited to dry thrust condition, on the performance of the aircraft operating at its maximum achievable flight Mach-number are investigated.

The flight duration and fuel consumed are the two primarily parameters of concern. Fundamentally, the flight duration is equal to the flight range divided by the flight velocity (see equation (11.1)). And the amount of fuel-consumed per unit flight-distance is equal to the fuel-consumption rate divided by the flight velocity (see equation (11.2)).

$$t = R_{flt} / V \tag{11.1}$$

$$\frac{w_{fuel}}{R_{flt}} = \frac{W_{fuel}}{V} \tag{11.2}$$

Technically, the aircraft's flight-condition and/or its control-surfaces are adjusted to achieve optimum performance during flight. To predict the aircraft performance accurately, the flight profile is to be divided into multiple segments; whereby the accuracy of the prediction increases with the number of segments. However, without sufficient exact data, the accuracy and reliability of the "multi-segments" approach will be doubtful. Therefore this study is limited to the aircraft's performance for per unit flight range.

The analysis has been conducted for the F16-EQ aircraft, Configuration 1, operating at its maximum achievable flight Mach-number (see Table 11.1). The aircraft with two-combustor engine can operate at higher maximum achievable flight Mach-number, therefore its flight duration to travel per unit distance is shorter than the aircraft with the baseline engine (see Figure 11.11). However the two-combustor engine is less efficient; thus the fuel-consumed is substantially higher than that of the baseline engine (see Figure 11.11). With the two-combustor engine replacing the baseline engine, there is a reduction of 10% to 30% flight duration, which is achieved with a penalty of averagely 50% increase in fuel-consumed.

The thrust produced by the baseline engine can be increased with an afterburner to match the two-combustor engine's dry thrust; thus both the engines can operate at equal maximum achievable flight Mach-number. The configuration of baseline engine with afterburner has lower cycle-efficiency; therefore requires

higher SFC when compared with that of the two-combustor engine producing comparable thrust (see Figure 11.12). With approximately the same maximum achievable flight Mach-number, the configuration of baseline engine with afterburner has the same reduction in flight duration as that achievable with the two-combustor engine. However, its penalty in the amount of fuel-consumed is higher than that of two-combustor engine: approximately 20% higher than the two-combustor engine (see Figure 11.13).

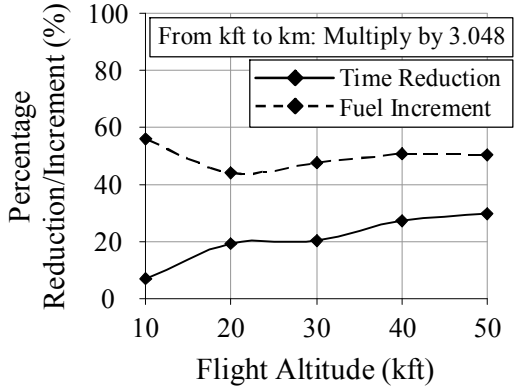

Figure 11.11. Two-combustor engine's performance, relative to the baseline engine, at respective maximum achievable flight Mach-number.

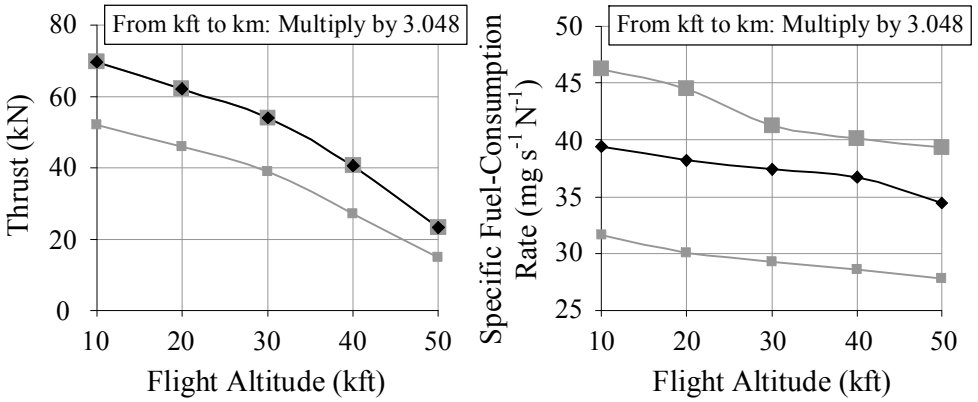

Figure 11.12. The performances of the baseline and two-combustor engines at maximum achievable flight Mach-number [—■— BLE —■— BLE+AB —◆— TCE].

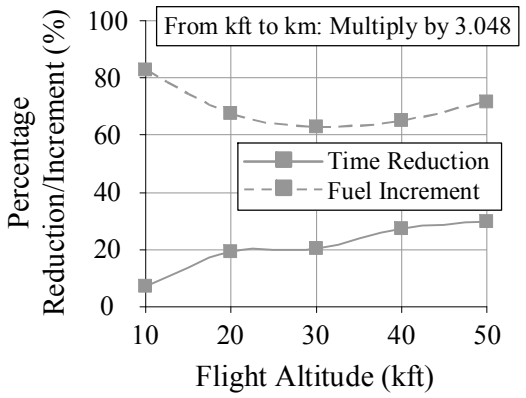

Figure 11.13. Performance of the baseline engine with afterburner, relative to the baseline engine, at the maximum achievable flight Mach-number of the two-combustor engine.

11.7 Aircraft's Performance under Optimal Cruise and Loiter Conditions

Equations (11.3) and (11.4) show the aircraft's weight-ratio under cruises and loiter conditions, respectively. Given the performances characteristics of both the aircraft and its propulsion system, the optimum flight conditions occurred for the aircraft's weight-ratio as close to unity as possible. Close examine of Equations (11.3) and (11.4) reveals that the optimum flight condition is also dependent on the flight altitude. With the differences in the characteristics of the baseline and two-combustor engines, the optimum flight conditions for aircraft powered by the respective engines could be at different altitude and flight Mach-number. Technically, the optimum flight conditions can be identified by sweeping the entire flight envelope. However, this approach would be of little value-add based on the limited available aircraft's characteristic data.

$$\frac{Wt_i}{Wt_{i-1}} = \exp\left(-\frac{R_{flt}}{V}\frac{SFC}{L/D}\right) \tag{11.3}$$

$$\frac{W_i}{W_{i-1}} = \exp\left(-E_{flt}\frac{SFC}{L/D}\right) \tag{11.4}$$

From the operation perspective, the users will have their own flight requirements, e.g. flight altitude and Mach-number. Usually these requirements are taken into consideration in the design and development of the aircraft and its engine. Presently, the author has no information with regard to these requirements. Reverse engineering to identify these requirements might be possible, but high levels of uncertainties/discrepancies are expected. Applying these requirements with limits aircraft data will results in more uncertainties in the results. Therefore, the study to identify the flight condition for optimum loiter and cruise conditions is not available in this study.

11.8 Conclusions

Studies are conducted to study the effects of two-combustor engine on the aircraft's performance when compared with that of baseline engine. Limited studies are conducted due to the lack of exact aircraft-performance data. The following summarize the findings: -

- ✓ The results show that aircraft with two-combustor engine has larger flight envelope and higher rate-of-turn when compared with that achievable with the baseline engine. However the above are achieved at the expenses of higher specific fuel-consumption rate. Nevertheless, when an afterburner is added to the baseline to produce comparable maximum achievable thrust of the two-combustor engine, the former will require higher specific fuel-consumption rate than the two-combustor engine.
- ✓ With both the baseline and two-combustor engine operating under dry thrust condition, the latter can operate at a higher flight Mach-number due to its higher achievable thrust; therefore the required duration for specific range will be reduced. However, the two-combustor engine being less efficient will consumed more fuel than the baseline engine. Similar to the previous paragraph, the use of the baseline engine with an afterburner is further less efficient than the two-combustor engine.

- ✓ When the aircraft is operating at cruise condition, the two-combustor engine is not a favorable option; its specific fuel-consumption rate is higher than that of the baseline engine.

In summary, when "moderate" high thrust is required, the two-combustor engine would be a favorable configuration than the baseline engine with an afterburner. For both baseline and two-combustor engines at maximum achievable dry-thrust, there exist a trade-off between reductions in flight duration against the increase in the amount of fuel consumed. When operating under cruise condition, the two-combustor engine is less efficient, thus not favorable when compared with to the baseline engine.

Chapter 12. Infrared Signature of the Engine's Exhaust-Cavity and Exhaust-Plume

12.1 Introduction

The signatures of the aircraft are crucial to its survivability and the success of its mission. The propulsion system is the main source of signatures, in particular the infrared signature [13-20]. The infrared-energy radiates from the engine's exhaust cavity (i.e. turbine, tail-pipe and exhaust nozzle) is dominating when viewed from the aft of the aircraft; whereas infrared-energy from the exhaust plume becomes more dominating when viewed from the side of the aircraft [14, 17-20]. In this study, empirical approaches (see Section 3.3.5) have been used to predict the signatures radiate from the engine's exhaust cavity and plume. Although it is a brief study, the predictions are sufficient to provide an indication on the level of infrared-energy radiates by the two-combustor engine relative to that of the baseline engine.

The study was conducted for Configuration 1 of the F16-EQ aircraft operating at an altitude of 30kft (i.e. 9.144km) (see Section 11.3.1). The engines operating under dry thrust, wet thrust and trim conditions are considered. The design-point conditions for the baseline and two-combustor engines are as shown in Table 6.1.

12.2 Engine's Exhaust-Cavity

12.2.1 Military (Dry) Thrust Condition

The infrared-energy radiates for the exhaust cavity of the baseline and two-combustor engines, over the selected range of flight Mach-number, are shown in Figure 12.1. Generally, due to its lower gas temperature, the infrared signature of the baseline engine's exhaust cavity is lower than that produces by the two-combustor engine. At lower range of flight Mach-number, there are various combinations of high-pressure and low-pressure turbines' entry-temperatures

(HPTET and LPTET) that enable the two-combustor engine to operate at respective maximum achievable thrust within respective envelope. To reduce the number of variable, only the option of two-combustor engine operating with HPTET identical to LPTET was considered.

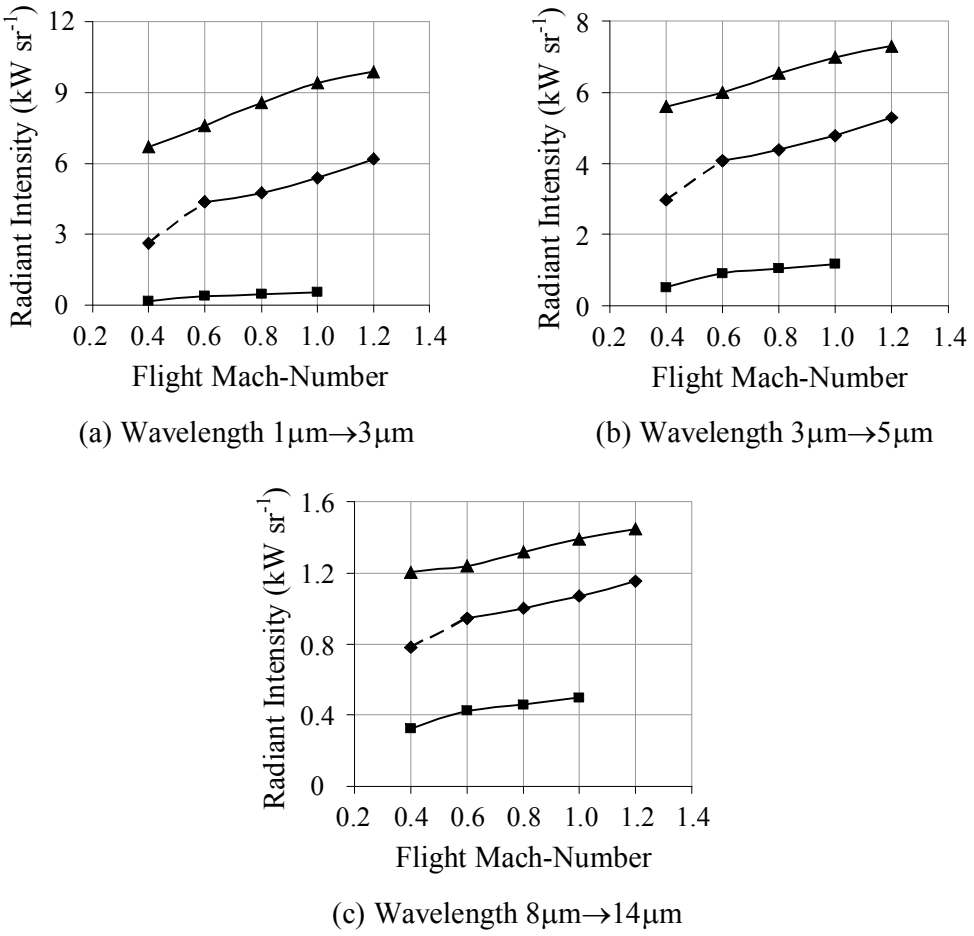

Figure 12.1. The exhaust-cavity's radiant intensities of the baseline (BLE) and two-combustor (TCE) engines [BLE BLE+AB TCE(TETs=1700K) TCE(TETs<1700K)].

The baseline engine with an afterburner (in partial operation) can achieve the identical operating envelope as that of the two-combustor engine. The mass-flow rate of the baseline and two-combustor engines are approximately equal (see Figure 12.2). However, the baseline engine's exit-flow has lower pressure; thus its gas-temperature has to be higher than that of the two-combustor engine so as to

produce the same level of thrust. With the level of radiation dominates by the flow temperature, the baseline engine (with afterburner) radiates higher infrared-energy than that of the two-combustor engine. The latter radiates at least 20% lower infrared-energy when compared with that of the baseline engine with an afterburner producing comparison thrust performance (see Figure 12.3).

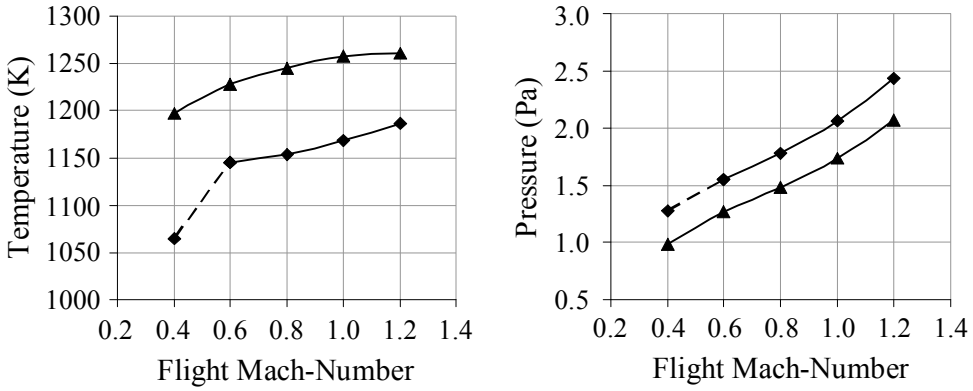

Figure 12.2. The nozzle's exit flow-properties of the baseline (BLE) and two-combustor (TCE) engines [—▲— BLE+AB —◆— TCE(TETs=1700K) - -◆- - TCE(TETs<1700K)].

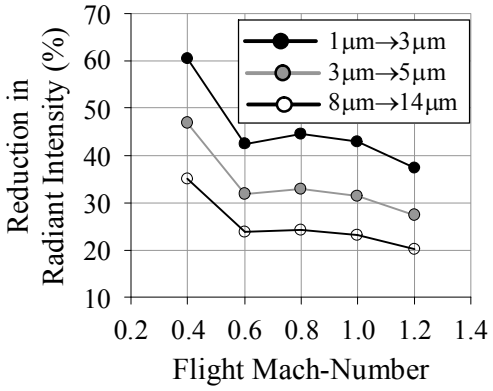

Figure 12.3. Reduction in the exhaust-cavity's radiant intensity of the two-combustor engine relative to that of the baseline engine with an afterburner.

12.2.2 Maximum (Wet) Thrust Condition

With afterburner used in both the baseline and two-combustor engine to produce the comparable thrust, the exhaust-cavity of the baseline engine radiates

higher radiant intensity when compared with that of the baseline engine (see Figure 12.4). There is substantial reduction (~7%→~24%, see Figure 12.5) in the radiant intensity of the exhaust-cavity when the two-combustor engine is replacement of the baseline engine. Due to the high exhaust temperature, the above-stated reduction is highest at the waveband 1μm→3μm when compared with the other two wavebands considered.

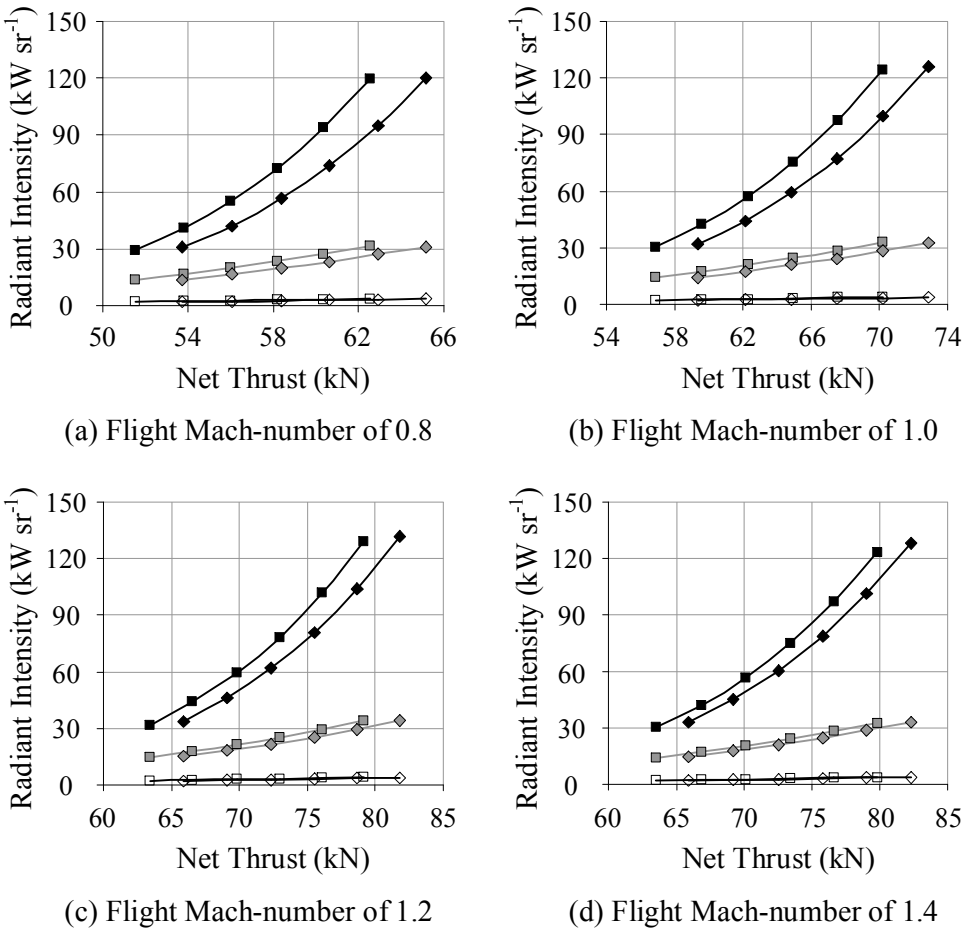

Figure 12.4. The exhaust-cavity's radiant intensities of the baseline (BLE) and two-combustor (TCE) engines [BLE(1μm→3μm) TCE(1μm→3μm) BLE(3μm→5μm) TCE(3μm→5μm) BLE(8μm→14μm) TCE(8μm→14μm)].

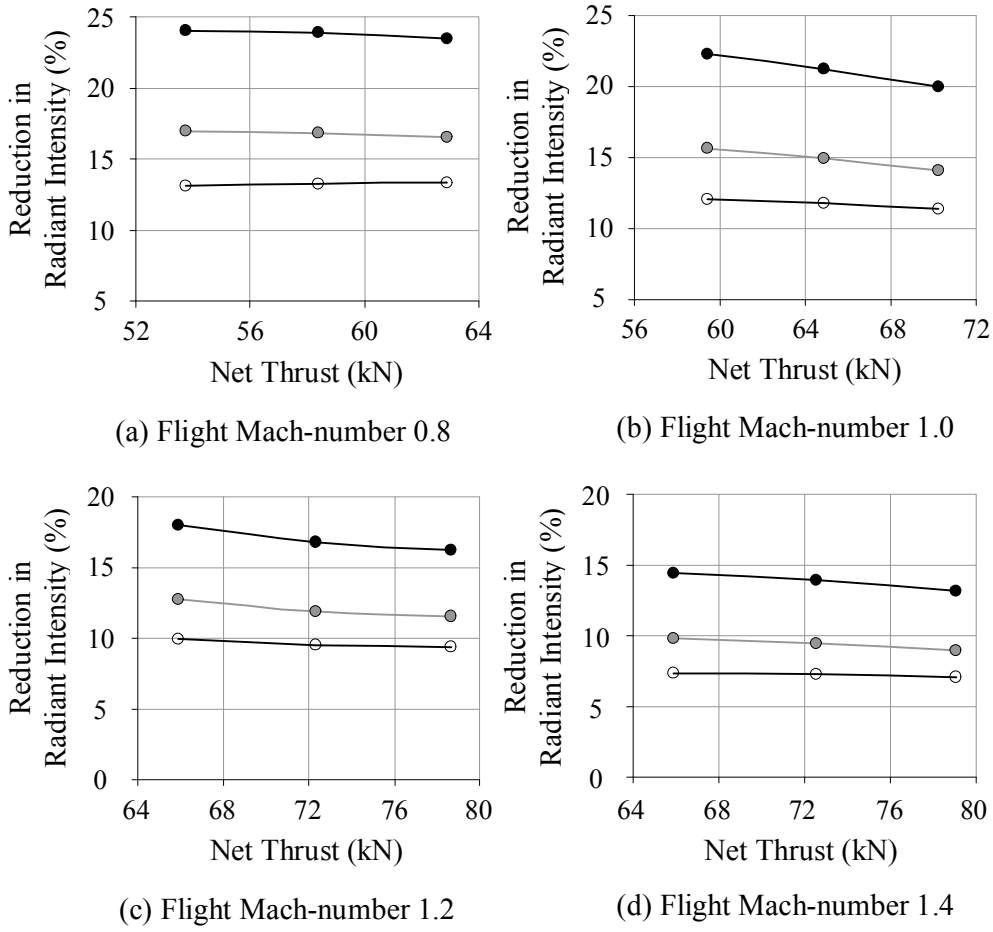

Figure 12.5. Reduction in the exhaust-cavity's radiant intensities of the two-combustor engine relative to that of the baseline engine

12.2.3 Cruise Condition

At cruise condition, the engine is throttled-down for the aircraft to operate under trim condition, i.e. thrust equal to drag and weight equal to lift. The baseline engine is throttled-down by reducing its turbine's entry-temperature (TET); whereas the thrust of the two-combustor engine is controlled by both the HPTET and LPTET. Two TETs-schedules have been considered, namely (i) both HPTET and LPTET throttled-down at the same rate simultaneously and (ii) the LPTET is throttled-down with the HPTET maintain at its maximum allowable

temperature. The option of high LPTET with low HPTET is less efficient (see Section 6.6), hence it is not considered here.

The two-combustor engine with the option of maintaining HPTET at its maximum allowable temperature radiates lower exhaust-cavity's radiant intensity than the option of keeping the HPTET and LPTET at the same temperature (see Figure 12.6). Nevertheless, regardless of TETs-schedules, the exhaust-cavity of the two-combustor engine radiates higher infrared radiant-intensity when compared with that of the baseline engine (see Figure 12.6); whereby the former could be 0.4→4.6 times higher depending on the flight Mach-number and waveband considered (see Figure 12.7).

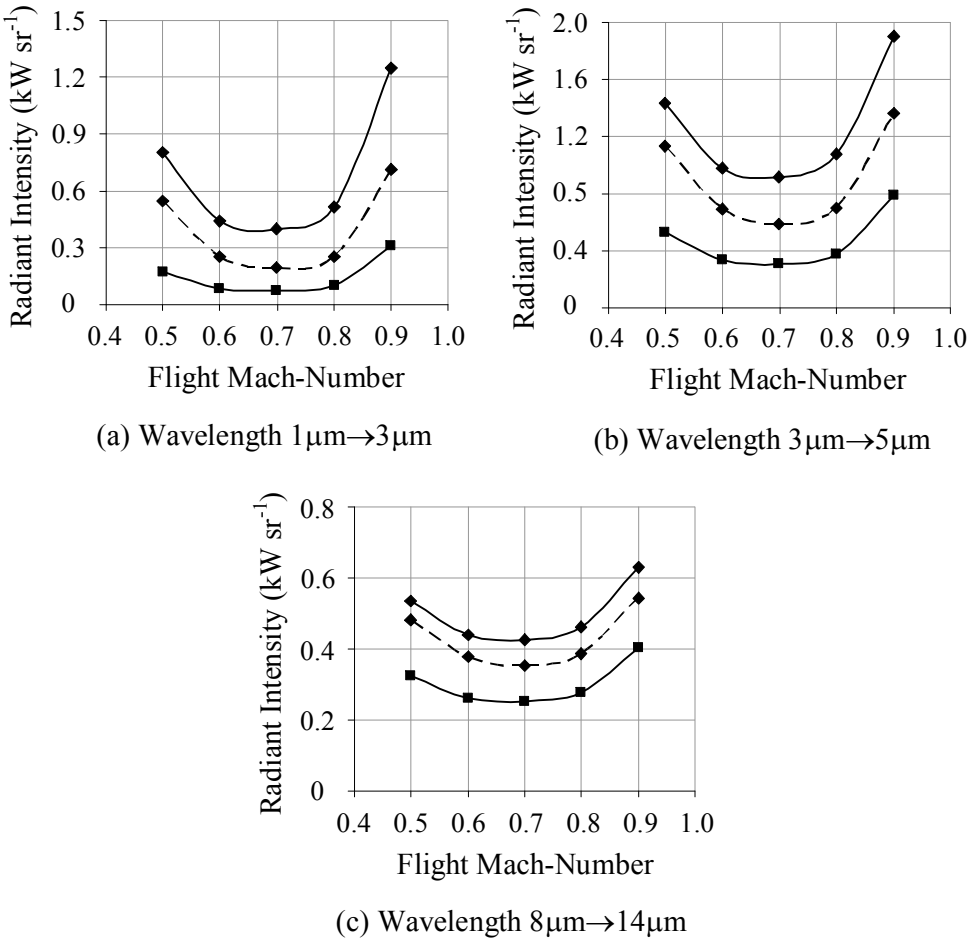

(a) Wavelength 1μm→3μm

(b) Wavelength 3μm→5μm

(c) Wavelength 8μm→14μm

Figure 12.6. The engines' exhaust-cavity's radiant intensities for the aircraft under trim condition [—■— BLE – ◆ – TCE(HPTET=max) —◆— TCE(HPTET=LPTET)].

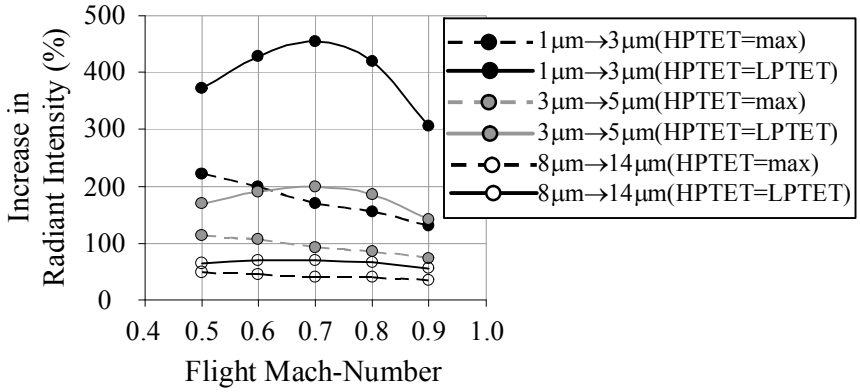

Figure 12.7. Increase in exhaust-cavity's radiant intensities of the two-combustor engine relative to that of the baseline engine.

12.3 Engine's Exhaust-Plume

12.3.1 Military (Dry) Thrust Condition

Figure 12.8 shows that radiant intensity of the engine's exhaust-plume at dry thrust condition; where the trends resemble that of the engine's exhaust-cavity (see Figure 12.1). The two-combustor engine's exhaust-plume has a higher radiant intensity than that of the baseline engine. When an afterburner is added to

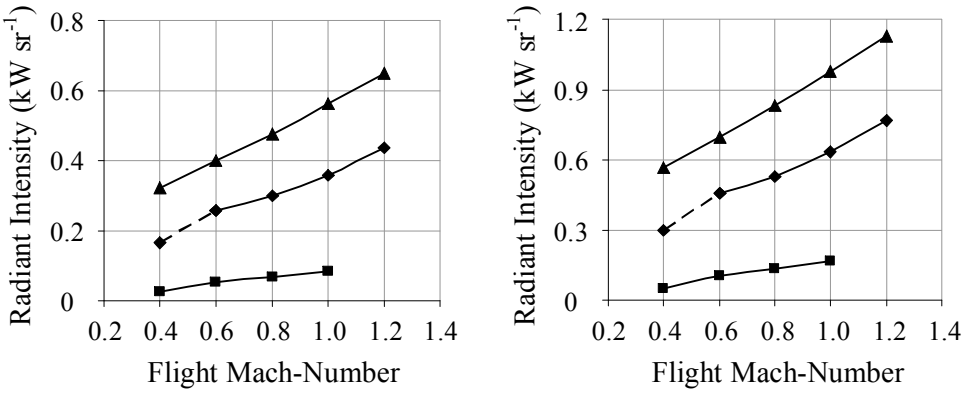

(a) Waveband 4.10μm→4.15μm (b) Waveband 4.45μm→4.55μm

Figure 12.8. The exhaust-plume's radiant intensities of the baseline (BLE) and two-combustor (TCE) engines [BLE BLE+AB TCE(TETs=1700K) TCE(TETs<1700K)].

the baseline engine to produce thrust comparable to that of the two-combustor engine's dry thrust, the former will has significantly higher exhaust-temperature; thus it produces significantly higher radiant intensity than that of the two-combustor engine.

12.3.2 Maximum (Wet) Thrust Condition

Afterburners are used in both the baseline and two-combustor engines to produce higher achievable thrust. The trends of the exhaust-plumes' radiant intensity are identical to that of the exhaust-cavity (see Section 12.2.2); where the baseline engine radiates lower infrared-energy when compared with that of the two-combustor engine with comparable wet thrust. With the use of the two-combustor engine, the reduction in the exhaust-plume's radiant intensity is in the range of ~15% to ~23% when compared with that of the baseline engine (see Figure 12.9).

12.3.3 Cruise Condition

For aircraft under cruise (i.e. trim) condition, the exhaust-plume's radiant intensity of the baseline engine is lower than that of the two-combustor engine; which trends are identical to that of the exhaust-cavity. The increase in the exhaust-plume's radiant intensity with the use of the two-combustor engine could be as high as ~2 times that of the baseline engine (see Figure 12.10). Considering two-combustor engine operates with its HPTET at its maximum allowable temperature, its penalty in the infrared radiant-intensity is lower when compared with the option of operating with HPTET and LPTET at same temperature. However, this reduction in the penalty in the exhaust-plume's radiant intensity is less obvious than that of that in the exhaust-cavity.

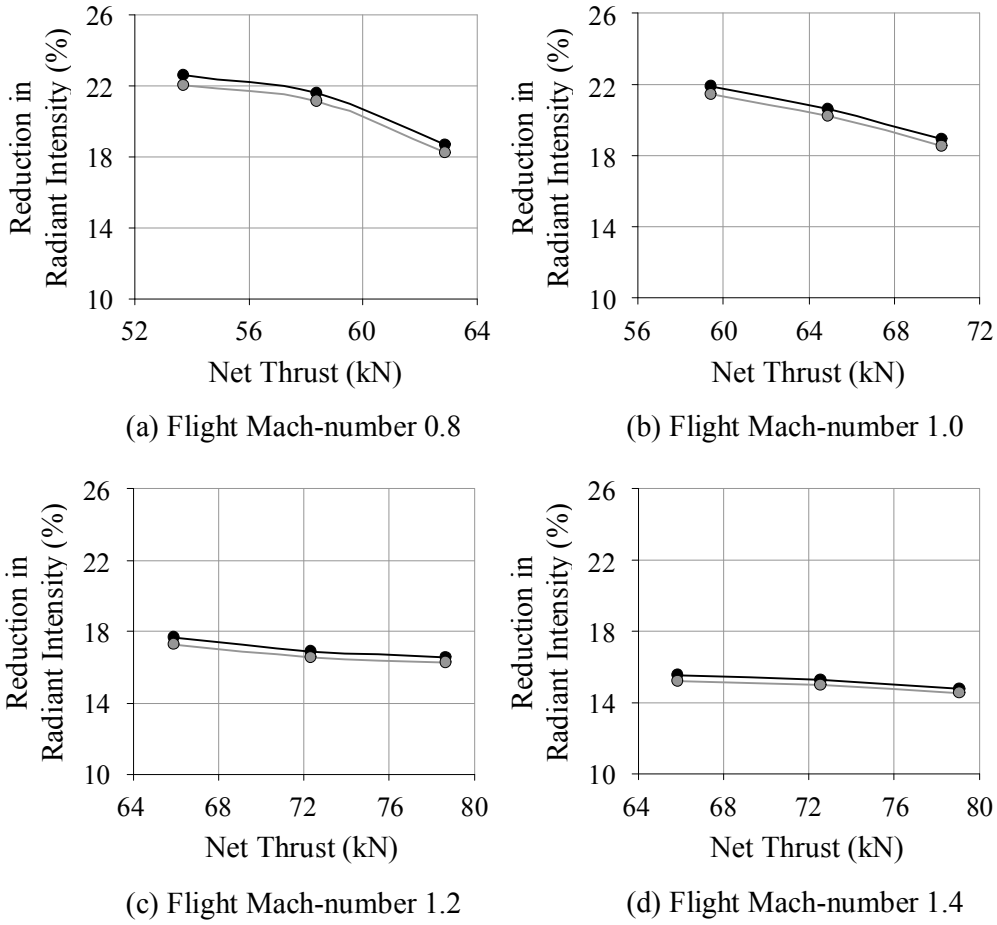

Figure 12.9. Reduction in the exhaust-plume's radiant intensities of the two-combustor engine relative to that of the baseline engine [4.10μm→4.15μm 4.45μm→4.55μm].

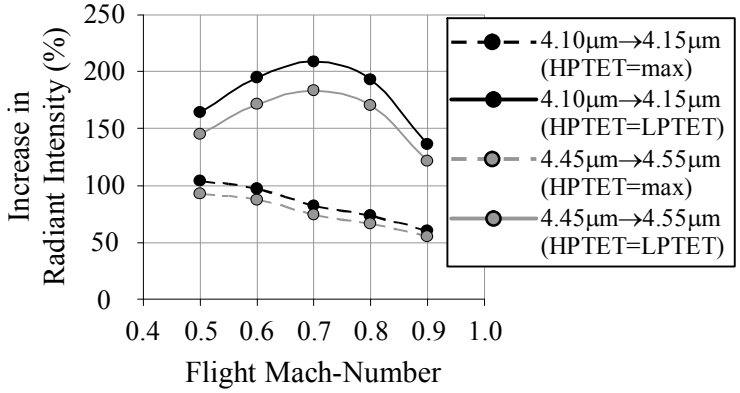

Figure 12.10. Increase in exhaust-plume's radiant intensities of the two-combustor engine relative to that of the baseline engine.

12.4 Conclusions

Empirical approaches have been adopted to investigate the effects of two-combustor engine on the aircraft's infrared-signature when compared with that of baseline engine. The infrared radiant-intensity of the engines' exhaust-cavities and plumes were predicted for engine under dry thrust, wet thrust and cruise conditions. The trends of the infrared radiant-intensity generates by the exhaust-cavity are identical to that of the exhaust-plume. Under maximum dry thrust condition, the signature of the two-combustor engine is higher than that of the baseline engine. However, when an afterburner is used in the baseline engine to generate comparable thrust to that of the two-combustor engine, the former generates higher signature than that of the two-combustor engine. When both the baseline and two-combustor engines are mounted with afterburner to generate comparable wet thrust, the former generates higher signature. When both engines are throttled-down to operate at cruise condition, the two-combustor engine generate higher signature than the baseline engine.

In summary, comparing the infrared signature generates by the baseline and two-combustor engine, the latter is more favorable configuration when high thrust is required (e.g. supersonic flight); whereas the baseline engine generates lower signature when lower thrust is needed (e.g. subsonic cruise).

Chapter 13. Conclusions and Recommendations

13.1 Conclusions

There are continual demands for military aero-engines to have higher specific thrusts and lower specific fuel-consumption rates (SFCs) over extended envelopes. With the maturing of the technologies concerned with the design and manufacture of conventional engines, the ability to further improve the basic-engine's performance is diminishing. Also, the infrared-energy radiation from the propulsion system has a great impact on the aircraft's survivability in a mission. Hence a novel cycle engine (i.e. a two-combustor engine) is proposed and investigated in attempt to improve the engine's aerodynamic performance and infrared-signature characteristic.

Based on the knowledge acquired from the extensive literature survey, systematic approaches were formatted with proven analytical methodologies for conducting the present study. Through the employment of engine performance-simulation program of high fidelity and also incorporating the exact turbine's cooling-flow rate, the characteristics and performances of the two-combustor engine are addressed with high order of accuracy. The key contribution is the establishment on the influences of the two-combustor engine on the performances of the selected fighter aircraft, in particular the transient behaviour, steady-state flight characteristics (e.g. flight-envelope) and infrared signatures. In order to ascertain the prospects and shortfalls of a two-combustor engine for military fighter, a proven conventional engine (i.e. F100-PW229 engine, based on open publications), for powering military fighter aircraft, was selected for benchmarking purposes. This research has revealed the potential of a two-combustor engine, relative to a proven conventional engine, on the enhancement of performances for an military fighter aircraft; with respect to both the aerothermodynamics and infrared characteristics. In particular, the results, findings and conclusions for the influences of two-combustor engine on aircraft's performance are not found in any up-to-date publication. In addition, the

availability of this research will allow engine and aircraft studies to include two-combustor solution in a more secure way than it was possible.

This research have been broken-down into different subjects pertaining to the aerothermodynamics performance of the two-combustor engine and its influences on the aircraft's behaviour. The results and findings for each subject are presented as an independent chapter in this thesis. Also, the discussions on the results and findings are adequate for conclusions to be drawn and included in the respective chapters. In this chapter, only the key conclusions are summarized; in particular, the key prospects and drawbacks of the two-combustor engine for the military fighter aircraft are emphasized.

The aerothermodynamics behaviours of the two-combustor engine under design-point conditions are revealed. A baseline engine having a performance equivalent to that of the F100-PW229 engine is selected for benchmarking. Interestingly, the two-combustor engine's maximum achievable specific thrust and thermal efficiency occur at approximately the same overall pressure-ratio (OPR). For a given OPR, the fan's pressure-ratio for maximum achievable specific thrust is lower than that for maximum achievable thermal efficiency. These two observations are different from those for the conventional engine. The author suggests that this is because the two-combustor engine's performance is dependent on both the main-combustor's and inter-stage turbine burner's (ITB's) operating-conditions. The effects of various design-parameters on the on-design performance of the two-combustor engine have been investigated: the key observations are highlighted below. By varying the design-parameters, it would be possible to identify an optimal two-combustor engine configuration. Nevertheless, its higher specific thrust is achievable only at the expenses of the higher SFC.

- ✓ The overall pressure-ratio for the two-combustor engine, operating at maximum achievable specific thrust, is slightly lower than that of the baseline engine.

- ✓ The implementation of ITB enables the two-combustor engine have a higher optimal pressure-ratio for the fan in comparison with that for the conventional engine.
- ✓ With the reduced turbines' entry-temperatures (TETs), i.e. reduced turbine's cooling-flow requirement, there is no configuration for the two-combustor engine with a higher specific thrust but lower SFC when compared with that of the baseline engine.
- ✓ The installation of an ITB "nearer" to the main-combustor reduced its SFC at the penalty of a lower specific thrust: the opposite was observed for the ITB when it was installed further "away" from the main-combustor.

The off-design performance of the two-combustor engine has been investigated under both full-throttle and part-throttle conditions. In the latter, the operation of the two-combustor engine was more efficient when the HPTET was kept at its maximum allowable temperature for comparable thrust. Nevertheless, regardless of the configuration and its throttling schedule, the two-combustor engine operated with a larger envelope by having a higher achievable thrust with a penalty for its SFC. The implementations of variable low-pressure turbine's nozzle-guiding-vanes and turbine's cooling-flow requirements have improved significantly the performance of the two-combustor engine. Nevertheless, there is no evidence that the two-combustor engine requires a lower SFC when compared with that of the baseline engine of comparable thrust.

To assess the physical impact of the implementation of the ITB, the methodologies for sizing of the conventional combustor and afterburner have been used to estimate the ITB's size. The installation of the ITB increases the engine's length. Nevertheless, together with an afterburner, the two-combustor engine could be marginally longer than that of the baseline engine, depending on the selected operating envelope for the two-combustor engine.

The transient behaviour and infrared characteristic are two specific subjects of interest regarding the actual operation of the two-combustor engine. Predicted using a simple methodology, the results reveal that the transient behaviour of the two-combustor engine is superior to that achievable by the baseline engine.

However, without detailed knowledge of the aircraft's control-loops, the exact effects of the two-combustor engine on the aircraft's transient-performance are not predictable. To investigate the engine's infrared characteristic, the infrared energy of the engine's exhaust-cavity (i.e. turbine, tail-pipe and exhaust nozzle) and exhaust-plume have been separately-predicted using empirical approaches. The results reveal that the two-combustor engine has a lower infrared radiation-intensity when compared with that emanating from the baseline engine with an afterburner producing a comparable thrust. However at the lower throttle setting (i.e. for the cruise condition), the two-combustor engine has a more intensive signature when compared with that from the baseline engine producing a comparable thrust.

Due to the lack of precise aerodynamic data for the aircraft, only limited studies concerning the effects of the two-combustor engine on the aircraft's performances have been investigated. The aircraft powered by the two-combustor engine has the larger operating envelope and higher rate-of-turn, but at the expenses of a higher SFC when compared with the use of the baseline engine. For the aircraft to operate at its maximum flight Mach-number achievable with the two-combustor engine, the baseline engine with an afterburner in partial operation is necessary. However, the latter configuration has a lower cycle-efficiency and hence higher SFC when compared with those of the two-combustor engine. For an aircraft in its cruise condition, the two-combustor engine requires a higher SFC than that needed by the baseline engine producing a comparable thrust.

Based on the above observations, the two-combustor engine is regarded as a more favourable engine for supersonic cruising due to its lower SFC and infrared-energy emissions when compared with that of the baseline engine includes an afterburner. However, the two-combustor engine is not a favorable option for subsonic cruise condition. The two-combustor engines will not surpass the conventional engine in all operational aspects. Nevertheless, the advantages of two-combustor engines (such as extended operating envelopes) might provide the motivation for their use.

13.2 Recommendations

The present study has clearly identified the niche areas for the two-combustor engine for military-fighter applications. Nevertheless, further studies have to be conducted in order to improve the accuracy of the present results and also to explore areas that have not been covered.

Transient-performance prediction codes of higher fidelity are required to improve the reliability and accuracy of the conclusions. Also the optimal path for acceleration and deceleration of the engine needs to be identified.

A more detail set of data on the aircraft's aerodynamic characteristics needs to be acquired so as to conduct the study at a higher resolution. Given the complete set of data, the study could extend the investigation to the influence of the two-combustor engine on the aircraft's performance over selected missions, e.g. surveillance mission.

With a validated infrared-signature prediction code, the infrared characteristics of the entire aircraft could be predicted. Then the exact contribution of infrared-energy from the two-combustor engine with reference to the baseline engine can be identified.

Combining the above-mentioned, a survivability study could also be conducted to assess the vulnerability of the aircraft undertaking air-superiority missions.

The complexity of the control of the two-combustor engine would be substantially increased by the implementation of the ITB. Therefore, it is desirable to investigate the feasibility of the two-combustor engine's control-system to ensure reliability and safety of the engine operation.

Only limited experience is available concerning the design of an ITB, in particular for aero-engines. Also, the gas temperature at the ITB's inlet (~1150K) is significantly higher than that at the inlet of the main combustor. Therefore it is necessary to study the design of the ITB to address the requirements of cooling-flow, combustion efficiency and pressure-losses.

References

1. Mason, R. A. (1987), Air power: An overview of roles, Brassey's Defence Publishers, London, UK.
2. Walker, J. R. (1989), Air superiority operations, Brassey's Defence Publishers, London, UK.
3. Elsam, M. B. (1989), Air defence, Brassey's Defence Publishers, London, UK.
4. Michael, K. (1989), Strategic offensive air operations, Brassey's Defence Publishers, London.
5. Walker, J. R. (1987), Air-to-ground operations, Brassey's Defence Publishers, London, UK.
6. Shaw, R. L. (1988), Fighter combat: The art and science of air-to-air warfare, Patrick Stephens Limited, Wellingborough.
7. Morgan, S. G. and Rogers, H. E. (1998), "Propelling the military into the future", International conference military aerospace technologies, p. 205-226, 8-10 Sep 1998.
8. Ruffles, P. C. (1998), "Delivering value to the customer through technology", International conference military aerospace technologies, p. 7-20, 8-10 Sep 1998.
9. Volpe, V. and Schiavone, J. M. (1993), "Balancing design for survivability", AIAA/AHS/ASEE aerospace design conference, 16-19 Feb 1993, AIAA, Irvine, CA, USA.
10. Rao, G. A. and Mahulikar, S. P. (2005), "New criterion for aircraft susceptibility to infrared guided missiles", Aerospace science and technology, Vol. 9, Issue 8, p. 701-712.
11. Doug, R. (1989), Stealth warplanes, Salamander Bks, London.
12. Fuhs, A. E. and Jenn, D. C. (1997), AIAA professional study on low observables, Amercian institute of aeronautics and astronautics.

13. Howe, D. (1991), "Introduction to the basic technology of stealth aircraft: Part I – Basic considerations and aircraft self emitted signals (Passive considerations)", Journal of engineering for gas turbines and power, Vol. 113, Issue 1, p. 75-79.

14. Ball, R. E. (2003), The fundamentals of aircraft combat survivability analysis and design (2nd ed), Amercian institute of aeronautics and astronautics, Inc., Reston, VA, USA.

15. Rao, G. A. and Mahulikar, S. P. (2002), "Integrated review of stealth technology and its role in airpower", The aeronautical journal, Vol. 106, No. 1066, p. 629-641.

16. Yi, B. (1995), "Combat-aircraft infrared-radiation characteristics and their infrared countermeasure and suppression technologies", China astronautics and missile abstracts, Vol. 2, p. 1-32.

17. Mahulikar, S. P., Sane, S. K., Gaitonde, U. N. and Marathe, A. G. (2001), "Numerical studies of integrated signature levels of complete aircraft", The aeronautical journal, Vol. 105, No. 1046, p. 185-192.

18. Rao, G. A. and Mahulikar, S. P. (2005), "Effect of atmospheric transmission and radiance on an aircraft infrared signature", Journal of aircraft, Vol. 42, No. 4, p. 1046-1054.

19. Rao, G. A. and Mahulikar, S. P. (2005), "Aircraft powerplant and plume infrared-signature modelling and analysis", 43rd AIAA Aerospace Sciences Meeting and Exhibit, 10-13 Jan. 2005, AIAA, Reno, NV, USA.

20. Mahulikar, S. P., Rao, G. A. and Kolhe, P. S. (2006), "Infrared signature of a low-flying aircraft and its rear-fuselage skin's emissivity optimization", Journal of aircraft, Vol. 43, No. 1, p. 226-232.

21. Wang, J. Y. (1995), "IR camouflage technology: State and development", Infrared and laser technology, Vol. 24, p. 1-4.

22. Tian, Z. H. (1996), "Summary of advanced infrared guided air-to-air missile-technology", China astronautics and missile abstracts, Vol. 3, p. 11-16.

23. Zhao, J. B. (1997), “Jamming of infrared guidance”, National air interlligence center, Feb 1997.

24. Davis, R. W. and Selegan, D. R. (1997), “Trends in future combat aircraft development”, AGARD symposium, 14-17 Apr 1997, Palaiseau, France.

25. Nicolai, L. M. (1997), “Considerations for affordable aerospace systems”, AGARD symposium, 14-17 Apr 1997, Palaiseau, France.

26. Jones, M. J. (2003), “A future military propulsion vision”, AIAA/ICAS international air and space symposium and exposition, 14-17 July 2003, Dayton, OH, USA.

27. Philippe, J. J. and Gmelin, B. (2003), “Rotorcraft challeneges and associated French-German research contribution”, AIAA/ICAS international air and space symposium and exposition, 14-17 Jul 2003, Dayton, OH, USA.

28. Williams, J. C. (1997), “Balancing affordability and performance in aircraft engines”, AGARD symposium, 14-17 Apr 1997, Palaiseau, France.

29. Skira, C. A. and Philpot, M. (1997), “Reducing costs for aircraft gas turbine engines”, AGARD symposium, 14-17 Apr 1997, Palaiseau, France.

30. Andriani, R., Ghezzi, U. and Ferri Degli Antoni, L. (1999), “Jet engines with heat addition during expansion: A performance analysis”, 37th AIAA aerospace sciences meeting and exhibit, 11-14 Jan 1999, Reno, NV, USA.

31. Andriani, R., Gamma, F., Ghezzi, U. and Infante, E. (2001), “Design proposals for constant temperature turbine engine for propulsion system”, 37th AIAA/ASME/SAE/ASEE joint propulsion conference and exhibit, 8-11 Jul 2001, Salt Lake City, UT, USA.

32. Liu, F. and Sirignano, W. A. (2000), “Turbojet and turbofan engine performance increases through turbine burners”, 38th AIAA aerospace sciences meeting and exhibit, 10-13 Jan 2000, Reno, NV, USA.

33. Liu, F. and Sirignano, W. A. (2001), “Turbojet and turbofan engine performance increases through turbine burners”, Journal of propulsion and power, Vol. 17, No. 3, p. 695-705.

34. Liew, K. H., Urip, E., Yang, S. L. and Siow, Y. K. (2003), "A complete parametric cycle analysis of a turbofan with interstage turbine burner", 41st AIAA aerospace sciences meeting and exhibit, 6-9 Jan 2003, Reno, NV, USA.

35. Liew, K. H., Urip, E., Yang, S. L., Mattingly, J. D. and Marek, C. J. (2004), "Performance cycle analysis of a two-spool, separate-exhaust turbofan with interstage turbine burner", 40th AIAA/ASME/SAE/ASEE joint propulsion conference and exhibit, 11-14 Jul 2004, Fort Lauderdale, FL, USA.

36. * Liew, K. H., Urip, E., Yang, S. L., Mattingly, J. D. and Marek, C. J. (2004), "Performance cycle analysis of a two-spool, separate-exhaust turbofan with interstage turbine burner", 40th AIAA/ASME/SAE/ASEE joint propulsion conference and exhibit, 11-14 Jul 2004, Fort Lauderdale, FL, USA.

37. Liew, K. H., Urip, E. and Yang, S. L. (2005) "Parametric cycle analysis of a turbofan engine with an interstage turbine burner", Journal of propulsion and power, Vol. 21, No. 3, p. 546-551.

38. Liew, K. H., Urip, E., Yang, S. L., Mattingly, J. D. and Marek, C. J. (2006) "Performance cycle analysis of turbofan engine with interstage turbine burner", Journal of propulsion and power, Vol. 22, No. 2, p. 411-416.

39. Liew, K. H. (2006), Aerothermodynamic cycle analysis of a dual-spool separate-exhaust turbofan engine with an interstage turbine burner (PhD thesis), Michigan Technological University.

40. Vogeler, K. (1998), "The potential of sequential combustion for high bypass jet engine", International gas turbine and aeroengine congress and exhibition, 2-5 Jun 1998, Stockholm, Sweden.

41. Eady, C. J. (1997), The effect of variable turbine flow capacity on the acceleration performance of a gas turbine engine (MSc thesis), Cranfield University.

42. Kristiansen, I. E. (2001), High bypass ratio three shaft turbofan engine with inter turbine reheat (MSc thesis), Cranfield University.

43. Yannakoulis, N. (2004), Introducing inter-turbine reheat in a high-bypass civil turbofan engine (MSc thesis), Cranfield University.

44. Treager, I. E. (1994), Aircraft gas turbine engine technology (2nd ed), Gregg Division McGraw-Hill, New York, USA.

45. Otis, C. (1991), Aircraft gas turbine powerplants (2nd ed), Casper, WY:IAP.

46. Mattingly, J. D. (2006), Elements of propulsion: Gas turbines and rockets, American institute of aeronautics and astronautics, Inc., Reston, VA, USA.

47. Hüenecke, K. (1997), Jet engines: Fundamentals of theory, design and operation, Airlife Publishing Ltd, England.

48. Whitford, R. (2004), Fundamentals of fighter design, The Crowood Press, Malborough, Wiltshire, USA.

49. Ballal, D. R. and Zelina, J. (2003), "Progress in aero engine technology (1939–2003)", 39th AIAA/ASME/SAE/ASEE joint propulsion conference and exhibit, 20-23 Jul 2003, Huntsville, AL, USA.

50. Yon, C. (2001), The selective bleed variable cycle engine: Implementation of a variable low pressure turbine (MSc thesis), Cranfield University.

51. Saravanamuttoo, H. I. H., Rogers, G. F. C., Cohen, H. and Straznicky, P. V. (2008), Gas turbine theory, Pearson Prentice Hall, Upper Saddle River, N.J., USA.

52. Perez Llarena, L. A. (1998), The selective bleed variable cycle engine: Design of compressors and valves (MSc thesis), Cranfield University.

53. Wood, A. S. (1996), Sizing and installation of the selective bleed variable cycle engine (MSc thesis), Cranfield University.

54. Andriani, R. and Ghezzi, U. (2002), "Off-design analysis of constant temperature turbine jet engine", 38th AIAA/ASME/SAE/ASEE joint propulsion conference and exhibit, 7-10 Jul 2002, Indianapolis, IN, USA.

55. Sirignano, W. A., Delplanque, J. P. and Liu, F. (1997), "Selected challenges in jet and rocket engine combustion research", 33rd

AIAA/ASME/SAE/ASEE joint propulsion conference and exhibit, 6-9 Jul 1997, Seattle, WA, USA.

56. Sirignano, W. A. and Liu, L. (1999), "Performance increases for gas-turbine engines through combustion inside the turbine", Journal of propulsion and power, Vol. 15, No. 1, p. 111-118.

57. Chiu, Y. T., King, P. S. and O'Brien, W. F. (2005), "A performance study of a super-cruise engine with isothermal combustion inside the turbine", 41st AIAA/ASME/SAE/ASEE joint propulsion conference and exhibit, 10-13 Jul 2005, Tucson, AZ, USA.

58. Chen, G., Hoffman, M. A. and Davis, R. L. (2004), "Gas-turbine performance improvements through the use of multiple turbine interstage burners", Journal of propulsion and power, Vol. 20, No. 5, p. 828-834.

59. Chen, G., Hoffman, M. A. and Davis, R. L. (2004), "Improvements in gas-turbine performance through the use of multiple turbine inter-stage burners", 42nd AIAA aerospace sciences meeting and exhibit, 5-8 Jan 2004, Reno, NV, USA.

60. Frutschi, H. U. (1994), Advanced cycle system with new GT24 and GT26 gas turbines – Historical background", ABB review, p20-25.

61. Nanhoff, H. and Thoren, K. 1994, GT24 and GT26 gas turbine - Sequential combustion: The key to high efficiencies", ABB Review, p. 4-7.

62. Joos, F., Brunner, P., Schulte-Werning, B., Syed, K. and Eroglu, A. (1996), "Development of the sequential combustion system for the ABB GT24/GT26 gas turbine family", ASME international gas turbine and aeroengine congress and exhibition, 10-13 Jun 1996, Birmingham, UK.

63. Mayer, A. and van der Linden, S. (1999), "GT24/26 advanced cycle system power plant progress for the new millenium", ASME international gas turbine and aeroengine congress and exhibition, 7-10 Jun 1999, Indianopolis, IN, USA.

64. Zelinak, J., Shouset, D. T. and Neuroth, C. (2005), "High-pressure tests of a high-g, ultra-compact combustor", 41st AIAA/ASME/SAE/ASEE joint propulsion conference and exhibit, 10-13 Jul 2005, Tucson, AZ, USA.

65. Zelina, J., Sturgess, G. J. and Shouse, D. T. (2004), "The behaviour of an ultra-compact combustor (UCC) based on centrifugally-enhanced turbulent burning rates", 40th AIAA/ASME/SAE/ASEE joint propulsion conference and exhibit, 11-14 Jul 2004, Fort Lauderdale, FL, USA.

66. Mawid, M. A., Park, T. W., Thornburg, H., Sekar, B. and Zelina, J. (2005), "Numerical analysis of inter-turbine burned (ITB) concepts for improved gas turbine engine performance", 43rd AIAA aerospace sciences meeting and exhibit, 10-13 Jan 2005, Reno, NV, USA.

67. Siow, Y. K. and Yang, S. L. (2002), "Numerical study and design of interstage turbine burner", 38th AIAA/ASME/SAE/ASEE joint propulsion conference and exhibit, 7-10 Jul 2002, Indianapolis, IN, USA.

68. Pachidis, V. A. (2006), Gas-turbine performance simulation, MSc course notes, Cranfield University.

69. Walsh, P. P. and Fletcher, P. (2004), Gas-turbine performance, Blackwell Science, Oxford.

70. Kurzke, J. (2003), Aero-engine design: A state of the art, von Karman Institute for Fluid Dynamics.

71. Young, J. B. and Wilcock, R. C. (2002), "Modelling the air-cooled gas turbine: Part 2 – Coolant flows and losses", Journal of turbomachinery, Vol. 124, p. 214-222.

72. Holland, M. J. and Thake, T. F. (1980) "Rotor blade cooling in high pressure turbines", Journal of aircraft, Vol. 17, p. 412-418.

73. Wilock, R. C., Young, J. B. and Horlock, J. H. (2005), "The effect of turbine blade cooling on the cycle efficiency of gas turbine power cycle", Journal of engineering for gas turbines and power, Vol. 127, p. 109-120.

74. Kurzke, J. (2002), "Performance modelling methodology: Efficiency definitions for cooled single And multistage turbines", ASME turbo expo, 3–6 Jun 2002, Amsterdam, The Netherlands.

75. Jones, B. (2008), Gas-turbine combustor, Short-course's course notes, Cranfield University.

76. ESDU (1981), Estimation of windmill drag and airflow of turbojet and turbofan engines, ESDU 81009, Performance Vol. 4, ESDU, London, UK.

77. Singh, R. (2006), Combustor, MSc course note, Cranfield University.

78. Koff, B. L. (1989), "F100-PW-229 higher thrust in same frame size", Journal of engineering for gas turbines and power, Vol. 111, p. 187–192.

79. Pilidis, P. (2006), Gas-turbine performance, MSc course note, Cranfield University.

80. Kurzke, J. (2004), GasTurb 10 – User's manual, Germany.

81. Jane's Information Group (2008), Jane's aero-engines, Jane's information group.

82. http://www.allstar.fiu.edu/aero/P&WEngines03.html

83. Hudson, R. D. (1969), Infrared system engineering, John Wiley & Sons, New York, USA.

84. Brandt, S. A., Stiles, R. J., Bertin, J. J. and Whitford, R. (2004), Introduction to aeronautics: A design perspective (2nd ed), American institute of aeronautics and astronautics, Inc., Reston, VA.

85. Cumpsty, N. A. (2003), Jet propulsion: A simple guide to the aerodynamic and thermodynamic design and performance of jet engines (2nd ed), Cambridge University Press, UK.

86. Raymer, D. P. (2006), Aircraft design: A conceptual approach (4th ed), American institute of aeronautics and astronautics, Inc., Reston, VA.

87. Jane's Information Group (2007), Jane's all the world's aircraft, Jane's information group.

88. http://en.wikipedia.org/wiki/F-16_Fighting_Falcon

89. http://www.aerospaceweb.org/aircraft/fighter/f16/

90. Jane's Information Group (2008), Jane's air-launched weapons, Jane's information group.

91 http://www.lockheedmartin.com/news/press_releases/2002/LockheedMartinUSAirForceCompleteFli.html

92. Mattingly, J. D., Heiser, W. H. and Pratt, D. T. (2002), Aircraft engine design (2nd ed), American institute of aeronautics and astronautics, Inc., Reston, VA.

93. http://en.wikipedia.org/wiki/Pratt_&_Whitney_F100

94. Lee, A. S., Singh, R. and Probert, S. D. (2008), "Performances of a two-combustor turbofan engine under design and off-design conditions", 44th AIAA/ASME/SAE/ASEE joint propulsion conference and exhibit, 21-23 July 2008, Hartford, CT, USA.

95. Yangom, S. (2006), Effect of variable cooling flow on gas turbine performance (MSc thesis), Cranfield University.

96. Ryman, B. (2003), The effect on gas turbine performance of air bleed for turbine cooling (MSc thesis), Cranfield University.

97. Sergent, H. (2000), Cooling air supply to high-pressure gas turbine blades (MSc thesis), Cranfield University.

98. Lefebvre, A. H. (1998), Gas turbine combustion (2nd ed), Taylor and Francis, London, UK.

99. http://fas.org/programs/ssp/man/uswpns/air/fighter/f16.html

100. Rolls-Royce (2005), The jet engine, Rolls-Royce, London, UK.

* Reference 36 is obtained directly from one of the author (Yang Song Lin).

Publications

1. Lee, A. S., Singh, R. and Probert, S. D. (2008), "Multi-combustor engines for military aircraft", 44th AIAA/ASME/SAE/ASEE joint propulsion conference and exhibit, 21-23 July 2008, Hartford, CT, USA.

2. Lee, A. S., Singh, R. and Probert, S. D. (2008), "Performances of a two-combustor turbofan engine under design and off-design conditions", 44th AIAA/ASME/SAE/ASEE joint propulsion conference and exhibit, 21-23 July 2008, Hartford, CT, USA.

3. Lee, A. S. and Singh, R. (2009), "Two-combustor engines for military aircraft", Aerospace technology seminar, Feb 2009, Singapore.

4. Lee, A. S., Singh, R. and Probert, S. D. (2009), "Modelling of F100-PW229 equivalent engine at sea-level static condition", 45th AIAA/ASME/SAE/ASEE joint propulsion conference and exhibit, 2-5 Aug 2009, Denver, CO , USA.

5. Lee, A. S., Singh, R. and Probert, S. D. (2009), "Effects of influential parameters on two-combustor engines' performances under design-point conditions", 45th AIAA/ASME/SAE/ASEE joint propulsion conference and exhibit, 2-5 Aug 2009, Denver, CO , USA.

6. Lee, A. S., Singh, R. and Probert, S. D. (2009), "Two-combustor engine's transient performance", 45th AIAA/ASME/SAE/ASEE joint propulsion conference and exhibit, 2-5 Aug 2009, Denver, CO , USA.

7. Lee, A. S., Singh, R. and Probert, S. D. (2009), "Two-combustor engine for military applications", 19th Conference of the international society for air breathing engines, 7-11 Sep 2009, Montréal, Québec, Canada (Accepted for Publication).

Appendix A. Constant-Temperature Turbine (CTT) Engine

Figure A1 shows the thermodynamic-cycle for turbojet engine with a constant-temperature turbine (CTT). The combustor process in the constant-temperature turbine in the CTT engine resembles that in the Carnot cycle, which is the most efficient cycle [39].

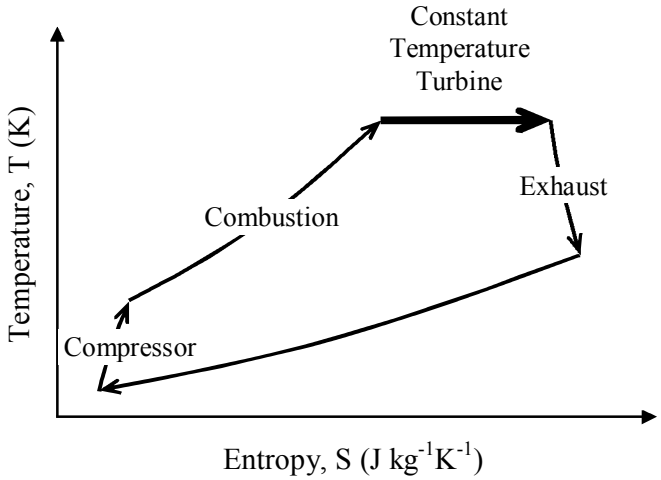

Figure A1. Temperature versus enthalpy diagram for constant temperature turbine (turbojet) engine.

Aero-Engine

Andriani et al [30, 31] had conducted investigation to reveal the performance of a CTT engine. The considered turbojet engine with afterburner produces higher specific thrust when compared with that achievable by a CTT tubojet-engine. However, the latter has a higher thermal efficiency. Andriani et al [54] extended the study to address the off-design performance of a single-spool CTT turbojet-engine. The CTT engine with variable area exhaust-nozzle allow higher mass-flow rate and thus produced higher thrust when compared with the equivalent CTT engine with a fixed exhaust-nozzle. This observation indicates that the implementation of the CTT posts a similar characteristics as that of an afterburner.

Analyses were also conducted by Sirignano et al [55, 56] to study the performance of a turbojet engine with CTT, which was designated as turbine-burner. The incorporating of the CTT increases the engine's specific thrust by 20% at the expenses of 10% increase in its specific fuel-consumption rate (SFC); where the equivalent increase in specific thrust will require a 50% increase in SFC if afterburner was used [56].

Chiu et al [57] investigated the effects of the implementation of CTT (which was designated as "turburner") in a turbofan engine for high-altitude supercruise application. Chiu et al had considered the performances of several engine-configurations with main-burner in combinations with inter-stage turbine burner (ITB), high-pressure (HP) turburner, low-pressure (LP) turburner and afterburner. The configuration with main burner and HP-turburner was chosen due to its superior performance when compared with the other the configurations. The implementation of HP-turburner increases the cruise-range by 4.6% or reduces the engine's mass-flow rate by 33% (i.e. a smaller engine is feasible) when compared with that achievable by the conventional turbofan engine. The analysis also revealed that turbofan with HP-turburner can provide higher thrust over larger envelope when compared with that achievable with the conventional engine.

Expectedly, the performance of the CTT engine is better than that achievable by the conventional engine. However, there are shortfalls in the analytical tool and model that will affect the accuracy of the predictions. Simple engine performance-simulation methodologies were adopted by Andriani et al [30, 31] and Sirignano et al [55, 56]. In addition, the requirement for extra cooling-flow rate for the CTT engine was not considered [30, 31, 57] or explicitly considered [55, 56]; therefore the performance of the CTT engine might over-predicted. Nevertheless, the results are sufficient to provide a first-order estimation on the performance of a CTT engine relative to a comparable conventional engine.

Industrial Gas Turbine

Sirignano et al [55, 56] also studied influences of the implementation of a CTT in a industrial gas-turbine. The predictions show that CTT gas-turbine

produces higher specific power, but lower thermal efficiency when compared with those of the conventional gas-turbine. However, together with heat re-generation, the CTT gas-turbine produces higher specific power at higher thermal efficiency when compared with those of the conventional industrial gas turbine. The engine performance-simulation methodology adopted was identical to that used for the prediction of the performance of the CTT aero-engine; also the exact requirement for turbine's cooling-flow rate was not explicitly considered.

Appendix B. Inter-stage Turbine Burner (ITB) Engine – Industrial Applications

Analyses were conducted by Chen et al [58, 59] to investigate the performance of a gas-turbine with an ITB incorporated. The requirement for extra turbine's cooling-flow rate with the implementation of inter-stage turbine burner (ITB) was incorporated. Chen et al claims that the ITB aero-engine has minimal performance improvements due to the requirement for higher turbine's cooling-flow rate. However, the methodology for the calculation of the turbine's cooling-flow rate, as well as the predictions on the performance of the aero-engine are not presented.

Chen et al [58, 59] extended to investigate the potential of incorporating an ITB in an industrial gas-turbine. The requirement for extra turbine's cooling-flow rate remains an issue. Therefore the study included the investigation on the effects of three cooling-methods, namely open-loop air-cooling, open-loop steam-cooling and closed-loop steam-cooling. The predictions reveal that gas turbine with open-loop steam-cooling produces the highest net power and efficiency, and the worst method is that with open-loop air-cooling. This is because steam is a better cooling medium than air.

Chen et al [58, 59] also went further to investigate the influences of the number of ITB on the gas-turbine performance. The predictions reveal that there is an decrease in the efficiency for the engine with more than one ITB. However, the prediction was not presented in the publications [58, 59]. Nevertheless, this finding is not found in any previous literatures, thus it is a valuable piece of information for future study on the performance of a ITB engine.

Appendix C. Turbine's Cooling-Flow Rate Prediction

Methodology Proposed by Walsh and Fletcher [69]

Figure C1 shows the correlations for the turbine's cooling-flow rate versus stator's outlet-temperature (SOT). For aero-engine applications, the cooling-flow rate is estimated based on its SOT under cruise condition. The defining of the engine's cruise condition could be ambiguous without knowing the exact design requirements for the engine. In addition, this method is for conventional engine, where the turbine's cooling-flow is mainly bled from the high-pressure compressor's (HPC's) exit. In the two-combustor engine, cooling flow is also required to cool the low-pressure turbine (LPT). The LPT is operating in a flow of lower pressure than that experienced by the HPT. Therefore the cooling flow for the LPT could be extracted from the front stages of the HPC. Hence, this method might not over-predict the LPT's cooling-flow rate.

Methodology Proposed by Kurzke [70]

Equations (C1) to (C3) are proposed by Kurzke to predict the turbine's cooling-flow requirements, in agreement with Figure C2. The value of A_1 (i.e. 0.03 to 0.07) depends on the type of cooling-mechanism incorporated, for maintaining the turbine at an acceptable surface temperature, which can range from simple radial holes to a combinations of multi-pass cooling with film cooling. Kurzke's proposed method is relatively straight-forward. However, this method might have excluded the effects of the implementation of thermal barrier coatings (TBC). The F100-PW229 engine has thermal coating applied on its turbine vanes and blades [78]. Therefore the employment of this method would result in an over-prediction of the turbine's cooling-flow rate.

$$\varepsilon_{ngv} = \left(T_{t/gas} - T_{metal}\right) / \left(T_{t/gas} - T_{t/cl}\right) = \phi_{cl/ngv} / \left(\phi_{cl/ngv} + A_1\right) \tag{C1}$$

$$\varepsilon_{rotor} = \left(0.9T_{t/sot} - T_{metal}\right) / \left(0.9T_{t/sot} - T_{t/cl}\right) = \phi_{cl/rotor} / \left(\phi_{cl/rotor} + A_1\right) \tag{C2}$$

$$\phi_{cl} = W_{cl} / W_{ref} \tag{C3}$$

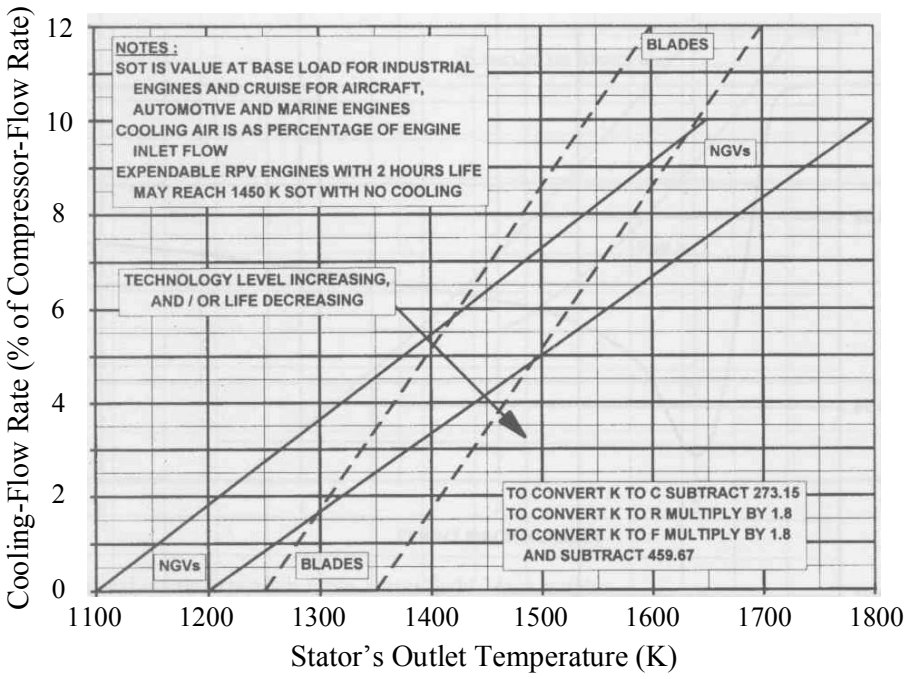

Figure C1. Turbine nozzle-guiding-vane's (NGV's) and rotor blade's cooling-flow requirements versus stator's outlet-temperature (SOT) [69].

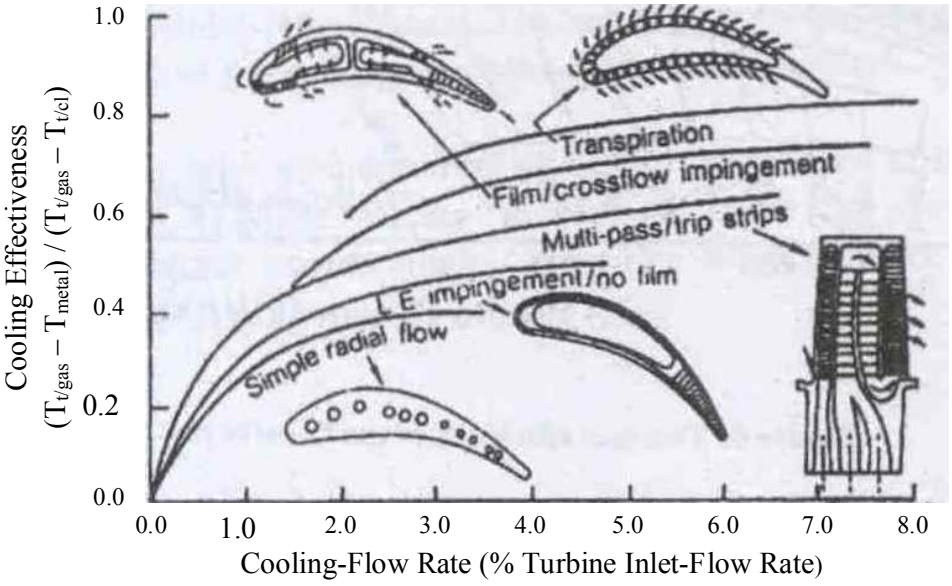

Figure C2. Cooling effectiveness of a turbine's vane or blade versus the cooling-flow requirement for the respective vane or blade [70].

Appendix D. Calculation of Combustor's Inlet Flow-Condition under Windmilling Conditions

This appendix presents the methodology introduces in Reference [75], which is designated as Windmilling-Method-B in this study. Given the engine's design-point condition, the combustor's inlet-flow condition (i.e. $P_{t/comb\text{-}in}$, $T_{t/comb\text{-}in}$ and $W_{comb\text{-}in}$) under specified windmilling can be calculated. (see Figure D1).

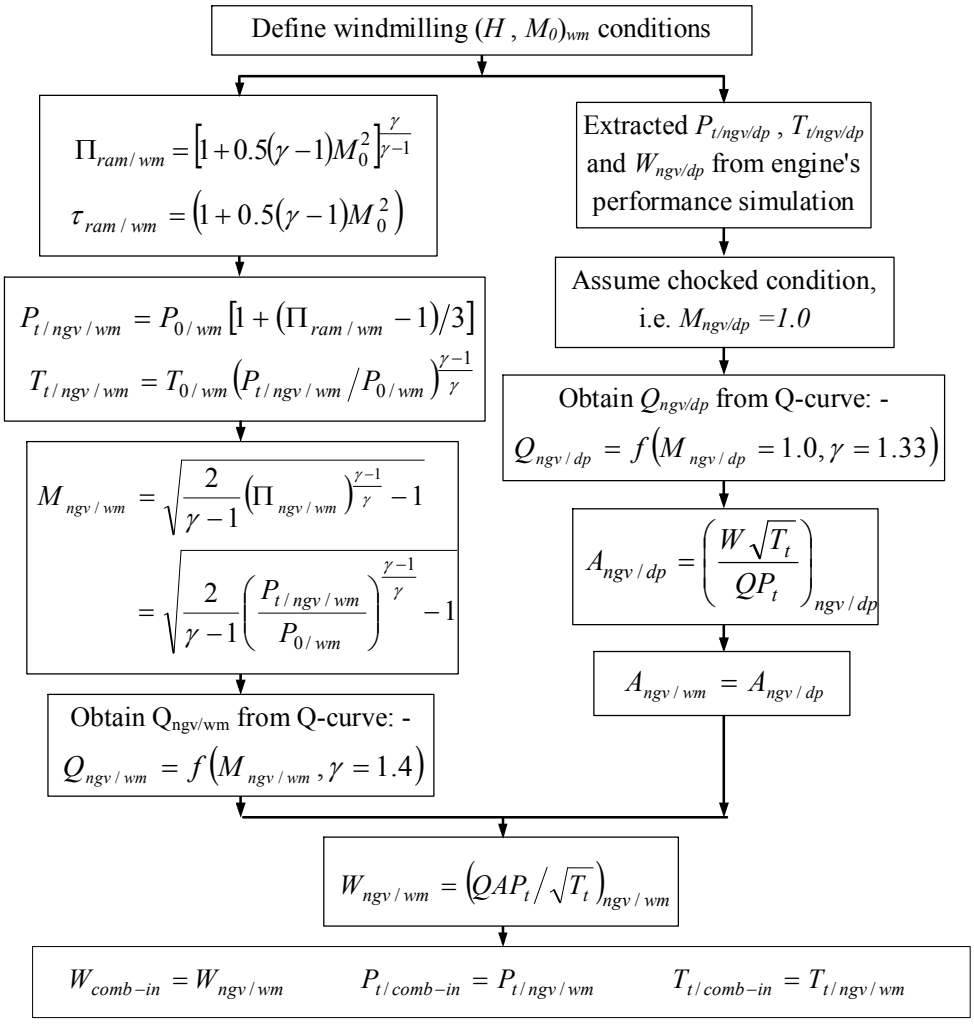

Figure D1. Flow chart on the methodology for Windmilling-Method-B.

Appendix E. Comparison of the Predictions from Windmilling-Method-A's and Windmilling-Method-B's

In the combustor-approach [77], the θ-parameter is used to measure the combustion efficiency and thus for sizing the combustor (Equation E1). The combustor's inlet-flow conditions at selected windmilling conditions were calculated using Windmilling-Method-A and Windmilling-Method-B. The calculation combustor's inlet-flow conditions were used to calculate the θ'-values in Equation E1 (see Table E1). The θ'-values calculates based on the combustor's inlet flow condition obtained from Windmilling-Method-B are lower than that from Windmilling-Method-A. Therefore given a specific θ-value requirement, i.e. combustion efficiency requirement, the combustor size calculates based on combustor's inlet-flow condition obtain from Windmilling-Method-B is larger than that from Windmilling-Method-A.

The following are two possible explanations for the differences in the combustor's inlet-flow condition, i.e. thus the θ'-value, calculated using Windmilling-Method-A and Windmilling-Method-B. Figure E2 shows the typical variations in the spool rotational-speed versus time for an engine under ram deceleration. Windmilling-Method-A is calculating the condition shortly after the engine flame-off; when there is still sufficient ram-pressure to drive the rotational of the compressor. As for Windmilling-Method-B, might be calculating under the windmilling condition whereby the spool rotational speed is near zero. Alternatively, Windmilling-Method-B could be meant for locked-rotor condition (see Figure E3). In the locked-rotor configuration, the compressor pressure-ratio will drop below unity; whereas in a free windmilling condition, the compressor pressure-ratio could be above unity depending on compressor design-point pressure-ratio and windmilling Mach-number. In either cases, the low combustor's inlet-pressure calculates using Windmilling-Method-B has significantly decrease the θ'-value; therefore a larger combustor will be needed to meet the θ-value requirement, i.e. combustion efficiency requirement.

The military aircraft, in particular fighter aircraft, has more flexibility than a civil aircraft. The former could perform a dive to increase its flight speed, thus increasing the ram-pressure and driving more air into the engine to drive the compressor. The use of Windmilling-Method-B might results in over-sizing the combustor for military aero-engine; therefore it is not adopted in this study.

$$\theta_{comb}{}' = \frac{\theta_{comb}}{A_{comb} D_{comb}^{0.75}} = \frac{P_{t4}^{1.75} \exp(T_{t4}/300)}{W_4} \qquad \text{(E1)}$$

Table E1. List of θ' calculated using the combustor's inlet flow condition obtained using Windmilling-Method-A and Windmilling-Method-B.

Flight altitude (kft/km)	**Flight Mach-number**	**Windmilling-Method-A**	**Windmilling-Method-B**
		θ' x10^8	**θ' x10^8**
30 / 9.144	0.305	6.07	2.74
40 / 12.192	0.390	2.70	1.44
50 / 15.240	0.50	1.47	0.81

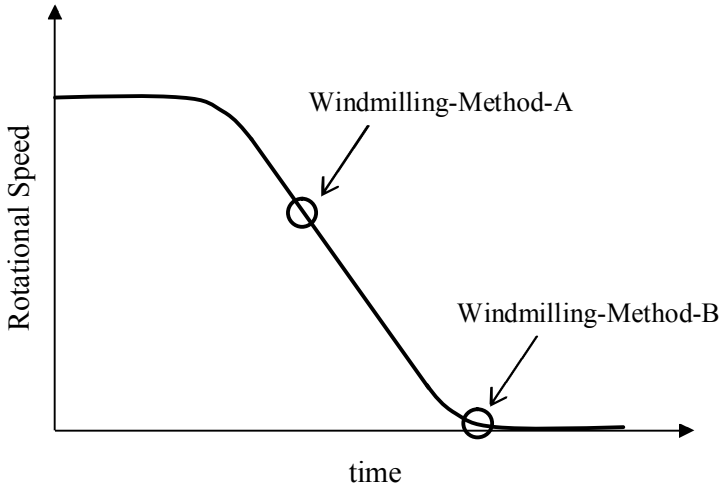

Figure E2. Typical spool's rotational speed during engine deceleration.

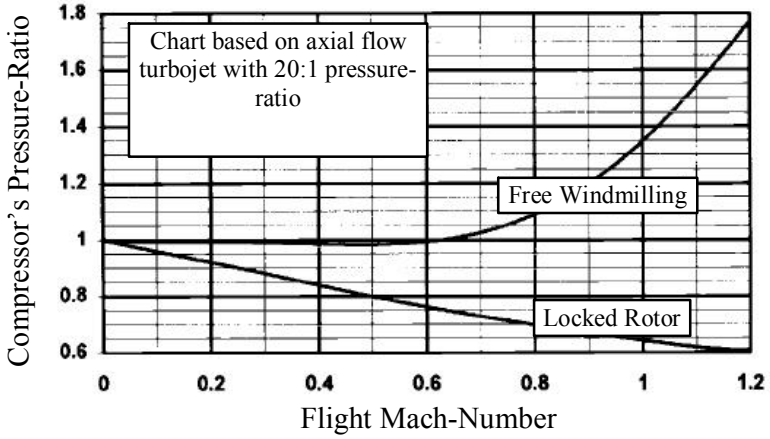

Figure E3. The compressor's pressure-ratios for free windmilling and locked-rotor conditions [69].

Appendix F. Conventional Combustor Sizing

The methodology presented by Walsh and Fletcher [69] is designated as CombSizing-Method-B and described here. The station numbers 0, 1, 3 and 4 are used to refer to the free-stream, engine's inlet, combustor's inlet and combustor's outlet, respectively (see Figure 2.21).

The combustor's flame-tube volume is sized based on the following combustor-loading (see Equation F1) and intensity (see Equation F2) criteria.

- ✓ The loading at sea-level static condition preferably to be lower than 5 kg s^{-1} $atm^{-1.8}$ m^{-3}.
- ✓ The loading at the highest altitude and lowest Mach-number in cold day to be less than 50 kgs^{-1} $atm^{-1.8}$ m^{-3} (in the worst case to be 75 kgs^{-1} $atm^{-1.8}$ m^{-3}).
- ✓ During altitude relight under windmilling condition, at the highest altitude and lowest Mach-number, the loading to be lower than 300 kgs^{-1} $atm^{-1.8}$ m^{-3}.
- ✓ The combustion intensity at sea-level static condition to be less than 60 MW atm^{-1} m^{-3}.

$$Vol_{flametube} = W_3 \Big/ \left(Loading * P_{t3}^{1.8} * 10^{0.00145*(T_{t3}-400)} \right) \tag{F1}$$

$$Vol_{flametube} = W_3 Q_{fuel} \eta_{mb} \Big/ P_{t3} I_{mb} \tag{F2}$$

After the sizing of the flame-tube volume, the following are steps taken to calculate the various dimensions of the combustor (see Figure F1).

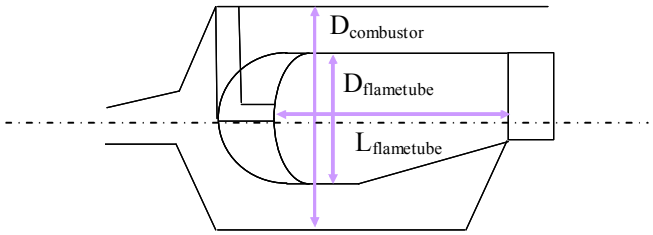

Figure F1. The dimensions defining the size of the combustor.

Calculate the cross-sectional area of the flame-tube ($A_{flametube}$): -

It is assumed that rich-burn (PHI=1.02) occurs at the primary zone of the flame-tube, hence enables the calculation of mass-flow rate into the primary zone (see Equation F3 and F4). It is further assumed that the flow Mach-number at the exit of primary zone is 0.02. Since stoichiometric reaction occurs at primary zone, the primary zone's exit gas is at 2300K. Using Equation F5, the cross-sectional area of the flame-tube can be calculated.

$$FAR_{pri-zone} = 1.02 * 0.067 = 0.0683 \tag{F3}$$

$$W_{air/pri-zone} = W_{fuel/mb} / FAR_{pri-zone} \tag{F4}$$

$$A_{pri-zone} = \left(\frac{W\sqrt{T_t}}{QP_t} \right)_{pri-zone} \tag{F5}$$

Calculate depth of the flame-tube ($D_{flametube}$): -

Equation F6 can be used to calculate the height of the flame-tube ($D_{flametube}$). In this case, the mean radius of the combustor is estimated from the drawing of the F100-PW229 engine (see Figure 5.1).

$$A_{pri-zone} = \pi * \left[\left(R_{mean} + \frac{D_{flametube}}{2} \right)^2 - \left(R_{mean} - \frac{D_{flametube}}{2} \right)^2 \right] \tag{F6}$$

Calculate flow area of the annulus (A_{ann}): -

It is assumed that the annulus-flow Mach-number is ~0.1. Using Q-curve, the cross-sectional area of the annulus can be calculated using Equation F7.

$$A_{ann} = \left(\frac{W\sqrt{T_t}}{QP_t} \right)_{ann} \tag{F7}$$

Calculate the depth of the combustor (D_{comb}): -

With the values of the combustor mean radius and the cross-sectional area of the flame-tube and annulus, the height of the combustor can be calculated using Equation F8.

$$A_{pri-zone} + A_{ann} = \pi * \left[\left(R_{mean} + \frac{h_{comb}}{2} \right)^2 - \left(R_{mean} - \frac{h_{comb}}{2} \right)^2 \right] \tag{F8}$$

Calculate length of flame-tube ($L_{flametube}$):

The length of the flame-tube can be calculated using Equation F9. The residence time can then be calculated using Equations F10 and F11. If the calculated residence time falls below the requirements, usually 3ms, the length of the flame-tube would have to be increased.

$$L_{flametube} = Vol_{flametube} / A_{pri-zone} \tag{F9}$$

$$V_{pri-zone/exit} = \left(M * \sqrt{\gamma Rt} \right)_{pri-zone/exit} \tag{F10}$$

$$t_{residence} = L_{flametube} / V_{pri-zone/exit} \tag{F11}$$

Appendix G. Sizing of the F100-EQ Engine's Combustor Using CombSizing-Method-B [69]

Three conditions are considered here: (i) the engine at maximum thrust at sea-level static, (ii) engine operating at highest altitude and lowest flight Mach-number and (iii) engine at windmilling condition at highest altitude and lowest flight Mach-number. Three altitudes, namely 30kft, 40kft and 50kft, are selected for comparisons for the last two conditions. The Windmilling-Method-A is used to calculate the combustors' inlet-flow condition under windmilling condition.

Under normal engine operating, Walsh and Fletcher [69] assumes that the flow at the annulus to be at Mach-number of 0.1. The amount of air entering the primary zone is calculated by assuming rich burn at equivalent ratio of 1.02 (see Appendix F). At windmilling condition, there is no recommendation on the Mach-number of the annulus flow and the amount of flow into the primary zone. The author assumes that 40% of the compressor's exit flow enters the primary zone of the combustor (see Figure G1). However, using an annulur Mach-number of 0.1, the calculated annulus area is significantly lower than required when the engine is under normal operation. With lower annulus mass-flow rate, the author thinks that it is more realistic to assume a lower annulus flow Mach-number, i.e. 0.05 (see Figure G2). With either assumption, the combustor size at the altitude of 50kft remains the worst case when comparing to that at 30kft and 40kft.

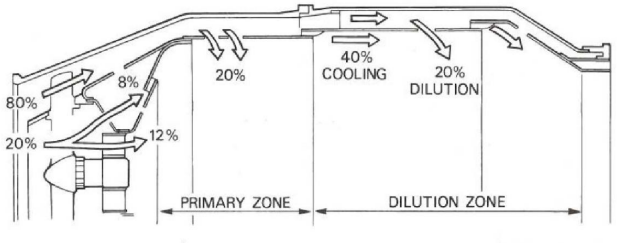

Figure G1. Typical flow distribution in a combustor [100].

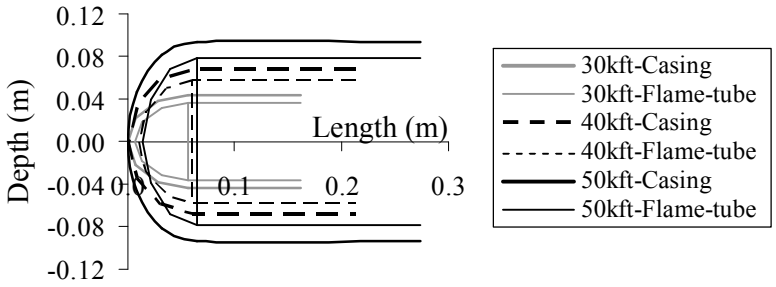

Figure G2. Sketches on the main combustor size for engine under windmilling conditions (annulus Mach-number ~0.05).

Figure G3 shows the calculated dimensions of the combustor in comparison with that estimated from the F100-PW229 engine's sketches (see Figure 5.1). Generally, the calculated flame-tube size is "fatter" when comparing to the estimated dimensions. At normal operation, the calculated length of the combustor is also significantly shorter than that of the estimated values. The flame-tube volume is calculated given the loading requirements and combustor inlet flow condition. With more flow into the primary zone, the flame-tube (i.e. combustor) will be "fatter" and "shorter". Alternative, the primary zone combustion temperature can be further reduced (<2300K) to decrease the flame-tube cross-sectional area, thus increases its length. However, these might not necessary agree with the physical operation of the combustor. Without going into detail design and analysis, the present author concludes that the combustor sized using CombSizing-Method-B does not match close with the dimensions estimated from the F100-PW229 drawing. Therefore it is not adopted for the calculation of the inter-stage turbine burner size.

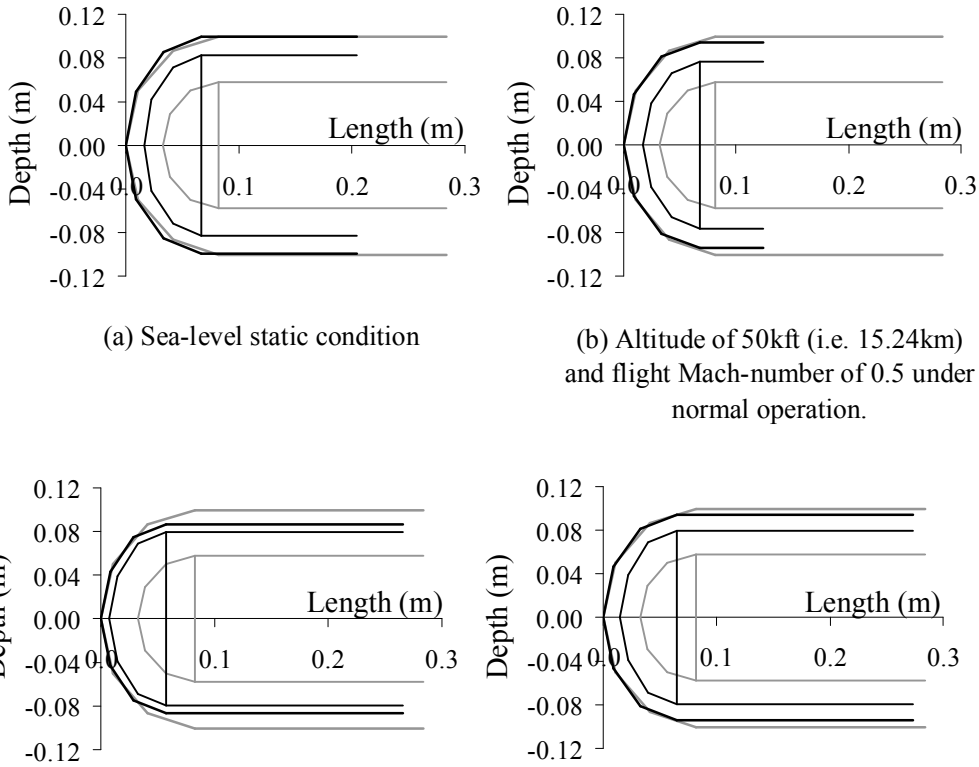

(a) Sea-level static condition

(b) Altitude of 50kft (i.e. 15.24km) and flight Mach-number of 0.5 under normal operation.

(c) Altitude of 50kft (i.e. 15.24km) and flight Mach-number of 0.5 under windmilling condition (Annulus Mach-number =0.1).

(d) Altitude of 50kft (i.e. 15.24km) and flight Mach-number of 0.5 under windmilling condition (Annulus Mach-number =0.05).

Figure G3. Sketches on the key dimensions of the combustor casing, flame-tube and fuel-injector calculated based on loading and intensity approaches in comparison with dimensions of F100-PW229 combustor estimated from drawing [Casing-Estimated Flame-tube-Estimated Casing-Calculated Flame-tube-Calculated].

Appendix H. Tabulating of Drag Polar for F16-EQ Aircraft "Clean" Configuration

The drag-polar of the F16 Falcon and generic aircraft available in public domain are tabulated. The aerodynamic characteristic of the F16-EQ aircraft is assumed to be identical to that of the F16 Falcon aircraft.

Figure H1 shows the variation of C_{Do} and k for generic high-performance military flightier [92. The author assumed that the data corresponds to "current" fighter aircraft will be more representative for the F16 Falcon aircraft.

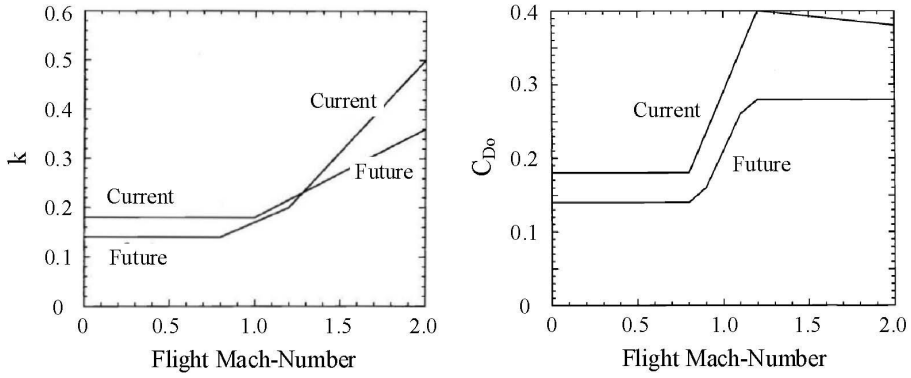

Figure H1. Variation of C_{Do} and k values with flight Mach-number for generic high-performance fighter aircraft [92].

Table H1 shows the values of C_{Do}, k_1 and k_2 for generating the F16's drag-polar [84]. The first-set of value is estimated C_{Do} and k values; whereas the second-set are "actual" values as designated in reference [84]. The present author interprets the "actual" as data from testing; thus "test data" instead of "actual" is used in this thesis.

Table H1. Comparison between test and estimated data [84].

Mach	Estimated Data			Test Data		
	C_{Do}	k_1	k_2	C_{Do}	k_1	k_2
0.30	0.0169	0.117	-0.0094	0.0193	0.117	-0.007
0.86	0.0169	0.117	-0.0094	0.0202	0.115	-0.004
1.05	0.0428	0.128	-0.0047	0.0444	0.16	-0.001
1.50	0.038	0.252	0	0.0448	0.28	0
2.00	0.0356	0.367	0	0.0458	0.37	0

Figure H2, also extracted from reference [84], shows the parasite drag coefficient, i.e. C_{Do}, of the F16 aircraft.

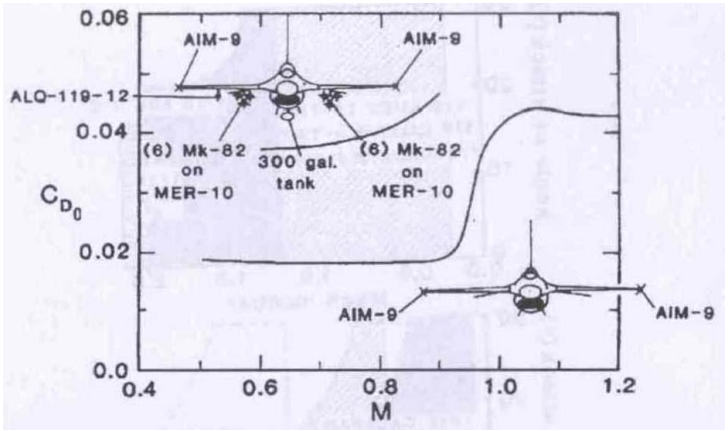

Figure H2. Parasite drag coefficient (C_{Do}) of F16 aircraft [84].

The F16 Falcon aircraft's parasite-drags obtained from the above-references are compared in Figure H3. It is observed that data smoothing was done, especially over the transonic regime, for data from reference [92]. Also the C_{Do} from reference [92] is lower than those from reference [84]. This could be because the F16 Falcon aircraft developed in the 1970s and reference [92] published in the 2000s. Both set of C_{Do} extracted from reference [84] match closely. It is also widely accepted to assume that test-data are reliable for further analysis. Therefore data from reference [84] will be used to tabulate the drag-polar for the F16-EQ aircraft. For Mach-number below 0.9 and above 1.1, the

C_{Do} values will be interpolated or extrapolate based on the test-data reproduced in Table H1. For transonic regime from Mach 0.9 to 1.1, the C_{Do} extracted from Figure H2 will be used. The values for k_1 and k_2 are linearly interpolated and extrapolated, over the flight Mach-number, based on data reproduced in Table H1. The above tabulated C_{Do}, k_1 and k_2 are for the F16-EQ aircraft with Aim-9 mounted at the wing-tip, hereby designated as F16-EQ aircraft "clean" configuration (see Table 3.3).

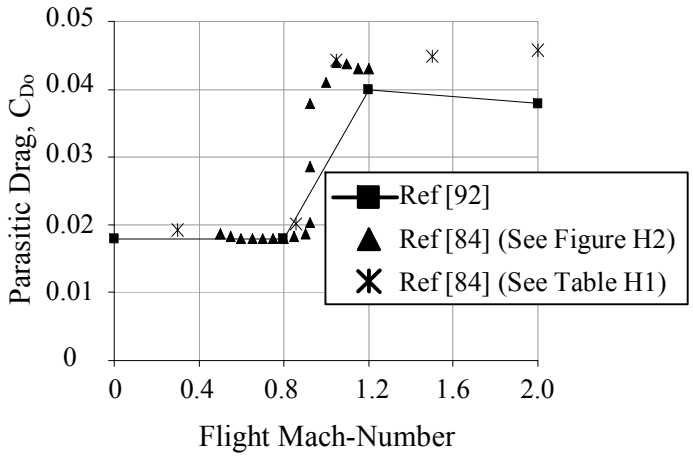

Figure H3. Comparison of C_{Do} values from references [84] and [92].

Appendix I.Performance Predictions for a Two-spool Separate-exhaust Turbofan Engine with and without an Inter-stage Turbine Burner (ITB) at the Design-point Condition.

Options: -

Engine Type:	Either	Conventional Engine (CE)
	Or	Two-combustor Engine (TCE)
Gas-Properties' Model:	Either	Constant Specific-Heat (CSH) model
	Or	Modified Specific-Heat (MSH) model
	Or	Improved Specific-Heat (ISH) model

Inputs Parameters: -

Flight Conditions:	P_0 , T_0 , M_0
Design Parameters:	W_0 , α , T_{t5} , T_{t7}, Π_{fan} , $\Pi_{overall}$
Components' Parameters:	$\Pi_{diff\text{-}max}$, Π_{mb} , Π_{itb} , τ_{diff} , $\tau_{fan\text{-}noz}$, τ_{noz}
	$\eta_{ploy/fan}$, $\eta_{ploy/lpc}$, $\eta_{ploy/hpc}$, $\eta_{ploy/hpt}$, $\eta_{ploy/lpt}$
	η_{mb}, η_{itb}, η_{noz}, $\eta_{fan\text{-}noz}$, $\eta_{mech/hp}$, $\eta_{mech/lp}$
Others:	Q_{fuel}

Equations [39]: -

Freestream Condition

$$a_0 = \sqrt{\gamma_0 R_0 T_0} \qquad V_0 = M_0 a_0$$

Ram Effects (Ram)

$$\Pi_{ram} = \left[1 + 0.5(\gamma_0 - 1)M_0^2\right]^{\frac{\gamma_0}{\gamma_0 - 1}}$$

$$\tau_{ram} = 1 + 0.5(\gamma_0 - 1)M_0^2$$

Inlets & Diffuser (Diff)

If $M_0 \le 1$, $\eta_{Rspec} = 1$

If $1 < M_0 < 5$, $\eta_{Rspec} = 1 - 0.075(M_0 - 1)^{1.35}$

Otherwise $\eta_{Rspec} = 800/\left(M_0{}^4 + 935\right)$

$$\Pi_{diff} = \Pi_{diff-\max}\eta_{Rspec}$$

Fan (Fan)

$$\tau_{fan} = \Pi_{fan}^{\left[(\gamma_2-1)/(\gamma_2\eta_{ploy/fan})\right]}$$

$$\eta_{fan} = \left(\tau_{fan}^{\eta_{ploy/fan}} - 1\right)/\left(\tau_{fan} - 1\right)$$

Low-pressure Compressor (LPC)

$$\tau_{lpc} = \Pi_{lpc}^{\left[(\gamma_2-1)/(\gamma_2\eta_{ploy/lpc})\right]}$$

$$\eta_{lpc} = \left(\tau_{lpc}^{\eta_{ploy/lpc}} - 1\right)/\left(\tau_{lpc} - 1\right)$$

High-pressure Compressor (HPC)

$$\tau_{hpc} = \Pi_{hpc}^{\left[(\gamma_3-1)/(\gamma_3\eta_{ploy/hpc})\right]}$$

$$\eta_{hpc} = \left(\tau_{hpc}^{\eta_{ploy/hpc}} - 1\right)/\left(\tau_{hpc} - 1\right)$$

Main combustor (MB)

$$FAR_{mb} = \left(Cp_5T_{t5} - Cp_4T_{t4}\right)/\left(Q_{fuel}\eta_{mb} - Cp_5T_{t5}\right)$$

High-pressure Turbine (HPT)

$$\tau_{hpt} = 1 - \frac{1}{\eta_{mech/hp}}\left(\frac{Cp_3T_{t3}}{Cp_5T_{t5}}\right)\left(\frac{\tau_{hpc}-1}{1+FAR_{mb}}\right)$$

$$\Pi_{hpt} = \tau_{hpt}^{\left[\gamma_5/\left[(\gamma_5-1)\eta_{ploy/hpt}\right]\right]}$$

$$\eta_{hpt} = \left(1 - \tau_{hpt}\right)/\left(1 - \tau_{hpt}^{\left(1/\eta_{ploy/hpt}\right)}\right)$$

Inter-stage Turbine Combustor (ITB)

If Engine Model is CE, then

$$\Pi_{itb} = 1$$

$$\tau_{itb} = 1$$

$$FAR_{itb} = 0$$

Otherwise (i.e. Engine Model is TCE)

$$FAR_{itb} = \left(Cp_7 T_{t7} - Cp_6 T_{t6}\right) / \left(Q_{fuel}\eta_{itb} - Cp_7 T_{t7}\right)$$

Low-pressure Turbine (LPT)

$$\tau_{lpt} = 1 - \frac{1}{\eta_{lp/mech}}\left(\frac{Cp_2 T_{t2}}{Cp_7 T_{t7}}\right)\left[\frac{\alpha\left(\tau_{fan} - 1\right) + \left(\tau_{lpc} - 1\right)}{\left(1 + FAR_{mb}\right)\left(1 + FAR_{itb}\right)}\right]$$

$$\Pi_{lpt} = \tau_{lpt}^{\left[\gamma_7 / \left[\left(\gamma_7 - 1\right)\eta_{ploy/lpt}\right]\right]}$$

$$\eta_{lpt} = \left(1 - \tau_{lpt}\right) / \left(1 - \tau_{lpt}^{\left(1/\eta_{ploy/lpt}\right)}\right)$$

Core's Exhaust-Nozzle (Noz)

$$P_{t10}/P_{10} = \left(P_0/P_{10}\right)\Pi_{ram}\Pi_{diff}\Pi_{lpc}\Pi_{hpc}\Pi_{mb}\Pi_{hpt}\Pi_{itb}\Pi_{lpt}\Pi_{noz}$$

$$M_{10} = \sqrt{2\left[\left(P_{t10}/P_{10}\right)^{\frac{\gamma_{10}-1}{\gamma_{10}}} - 1\right] \Big/ \left(\gamma_{10} - 1\right)}$$

$$\frac{T_{10}}{T_0} = \frac{T_{t10}/T_0}{\left(P_{t10}/P_0\right)^{\frac{\gamma_{10}-1}{\gamma_{10}}}} = \frac{\left(T_{t7}\tau_{lpt}\right)/T_0}{\left(P_{t10}/P_0\right)^{\frac{\gamma_{10}-1}{\gamma_{10}}}}$$

$$V_{10}/a_0 = M_{10}\sqrt{\left(\gamma_{10}R_{10}T_{10}\right)/\left(\gamma_0 R_0 T_0\right)}$$

Fan Exhaust-Nozzle (Fan-Noz)

$$P_{t13}/P_{13} = \left(P_0/P_{13}\right)\Pi_{ram}\Pi_{diff}\Pi_{fan}\Pi_{fan-noz}$$

$$M_{13} = \sqrt{2\left[\left(P_{t13}/P_{13}\right)^{\frac{\gamma_{13}-1}{\gamma_{13}}} - 1\right] \Big/ \left(\gamma_{13} - 1\right)}$$

$$\frac{T_{13}}{T_0} = \frac{T_{t13}/T_0}{\left(P_{t13}/P_0\right)^{\left[\left(\gamma_{13}-1\right)/\gamma_{13}\right]}} = \frac{\tau_{ram}\tau_{diff}\tau_{fan}\tau_{fan-noz}}{\left(P_{t13}/P_0\right)^{\left[\left(\gamma_{13}-1\right)/\gamma_{13}\right]}}$$

$$V_{13}/a_0 = M_{13}\sqrt{\left(\gamma_{13}R_{13}T_{13}\right)/\left(\gamma_0 R_0 T_0\right)}$$

Performance [39]: -

$$F_{net} = W_{10}V_{10} + W_{13}V_{13} - W_0 V_0$$

$$SFC = W_{fuel}/F_{net}$$

$$\eta_{th} = \left(W_{10}V_{10}^2 + W_{13}V_{13}^2 - W_0V_0^2\right)/\left(2W_{fuel}Q_{fuel}\right)$$

where

$$W_{fuel} = W_0\left[\left(1+FAR_{mb}\right)\left(1+FAR_{itb}\right)-1\right]/\left(1+\alpha\right)$$

$$W_{10} = W_0\left(1+FAR_{mb}\right)\left(1+FAR_{itb}\right)/\left(1+\alpha\right)$$

$$W_{13} = W_0\left(\frac{\alpha}{1+\alpha}\right)$$

Appendix J. Performance Predictions for the Two-spool Separate-exhaust Turbofan Engine, with and without an Inter-stage Turbine Burner (ITB), under Off-design Conditions.

Inputs: -

Flight conditions: P_0, T_0, $M_0(a_0)$

Constants (Same values as in design-point condition): -

Component efficiencies: η_{fan}, η_{lpc}, η_{hpc}, η_{mb}, η_{hpt}, η_{itb}, η_{lpt}, η_{noz}, $\eta_{fan\text{-}noz}$

Component pressure-ratios: Π_{fanR} , Π_{lpcR} , Π_{hpcR} , Π_{hptR} , Π_{lptR}

Component temperature ratios: τ_{fanR} , τ_{lpcR} , τ_{hptR} , τ_{lptR}

Others: α_R , T_{t5R} , T_{t7R} , $MFP(M_{9R})$, $MFP(M_{12R})$, Q_{fuel}

Assumptions: -

The flow in the HPT and LPT are choked. Hence the mass-flow parameters (MFPs) for the HPT and LPT are constant.

All flow areas are invariant, except for the LPT's NGV and core exhaust nozzle.

The pressure-ratios across the combustors are constant.

The slight variation in fuel-air ratio is ignored

Equations [39]: -

Freestream Condition (0)

$$a_0 = \sqrt{\gamma_0 R_0 T_0} \qquad V_0 = M_0 a_0$$

Ram Effect (Ram)

$$\Pi_{ram} = \left[1 + 0.5(\gamma_0 - 1)M_0^2\right]^{\frac{\gamma_0}{\gamma_0 - 1}}$$

$$\tau_{ram} = 1 + 0.5(\gamma_0 - 1)M_0^2$$

Inlets & Diffuser (Diff)

If $M_0 \le 1$, $\eta_{Rspec} = 1$

If $1 < M_0 < 5$, $\eta_{Rspec} = 1 - 0.075(M_0 - 1)^{1.35}$

Otherwise $\eta_{Rspec} = 800/\left(M_0{}^4 + 935\right)$

$$\Pi_{diff} = \Pi_{diff-\max}\eta_{Rspec}$$

Turbine's Entry Temperature

If $\theta_0 > \theta_{0R}$, $T_{t5} = T_{t5R}$ $T_{t5} = T_{t5R}$

Otherwise, $T_{t5} = T_{t5R}(\theta_0/\theta_{0R})$ $T_{t7} = T_{t7R}(\theta_0/\theta_{0R})$

where $\theta_0 = \tau_{ram}\left(T_0/T_{ref}\right)$

Fan (Fan)

$$\tau_{fan} = 1 + \eta_{lp/mech}\left(\tau_{fanR} - 1\right)\left(\frac{Cp_7T_{t7}}{Cp_2T_{t2}}\right)\left(\frac{\left(1-\tau_{lpt}\right)\left(1+FAR_{mb}\right)\left(1+FAR_{itb}\right)}{\left(\tau_{lpcR}-1\right)+\alpha\left(\tau_{fanR}-1\right)}\right)$$

$$\Pi_{fan} = \left[1 + \eta_{fan}\left(\tau_{fan}-1\right)\right]^{\frac{\gamma_2}{\gamma_2-1}}$$

Low-pressure Compressor (LPC)

$$\tau_{lpc} = 1 + \left(\tau_{fan}-1\right)\left(\tau_{lpc}-1\right)_R/\left(\tau_{fan}-1\right)_R$$

$$\Pi_{lpc} = \left[1 + \eta_{lpc}\left(\tau_{lpc}-1\right)\right]^{\frac{\gamma_2}{\gamma_2-1}}$$

High-pressure Compressor (HPC)

$$\tau_{hpc} = \eta_{hp/mech}\left(1+FAR_{mb}\right)\left(1-\tau_{hpt}\right)\left(Cp_5T_{t5}\right)/\left(Cp_3T_{t3}\right)$$

$$\Pi_{hpc} = \left[1 + \eta_{hpc}\left(\tau_{hpc}-1\right)\right]^{\frac{\gamma_3}{\gamma_3-1}}$$

Main Burner (MB)

$$FAR_{mb} = \left(Cp_5T_{t5} - Cp_4T_{t4}\right)/\left(Q_{fuel}\eta_{mb} - Cp_5T_{t5}\right)$$

High-pressure Turbine (HPT)

$$\tau_{hpt} = 1 - \eta_{hpt}\left(1 + \Pi_{hpt}^{[(\gamma_5-1)/\gamma_5]}\right)$$

$$\Pi_{hpt} = \Pi_{hptR}\sqrt{\tau_{hpt}/\tau_{hptR}}$$

Inter-stage Turbine Burner (ITB)

$$FAR_{itb} = \left(Cp_7T_{t7} - Cp_6T_{t6}\right)/\left(Q_{fuel}\eta_{itb} - Cp_7T_{t7}\right)$$

Low-pressure Turbine (LPT)

$$\tau_{lpt} = 1 - \eta_{lpt}\left(1 + \Pi_{lpt}^{\left[(\gamma_7 - 1)/\gamma_7\right]}\right)$$

$$\Pi_{lpt} = \Pi_{lptR}\sqrt{\tau_{lpt}/\tau_{lptR}}\left(MFP(M_{9R})/MFP(M_9)\right)$$

Core Exhaust Nozzle (Noz)

$$\frac{P_{t10}}{P_{10}} = \frac{P_0}{P_{10}}\Pi_{ram}\Pi_{diff}\Pi_{lpc}\Pi_{hpc}\Pi_{mb}\Pi_{hpt}\Pi_{itb}\Pi_{lpt}\Pi_{noz}$$

$$M_{10} = \sqrt{2\left[\left(P_{t10}/P_{10}\right)^{\frac{\gamma_{10}-1}{\gamma_{10}}} - 1\right] \Big/ \left(\gamma_{10} - 1\right)}$$

$$\frac{T_{10}}{T_0} = \frac{T_{t10}/T_0}{\left(P_{t10}/P_0\right)^{\frac{\gamma_{10}-1}{\gamma_{10}}}} = \frac{\left(T_{t7}\tau_{lpt}\right)/T_0}{\left(P_{t10}/P_0\right)^{\frac{\gamma_{10}-1}{\gamma_{10}}}}$$

$$V_{10}/a_0 = M_{10}\sqrt{\left(\gamma_{10}R_{10}T_{10}\right)/\left(\gamma_0 R_0 T_0\right)}$$

If $M_{10} >= 1$, $M_9 = 1$

Otherwise, $M_9 = M_{10}$

$$MFP(M_9) = M_9\sqrt{\left(\gamma_9/\gamma_9\right)\left[1 + 0.5\left(\gamma_9 - 1\right)M_9^2\right]^{\frac{\gamma_9+1}{2(1-\gamma_9)}}}$$

Fan Exhaust Nozzle (Fan-Noz)

$$P_{t20}/P_{20} = \left(P_0/P_{20}\right)\Pi_{ram}\Pi_{diff}\Pi_{fan}\Pi_{fan-noz}$$

$$M_{13} = \sqrt{2\left[\left(P_{t13}/P_{13}\right)^{\frac{\gamma_{13}-1}{\gamma_{13}}} - 1\right] \Big/ \left(\gamma_{13} - 1\right)}$$

$$\frac{T_{13}}{T_0} = \frac{T_{t13}/T_0}{\left(P_{t13}/P_0\right)^{\frac{\gamma_{13}-1}{\gamma_{13}}}} = \frac{\tau_{ram}\tau_{diff}\tau_{fan}\tau_{fan-noz}}{\left(P_{t13}/P_0\right)^{\frac{\gamma_{13}-1}{\gamma_{13}}}}$$

$$V_{13}/a_0 = M_{13}\sqrt{\left(\gamma_{13}R_{13}T_{13}\right)/\left(\gamma_0 R_0 T_0\right)}$$

Bypass Ratio (α)

$$\alpha = \alpha_R\left(\frac{\Pi_{lpcR}\Pi_{hpcR}/\Pi_{fanR}}{\Pi_{lpc}\Pi_{hpc}/\Pi_{fan}}\right)\left(\frac{MFP(M_{12})}{MFP(M_{12R})}\right)\sqrt{\frac{T_{t5}/T_{t5R}}{T_0\tau_{ram}\tau_{fan}/T_{0R}\tau_{ramR}\tau_{fanR}}}$$

Total Mass-flow Rate (W_0)

$$W_0 = W_{0R}\left(\frac{1+\alpha}{1+\alpha_R}\right)\left(\frac{P_0\Pi_{ram}\Pi_{diff}\Pi_{lpc}\Pi_{hpc}}{P_{0R}\Pi_{ramR}\Pi_{diffR}\Pi_{lpcR}\Pi_{hpcR}}\right)\sqrt{\frac{T_{t5R}}{T_{t5}}}$$

Performance [39]: -

$$F_{net} = W_{10}V_{10} + W_{20}V_{20} - W_0V_0$$

$$SFC = W_{fuel}/F_{net}$$

$$\eta_{th} = \left(W_{10}V_{10}^2 + W_{13}V_{13}^2 - W_0V_0^2\right)/\left(2W_{fuel}Q_{fuel}\right)$$

Appendix K. Assigning of Gas Properties to the Engine's Stations

Station 0 (=freestream)

$(Cp, R, \gamma)_0 = \text{function} (T_0 , FAR_0 = 0)$

Stations 1, 2, 3

If the CSH or MSH model is used, then

$Cp_1 = Cp_0 , Cp_2 = Cp_0 , Cp_3 = Cp_0$

$R_1 = R_0 , R_2 = R_0 , R_3 = R_0$

$\gamma_1 = \gamma_0 , \gamma_2 = \gamma_0 , \gamma_3 = \gamma_0$

Otherwise

$(Cp, R, \gamma)_x = \text{function} (T_{tx} , FAR_x = 0)$ where x = 1, 2, 3

Station 4

If the CSH model is used, then

$Cp_4 = Cp_0 , \quad R_4 = R_0 , \gamma_4 = \gamma_0$

Otherwise

$(Cp, R, \gamma)_4 = \text{function} (T_{t4} , FAR_4 = 0)$

Station 5

$(Cp, R, \gamma)_5 = \text{function} (T_{t5} , FAR_5)$

Station 6

If the CSH model is used, then

$Cp_6 = Cp_5 , \quad R_6 = R_5 , \gamma_6 = \gamma_5$

Otherwise

$(Cp, R, \gamma)_6 = \text{function} (T_{t6} , FAR_6)$

Station 7

For CE engine type: -

If the CSH model is used, then

$Cp_7 = Cp_5$, $R_7 = R_5$, $\gamma_7 = \gamma_5$

Otherwise

$(Cp, R, \gamma)_7 = \text{function} (T_{t7} , FAR_7)$

For TCE engine type: -

$(Cp, R, \gamma)_7 = \text{function} (T_{t7} , FAR_7)$

Station 8=9=10

For CE engine type: -

If CSH or MSH model is used, then

$Cp_8 = Cp_5$, $R_8 = R_5$, $\gamma_8 = \gamma_5$

Otherwise

$(Cp, R, \gamma)_7 = \text{function} (T_{t7} , FAR_7)$

For TCE engine type: -

If CSH or MSH model,

$Cp_8 = Cp_7$, $R_8 = R_7$, $\gamma_8 = \gamma_7$

Otherwise

$(Cp, R, \gamma)_8 = \text{function} (T_{t8} , FAR_8)$

Station 11=12=13

If CSH or MSH model is used, then

$Cp_{11} = Cp_0$, $R_{11} = R_0$, $\gamma_{11} = \gamma_0$

Otherwise

$(Cp, R, \gamma)_{11} = \text{function} (T_{t11} , FAR_{11} = 0)$

Appendix L. Equations for the Calculations of the Gas-Properties

Input Parameters

T , FAR

Equations [46]

$$Cp_{air} = \left(C_0 + C_1T + C_2T^2 + C_3T^3 + C_4T^4 + C_5T^5 + C_6T^6 + C_7T^7\right)_{air}$$

$$Cp_{product} = \left(D_0 + D_1T + D_2T^2 + D_3T^3 + D_4T^4 + D_5T^5 + D_6T^6 + D_7T^7\right)_{product}$$

$$Cp = \frac{Cp_{air} + Cp_{product}FAR}{1 + FAR} \times 4186.8$$

$$R = \frac{1.9857117}{28.97 - 0.946186 \times FAR} \times 4186.8$$

$$\gamma = \frac{Cp}{Cp - R}$$

The units of Cp and R are kJ kg^{-1} K^{-1} and γ is dimensionless.

where

Air:

C_0=2.502E-01 C_1=-5.154E-05 C_2=6.552E-08 C_3=-6.718E-12

C_4=-1.513E-14 C_5=7.622E-18 C_6=-1.453E-21 C_7=1.012E-25

Product (Fuel-air combustion product):

D_0=7.382E-02 D_1=1.226E-03 D_2=-1.377E-06 D_3=9.969E-10

D_4=-4.205E-13 D_5=1.021E-16 D_6=-1.334E-20 D_7=7.268E-25

Outputs

Cp , R , γ

Appendix M. Comparison of the Performance of a Low-bypass Engine with Two and Three Compressors Configurations

The compression system for the F100-EQ engine consists of a fan and a high-pressure compressor (HPC). The effects of modelling the HPC as a "single-compressor" or "two-compressor" are addressed here. The considered engine configurations are shown in Figure M1 and the corresponding design-point conditions are shown in Table M1. For ease of comparison, only cooling-flow for the high-pressure turbine (HPT) bled from the HPC's exit-flow is considered.

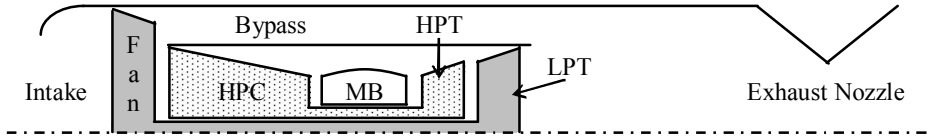

(a) Two compressors and two turbines configuration

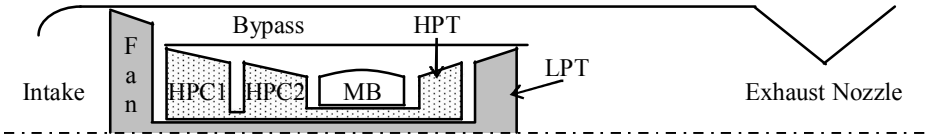

(b) Three compressors and two turbines configuration

Figure M1. Sketch of low-bypass two-spool mixed-exhaust turbofan engine.

Figures M2 and M3 show the behaviours of the engine modelled via two-compressor and three-compressor configurations. There are marginal differences in the behaviours of the two engine-configurations under off-design conditions. This comparison shows that the mean of modelling the high-pressure compressor via two-compressor is feasible.

Table M1. Design points for two-compressor and three-compressor engine configurations.

Parameters	**Two-compressor Configuration**	**Three-compressor Configuration**
Flight altitude, H (km)	0	0
Flight Mach-number, M_0	0	0
Fan's pressure-ratio, FPR	3.55	3.55
HPC1 pressure-ratio, HPC1's PR	N.A.	2.23
Overall pressure-ratio, OPR	32.4	32.4
Bypass ratio, BPR	0.36	0.36
Mass-flow rate, W (kg s^{-1})	100	100
Turbine's entry-temperature, TET (K)	1700	1700

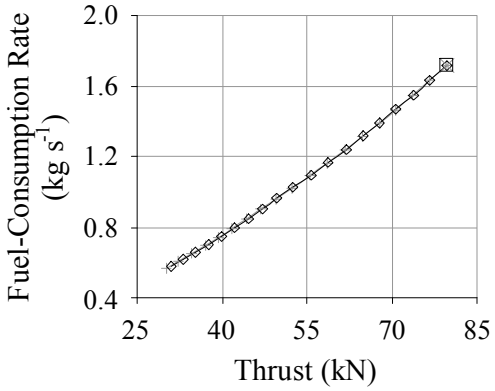

Figure M2. The fuel-consumption rate versus thrust for the engines of two-compressor and three-compressor configurations [Two-compressor(DP) Two-compressor(OD) Three-compressor(DP) Three-compressor(OD)].

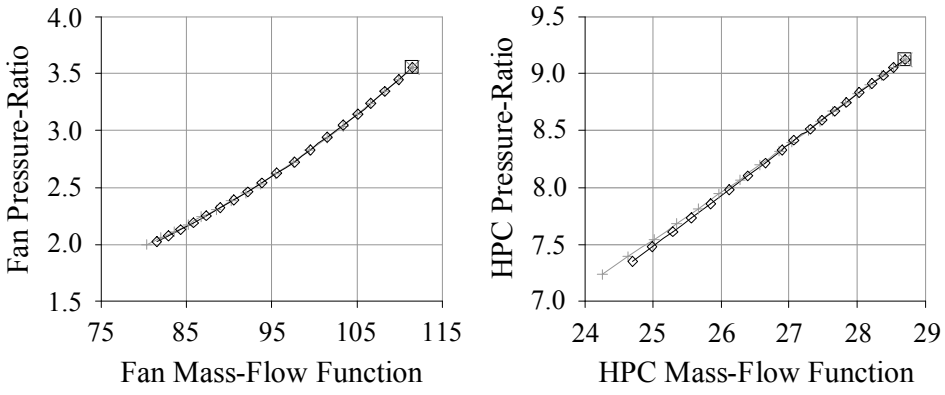

Figure M3. The behaviours of the fan and high-pressure compressor (HPC) for the engines of two-compressor and three-compressor configurations [Two-compressor(DP) Two-compressor(OD) Three-compressor(DP) Three-compressor(OD)].

Appendix N. Comparison of the Performances of the Engines with Mixed and Separated Exhaust-Nozzles

The design-point conditions for the considered engines are shown in Table N1. In the modelling of the engine with mixed exhaust-nozzle, a convergent-divergent nozzle of variable geometry is adopted. However, in the modelling of the engine with separated exhaust-nozzle, the core's and fan's exhaust-nozzles are convergent-divergent nozzles of variable and fixed geometries, respectively. This is because the employed engine performance-simulation program, i.e. TURBOMATCH, has an limitation on the maximum number of variable parameters.

Table N1. Design points for the engines with mixed and separate exhaust-nozzles.

Parameter	**Value**
Flight altitude, H (km)	0
Flight Mach-number, M_0	0
Fan's pressure-ratio, FPR	3.6
Overall pressure-ratio, OPR	32.4
Bypass ratio, BPR	0.36
Mass-flow rate, W (kg s^{-1})	100
Turbine's entry-temperature, TET (K)	1500
Cooling-flow (%)	0.0

The predictions of the fuel-consumption rate versus thrust for the engines with mixed and separated exhaust-nozzle are slightly different (see Figure N1). However, there are significant differences in the behaviours of the fan and high-pressure compressor (HPC) for the considered two engine-configurations (see Figure N2). Therefore to enhance the reliability of the outcomes of an study, it is necessary to model the engine as close to the actual configuration as possible.

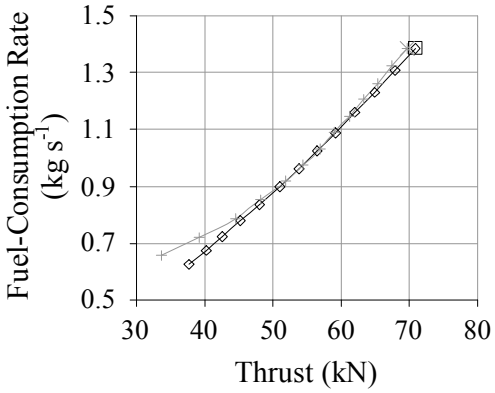

Figure N1. The fuel-consumption rate versus thrust for the engines with mixed and separated exhaust-nozzle [× Separated(DP) —+— Separated(OD) □ Mixed(DP) —◇— Mixed(OD)].

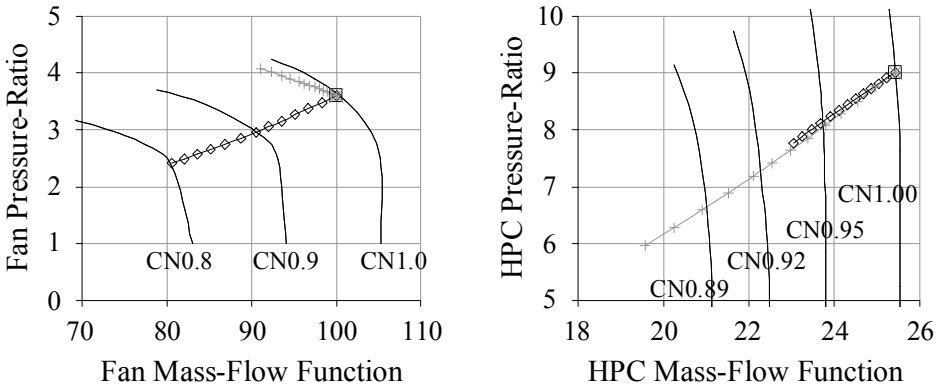

Figure N2. The behaviours of the fan and high-pressure compressor (HPC) for the engines with mixed and separated exhaust-nozzle [× Separated(DP) —+— Separated(OD) □ Mixed(DP) —◇— Mixed(OD)].